



UNIVERSITY OF STRASBOURG

A dissertation presented
by

Zsuzsanna Tamara Nagy

Synthesis of Self-Organized Dendrimers and Dendronized Nanohybrids and their Physical Properties

Submitted to
the **Doctoral school of Physics and Physical Chemistry**
University of Strasbourg

In partial fulfilment of the requirements for the degree of

Doctor of Philosophy

Organic Chemistry and Materials Science

14th September 2012

The Institute of Physics and Chemistry of Materials of Strasbourg
Department of Organic Materials
CNRS UMR 7504

Thesis directors:

Dr. Daniel GUILLON,
Dr. Bertrand DONNIO,

DR1 (CNRS) IPCMS, Dr ECPM, Strasbourg, France
DR2 (CNRS) IPCMS, UMR 7504 -CNRS, France

Reporters:

Prof. Didier ASTRUC,
Prof. Georg H. MEHL,

reporter, University of Bordeaux, France
reporter, University of Hull, England

Other members of the committee:

Dr. Marie-Pierre KRAFFT,
Prof. Jean-François STUMBÉ,

DR2 (CNRS) ICS, UPR 22-CNRS, Strasbourg, France
ENSCMu / UHA, Mulhouse, France

ÉCOLE DOCTORALE de PHISIQUE et CHIMIE-PHISIQUE
IPCMS/DMO

THÈSE

présentée par:

Zsuzsanna Tamara NAGY

soutenue le : **14 Septembre 2012**

pour obtenir le grade de:

Docteur de l'université de Strasbourg

Discipline/ Spécialité:

Chimie Organique Moléculaire et Chimie des Matériaux

Synthèse de dendrimères et de nanohybrids dendronisés, auto- organisés et étude de leurs propriétés physiques

THÈSE dirigée par :

M. GUILLON Daniel

DR1 (CNRS), IPCMS, Dr, ECPM, Strasbourg, France

M. DONNIO Bertrand

DR2 (CNRS), IPCMS, UMR 7504 - CNRS, Strasbourg, France

RAPPORTEURS :

M. ASTRUC Didier

Professeur de l'Université de Bordeaux, France

M. MEHL Georg H.

Professeur de l'University of Hull, England

AUTRES MEMBRES DU JURY :

Mme. KRAFFT Marie-Pierre

DR2 (CNRS), ICS, UPR 22, Strasbourg, France

M. STUMBÉ Jean-François
France

Professeur de l'UHA, ENSCMu / UHA, Mulhouse,

*“Prediction is very difficult, especially
if it's about the future”*

Niels Henrik David Bohr

Acknowledgements

This thesis work has been carried out in the last three years at the Department of Organic Materials (DMO) of the Institute of Physics and Chemistry of Materials of Strasbourg (IPCMS), CNRS - Strasbourg University (UMR7504), Strasbourg and has been supported by the European Commission, FP7 program, Marie Curie Actions - Initial Training Network, "DENDREAMERS" project (No. 215884-2.).

First, I must thank my supervisors Dr. Bertrand Donnio and Dr. Daniel Guillon to give me the opportunity to conduct my PhD research under their guidance, for their help and patience which made this work possible and for me to have become a better scientist.

I would like to acknowledge Prof. Didier Astruc, Prof. Georg Mehl, Dr. Marie-Pierre Krafft and Prof. Jean-Francois Stumbe for having accepted to evaluate my thesis and to participate in the committee.

Also, I would like to thank Prof. José L. Serrano, project coordinator, for letting me participate in the "Dendreamers" project which allowed me to meet with some great people, to Dr. Jean-Louis Gallani, department leader, and to Dr. Jean-Pierre Bucher, director of the "Ecole Doctorale de Physique et Chimie-Physique" of the Strasbourg University, for allowing me to carry out lab-work at the department and to carry out my PhD studies at the doctoral school.

I thank Prof. Joachim Stumpe for welcoming me in Potsdam for two weeks and for this most useful collaboration.

I am greatly thankful to Dr. Benoît Heinrich for his kindness, availability and all his help in DSC, SAXS and everything else related to the lab. Sharing his knowledge allowed me to understand liquid crystals better. I thank the technical staff of the DMO: Emilie Voirin for her help around the lab, Emilie Couzigne for ordering chemicals, and Nicolas Beyer for considering our needs during the lab building and his help out of work. I thank Rose-Marie Weller for her competence and helping me in administration. I thank also my colleagues, particularly Antonio for his buoyancy, George for being George, Marie for her kindness and her help with my early chemistry and of course, foremost Kálmán who provided the most help in the lab and support during my writing and beside being a colleague most importantly being my partner for a long and colourful period in my life.

I would like to thank the assistance provided by the following contributors: Dris Ihiawakrim (DSI) for the TEM measurements, the great pictures and his cheerfulness, Didier Burger (DCMI) for the TGA measurements and Jean-Marc Strub (ECPM) for MALDI-ToF analysis.

I must extend special thanks to John R. Fyson (Monty) for his generosity, kindness and the time he devoted to read my thesis and for the comments which were not only helpful but cheered me up.

I am very grateful to all my friends for their friendship and support, in Strasbourg and all around the world but especially to the ones in Hungary. Despite the distance and the six years I have left the country I could turn to them and talk as if I had never left. I also thank to my family for their support and encouraging me to work abroad. And again and last I thank Kálmán for everything.

Table of content

Acknowledgements	i
Table of content.....	iii
List of Abbreviations.....	vi
Abstract	viii
Chapter I. - Self-Organized dendrimers	
I.1 Introduction	1
I.1.1 Dendrimers	1
I.1.1.1 General structure of dendrimers	3
I.1.1.2 Synthesis methods	4
I.1.2 Liquid Crystals	5
I.1.2.1. Classification of liquid crystals	6
I.1.2.2. Thermotropic liquid crystals	7
I.1.3 Liquid crystal dendrimers	11
I.1.3.1 Thermotropic liquid crystal dendritic structures	11
I.1.4 Photoinduced anisotropy of liquid crystal azodendrimers.....	15
I.1.4.1. Azobenzene derivatives.....	15
I.1.4.2. Light-driven azodendrimers.....	18
I.1.5 Objective of the thesis, I.....	23
I.2 Results and Discussion - Syntheses.....	25
I.2.1 Synthesis of mesogenic units and branching points.....	25
I.2.2 Synthesis of Trimers	30
I.2.3 Synthesis of phloroglucinol based first generation dendrimers	33
I.2.4 Synthesis of benzyl alcohol based dendrimers.....	38
I.2.5 Synthesis of Cinnamic acid ester derivatives	43
I.3 Results and discussion - Characterization.....	45
I.3.1 Characterization by Nuclear Magnetic Resonance spectroscopy.....	45
I.3.2 Characterization by Mass Spectroscopy	52
I.3.3 Characterization by Elemental analysis.....	54
I.3.4 Mesomorphic properties and self-assembly.....	54
I.3.4.1 Mesomorphism of Trimers	59
I.3.4.2 Mesomorphism of PG Dendrimers	68
I.3.4.3 Mesomorphism of BA Dendrimers.....	79

I.3.4.4	Self-organization of PG and BA dendrimers	86
I.3.5	Photochemical behaviour	90
I.3.5.1	Photochemical behaviour of trimers	92
I.4	Conclusions and Outlooks	98
I.5	Experimental part.....	102
I.5.1	Synthesis of mesogenic units and branching points.....	102
I.5.2	Synthesis of Dendrons and Trimers	108
I.5.3	Synthesis of PG dendrimers.....	116
I.5.4	Synthesis of BA dendrimers.....	129
I.4.4	Synthesis of Cinnamic acid esters	141
I.6	References.....	144
Chapter II – Dendronized Gold Nanohybrids		
II.1	Introduction	153
II.1.1	Gold Nanoparticles.....	153
II.1.1.1	History of gold and gold nanoparticles.....	153
II.1.1.2	Syntheses of AuNPs.....	155
II.1.1.3	Ligand-exchange and coupling on AuNPs.....	156
II.1.2	Liquid-crystalline Dendronized Gold Nanohybrids	158
I.1.2.1	Dendronized gold nanohybrids	158
I.1.2.2	Liquid-crystalline gold nanohybrids and self-assembly.....	163
II.1.3	Objective of the thesis, II.	169
II.2	Results and discussion - Syntheses.....	170
II.2.1	Synthesis of gold nanoparticles.....	170
II.2.2	Synthesis of Ligands	174
II.2.3	Synthesis of dendronized gold nanohybrids.....	176
II.3	Results and discussion - Characterization.....	181
II.3.1	Characterization of gold nanoparticles	181
II.3.2	Characterization of Thiols.....	185
II.3.3	Characterization of Dendronized Gold Nanohybrids	189
II.3.4	Self-Assembly of dendronized gold nanohybrids	195
II.4.	Conclusions and outlooks.....	203
II.5	Experimental part.....	206
II.5.1	Gold Nanoparticles.....	206
II.5.2	Thiolated ligands	207

II.5.3	Dendronized Gold Nanohybrids.....	213
II.6	References.....	214
	Résumé de la These	219
	Annex - structures	231

List of Abbreviations

AuNP	Gold nanoparticle
AZB	Alkoxy-azobenzene
BA	Benzyl alcohol
BPH	Alkoxy-biphenol
calcd	Calculated
Col	Columnar phase
Cr	Crystalline phase
DEN	Dendrimer-encapsulated nanoparticles
DIAD	Diisopropyl azodicarboxylate
DMF	Dimethylformamide
DSC	Differential scanning calorimetry
DT	Dodecanethiol
EA	Elemental analysis
G	Glassy state
I	Isotropic liquid
LC	Liquid crystal
LPL	Linearly polarized light
N	Nematic phase
NBS	<i>N</i> -bromosuccinimide
NCD	Nanoparticle-cored dendrimers
NMR	Nuclear magnetic resonance
NP	Nanoparticle
OA	1-octylamine
OCB	4'-Hydroxybiphenyl-4-carbonitrile
PAMAM	Polyamidoamine
PG	Phloroglucinol
POM	Polarized optical microscopy
SANS	Small-angle neutron scattering
SAXS	Small-angle X-ray scattering
sd	Standard deviation
Sm	Smectic phase
SRG	Surface relief grating
TBAF	Tetra- <i>n</i> -butylammonium fluoride

TBDMS	<i>Tert</i> -Butyldimethylsilyl
TEM	Transmission electron microscopy
T _g	Glass transition temperature
TGA	Thermogravimetric analysis
THF	Tetrahydrofuran
THP	Tetrahydropyranyl
TOAB	Tetraoctylammonium bromide
UV-Vis	Ultraviolet-Visible
XRD	X-ray diffraction

Abstract

Self-assembly of single molecules into supramolecular systems and self-organization of supermolecular structures into highly complex and functional networks, where liquid-crystalline materials (LCs) continuously emerge as prime candidates, are of interest in life and material sciences. The need to expand further the range of mesomorphic organization, develop original materials where different functionality can be added (*i.e.* multifunctional), and to design “multitask materials” with tunable properties are particularly interesting and crucial challenges for potential uses in future technologies. Dendrimers because of their special structures which provide diversity and high functionality are ideal to build up such supermolecules as well as hybrid materials.

Gold nanoparticles (AuNP) based hybrid materials are especially interesting because of the size-dependent properties of the AuNPs which can be controlled by syntheses conditions. One of the great challenges of nanomaterials is the development of efficient methods for the fabrication of ordered structures. Structured nanomaterials are desirable for potential application based on unusual optical properties, *e.g.* negative refractive index. The self-assembly of the hybrids into 2D or 3D networks can be modulated by the shape and size of NPs and by the density of the grafted protodendritic ligands.

On the one hand, this project is focused on the design and synthesis of multifunctional supermolecules (liquid crystal, dendritic, photoresponsive) which are suitable for making thin films where photoinduced optical anisotropy and surface relief gratings can be generated. We also investigated the mesomorphic behaviour of these dendrimers. On the other hand, we grafted structurally related protodendritic mesogenic ligands to monodisperse AuNPs to elaborate the liquid crystalline properties in order to induce self-assembly. A set of dendronized gold nano hybrids was synthesized to carry out this study.

In the first part of this thesis, we will describe the successful synthesis of several sets of unconventional zero (trimers) and first generation dendritic structures with different branching points (phloroglucinol (PG) or benzyl alcohol (BA)) bearing calamitic alkoxy-azobenzene (AZB) based chromophores whose relative molar proportion is selectively varied by exchanging with the other calamitic mesogens (alkoxy-biphenyl (BPH) or cyanobiphenyl (OCB)). Divergent synthesis and selective functionalization were applied to the trimers and a convergent method was applied to increase the generation number. Essentially all the synthesized systems behave as thermotropic liquid crystals. Various types of smectic (SmA/B/C/F/I) and nematic phases have been induced as expected, since all mesogenic groups

are calamitics. In most of cases, the heterolithic structures show original and highly separated multilayered smectic phases – except in one case, a columnar phase occurred due to the sliding of undulated planes. The nature and the symmetry of the phases could be changed by modifying the structure of the dendrimers (relative molar proportions of the mesogenic units, the branching points *etc.*) The effects of the structural modifications on the mesomorphism have been investigated by differential scanning calorimetry (DSC) and small-angle X-ray diffraction (SAXS) experiments, combined with dilatometry. Optical properties of the trimers were investigated by a collaborative partner and one of them has been shown to induce exceptionally high optical anisotropy (dichroism 0.77) in a thin film made from an AZB-containing trimer. In case of first generation dendrimers more heterolithic systems have fulfilled the required physical properties for optical measurement, such as high glass transition temperature (T_g) and good solubility, which makes them ideal candidate for induction of optical anisotropy. These measurements are still in progress.

In the second part we will describe the successful synthesis of dendronized gold nano hybrids, using the protodendritic ligands from the synthesis of the dendrimers by changing the focal point to the thiol anchoring function. Their self-assembly and liquid crystalline properties were also investigated. In order to build up hybrid structures, first small (2-8 nm), monodisperse gold nanoparticles were synthesized. In order to achieve low-dispersity, direct synthesis was applied: a modification of Brust's two phase method, which underwent several different modifications. In the second step, for the synthesis of the hybrids, solvent-mediated ligand exchange was applied, which allows preserving the original size of the AuNPs, but lowers the density of the mesogenic units, compared to direct grafting reactions. The density of mesogenic units, which were induced in the organic layers of the hybrid, was varied according to the applied generation of the dendritic ligands. In order to investigate the liquid crystalline properties of the hybrids, it is particularly important to assure the purity of the sample as free ligands can modify the liquid crystalline behaviour. The self-assembly has been investigated by transmission electron microscopy (TEM) and the liquid crystalline properties by SAXS, small-angle neutron scattering (SANS), DSC and polarized optical microscopy (POM). In case of the first generation AZB containing gold nano hybrids, optical texture was observed, which indicates the successful induction of liquid crystalline properties.

Chapter I

Self-Organized Dendrimers

1.1 Introduction

This chapter addresses the discussion of the synthesis and characterization of multifunctional polyether trimers and dendrimers bearing different protomesogenic functional groups that exhibit liquid crystalline and photoresponsive properties. One of the functional groups is a chromophore, namely azobenzene, and its relative molar proportion is modulated by exchanging it with the other mesogens. The mesomorphic properties of the products have been investigated in detail and some optical measurements have been carried out and will also be presented. The chapter consists of five main sections.

First we will introduce the dendrimers, the typical architectures and the most common synthetic methods. This will be followed by the introduction of liquid crystals (LC) and in more detail thermotropic liquid crystals, typical mesogenic structures and their self-organizations. Then a specific class of the dendrimers, the LC dendrimers, will be presented in brief and finally azobenzenes, their photoisomerization properties and their dendritic derivatives will be introduced, dependent on the position of the chromophore in the dendritic structure.

In the following two sections we will present the results. First the synthetic methods, which have been used to carry out the successful syntheses of the dendrimers. Trimers have been built up using a combination of divergent procedure and selective functionalization and mainly convergent procedures to obtain the first generation dendrimers. We also attempted to investigate other chromophores and the synthesis of materials bearing a cinnamic acid ester group will also be shown. This will be followed by the characterization of materials according to their mesomorphic and optical properties. After the general characterization (NMR, Mass spectroscopy, *etc.*), the mesomorphic properties of the final products (trimers, dendrimers) will be discussed and compared by DSC, SAXS and polarized optical microscopy (POM) results. Then the optical properties of the azobenzene containing trimers and finally, after the conclusion, the detailed syntheses steps will be presented in the experimental part.

1.1.1 Dendrimers

The increased demand to expand further and develop original and multifunctional materials, dendritic molecular systems, with perfectly controlled geometry (symmetrical or not) and identifiable molecular sub-units, are potentially interesting candidates. Their intrinsic advantages, such as intricate molecular systems, which combine traits of discrete low-molecular-weight materials (monodisperse) with those of polymers (various degrees of conformational flexibility, size-modulated viscosity, glass transition, *etc.*), represent an attractive way of adding functionality (*e.g.*, multifunctional and high control of functional specificity and

hierarchy) and designing “multitask materials” with tunable properties¹. The various types of dendritic materials can be divided into sub-classes, such as dendrimers and dendrons, hyperbranched polymers, dendrigraft polymers and dendronized polymers^{2,3} (Figure 1), but here we will focus and present only the dendrimers.

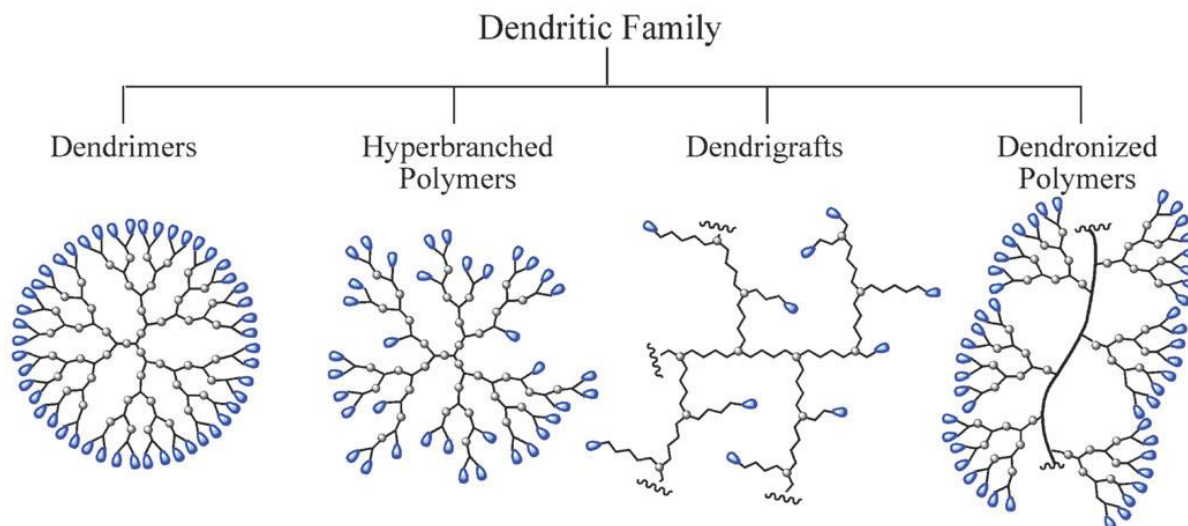


Figure 1 Schematic picture of sub-classes within the dendritic family³

In 1952 Flory began a systematic study of hyperbranched materials and reported a theory about the synthesis of highly branched polymers which can be carried out by polycondensation of an AB_2 monomer where the two functional groups can react with each other^{4,5}. However, only after Vögtle, who first reported the synthesis of defined branched structures by an iterative synthetic procedure⁶ (originally called “cascade synthesis”), a large interest in hyperbranched polymers has opened up, and the field of dendrimers became independent from polymers. First, Tomalia *et al.* synthesized dendrimers (poly(amidoamine), PAMAM) at Dow Chemical, in 1979, which was published later^{7,8}. Parallel to this work Newkome reported the synthesis of arborol dendrimers⁹. Fréchet introduced a new synthesis method (see later) in 1990 and built up polyether dendrimers¹⁰. In 1994, Meijer and co-workers demonstrated first the potential of the dendrimers as hosts and encapsulation of a molecule inside a dendrimer, in the so-called “dendritic box”¹¹ which was based on a poly(propyleneimine) (PPI) dendrimer.

Since then, the interest for the synthesis of new dendritic materials having specific properties has exceptionally increased and more comprehensive reviews and books were written on dendrimer syntheses^{1,12,13,14} and their supramolecular properties and applications^{11,15,16,17,18,19} (by Newkome’s, Vögtle’s, Zimmerman’s, Tomalia’s, Astruc’s and Meijer’s group).

1.1.1.1 General structure of dendrimers

Dendrimers are hyperbranched symmetrical structures (*e.g.* tree-branches, snowflake). The word comes from the Greek word “dendron” which means tree and “meros” means part. Dendrimers in chemistry are monodisperse supermolecules with regular, star-like, highly branched architecture. They are composed of concentric layers of repeating units emanating from a central core and the number of layers is defined as the generation of the dendrimers (G_i). The branching points are part of the layers and connect the core, through its functionality (chemical bonds), to the terminal groups (often functional groups) (Figure 2). Dendrons are highly branched wedge-shaped macromolecules but the bonds emerge radially from a central focal point, which is the single reactive function of the dendritic section (Figure 2).

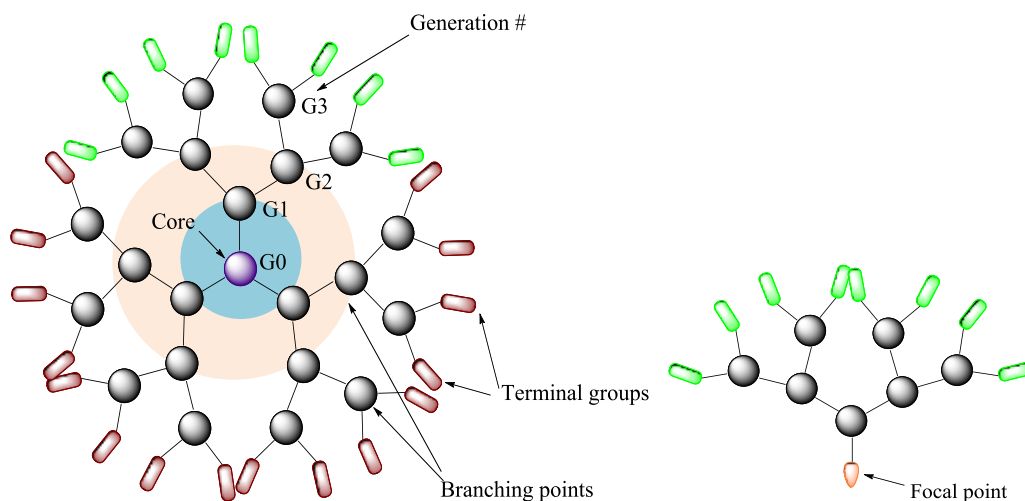


Figure 2 Schematic presentation of a dendrimer (left) and a dendron (right)

The generations are interdependent and create a unique molecular shape, leading to intrinsic properties such as high solubility and low viscosity. The functional groups can be located not only at the termini but in the dendritic interior (1.1.4.2). They can carry molecules encapsulated in their interior or attached to the surface²⁰. Dendrimers' structural diversity is great^{12,21,22,23} where the generation number, the degree of branching, the chain density and the functionality can be modulated (Figure 3).

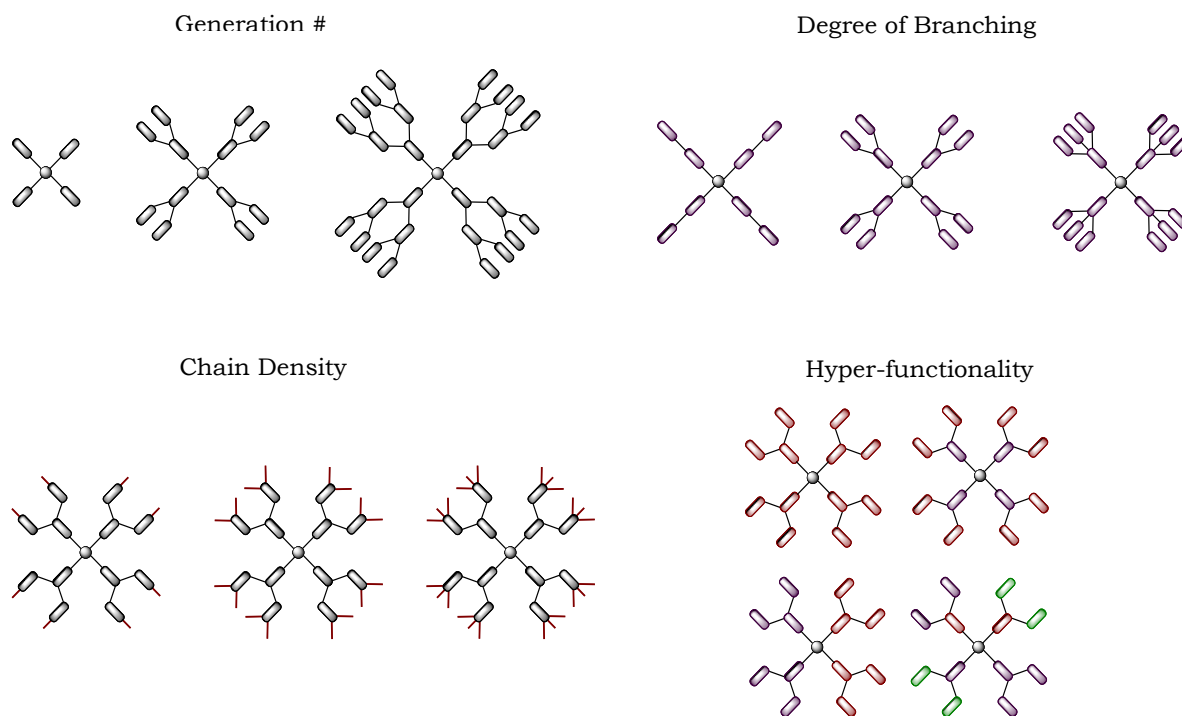


Figure 3 Schematic presentation of the structural diversity of dendrimers

1.1.1.2 Synthesis methods

Dendrimers can be prepared with high regularity and controlled molecular weights using traditional methods of organic chemistry (*e.g.* ether coupling, esterification, click chemistry²⁴) based on iterative sequences of synthesis steps, such as activation then coupling and deprotection, to increase the generation number. There are two general methods for the synthesis of dendrimers (see Fig. 4 and Fig. 5). Divergent synthesis was used originally by Tomalia⁷ and Newkome⁹, but Fréchet¹⁰ pioneered a convergent synthesis. The two methodologies are complementary and the approach being used depends on the features of the targeted molecule. In divergent synthesis, it is more complicated to obtain pure and structurally uniform dendrimers, as the number of reactions exponentially increases at each step of growth, but on a large scale and for higher generation dendrimers, it can be favoured. Structural control increased using convergent approaches, on one hand due to the “ease” of purification methods, and on the other hand the differentiated functionalities of the focal point and the periphery²⁰.

The ***divergent method*** starts from the core, of which the multiplicity can be varied (two or higher), and proceeds radially outward toward the dendrimer periphery. In the case of symmetric dendrimers the reactive groups of the core is reacted with the selectively protected monomer, which introduces a new latent branching points. After the first generation of the dendrimer has been grown, the functional groups on the periphery are activated and further

reacted with the monomer. The procedure is repeated stepwise by activation and coupling of the monomer resulting in an increased generation number (Figure 4).

Divergent strategy

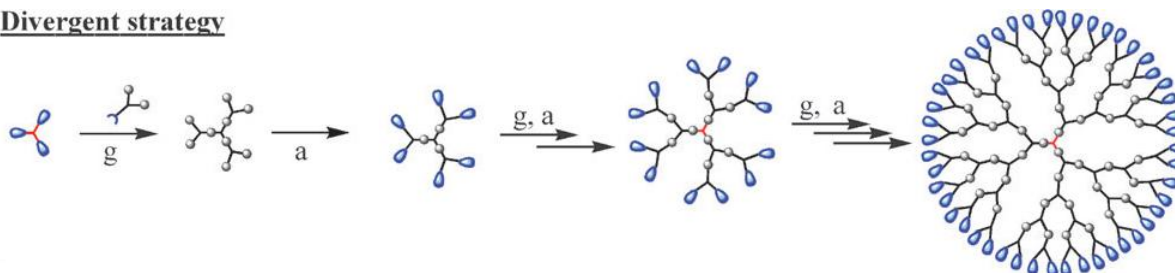


Figure 4 Divergent growth approach; g: dendritic growth, a: activation of surface groups³

In the **convergent method** the growth starts at what will become the periphery of the dendrimer, and the individual branches or dendrons are built sequentially, proceeding inward by selective deprotection/activation and coupling. The dendrons built up in this way coupled to the core in the last step (Figure 5). The convergent approach provides control over the nature and location of the groups that are placed at the periphery of the molecule.

Convergent strategy

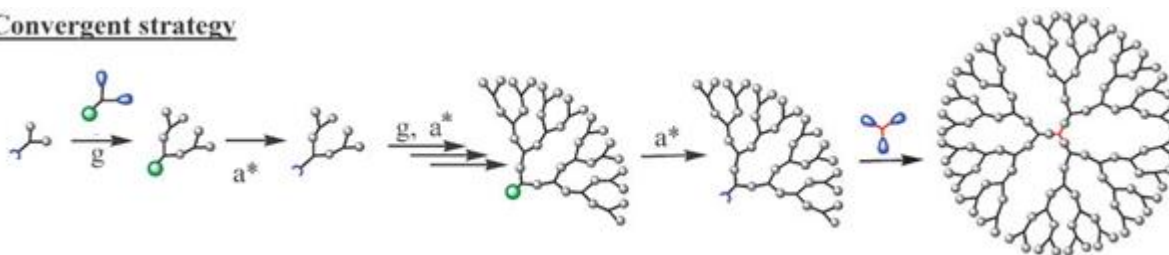


Figure 5 Convergent growth approach; g: dendritic growth, a*: activation of core³

There are many complementary methods^{14,15} developed in order to increase the efficiency of the process, such as the double-stage convergent growth approach²⁵, the hypercore or branched monomer approach^{26,27}, the double-exponential dendrimer growth²⁸, the click chemistry²⁹ and the orthogonal coupling strategies³⁰.

1.1.2 Liquid Crystals

Since 1888, when Friedrich Reinitzer, an Austrian botanical physiologist, observed the phenomenon which was named liquid crystal (LC) by Otto Lehman, a German physicist^{31,32} and since George H. Heilmeyer's research work, which led to the first liquid crystal display (LCD, IEEE Milestone) in 1968, the LCD TV industry revenue has grown to \$99b (figures from 2010). This short insight can point out why there is such a great interest in LCs. However this revenue is predicted to peak and will decrease as AMOLED (active-matrix organic light-emitting diode)

will penetrate the TV market and will replace the LCDs³³, just as LCDs surpassed cathode ray tubes (CRTs) in 2007. But, LCs are not only interesting for display industry.

Supramolecular chemistry is a powerful tool to elaborate preprogrammed self-assemblies of single molecules, interacting by non-covalent intermolecular forces and specific molecular recognition criteria, into highly complex and detailed functional networks mimicking living systems, of interest in life and material sciences^{34,35,36}. LC materials continuously emerge as prime candidates for the construction of supramolecular or supermolecular systems due to their dynamic nature, function-integration and stimuli-responsiveness³⁷. This class of 'soft' materials, which combines order with fluidity within various types of mobile and low-dimensional periodic structures, seems suited to the future development of organic-based organization-dependent technological (e.g. optic- and electronic-based) and biological (molecular machines, guest-host systems, sensors, catalysts, switches, signal amplification devices, therapeutic and transfecting agents, *etc*) applications^{38,39,40,41,42}. Moreover, the properties of the single molecules can be transferred and considerably enhanced within ordered supramolecular soft assemblies, and occasionally new properties and functions may emerge^{43,44,45}.

1.1.2.1. Classification of liquid crystals

Liquid crystals exist between crystalline solids and isotropic liquid phases³⁷ and they can flow like fluids besides having retained some of the anisotropic properties of crystals. Many organic substances exhibit phase transitions between single crystal and isotropic liquid states whose physical properties are intermediate between those of a crystal and a liquid and can be characterized by their molecular positional and orientational order and their anisotropic properties. The name "liquid crystals" is not accurate and that are more properly called "mesomorphic" (from the Greek mesos (middle) and morph (form)), as was introduced by O. Lehmann³² or "mesogens" which exhibit mesomorphism (having mesophases). The first classification of mesophases, established by Friedel⁴⁶ in 1922, was based on order and symmetry and distinguished three classes: smectic, nematic and cholesteric, but the most important classification of LCs is based on the stimulus how the mesomorphism was generated. According to this we can categorize them into two main distinct types: lyotropic and thermotropic LCs.

- In ***lyotropic LCs*** the mesophase is generated as a function of a solvent, its concentration and of temperature. Molecules which exhibit such phases are mainly amphiphilic.

- In **thermotropic LCs** the phase transitions occur due to temperature change and molecules with anisotropic shape tend to form this type of mesomorphism. In this work we mainly focused on thermotropic liquid crystals; this class will be presented in more detail.

1.1.2.2. Thermotropic liquid crystals

Conventional low-molecular weight thermotropic mesogens mostly possess a molecular structure that contains two segments which are different in chemical or structural character^{47,48} e.g. rod-like (calamitic) or disk-like (discotic) molecules equipped with flexible alkyl or perfluorinated end-chains providing the necessary mobility^{37,49}. When such types of molecules self-organize, the rigid aromatic parts tend to pack together and also the flexible aliphatic chains, resulting in the so-called local microphase-segregation^{48,50}. Generally rod-like molecules organize themselves into lamellar structures (smectic phases) or nematic phase, while disk-like molecules do into columnar phases (Figure 7). The discovery that other types of amphipathic molecules based on different structural paradigms (bent core⁵¹ or T- and X-shapes^{52,53,54,55}) also exhibit mesophases (polar phases (Figure 7) or polygonal honeycombs, respectively) revived considerable interest in the design of molecules for pre-programmed self-assemblies with increasing complexity⁵⁶.

In thermotropic LCs the orientational order (which is described by the director, n) is well defined and the molecules' axes are oriented in the same direction. The positional order is less organized, compared to crystals, and can exhibit short-range or long-range order.

In **nematic phases** (N) molecules only possess orientational order (Figure 6). This is the less ordered LC phase.

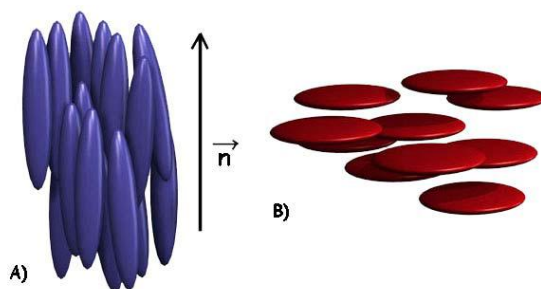


Figure 6 Schematic representation of the nematic phase of calamitic (left, a) and discotic (right, b) molecules

The degree of order of the nematic mesophase can be described by the order parameter⁵⁷:

$$S = \frac{1}{2} \langle 3\cos^2\theta - 1 \rangle$$

Where θ is the angle between the main axis of the molecule and the director. For crystals, $S=1$, for isotropic liquid $S=0$ and for nematic phase this value is comprised between 0.4-0.9 generally.

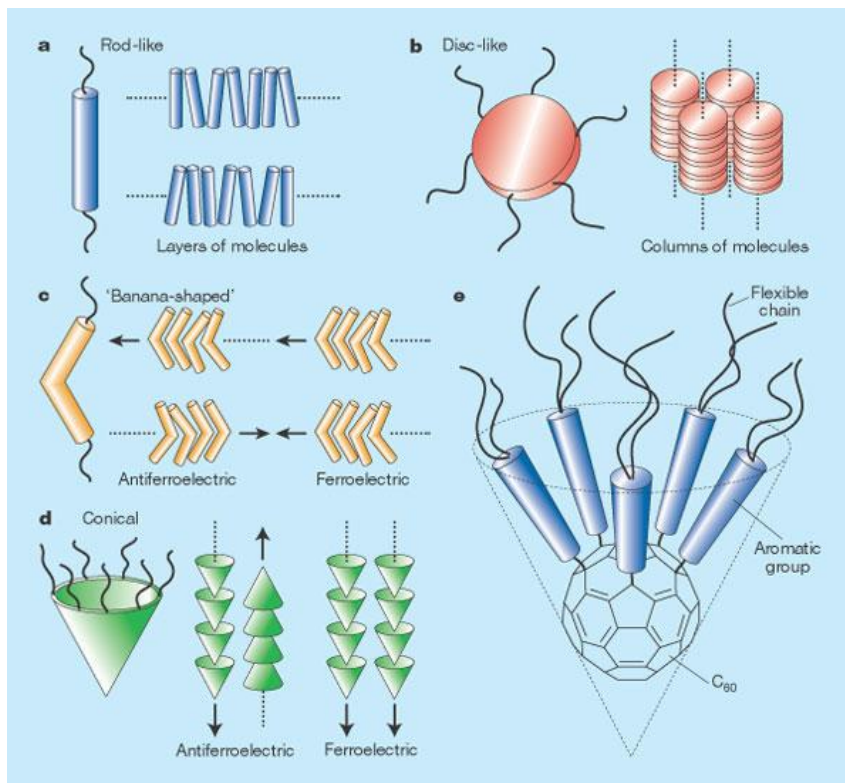


Figure 7 **a**, Rod-like molecules organize themselves into layers, **b**, disc-like molecules form columns that can be arranged parallel to each other in a two-dimensional lattice. **c**, A bend introduced in the rigid core leads to 'banana-shaped' molecules. The rotation of these molecules around their long axis is restricted and they adopt a directed order within the layers. Depending on the bending direction in adjacent layers, either antiferroelectric or ferroelectric smectic phases may result. **d**, Molecules with a conical shape can lead to a polar order within columns. The polar direction of neighbouring columns may be parallel or antiparallel. **e**, "Shuttlecock-shaped" molecules based on the C₆₀ molecule, whose distinctive shape leads to directed organization in columns (taken from C. Tschierske⁴⁹)

A special case of the nematic phase is a chiral nematic phase, commonly called cholesteric. Chirality results when the molecule has a chiral center and causes rotation of the director, describing a helix.

Smectic (or lamellar) **phases**⁵⁸ are formed mainly by calamitic mesogens, organized into layers while preserving the orientational order. The layers are not rigid and are able to slide over one another. We can distinguish two main types of smectic phases: orthogonal or tilted; and these groups can be further divided according to the extent of the positional order within the layers, such as if short-range or long-range positional order occurs (Figure 8). In orthogonal phases the director is perpendicular to the layer planes. If only short-range positional order is present, the layers are defined by a one-dimensional electronic density; then the phase is called smectic A (SmA). If the director is tilted at an angle to the layers, then these are tilted phases. In

the case of short-range positional order in the plane, the phase called smectic C (SmC). In general the SmA phase appears in a temperature range above that of SmC phase.

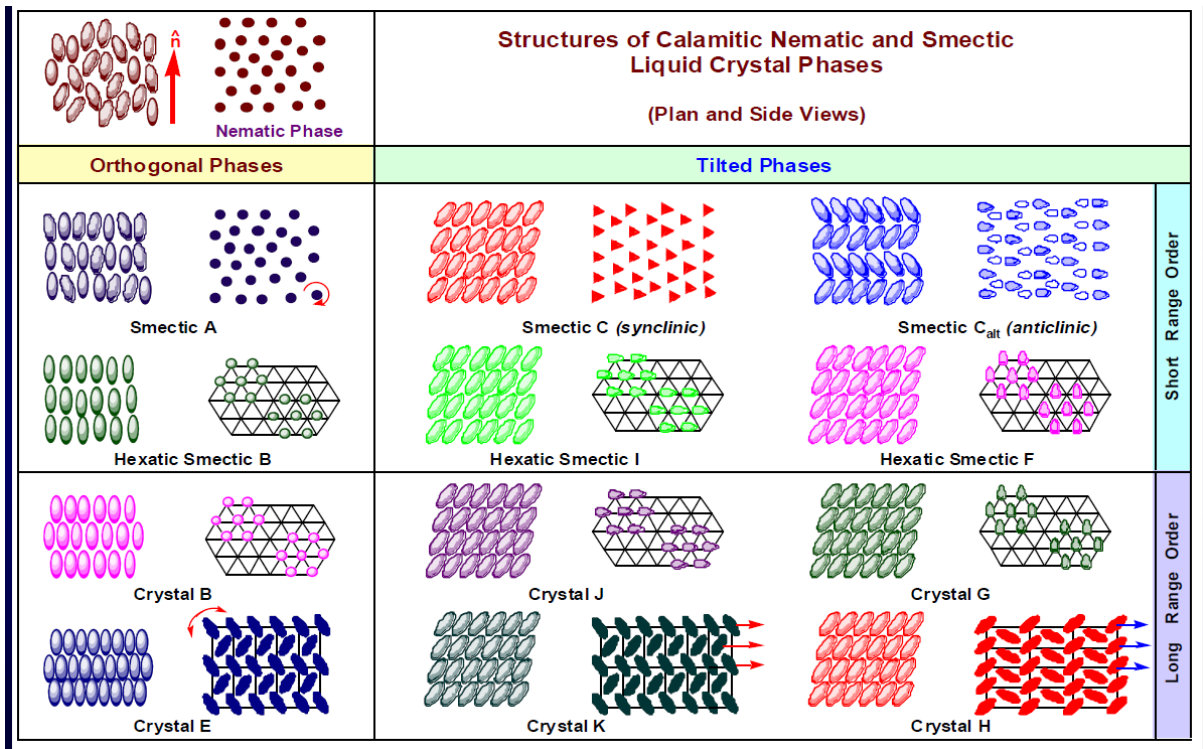


Figure 8 Schematic presentation of smectic LC phases (taken from York univ.)

If the in-plane (short-range) positional order is increased, the ordered layers are weakly-coupled and possess a long-range bond orientation; in this case we talk about hexatic smectic phases. Such a phase if orthogonal is called a hexatic smectic B phase (SmB^h) and if tilted it is called a hexatic smectic I (SmI) or a hexatic smectic F (SmF) phase (Figure 8, Figure 9). In all cases, diffusion between the layers occurs, the phases are fluid but more viscous and inter-layer correlations appear.

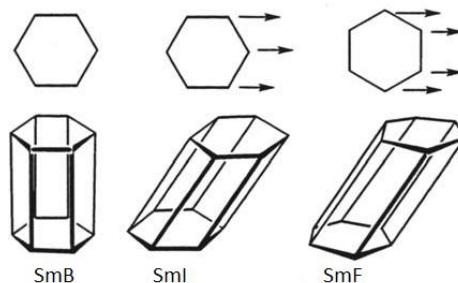


Figure 9 Schematic presentation of SmB, SmI (tilt to apex of hexagonal net) and SmF (tilt to side of hexagonal net) phases⁵⁹

Other types of smectic phases with polar ordering are generated by chiral mesogens or bent-mesogens⁵¹. In crystal B (orthogonal), J and G (tilted) phases, positional long-range orientation

occurs and the rotation around the molecular long axes is concerted, while E (orthogonal), K and H (tilted) phases possess three dimensional order within the layers and a substantial orientational disorder. They are still layered but less fluid than the non-crystal smectics. Theoretical thermodynamic ordering of the phases, due to the decrease in order, maybe (and mostly) the following during temperature change:

Iso Liq - N - SmA - SmC - SmB^h - SmI - SmB - SmF - SmJ - SmG - SmE - SmK - SmH

But phase inversion may occur (re-entrance).

Columnar phases are most often formed by the stacking of discotic molecules, which are packed parallel into 2D ordered lattices^{37,40}. According to the 2D lattice symmetry of the columnar packing, the phases can be hexagonal (Col_h), rectangular (Col_r), oblique (Col_o) or square (Col_s) (Figure 10).

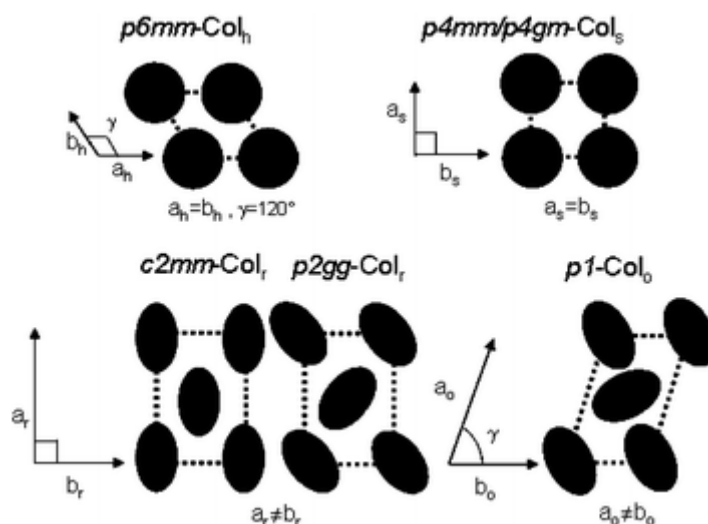


Figure 10 2D lattices of LC columnar phases. The cross-section of the columns are presented with respect to the plane symmetry⁵⁹

Columnar mesophases can be formed not only by discotic molecules but from polycatenar mesogens as well^{60,61,62,63} which are generally composed of a long, rod-like, aromatic rigid core ending in two moieties bearing several flexible chains. In this case, the sublayer formed by the rigid cores undergoes undulations when its thickness is at a maximum, in order to keep the aliphatic part efficiently excluded from the sublayers of the rigid cores. When the maximum of the undulations reaches the whole thickness of the sublayer, it breaks into columns, separated by the aliphatic chains. Columnar structures can also be formed by *e.g.* with bent or T-shaped molecules⁵².

Cubic phases are common in lyotropic liquid crystals, but was only much later reported as a thermotropic mesophase^{64,65,66}. Due to the cubic symmetry, no anisotropy occurs and the phase shows no birefringence when observed under polarized optical microscopy. Their three

dimensional organization can be distinguished into two classes: micelles, where the micellar phases of molecules arranged in a cubic lattice, or bicontinuous phases formed by two mutually interpenetrating networks.

1.1.3 Liquid crystal dendrimers

In order to increase further the range of mesomorphic organizations, supra- and supermolecular liquid crystal systems have been designed and synthesized^{22,67,68,69,70,71,72}, where adding functions with a precise nature and location is well controlled. Mesomorphic functional dendrimers^{16,20,50,59,73,74} have increased interest because of their useful properties, control of functionality and molecular architecture which are essential in molecular engineering of liquid crystals for controlling the self-organization process which leads to mesophase formation. Here we do not aim to present supramolecular LC dendrimers or as often referred to as dendromesogens, of which an excellent and comprehensive review was written by Percec²², but briefly introduce supermolecular LC dendrimers of which Donnio and Guillon have made comprehensive reviews^{50,59}.

The basic structure of these functional supermolecules usually consists of protomesogenic units linked together through flexible spacers (alkyl, siloxane chains, *etc*) to generate linear oligomeric systems^{75,76,77}. Alternatively a central focal multivalent node is created to yield molecular structures with branched architectures such as polypedes^{48,68,78} and dendrimers^{50,79}. The structural diversity offered by such supermolecular LCs (connectivity, topology, restricted flexibility) often present unusual morphologies induced by the segregation, at the molecular level, between the various building species^{48,68,80,81}.

1.1.3.1 Thermotropic liquid crystal dendritic structures

The idea to induce liquid crystal properties in a dendrimer came from Kim's work, who induced a nematic lyotropic LC phase in a hyperbranched polyamide⁸². Percec was the first to synthesise thermotropic LC dendrimers⁸³ which was followed by the synthesis of carbosilane dendrimers which were functionalized by mesogenic end-groups at the periphery⁸⁴. Since then silicon-containing LC dendrimers are one of the most widely studied side-chain LC dendrimers.

The location of the mesogenic or pro-mesogenic groups can be varied in the structure of the dendrimers. In *side-chain LC dendrimers* these groups are attached to the termini of the flexible dendritic network (Figure 11). Silicon-containing dendrimers are such a type and Shibaev *et al.* carried out detailed investigations with different functional groups, *e.g.* cyanobiphenyl⁸⁵, methoxyphenyl benzoate⁸⁶, or anisic acid⁸⁷ derived mesogens, and generation numbers. The dendrimers, contrary to the monomer's nematic mesophase, exhibited smectic

phases, and the stability was increased upon “dendrimerization” resulting from the enhanced microphase separation.

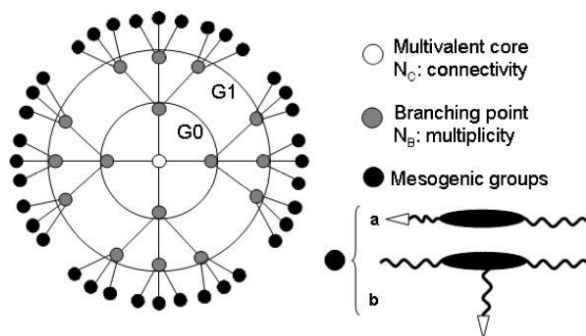


Figure 11 Schematic 2D representation of a side-chain dendrimer. The mesogen is terminally (a) or laterally (b)⁵⁰

By increasing the generation number, polymorphism with columnar meso-structures⁸⁸ was observed (Figure 12). The lamellar structure at lower temperature is stable, but increasing the temperature results in reduced interactions between the molecules and in the dendrimers the terminal groups expand around the central core, which results in undulation of the layers. Thus, first they self-organize in a rectangular symmetry as the neighbours still influence each other, but this influence decreases by increasing the temperature and results in hexagonal symmetry (Figure 12) with minimal space.

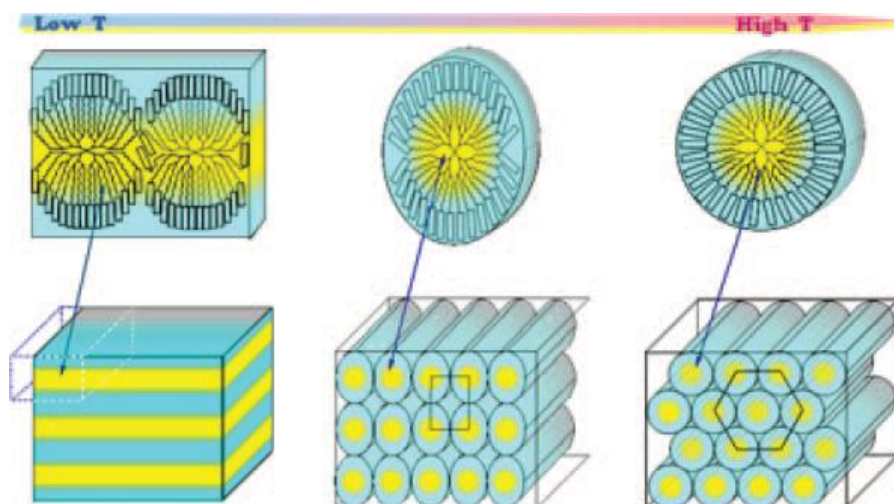


Figure 12 Models of structures formed by LC dendrimer G5 at different temperatures: (left) lamellar structure (middle) Columnar structure with rectangular ordering of ellipsoidal (right) Columnar structure with hexagonal ordering of rounded columns⁸⁸

When carbosilane dendrimers were functionalized with azobenzene functional groups, a smectic mesophase was induced which could be destroyed and transformed into an isotropic liquid by UV-irradiation due to the photoisomerization of the chromophores into the less

isotropic cis form⁸⁹. A room temperature nematic phase was induced in a carbosilazane dendrimer by Mehl⁹⁰. The ligand was laterally attached to the core, which required a large space, preventing it from lamellar organization.

PPI dendrimers showing a SmA⁹¹ phase were described, using cyanobiphenyl functional groups on the periphery, and Col_h using non-mesogenic groups⁹². In case of cyanobiphenyls, the flexibility of the dendritic interior allows the stacking of the functional groups which results in self-organization into lamellar layers (Figure 13).

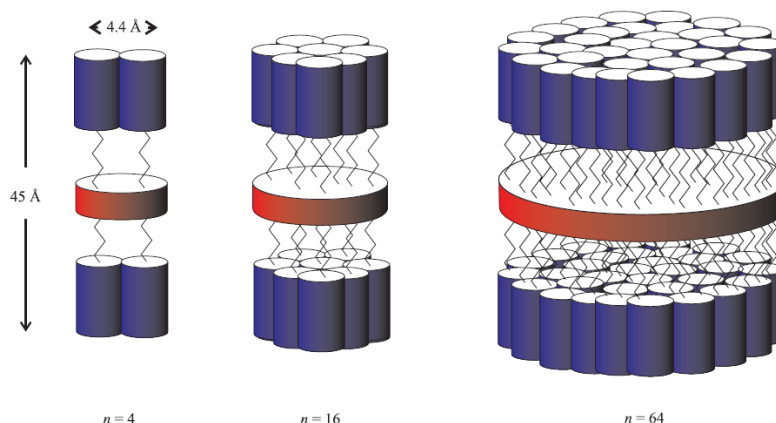


Figure 13 Proposed model for the organization of mesogenic dendrimers into smectic layered mesophases, depicted for the first ($n=4$), third ($n=16$), and fifth-generation ($n=64$)⁹¹

Serrano *et al.*⁹³ made a systematic study on both PPI and PAMAM dendrimers and found that depending on the number of the terminal alkoxy chains, attached to the peripheral mesogenic units at the periphery, smectic or Col_h phases could be selectively formed.

In **main-chain LC dendrimers** anisotropic groups are present at every level of the dendritic structure and the conformational freedom is strongly reduced. The first of this type of dendrimers were the “willow-like” dendrimers based on terphenylene monomers⁸³ and formed nematic and smectic phases due to the parallel self-organization of the subunits which provided an overall rod-like shape. Donnio *et al.* prepared octopus-like dendrimers⁹⁴ where the mesogenic groups are connected together through flexible alkyl chains in the dendritic branches which were connected to a tetra-podand core. The type of the mesophase, similarly to Serrano’s PPI dendrimers, depends on the number of the terminal chains. When only one terminal aliphatic chain per unit is present, a smectic mesophase is exhibited due to the parallel arrangement of the mesogenic units on both sides of the core, resulting in a large rod and a highly segregated lamellar structure. When the number of terminal aliphatic chains is increased, the parallel ordering of the mesogenic groups is difficult and an oblate conformation results. This conformation is a consequence of the curvature of the “octopus” into a wedge-like form,

which self-assembles into supramolecular discs or columns and results in an induction of a Col_h phase (Figure 14).

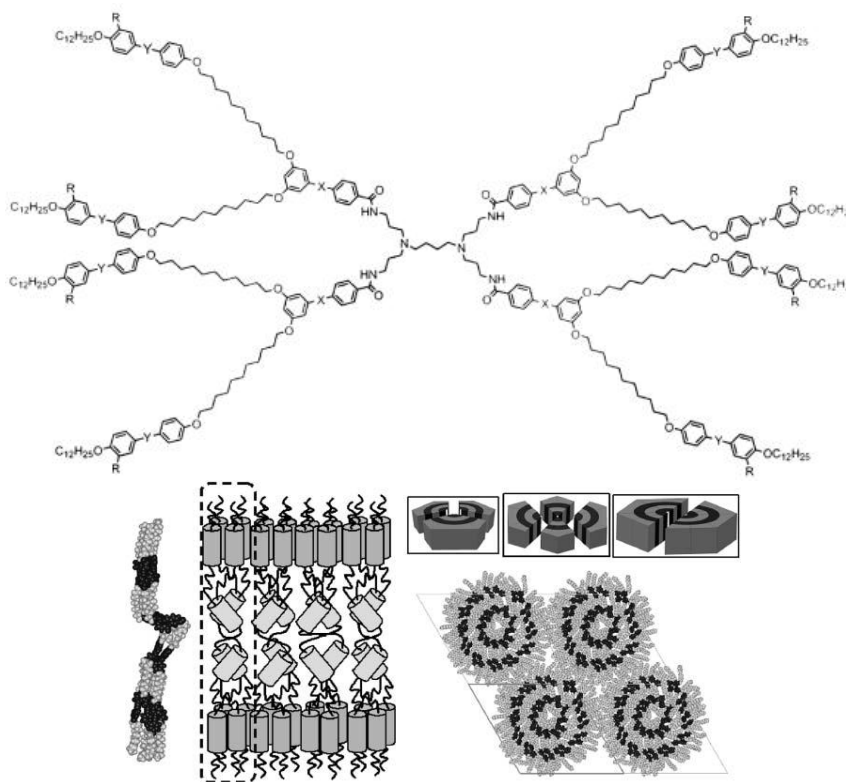


Figure 14 Structures of the multilayer smectic and onion columnar phases: grey = aliphatic continuum; black = aromatic segments⁹⁴

In *shape-persistent LC dendrimers* the dendritic interior is completely rigid, conjugated and intrinsically discotic. From first to the fourth generation tolan based dendrimers exhibited columnar mesophases over a wide temperature range, and the clearing point increased with increasing the generation number⁹⁵. Higher generations did not exhibit mesophases.

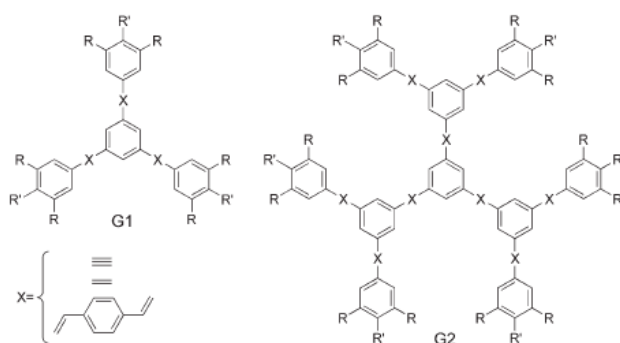


Figure 15 Schematic structures of the G1 and G2 shape-persistent dendrimers (tolanoid: R = CO₂(CH₂CH₂O)₃Me, R' = H; stilbenoid: R = R' = OC_nH_{2n+1}, n = 6,12)⁵⁹

With this brief presentation of the wide variety of the LC dendrimers, we have tried to demonstrate that even small modifications of the dendritic structure open the door to a large and rich variety of mesomorphism. The judicious choice and careful molecular design of the primary constitutive building blocks permits us to partially predict the nature of such supermolecular systems, although the strict control of self-organizing processes and the function transfer from nano- to micrometric scale by molecular engineering still remains challenging.

1.1.4 Photoinduced anisotropy of liquid crystal azodendrimers

Azobenzenes and their derivatives are well known for their reversible photoisomerization properties and from the photochemical reactions that arise in them⁹⁶. Photoinduced anisotropy, which allows defined preparation of anisotropic films or holographic gratings, was observed in thin films due to angular-dependent photoisomerization and photo-orientation effects. A comprehensive summary made by Cojocariu and Rochon discusses azopolymers⁹⁷. This work is based on Almeria Natansohn's work who investigated azobenzene-containing materials, their photoinduced motion, and the possibility of large mass movement well below the glass transition temperature.

1.1.4.1. Azobenzene derivatives

Azobenzenes are elongated proto-mesogenic chromophores. When their termini are modified by alkoxy groups, they show LC properties³⁷. Photochemical *trans-cis* isomerization can be induced by UV or visible light; this process is induced by the electronic excitation of an electron from either the highest occupied nonbonded orbital (n) or the highest occupied π orbital to the lowest unoccupied π orbital (π^*). A nonradiative decay from the excited states forces the molecule back to the ground state either in the *cis* or the *trans* state. The ground state of *trans* lies lower than that of *cis*-isomer resulting in a return to the *trans* state photochemically or thermally (Figure 16).

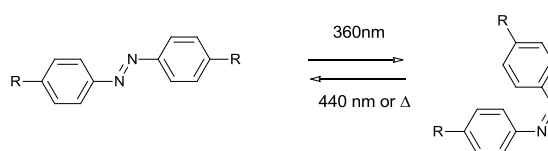


Figure 16 Trans-cis isomers of azobenzene derivative

Isomerization of azobenzenes can be monitored by UV-Vis spectroscopy as its $\pi \rightarrow \pi^*$ band is intense in the UV region and the $n \rightarrow \pi^*$ band is rather weak in the visible region. This change

also induces a large structural change (conformation and size). The rate and the extent of isomerization, as well as the composition of the photostationary state, depends on the ring substituents and the overall molecular structure.

In azo-containing materials (bound to or doped into), the photoisomerization induces series of motions which could be classified in three types: at molecular, nanoscale, and micrometer level⁹⁷.

- Motion at molecular level is the chromophore motion that results from the interaction between the mesogenic azo molecules and Linearly Polarized Light (LPL). *Trans*-azobenzene has a highly anisotropic shape and its transition moment axis directed along its main molecular axis. The probability that the azo unit absorbs a photon and isomerizes is proportional to $\cos^2\varphi$ where φ is the angle between the polarization direction of the light and the azobenzene transition dipole moment. Thus, only azobenzenes groups having a component dipole parallel to the light polarization direction will absorb and consequently photoisomerize. While undergoing multiple *trans-cis-trans* isomerization cycles, the chromophores move and reorient slightly their optical transition moment axis, and hence their long axis (Figure 17). When they happen to fall perpendicular to the light polarization, they become less active to light. Thus, optical dichroism as well as birefringence is induced in azobenzene containing (*e.g.* polymer) films due to a global rearrangement.

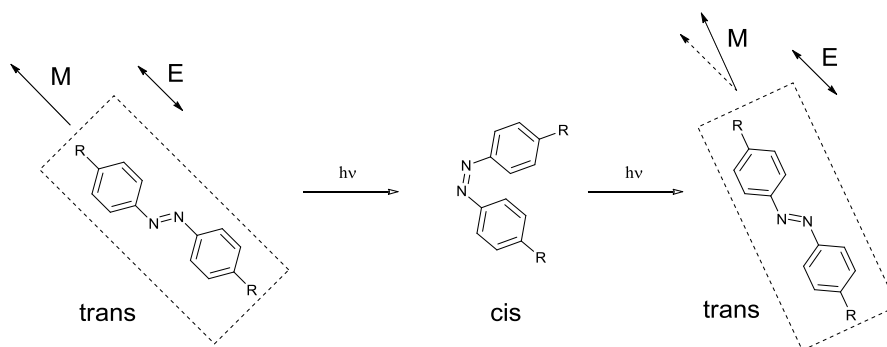


Figure 17 Reorientation of a substituted azobenzene through *trans-cis-trans* isomerization; E: electric field vector; M: optical transition moment axis⁹⁷

- Motions at the nanoscale level are the motions of the photochrome in an organized environment (*e.g.* LC domains). Competition between the two principles of ordering occurs in this case. One of the ordering impacts is the LPL which aligns the photochromes perpendicular to the direction of the LPL; the other is the initial order of the system. The high photoisomerization quantum yield of azobenzenes coupled with the strong driving force for angular-dependent photoselection leads in the end to a reorientation of the whole LC or crystalline domains in a direction perpendicular to the light polarization.

- Motions at micrometer level are those of massive movements of the material over a long distance which accompanies the photoisomerisation of azobenzenes. This occurs upon exposing the azo film to a periodic holographic pattern of linearly or circularly polarized light (CPL). The motion in this case is not limited to the mesogenic chromophore, but involve the whole system. This motion occurs below the glass transition temperature (T_g).

The three types of light-induced motions affect the orientation of the dyes. The photoinduced orientation of azo groups was found to be more stable in LC polymers than in azo-doped polymers which were the first materials where the photoinduced birefringence was reported⁹⁸. There are many parameters which can affect the induction of photoanisotropy.

From these studies, it was implied that the presence of some spacer was needed between the backbone and the azo groups. The spacer would give enough flexibility for the side mesogen groups to move about for orientation and to form the LC phase. But it was shown that motion of the side chromophores can occur below the T_g and photoinduced birefringence could be stored with comparable efficiency and a much better speed than on amorphous polymers⁹⁹. The other parameter is the bulkiness of the azobenzene, which has an important role in photo-orientation as it hinders the motion of the chromophore and affects both the level and the rate of photo-orientation. Also the nature of the azo groups is crucial. Pseudo-stilbene-type (electron donor/electron acceptor substituted) chromophores are among the best candidates for optical induced ordering and stability. A faster growth and a higher level of birefringence can be obtained if the material absorbs in the visible range and the *cis*- and *trans*-isomer spectra are superimposed, so the irradiation with a laser (514 or 488 nm) will activate both *trans-cis* and *cis-trans* isomerization processes. This leads to a large number of *trans-cis-trans* isomerization cycles per unit time. Increasing the strength of the azo dipole can cause an irreversible photodegradation process. The linkage between the azo chromophore and the polymer backbone affects both the mechanical properties (*i.e.*, T_g) and the motion of the azo groups, thus their orientation. A rigid link restricts the chromophore's motion, thus making it harder to induce orientation, but it also confers better stability of the induced anisotropy after the light is turned off¹⁰⁰. Increasing the length of the spacer causes the T_g and the stability of the photoinduced anisotropy to decrease, but the mobility of chromophores is higher, the thermal back relaxation is more favourable and the reorientation process is faster. Higher azo content resulted in better photoinduced birefringence¹⁰¹. For ordered systems such as LC polymers, there is another way to enhance the photoinduced anisotropy. That is thermal amplification¹⁰² and it occurs when a photo-oriented azo LC polymer film is annealed above the T_g within the mesophase. The amplification of the photoinduced orientation by self-organization depends on several parameters, including the initial degree of organization within the thin film, the ordering

tendency of the polymer (in-plane or out-of-plane), the amount of aggregation, the thermal history of the samples, *etc.* When azopolymer films are exposed to a periodic pattern created by the interference of two polarized beams provided by an Ar⁺ laser longer than a few seconds, a large-scale polymer mass transport leads to the creation of micrometer-deep Surface Relief Gratings (SRG)s¹⁰³.

Azobenzene-functionalized oligopeptides can efficiently be used for creating anisotropic optical films and SRGs, which are of great interest for developing elements for different technical applications, such as optical data storage (optical memories and holographic data storage devices) ^{104,105,106,107} or optical elements (e.g. anisotropic polarizers, retarders, anisotropic emitters, or polarization gratings)^{108,109}. The photo-alignment of photosensitive liquid crystals has some advantages compared to conventional orientational techniques (Langmuir – Blodgett technique, mechanical stretching, traditional rubbing technique *etc.*) such as tilt angle, defined control of the orientation direction and pixel-wise orientation at room temperature¹¹⁰. Photoinduced orientation by LPL can be significantly amplified by annealing at the temperature of mesophase^{101,111}. Azobenzene-containing materials, because of the angular-selective trans-cis photoisomerization cycles and rotational diffusion in the steady state, are ideal for photo-orientation which induces the optical anisotropy; however, they can quench the emission of the fluorophores¹¹¹. In this case, cinnamate as an alternative photosensitive group can also be considered¹¹².

1.1.4.2. Light-driven azodendrimers

Nowadays photosensitive LC polymers (LCP), where the mesogenic and fluorophore functions are randomly distributed along the polymer backbone, are used to create anisotropic optical films, but using random co-polymers does not provide a well determined ratio or sequence of different functional groups in one molecule. Synthesis and application of a new class of compounds such as azobenzene-functionalized dendrimers (azodendrimers), have drawn a great deal of interest due to the useful properties including high photosensitivity, low-melting point, solution viscosity¹¹³ and those with other responses to light, have numerous potential applications due to the possibility of inducing macroscopically ordered materials by noncontact methods^{114,115}. Dendrimers with mesogenic functional groups allow molecular engineering of LC properties by the modification of the dendritic connectivity and controlling the self-assembling ability⁵⁹; therefore, changing from LCPs to LC dendrimers could be of great interest as far as structures (hierarchy of the functionality), properties (amplification) and processing (thin film) are concerned. Several interesting phenomena seen with azodendrimers, *e.g.* irradiation of some of these dendrimers by actinic light does not induce simultaneous

photo-orientation and photoisomerisation of the trans-cis transition⁸⁹. A recent review was published by Caminade on various types of light-driven azobenzene-containing dendrimers and dendrons and their photoresponsive properties¹¹⁵. The azobenzenes groups in the dendrimers can be located at termini, at the core or incorporated in the layers of dendrimers and these dendrimers can be categorized according to the location of azobenzene function (Figure 18)¹¹⁴. The location of the azobenzenes has an influence on the photoisomerization properties. In this section following Caminade's detailed review, we show some representative examples of different types of azodendrimers.

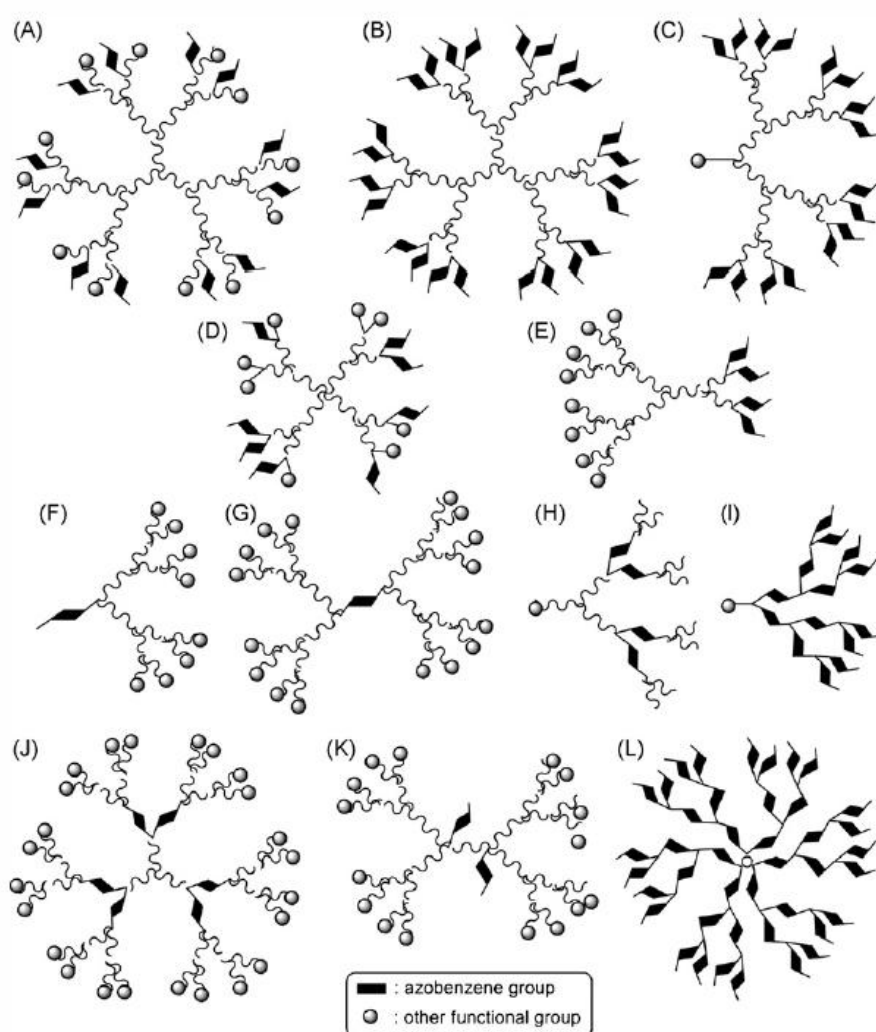


Figure 18 Schematic representation of the various types of dendrimers (A, B, D, E, G, J, K, L) and dendrons (C, F, H, I) having azobenzene group(s) in their structure (taken from Caminade¹¹⁴)

First azodendrimers¹¹⁶ were reported with **azobenzenes at the termini** where half of the terminal groups were azobenzenes (Figure 18, A). Other azodendrimers were synthesised from the first to fourth generation, in a similar way with strict 1:1 ratio of functional groups, and

the proportion of *cis* isomers at the photostationary equilibrium in solvent was found to depend on the wavelength of the irradiation¹¹⁷. In some cases, the high density of azobenzenes at the periphery, in not LC dendrimers, resulted in H-aggregates¹¹⁸ in thin films; but in other cases *e.g.* using PAMAM dendrimers, high dichroism was induced by polarized UV light irradiation. Using films, the percentage of the *cis* isomers is reduced compared to a solution, after irradiation. In another report, using poly(alkyl aryl ether) dendrimers from generation 0 to 3, aggregates in thin solid films occurred which exhibited fluorescence¹¹⁹ (Figure 19); in this case the dendrimers did not show liquid crystalline behaviour contrary to their mesogens.

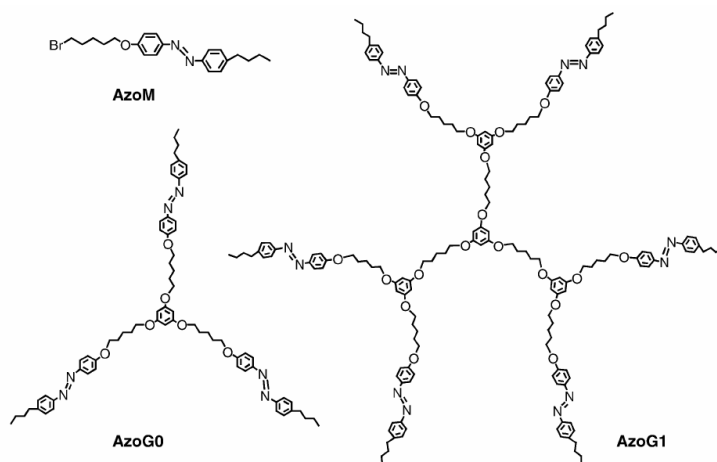


Figure 19 Structure of zero and first generation poly(alkyl aryl ether) dendrimers¹¹⁹

When ***azobenzenes are located at the core of the dendrimers*** the generation number has a strong influence on the photoresponsive behaviour and numerous examples of such types of azodendrimers confirm this behaviour. These dendrimers have azobenzene at the core with two identical chemical functions and most commonly polyether internal structures. They are generally obtained by grafting two dendrons to the azobenzene in the last step (convergent method). *Trans-cis* photoisomerization was shown to depend on the generation number (Figure 20) by a systematic study, but not the *cis-trans* photoisomerization¹²⁰. The surrounding dendrimer groups were found to affect the thermal isomerization mechanism by decreasing the freedom of movement of the activated state of the azobenzene chromophore.

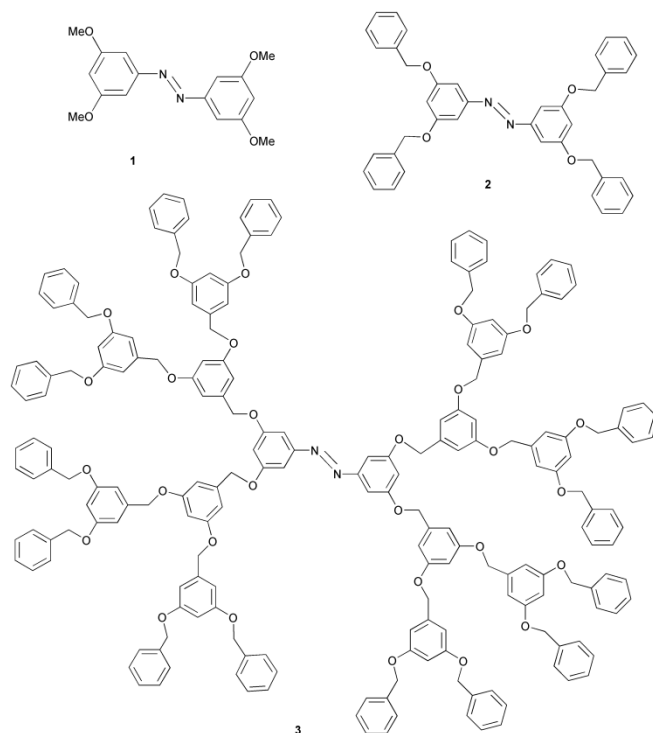


Figure 20 3,3',5,5'-Tetramethoxyazobenzene and related *meta* substituted azobenzene dendrimers¹²⁰

In other cases, both photoisomerization and thermal isomerization decrease with increasing the generations^{121,122}. The flexibility of the linker, through the dendritic interior connected to the azobenzene, has also an influence on the efficiency of trans-cis isomerization, and the changes are larger for rigid structures^{123,124}.

When **azobenzenes are in the internal structure of the dendrimers**, one can distinguish multiple discrete states upon irradiation^{125,126} (Figure 21). Most of these dendrimers were built up using a convergent method, by grafting the dendrons, which contain the azobenzenes in their interior as a single layer, to the core. The number of the chromophores can be varied according to the core and generation number. In some cases, a divergent procedure was applied resulting in single or multiple layers of the azobenzene in their dendritic structure. In the case of multiple layers, steric hindrance and resistance toward isomerization occurs. An interesting example of this type of dendrimers, a fluorescent dendritic hosts with photoswitchable properties with site-specific placement of three different types of function (PDI, pyridine, and azobenzene) were synthesised¹²⁷ where the host can be utilized to actively encapsulate guest molecules into its interior cavities.

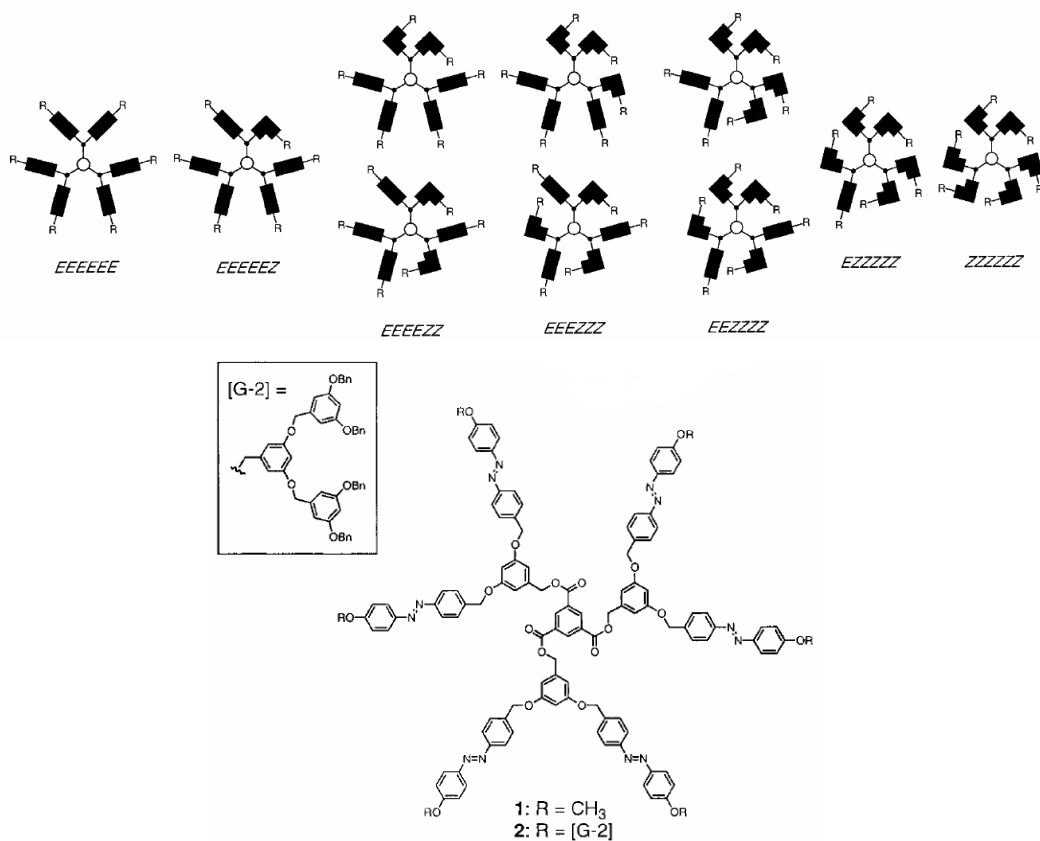


Figure 21 Benzyl aryl ether dendrimer incorporating azobenzenes at a single layer in the dendritic structure, and the schematic representation of the 10 configurational isomers of dendrimers 1 and 2¹²⁶

1.1.5 Objective of the thesis, I.

One of the goals of supramolecular chemistry is to construct devices capable of fulfilling tasks at the molecular level. Dendrimers have been a bountiful source for the development of new molecules, including hybrid systems, with specific properties. The multifunctional properties, which can be developed in dendrimers, make them especially interesting. As was introduced in previous sections, anisotropic optical films and SRG are of great interest for creating elements for different technological applications and azobenzene-containing materials are ideal for photo-orientation which induces optical anisotropy.

This discussion is divided into three parts which build on each other - the first two parts are presented in this chapter and the third part which deals with the dendronized gold nano-hybrids is presented in Chapter II - :

- First, the synthesis of multifunctional polyether dendrimers, where different properties (photoresponsive and liquid crystalline) are combined in one molecule. Protomesogenic alkoxy-azobenzene-based (AZB) chromophores are selectively incorporated within the supramolecular structures and their relative molar proportions varied in a stepwise controlled manner. In this way homogeneous (where all functional groups are the same) or heterogeneous (functional groups are different) structures can be built up, combining the AZB with other calamitic mesogens (Figure 22) and the mesomorphic behaviour modulated.

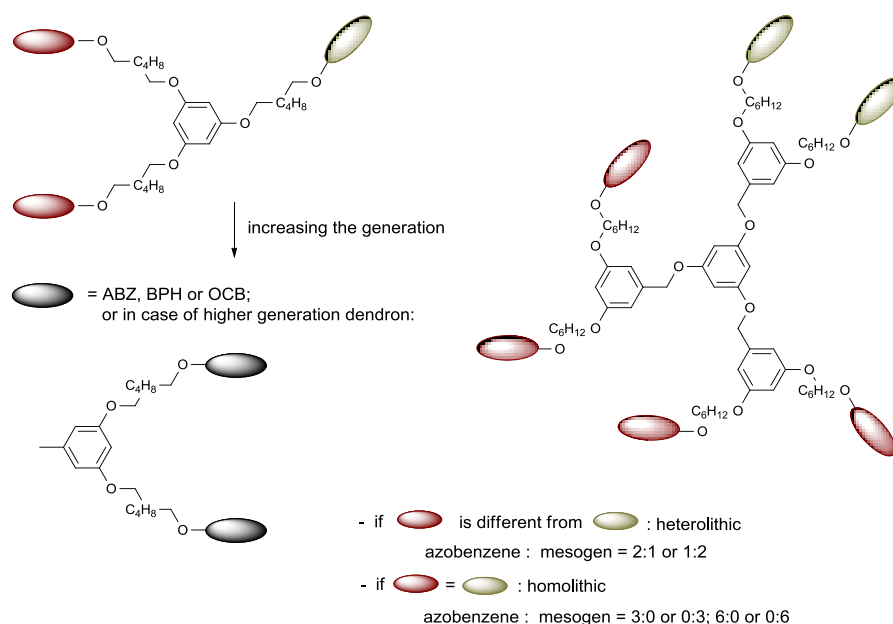


Figure 22 General structures of designed multifunctional dendrimers

In order to study the relationship between the architecture and the mesomorphic properties, pertinent structural parameters were varied, such as generation, length of spacer, branching

points, mesogenic proportion. The design of these dendrimers is determined by the special needs described in the second part:

- The second part was performed to study optical properties of materials. This required multifunctional dendrimers which fulfil specific conditions in order to allow carrying out optical studies, such as the induction of optical anisotropy and SRG. These properties are the following:

- glass transition temperatures (T_g) above 25°C
- good film forming tendency
- forming isotropic films as initial state
- low-tendency to aggregation at high concentration of chromophores
- amorphous state and/or LC mesophases
- photosensitivity

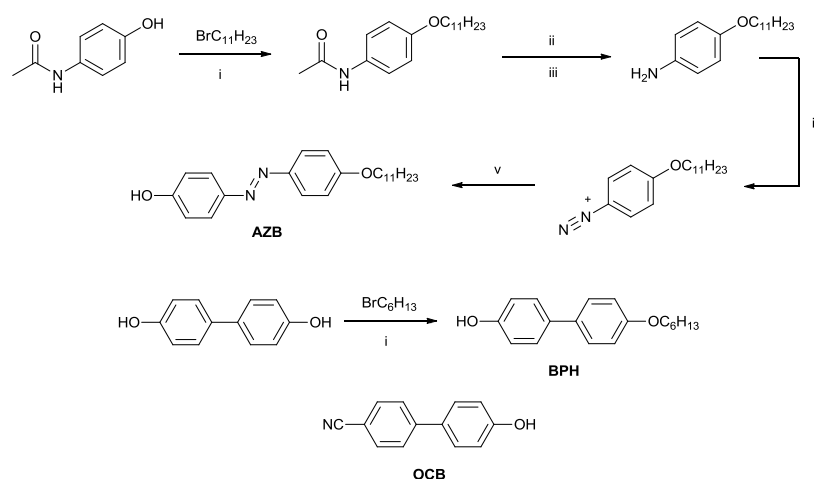
In order to accomplish these properties, we used azobenzene as a photoresponsive group and dendrimers which were designed to allow us to induce mesomorphic behaviour and vary the molar proportion of the chromophore in one molecule ensuring the low-tendency for aggregation. The dendrimer structure was built up by ether bonding providing flexibility and increased thermal stability. The additional protomesogenic groups, such as alkoxy biphenyl and cyanobiphenyl, and the flexible alkyl chains, which attach the calamitic mesogens to the core, ensure the liquid crystallinity.

The third part of this thesis work, which is related to the dendronized gold nanohybrids, is described in the Chapter II. and the objective of this part is presented there.

1.2 Results and Discussion - Syntheses

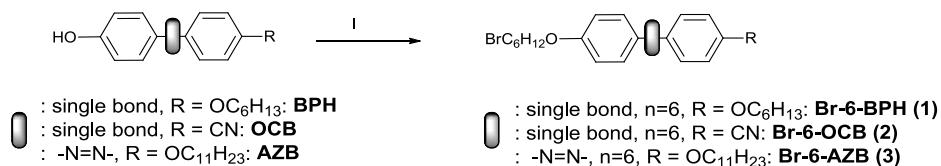
1.2.1 *Synthesis of mesogenic units and branching points*

The synthesis of functional groups was carried out in a way similar to literature procedures (4-hydroxy-4'-(undecyloxy)azobenzene (AZB)¹²⁸, 4'-(hexyloxy)biphenyl-4-ol (BPH)¹²⁹, except 4'-hydroxybiphenyl-4-carbonitriles (OCB) which is commercially available). The synthesis of AZB started from the alkylation of 4-hydroxyacetanilide via Williamson etherification followed by hydrolysis. The generated amine was converted into the diazonium sodium salt which was reacted directly with phenol in electrophilic aromatic substitution to yield the product **AZB**. Synthesis of BPH was carried out by ether coupling of 1-bromohexane with the 4,4'-dihydroxybiphenyl, giving the monoalkylated product (**BPH**) (Scheme 1).



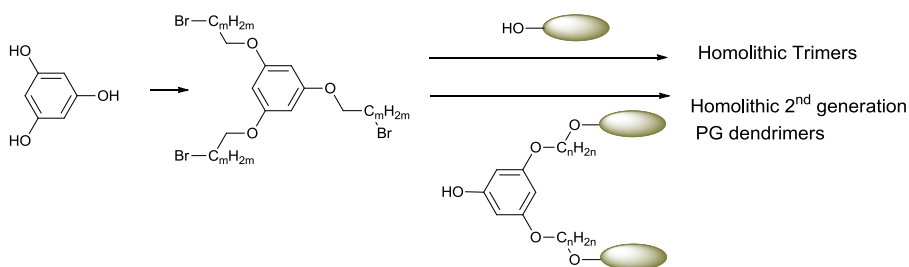
Scheme 1 Synthesis of AZB and BPH functional group. *Reagents and conditions:* (i) K_2CO_3 , DMF, $95^\circ C$, (ii) 40 wt. % H_2SO_4 , $100^\circ C$, 4h, (iii) NaOH, toluene/water, reflux (iv) 18 wt.% HCl, $NaNO_2$ (v) phenol, NaOH, H_2O , $0^\circ C$; **AZB** 49%; **BPH** 42%

The synthesis of trimers or dendrimers can be carried out by a convergent, a divergent procedure or by selective functionalization. In the convergent method the dendrimers are built up from the periphery (functional groups) towards to the core. In this case, first the linkers are attached to functional groups which can be further reacted with branching points or with the core. The mesogenic brominated monomers (**1**, **2**, **3**) were obtained by the mono bromoalkylation of the functional groups (**AZB**, **BPH**, **OCB**) with 1,6-dibromohexane via bimolecular nucleophilic substitution (Scheme 2).



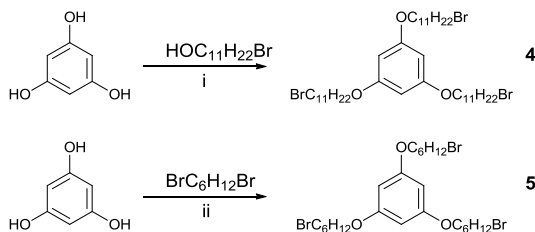
Scheme 2 Synthesis of bromoalkylated functional groups (Br-6-M, M=BPH, OCB, AZB). *Reagents and conditions:* (i) K₂CO₃, 1,6-bibromohexane, acetone, reflux

The divergent method is the opposite: dendrimers are built up from the core to the direction of the periphery. In this case, first the linkers are attached to the core which can be reacted with functional groups or, in order to obtain higher generation, with branching points and so on. In order to build up homolitic trimers or increase the generation number of the homolitic (all blocks are identical) structures, the phloroglucinol was bromoalkylated by attaching linkers with bromide function to all the three hydroxyl groups through etherification steps. These tribromide derivatives can be reacted with functional groups (AZB, BPH or OCB) or higher generation dendritic ligands to obtain trimers or first generation homolitic dendrimers, respectively (Scheme 3).



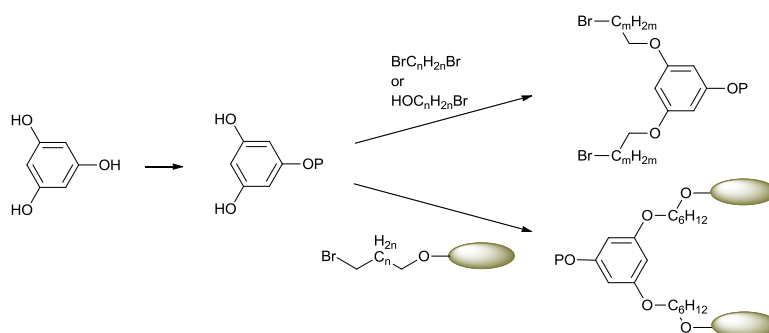
Scheme 3 General synthetic scheme of homolitic trimers and dendrimers using tribromide derivatives

1,3,5-Tris-(11-bromoundecyloxy)benzene (**4**) was synthesized via Mitsunobu reaction; first performing betaine by addition of DIAD to the triphenylphosphine in THF at 0°C, followed by the phloroglucinol and finally 11-bromo-1-undecanol¹³⁰. The synthesis of the tribromide derivative with linker C6 (**5**) - 1,3,5-Tris-(6-bromohexyloxy)benzene) - was achieved from the complete etherification of the phloroglucinol with 1,6-dibromohexane¹³¹ via a Williamson reaction (Scheme 4). Both reactions provided similar yields.



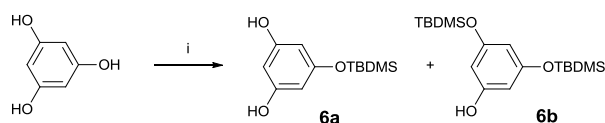
Scheme 4 Synthesis of tribromide PG-derivatives. *Reagents and conditions:* (i) DIAD, PPh₃, THF, 0°C to reflux, 51%; (ii) K₂CO₃, 18-crown-6, acetone, reflux, 54%

In order to incorporate protomesogenic alkoxyazobenzene-based chromophores in different proportions within a molecular structure and/or to increase the generation numbers of the phloroglucinol based dendrimers, the selective protection of one of the hydroxyl group of the phloroglucinol was essential (Scheme 5). Hydroxyl groups usually can be protected by forming ethers or esters. The *tert*-Butyldimethylsilyl (TBDMS) group is a sufficient protective group for alcohols, since TBDMS ethers can be easily prepared under mild conditions and are stable under a wide range of reaction conditions (e.g. from pH 4-6 to pH 10-12 at room temperature, in reducing media toward e.g. LiAlH_4 reducing agent - however loss of the silyl group during LiAlH_4 reduction can occur¹³²) and usually removed with fluoride ions or with aqueous acids. The tetrahydropyranyl (THP) group is ideal under basic conditions (stable from pH=4 to pH>12, 150°C, and toward e.g. NaH) and can be easily removed under mild acidic condition. Benzoic acid esters (Bz) are also stable under a wide range of conditions: from pH <1 to pH >12 at rt. and with base¹³³ e.g. NaH, and most commonly removed under strong basic conditions refluxing with KOH in THF/ H_2O solvent media. Synthesis of trimers or dendrimers was carried out by repetition of etherification reactions which were performed under basic conditions and for that reason such protective groups were considered which are stable in this environment (TBDMS, Bz, THP).



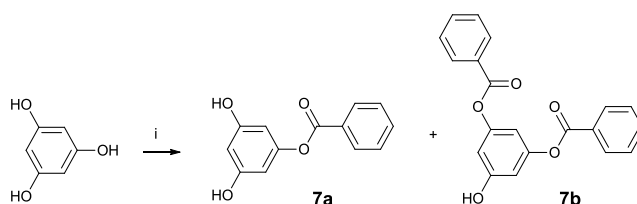
Scheme 5 General synthetic scheme of heterolithic trimers and dendrimers using protected phloroglucinol

TBDMS protected phloroglucinol (**6a**) was synthesized via bimolecular nucleophile substitution by adding TBDMSCl to the phloroglucinol in the presence of imidazole in DMF. During the reaction the diprotected by-product (**6b**) was also generated and isolated in low yields (Scheme 6).



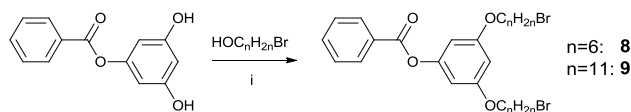
Scheme 6 Synthesis of TBDMS protected phloroglucinol. *Reagents and conditions:* (i) TBDMSCl, imidazole, DMF, rt, 40%

To accomplish the tetrahydropyranylation of alcohols, many reagents have been developed and used (I_2 , cyanuric chloride, bromodimethylsulfonium bromide¹³⁴, etc.). However, no report was found on the protection of phloroglucinol. The protection of the phenolic hydroxyl group of the phloroglucinol by 3,4-dihydro-2H-pyran (DHP) was attempted by different methods, using $CaCl_2$, PPTS¹³⁵ and catalytic ferric sulphate hydrate¹³⁶. None of these reactions led to the desired product and for this reason it will not be detailed in the experimental part. Benzoate protected phloroglucinol: 3,5-dihydroxyphenyl benzoate (**7a**) was synthesised according to the literature¹³⁷ adding benzoyl chloride to anhydrous phloroglucinol in presence of pyridine in THF. Di- (**7b**) and tri-protected by-products also occurred (Scheme 7).



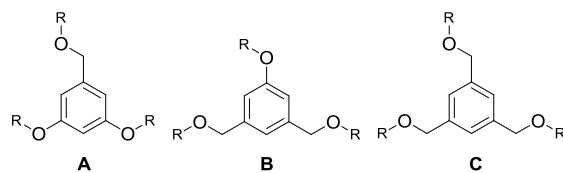
Scheme 7 Synthesis of Bz protected phloroglucinol. *Reagents and conditions:* (i) benzoyl chloride, pyridine, THF, reflux, 42%

Attaching the linkers to the protected phloroglucinol provides the possibility to build up heterolithic and/or higher generation dendrimers by divergent methods. Synthesis of the dibromide derivatives (**8**, **9**) was carried out in a similar way to the tribromide derivative (**4**). 3,5-Dihydroxyphenyl benzoate was bromolactylated by 6-bromo-hexane-1-ol or 11-bromo-undecane-1-ol via Mitsunobu reaction providing the 3,5-bis(6-bromohexyloxy)phenyl benzoate (**8**) and 3,5-bis(11-bromoundecyloxy)phenyl benzoate (**9**), respectively, in good yield (Scheme 8).

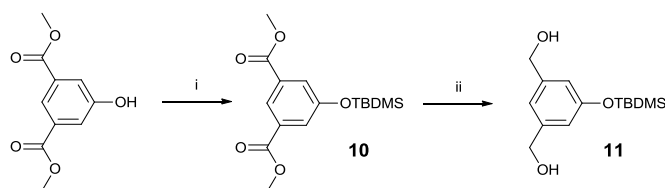


Scheme 8 Synthesis of dibromide derivatives. *Reagents and conditions:* (i) DIAD, PPh_3 , THF, 0°C to reflux

Changing the type of the branching points provides opportunities to investigate the effect on liquid crystallinity. We considered benzyl group based branching points for the comparison as the following:

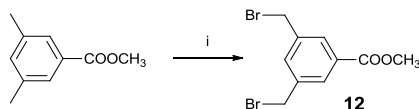


Structures of type **A** can be prepared directly from 3,5-dihydroxybenzyl alcohol (BA) which is commercially available. Structures **B** type can be synthesised from protected 3,5-di(hydroxymethyl)phenol and structures **C** from 3,5-bis(bromomethyl)benzoate as intermediates, which can be further reacted with bromides or alcohols in ether coupling reactions. To obtain **B** types structures, first the phenol function of dimethyl 5-hydroxyisophthalate was protected with (tert-butyl)dimethylsilyl ether (**10**) by treatment with TBDMSCl in the presence of 1H-imidazole. The reaction yield was improved (from 86% to 99%) and the process simplified by changing the solvent from DMF to CH_2Cl_2 . This was followed by reduction with LiAlH_4 resulting the TBDMS protected 3,5-di(hydroxymethyl)phenol¹³⁸ (**11**) (Scheme 9).



Scheme 9 Synthesis of TBDMS protected 3,5-di(hydroxymethyl)phenol. *Reagents and conditions:* (i) imidazole, TBDMSCl, CH_2Cl_2 , rt, 99%, (ii) LiAlH_4 , THF, 0°C , 49%

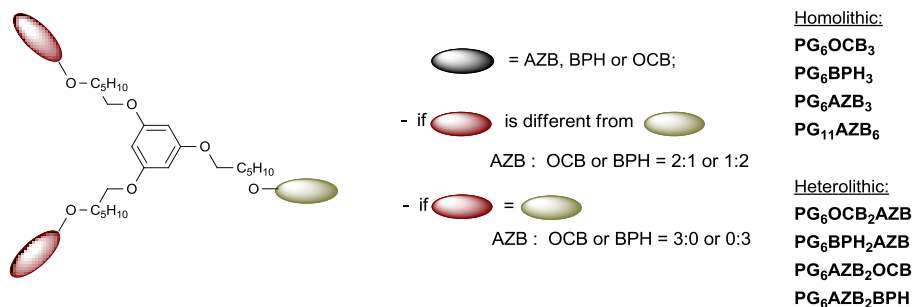
To obtain **C**-like structures methyl 3,5-dimethylbenzoate was brominated with an excess of *N*-bromosuccinimide (NBS) in CCl_4 to the corresponding vic- and gem-dibrominated mixtures which were then reduced with diethyl phosphite and *N,N*-diisopropylethylamine^{139,140} to afford the desired vic-dibromide (**12**) (3,5-bis(bromomethyl)benzoate) in satisfactory yield and high purity (Scheme 10).



Scheme 10 Synthesis of 3,5-bis(bromomethyl)benzoate. *Reagents and conditions:* (i) NBS, AIBN, CCl_4 , 80°C , 39%

1.2.2 Synthesis of Trimers

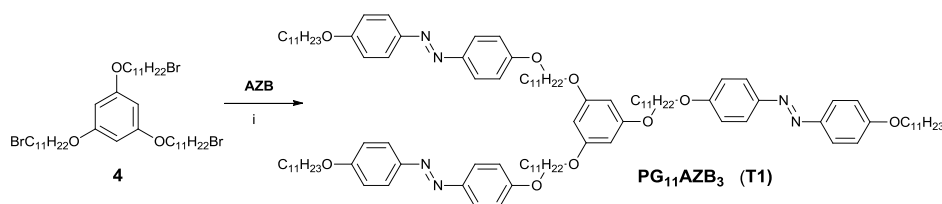
In the syntheses of the set of dendrimers, first the phloroglucinol based dendrons and trimers have been prepared using the various building blocks (mesogens, brominated mesogens and branching points), whose syntheses were described in the previous part.



Scheme 11 General structure of the zero generation (G0) PG based dendrimers

The various homolithic and heterolithic phloroglucinol-based (PG) trimeric and dendritic materials hereafter abbreviated as $PG_zAZB_xBPH_{3-x}$ or $PG_zAZB_xOCB_{3-x}$, for trimers and $PG_zAZB_{2x}BPH_{6-2x}$ or $PG_zAZB_{2x}OCB_{6-2x}$ for first generation dendrimers, where $z = 6$ or 11 is the number of methylene units within the alkyl spacer between PG and the peripheral mesogenic units. The AZB/BPH or AZB/OCB ratios were varied within the supermolecular structure ($x=1, 2$ or 3) in case of trimers according to the sequence $3:0 \rightarrow 2:1 \rightarrow 1:2 \rightarrow 0:3$ and in case of dendrimers according to the sequence $6:0 \rightarrow 4:2 \rightarrow 2:4 \rightarrow 0:6$.

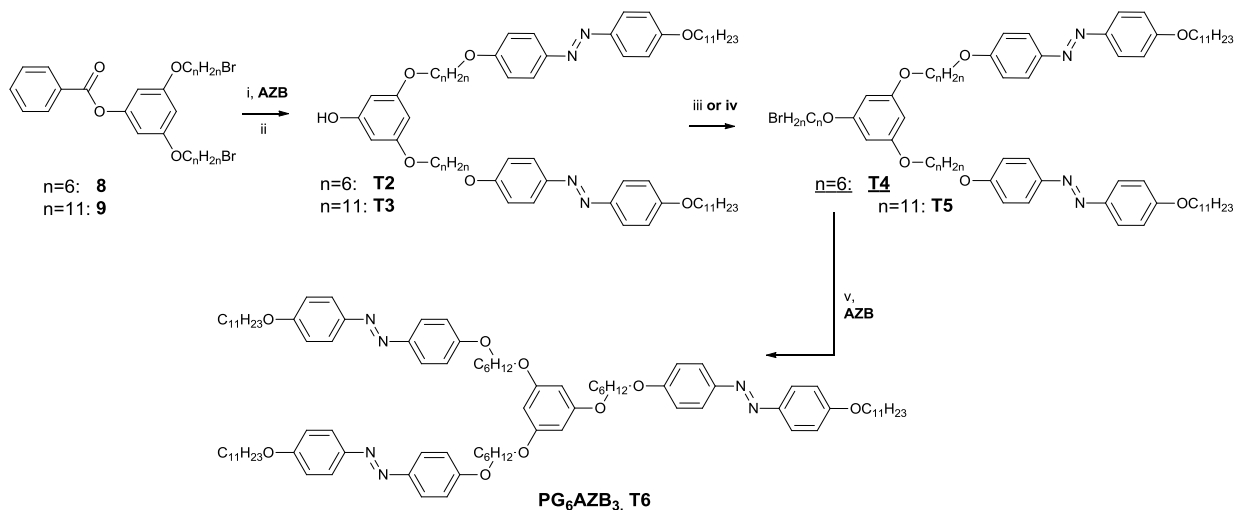
In order to build up the homolithic trimer bearing AZB function with linker C11 ($PG_{11}AZB_3$ (**T1**)), the synthesis was carried out from the core to the direction of the functional groups by reacting the tribrominated core (**4**) through an ether coupling reaction with the **AZB** (Scheme 12).



Scheme 12 Synthesis of $PG_{11}AZB_3$ (**T1**). *Reagents and conditions:* (i) K_2CO_3 , KI, THF, reflux

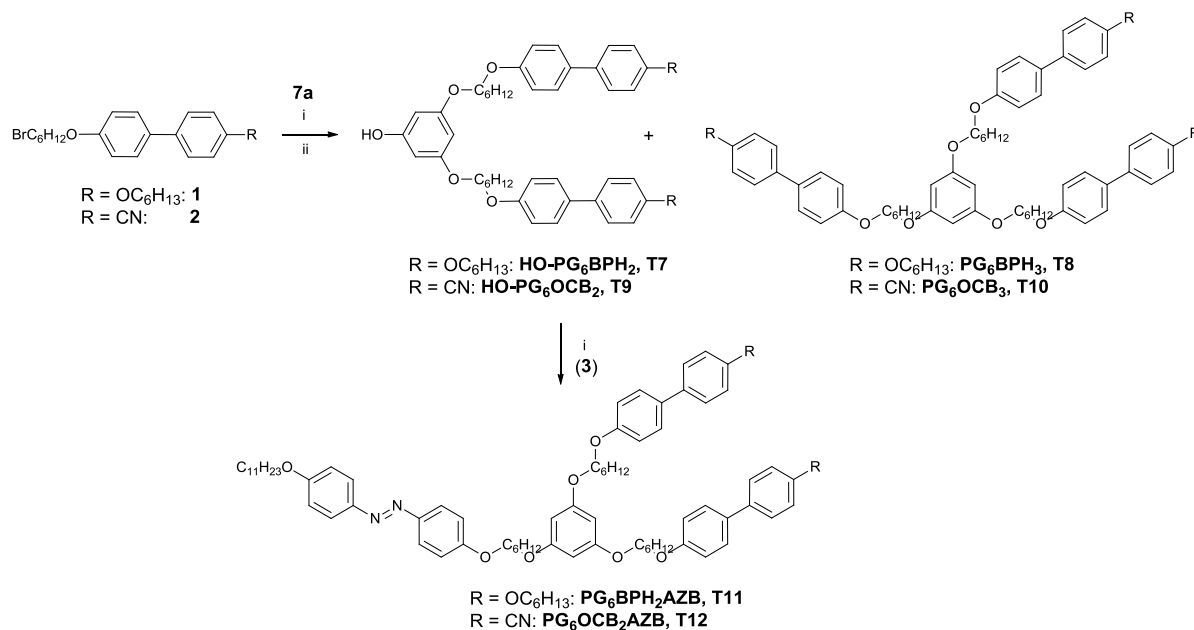
A different method was used to build up the other homolithic AZB trimer with C6 linker. First the difunctionalized phenolic dendron (**T2**, $HO-PG_6AZB_2$) was synthesized using Williamson etherification of the dibromide derivative (**8**) with the **AZB**, followed by hydrolysis. **T2** has been a useful precursor for the synthesis of other materials (mixed trimers with a higher proportion

of AZB or higher generation dendrimers). Then, in the second stage, the ether coupling of **T2** with a large excess of 1,6-dibromohexane resulted in the first generation bromide derivative (**T4**) and the subsequent ether coupling with **AZB** provided the homogeneous trimer PG₆AZB₃ (**T6**). The related first generation phenolic dendron, HO-PG₁₁AZB₂ (**T3**), and the bromide derivative (**T5**) with C11 linker, were obtained similarly (Scheme 13)



Scheme 13 Synthesis of phloroglucinol based dendrons: HO-PG₆AZB₂ (**T2**) and HO-PG₁₁AZB₂ (**T3**) and homolitic trimer (**T6**) *Reagents and conditions:* (i) K₂CO₃, DMF or THF, reflux, (ii) KOH, THF/H₂O, reflux, (iii) n=11: BrC₁₁H₂₂Br, K₂CO₃, THF, reflux, (iv) BrC₆H₁₂Br, K₂CO₃, 18-crown-6, THF, reflux, (v) K₂CO₃, DMF, 70°C

In order to obtain the useful phenolic intermediates bearing the other mesogens (HO-PG₆M₂: M=BPH or OCB) the same method was not sufficient. The lower reactivity of the phenolic OH of the BPH or OCB - compared to the AZB - resulted in very low yields due to the simultaneous in situ cleavage of the Bz protective group from the 3,5-bis(6-bromohexyloxy)-phenyl benzoate (**8**). The evolved phenolic group further reacted with the bromide which ended up in the formation of polymeric by-products from which the separation was particularly difficult. To allow the synthesis of the first generation phenolic dendrons of the mesogenic units (BPH, OCB) the direction of the reaction was changed. In this way, we attached the bromide derivatives of the functional groups (**1**, **2**) to the 3,5-dihydroxyphenyl benzoate (**7a**) - whose reactivity is higher - and the following hydrolysis resulted in the products (**T7**, **T9**), but with lower yields as compared to the AZB dendrons' (**T2** or **T3**). During the etherification, the simultaneous in situ deprotection of the 3,5-dihydroxyphenyl benzoate also took place resulting in the homogenous trimers (PG₆BPH₃ (**T8**) and PG₆OCB₃ (**T10**)), as by-products, which were isolated during the purification process (Scheme 14).

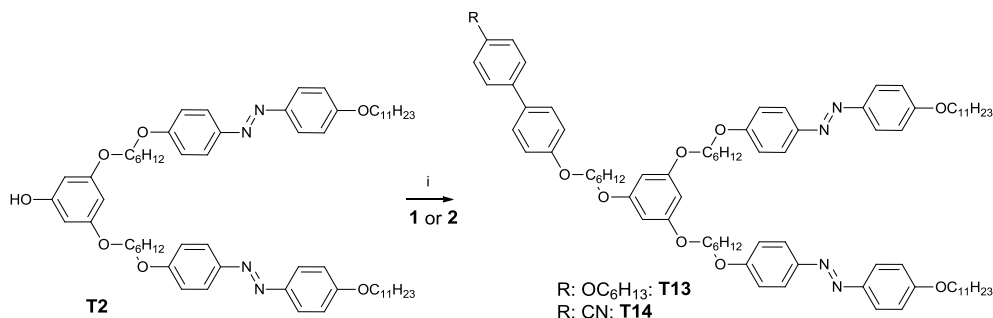


Scheme 14 Synthesis of the **HO-PG₆M₂**, M=OCB or BPH, homolithic and heterolithic trimers. *Reagents and conditions:* (i), K₂CO₃, 18 crown-6, DMF or acetone or DMF/THF (ii) KOH, THF/acetone, reflux

To increase the yield, the synthesis of **T7** was carried out several times in different solvents and using different purification procedures. Firstly, the etherification was carried out in DMF, and then the reaction mixture was worked up (washing, drying). After the purification by silica gel column chromatography, the protected intermediate (Bz-PG₆BPH₂) was obtained with 79% yield. This was followed by the hydrolysis resulting in the first generation phenolic dendron (**T7**) with 67%, giving an overall 53% yield. The DMF solvent was exchanged: with THF (longer reaction time), 3-pentanone (low yield), THF/acetone (similar yield). Alternatively the purification of the intermediate was skipped which also resulted in similar yield, but no significant improvement was achieved. In case of OCB, there was no purification performed after the etherification step. We also changed the protection of the branching points and used TBDMS protected phloroglucinol (**6a**) for ether coupling. The TBDMS group' under the aqueous basic condition of Williamson etherification with K₂CO₃, proved less stable than the benzoate and resulted in a poorer yield. Changing from aqueous basic condition to NaH, using 15-crown-5 as the catalyst, resulted in an increase of side reactions i.e. formation of alkenes by elimination of bromide. Because of the lack of improvement of yield, these reactions will not be detailed in the experimental part.

The heterogeneous trimers (PG₆BPH₂AZB (**T11**) and PG₆OCB₂AZB (**T12**)) were obtained in one step by etherification of the intermediate phenolic derivatives (HO-PG₆BPH₂ (**T7**) and HO-PG₆OCB₂ (**T9**)) with the brominated AZB monomer (**3**) (Scheme 14). Accordingly, the

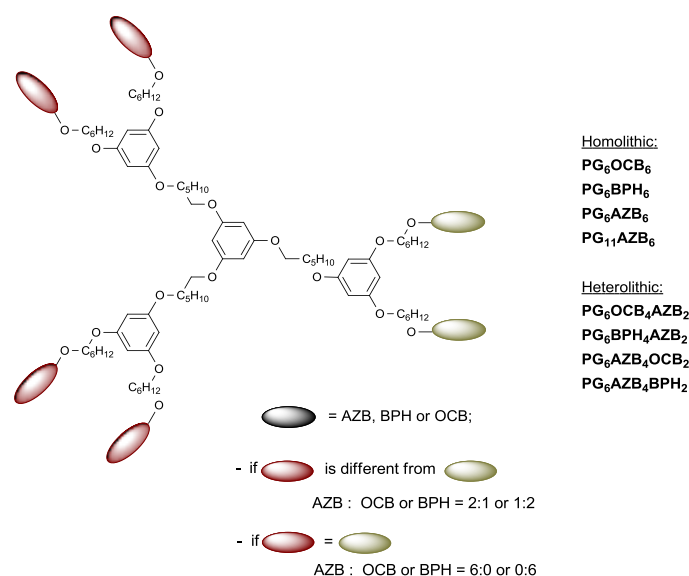
PG₆AZB₂BPH (**T13**) and PG₆AZB₂OCB (**T14**) were obtained by attaching the bromide derivatives of the mesogens (**1** and **2**) to the HO-PG₆AZB₂ (**T2**) (Scheme 15).



Scheme 15 Synthesis of the heterolithic trimers PG₆AZB₂M (M=BPH or OCB). *Reagents and conditions:* (i), K₂CO₃, KI, 18 crown-6, THF or DMF/THF

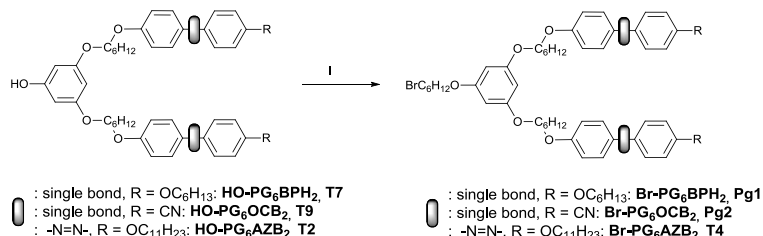
1.2.3 Synthesis of phloroglucinol based first generation dendrimers

In order to carry out a systematic and comprehensive study, we increased the generation number of the phloroglucinol based trimers and investigated the effect on the mesomorphic behaviour. We used the phenolic derivatives (**T2**, **T3**, **T7**, **T9**) of the mesogenic units (AZB, BPH, OCB), which were synthesized during the synthesis of the trimers, as building blocks. These blocks were attached to a phloroglucinol core through a linker with the same length as the phenolic derivatives were built up from (*e.g.* C6 in case of HO-PG₆AZB₂ (**T2**) or C11 in case of the HO-PG₁₁AZB₂ (**T3**) building block). The proportion of the mesogens in one molecule was varied likewise in case of trimers (AZB : BPH/OCB → 6:0 → 2:1 → 1:2 → 0:6) but each molecule bearing six mesogenic units (Scheme 16).



Scheme 16 General structure of the first generation PG based dendrimers

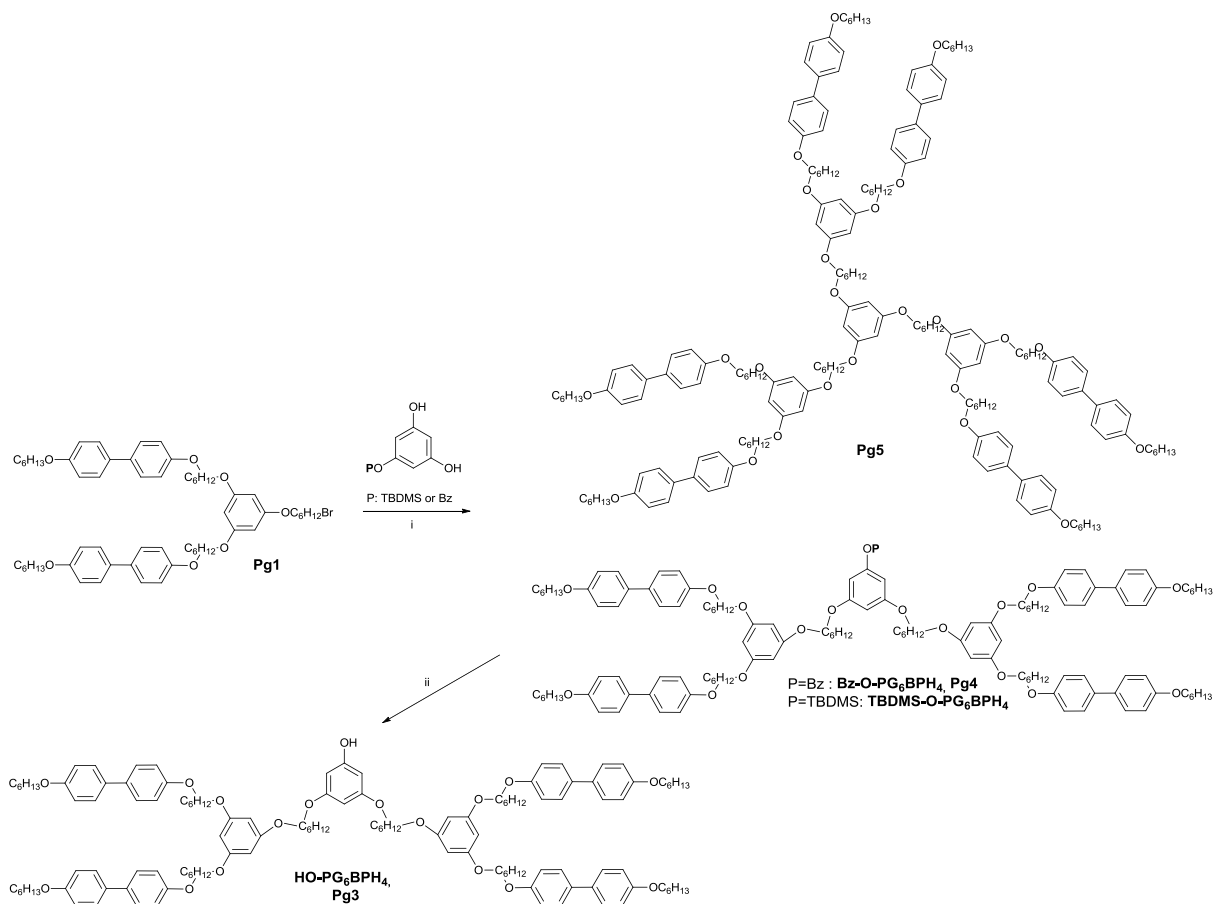
The synthesis of the first generation dendrimers was carried out by a multistep convergent procedure by repetition of etherification steps. The bromoalkylation of the first generation phenolic dendrons (HO-PG₆M₂: **T2**, **T7**, **T9**; see synthesis in I.2.2) with 1,6-dibromohexane led to the first generation bromide derivatives (Br-6-PG₆M₂: **PG1**, **PG2**, **T4**)(Scheme 17).



Scheme 17 Synthesis of the **Br-6-PG₆M₂**: M=OCB, AZB or BPH. *Reagents and conditions:* (i) 1,6-dibromohexane, K₂CO₃, 18 crown-6, acetone/THF, reflux

This was followed by a Williamson etherification of these bromide derivatives (Br-6-PG₆M₂: **Pg1**, **Pg2**, **T4**) with the 3,5-dihydroxyphenyl benzoate (**7a**) and the consecutive deprotection led to second generation phenolic derivatives (**Pg3**, **Pg6**, **Pg8**) (Scheme 18 and Scheme 19). Analogous to the synthesis of the first generation phenolic intermediates, the simultaneous in situ deprotection of the monoprotected phloroglucinol during the etherification step resulted the first generation homolithic dendrimers as by-products, which were isolated (PG₆M₆: M=BPH (**Pg5**) or OCB (**Pg7**)). The isolation of the homolithic PG₆AZB₆ (**Pg9**) was not successful and its synthesis was carried out with a different method (see later).

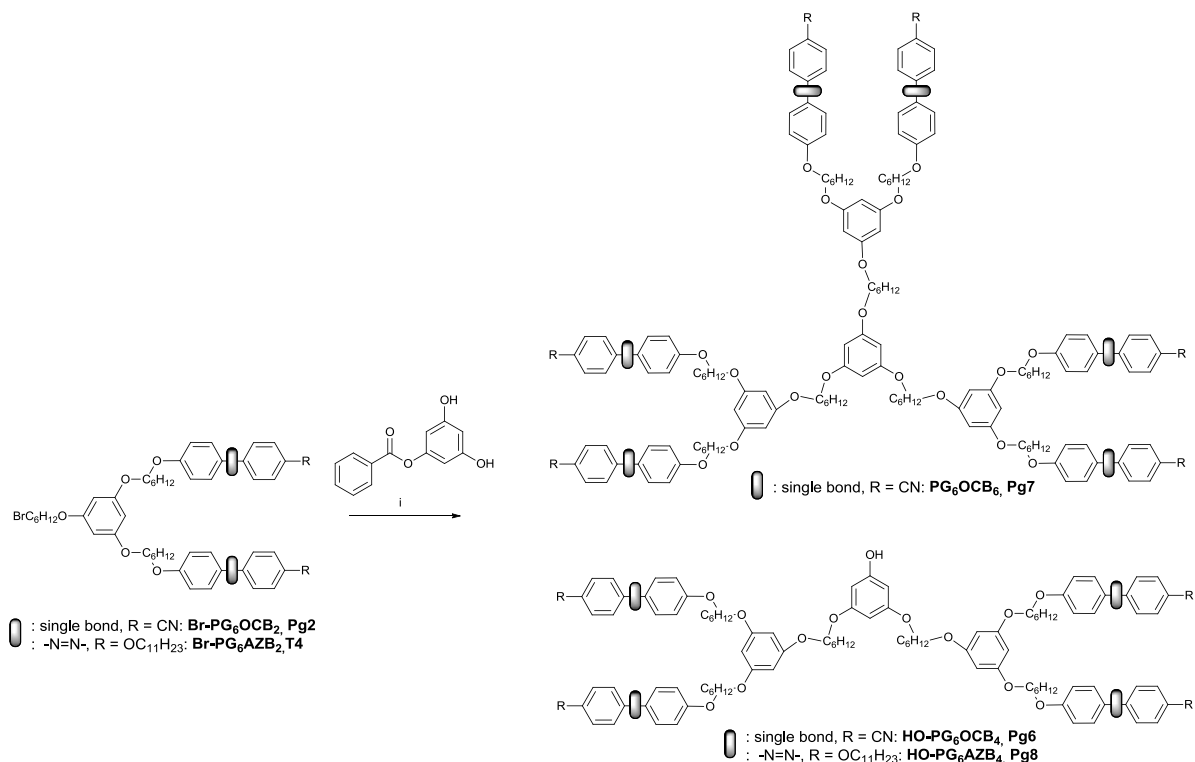
The etherification step to gain the four-fold BPH functionalized phenolic derivative was carried out several times in order to find the optimal reaction conditions. First, benzoic acid ester protected phloroglucinol (3,5-dihydroxyphenyl benzoate, **7a**) was used as a selectively protected core to attach to the bromide derivative (Br-6-PG₆BPH₂, **Pg1**) in DMF, resulting the protected intermediate (**Pg4**). This was followed by the deprotection step which was performed in the presence of KOH in THF/water to obtain four-fold functionalized second generation dendron (HO-PG₆BPH₄, **Pg3**) (Scheme 18). This method resulted in a very low yield. The etherification was also carried out with TBDMS protected phloroglucinol in THF using TBAF for the consecutive deprotection step. This protective group proved less stable than the benzoate, under these conditions, resulting in mainly the first generation homolithic dendrimer (PG₆BPH₆, **Pg5**). Finally, using the benzoate protected phloroglucinol (**7a**) in the Williamson etherification but changing the deprotection step for more mild conditions and using 1-butylamine¹⁴¹, provided the desired phenolic product (HO-PG₆BPH₄, **Pg3**) in good yield (Scheme 18).



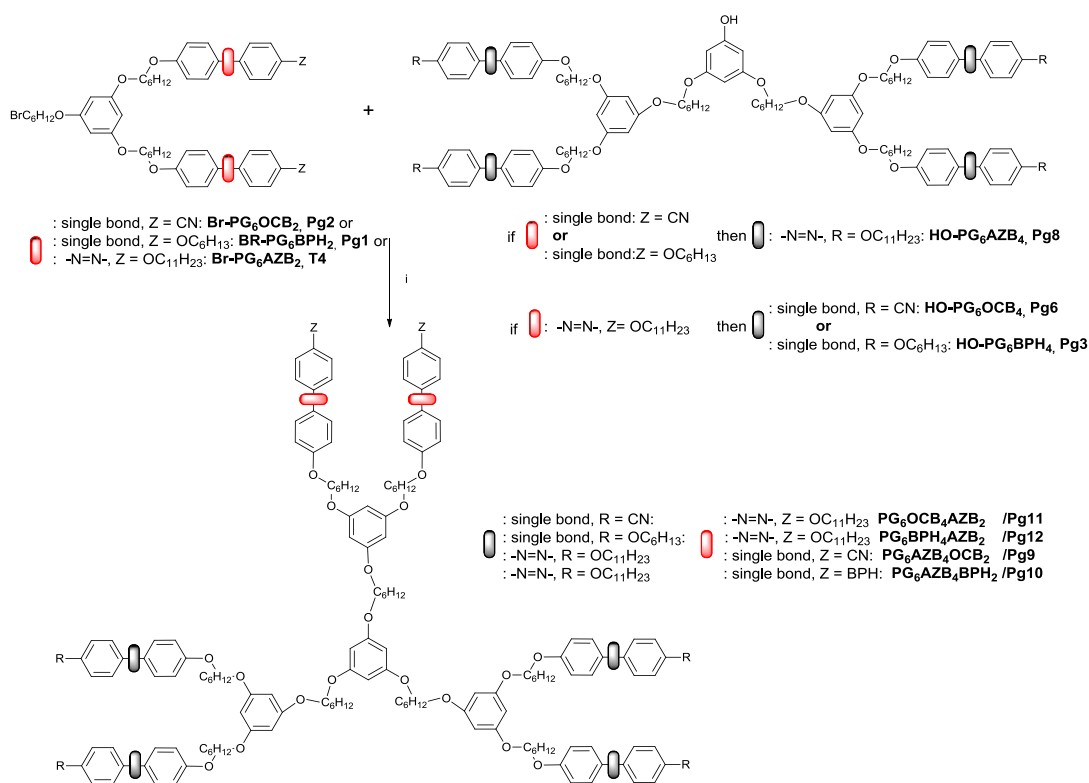
Scheme 18 Synthesis of the HO-PG₆BPH₄ (**Pg3**). *Reagents and conditions:* (i) K₂CO₃, 18 crown-6, KI, acetone/THF, reflux, (ii) P=Bz: KOH, THF/H₂O, reflux; 1-butylamine, THF, reflux; P=TBDMS: TBAF, THF, rt;

In the following, this last method and condition was used to build up the second generation phenolic dendrons bearing the other mesogens (OCB (**Pg6**) and AZB (**Pg8**)) (Scheme 19). The last step of the synthesis of first generation heterolithic dendrimers was the Williamson etherification of the second generation phenolic derivatives (HO-PG₆M₄: **Pg3**, **Pg6**, **Pg8**) with the corresponding bromide derivatives (Br-6-PG₆M₂: **Pg1**, **Pg2**, **T4**) (Scheme 20):

- HO-PG₆AZB₄ (**Pg8**) was reacted with the Br-6-PG₆BPH₂ (**Pg1**) or Br-6-PG₆OCB₂ (**Pg2**) to obtain PG₆AZB₄BPH₂ (**Pg10**) and PG₆AZB₄OCB₂ (**Pg9**), respectively
- and in order to obtain their conjugates (PG₆OCB₄AZB₂ (**Pg11**) and PG₆BPH₄AZB₂ (**Pg12**): HO-PG₆OCB₄ (**Pg6**) or HO-PG₆BPH₄ (**Pg3**) was reacted with Br-6-PG₆AZB₂ (**T4**), respectively (Scheme 20). The purification of the first generation dendrimers was especially difficult.

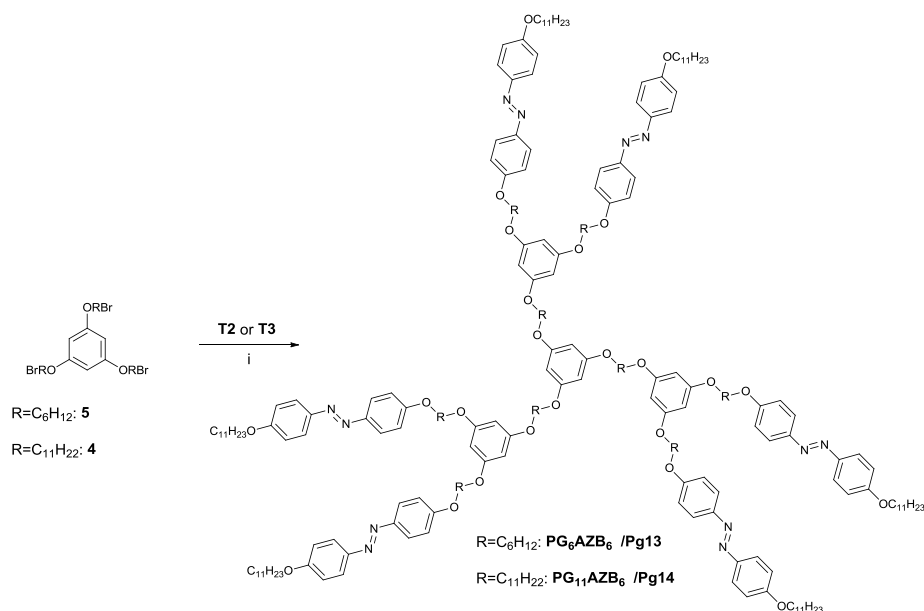


Scheme 19 Synthesis of the **HO-PG₆M₄** (M=OCB, AZB). *Reagents and conditions:* (i) K₂CO₃, 18 crown-6, KI, acetone/THF, reflux, (ii) 1-butylamine, THF, reflux;



Scheme 20 Synthesis of heterolithic first generation dendrimers. *Reagents and conditions:* (i) K₂CO₃, 18 crown-6, KI, THF, reflux,

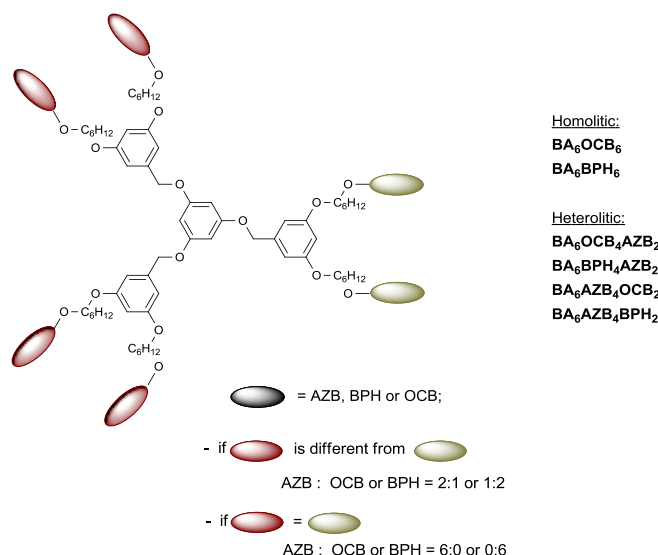
The synthesis of the homolithic PG₆AZB₆ (**Pg13**) and PG₁₁AZB₆ (**Pg14**) was achieved from the complete etherification of the tribromide derivatives (**5** and **4**) with the first generation phenolic derivatives of the AZB (**T2** or **T3**) (Scheme 21).



Scheme 21 Synthesis of homolithic first generation dendrimers PG₆AZB₆ and PG₁₁AZB₆. *Reagents and conditions:* (i) K₂CO₃, 18 crown-6, KI, DMF, 80°C

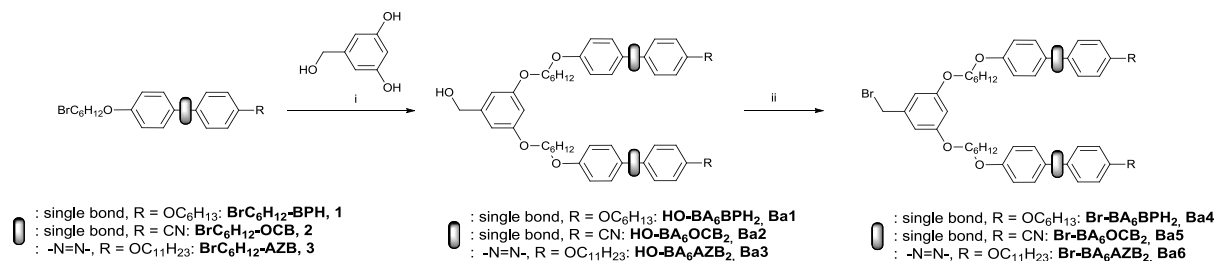
1.2.4 Synthesis of benzyl alcohol based dendrimers

In order to investigate the effect of branching points on the physical properties, we exchanged the phloroglucinol branching points to 3,5-dihydroxybenzyl alcohol based ones (Scheme 22).



Scheme 22 Benzyl alcohol (BA) based dendrimers

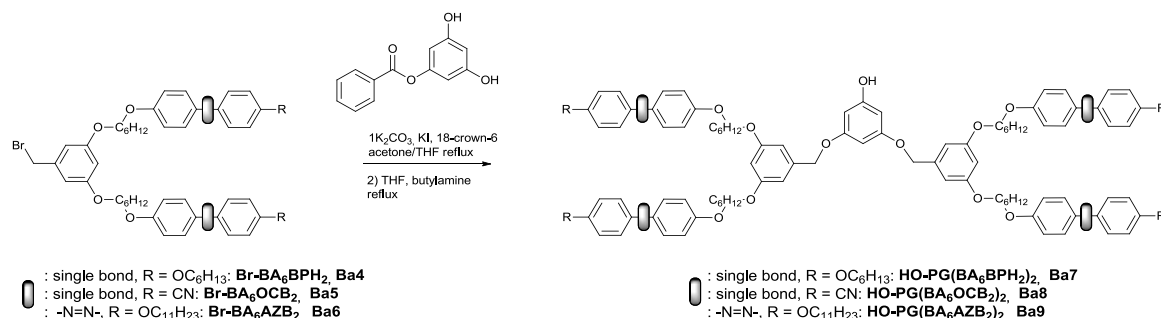
The synthesis of dendrimers with benzyl alcohol branching points was carried out by a convergent procedure by repetition of etherification and bromination steps. First 3,5-dihydroxybenzyl alcohol was reacted with the bromoalkylated functional groups (For **1**, **2**, **3** - synthesis details, see in the part of branching points (I.2.1)), by Williamson etherification, which gave the proto-mesogenic benzyl alcohol intermediates ($\text{HO-BA}_6\text{M}_2$: $\text{M}=\text{BPH}$ (**Ba1**) or OCB (**Ba2**) or AZB (**Ba3**)). These intermediates were converted to the corresponding benzyl bromide groups using different methods, such as the Appel reaction ($\text{CBr}_4/\text{PPh}_3$), the bromination with PBr_3 ¹⁴² or with trimethylsilyl bromide¹⁴³ (TMSBr) which resulted the first generation benzyl bromide derivatives ($\text{Br-BA}_6\text{M}_2$: $\text{M}=\text{BPH}$ (**Ba4**) or OCB (**Ba5**) or AZB (**Ba6**)) (Scheme 23).



Scheme 23 Synthesis of the $\text{Br-Ba}_6\text{M}_2$. *Reagents and conditions:* (i) 3,5-dihydroxybenzyl alcohol, K_2CO_3 , KI, 18 crown-6, acetone/THF, reflux; (ii) PBr_3 , CH_2Cl_2 , 0°C ; $\text{CBr}_4/\text{PPh}_3$, THF, rt; TMSBr , rt

In some cases, the yield of Williamson etherification of 3,5-dihydroxybenzyl alcohol with the bromide derivative of the functional groups (Br-6-M) was improved using 18-crown-6 catalyst (from e.g. 72% to 84%, see Experimental part). During bromination, using $\text{CBr}_4/\text{PPh}_3$, in most cases benzyl chloride by-product was produced as well. It was not possible to separate this from the bromide product and gave a poor yield. Using trimethylsilyl bromide (TMSBr) resulted in a very poor yield, after a very long reaction time. The use of PBr_3 led to the corresponding benzyl bromide derivative in good yield with the simplest protocol. We also tried tosylation of the benzyl alcohol groups with *p*-toluenesulfonyl chloride (TsCl) in the presence of Et_3N to convert the alcohol to a good leaving group (sulfonate ester) but the reaction was not successful and will not be detailed in the experimental part.

At this point two different syntheses protocols were used to get either homolithic or heterolithic dendrimers. Heterolithic dendrimers were obtained by the Williamson etherification of the benzyl bromide derivatives (**Ba4**, **Ba5**, **Ba6**) with the mono-protected core (**7a**, 3,5-dihydroxyphenyl benzoate) and subsequent deprotection resulted the phenolic derivatives ($\text{HO-PG}(\text{Ba}_6\text{M}_2)_2$; M=BPH (**Ba7**) or OCB (**Ba8**) or AZB (**Ba9**)), (Scheme 24), in fairly good yields (50-60%).

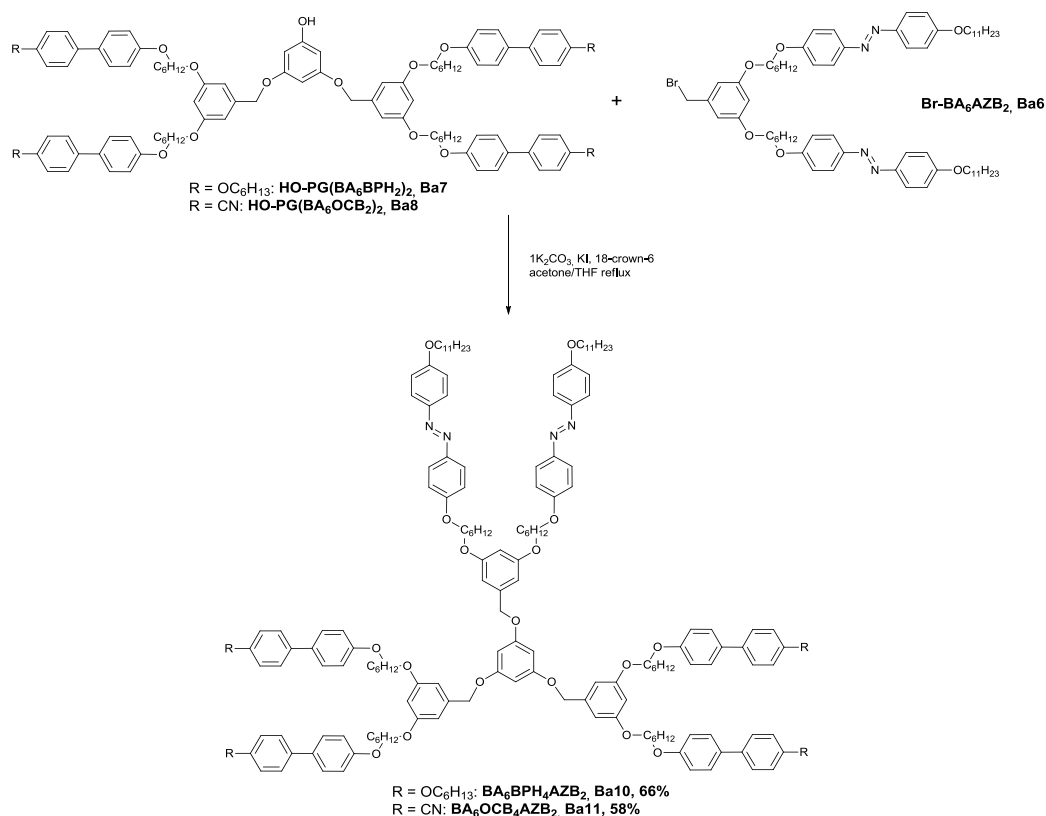


Scheme 24 Synthesis of the $\text{HO-PG}(\text{Ba}_6\text{M}_2)_2$. *Reagents and conditions:* (i) K_2CO_3 , KI, 18 crown-6, acetone/THF, reflux; (ii) THF, 1-butylamine, reflux

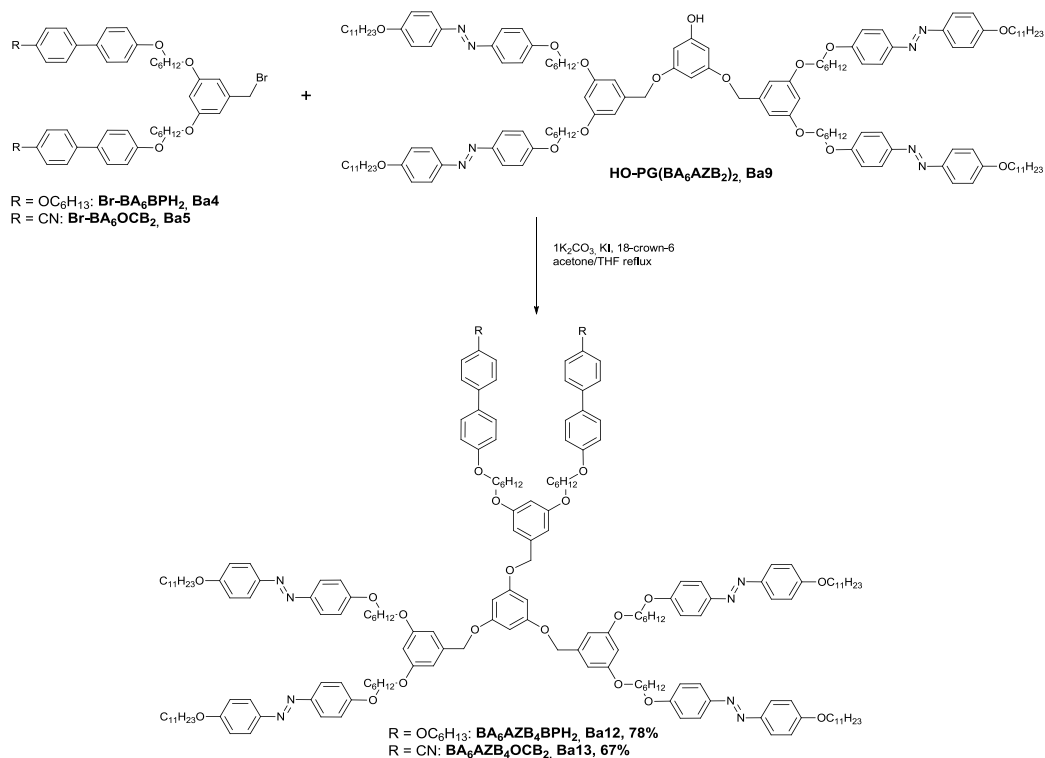
On this occasion, also occurred the simultaneous in-situ deprotection of the 3,5-dihydroxyphenyl benzoate as a side reaction, but unlike for the trimers, it was not possible to isolate the by-product homolithic dendrimers. Consequently, another protocol was used to obtain the homolithic dendrimers (see later). The synthesis of $\text{HO-PG}(\text{Ba}_6\text{OCB}_2)_2$ (**Ba8**) was carried out several times. The first time, after the etherification the reaction mixture was worked up (washing, drying) but the consecutive purification by silica gel column chromatography failed, because of poor separation and did not provide the pure protected product $\text{Bz-PG}(\text{Ba}_6\text{OCB}_2)_2$ using any solvent combination. The second time, the workup (washing, drying) was carried out in the same way as the first time, but there was no further purification until the deprotection reaction. The purification took place after the cleavage of the

protective group, which provided a much better separation; this method resulted in around a 50% yield. And finally, the etherification and the deprotection step took place in the same pot, only cooling down the reaction mixture, after the etherification step finished, before adding the 1-butylamine to the mixture. This method also provided about a 50% yield after workup and purification procedure. Because of its simplicity and the similar yield, we used this method for the synthesis of the phenolic derivatives (HO-PG(Ba₆M₂)₂), which is described in the Experimental part.

The subsequent etherification of the phenolic derivatives (HO-PG(Ba₆M₂)₂: **Ba7**, **Ba8**, **Ba9**) with the corresponding benzyl bromide derivative (Br-BA₆M₂: **Ba4**, **Ba5**, **Ba6**) provided the heterolithic dendrimers with benzyl alcohol branching points (BA₆BPH₄AZB₂ (**Ba10**), BA₆OCB₄AZB₂ (**Ba11**), BA₆AZB₄BPH₂ (**Ba12**), BA₆AZB₄OCB₂ (**Ba13**)), (Scheme 25 and Scheme 26).

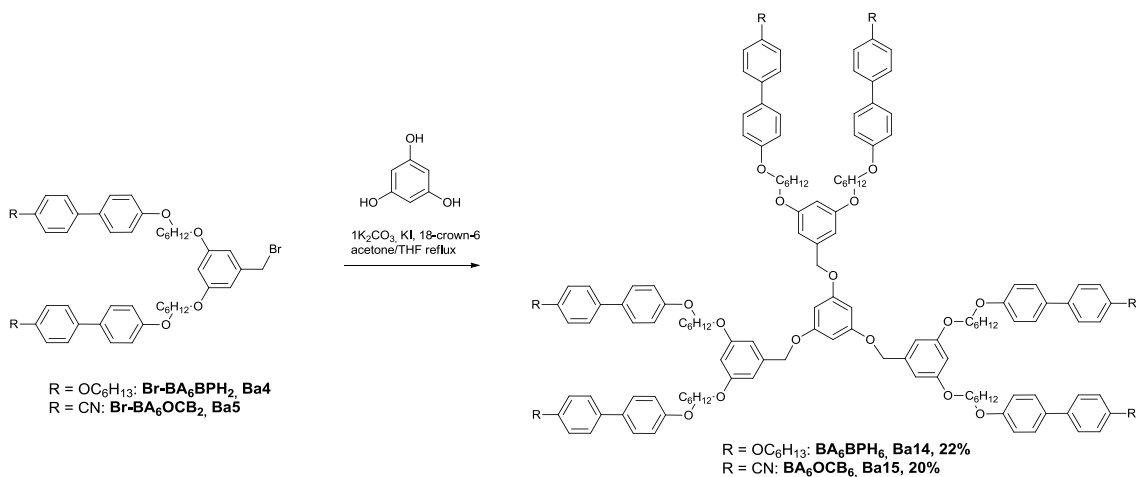


Scheme 25 Synthesis of BA₆BPH₄AZB₂ (**Ba10**), and BA₆OCB₄AZB₂ (**Ba11**) Reagents and conditions: (i) K₂CO₃, KI, 18 crown-6, acetone/THF, reflux;



Scheme 26 Synthesis of BA₆AZB₄BPH₂ (**Ba12**) and BA₆AZB₄OCB₂ (**Ba13**). *Reagents and conditions:* (i) K₂CO₃, KI, 18 crown-6, acetone/THF, reflux

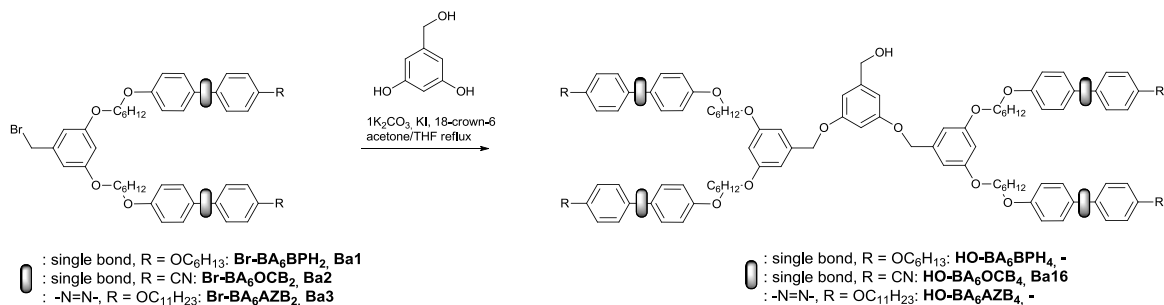
Homolithic dendrimers (BA₆BPH₆ (**Ba14**), BA₆OCB₆ (**Ba15**)) were directly obtained by the Williamson etherification of the benzyl bromide derivatives (**Ba4**, **Ba5**) with the phloroglucinol core (Scheme 27).



Scheme 27 Synthesis of BA₆BPH₆ (**Ba14**) and BA₆OCB₆ (**Ba15**) *Reagents and conditions:* (i) K₂CO₃, KI, 18 crown-6, acetone/THF, reflux;

It is possible to further increase the generation numbers by repeating the etherification and bromination steps between the branching points and the bromide derivative of the higher generation dendrons. We attempted to synthesize the second generation dendrons by

etherification of the first generation benzyl bromide derivatives (**Ba1**, **Ba2**, **Ba3**) with the 3,5-dihydroxybenzil-alcohol core (Scheme 28).

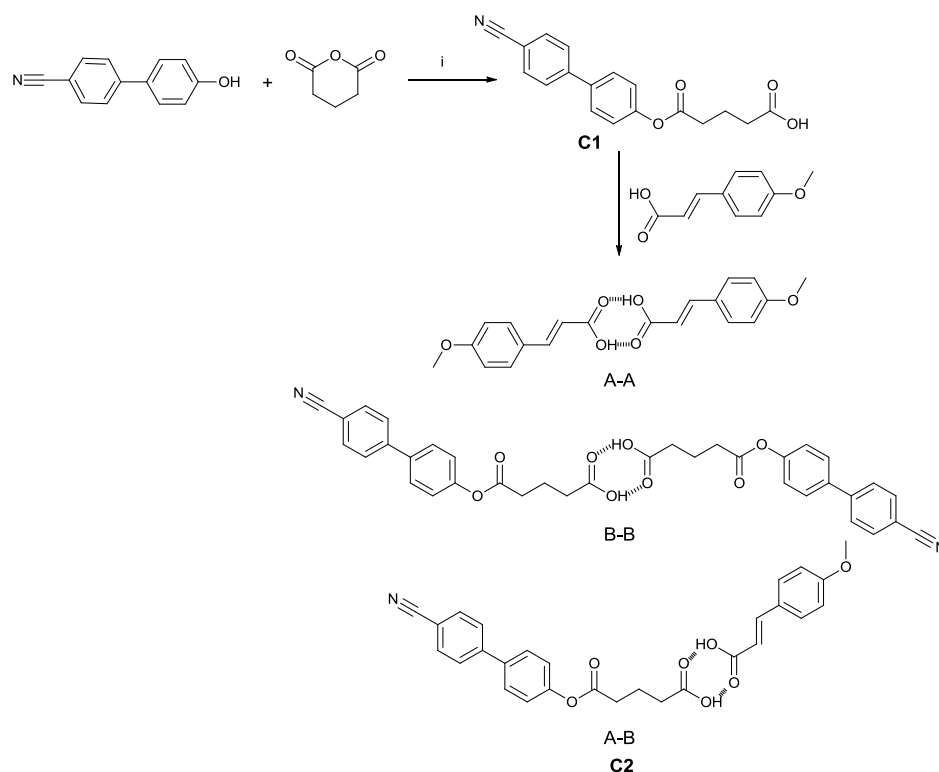


Scheme 28 Synthesis of the **HO-Ba₆M₄**. *Reagents and conditions:* (i) K₂CO₃, KI, 18 crown-6, acetone/THF, reflux

In case of AZB functional groups, the reaction was unsuccessful; in case of BPH the reaction provided a very low yield and for that reason will not be detailed in the experimental part. However, the second generation HO-BA₆OCB₄ dendron (**Ba16**) was synthesised in good yield.

1.2.5 Synthesis of Cinnamic acid ester derivatives

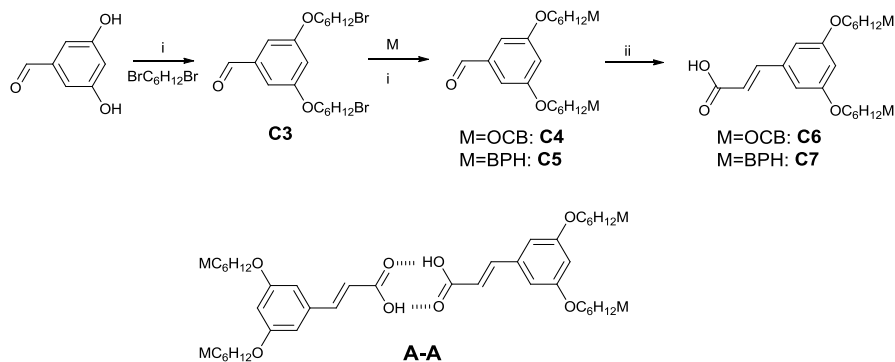
Cinnamic acid esters are also interesting for induction of optical-anisotropy caused by molecular photoreactions and photo-cycloadditions upon irradiation by polarized light. In the case of cinnamic acid derivatives we wanted to build up non-covalent, hydrogen bonding between the moieties. Cinnamic acid derivatives can form hydrogen bonded dimers through the carboxyl groups. Two types of systems were synthesised. The first set was assigned to 4-methoxycinnamic acid (commercially available) forming hydrogen bonds with the carboxyl group of a mesogen containing molecule, namely with 4'-cyanobiphenyl hydrogen glutarate¹⁴⁴ (**C1**). In this case three types of hydrogen bonded dimers can be formed (**C2**): between the two cinnamic acid derivatives (A-A system), the two glutarate derivatives (B-B system) or the cinnamic acid and glutarate derivative (A-B system) (Scheme 29).



Scheme 29 Synthesis of 4'-cyanobiphenyl hydrogen glutarate and hydrogen bonded system with cinnamic acid derivative. *Reagents and conditions:* (i) N,N-Diisopropylethylamine, THF, reflux

The second set of molecules forming hydrogen-bonding (A-A type systems) contained both, the cinnamic acid function and the mesogen in one molecule. Two molecules were synthesised in this set: one of them bearing OCB and the other BPH functional groups in order to induce LC properties. First step was the bromoalkylation of the 3,5-dihydroxybenzaldehyde with 1,6-dibromohexane via Williamson etherification. The resulting bromide derivative (**C3**) was

reacted with the mesogens - OCB or BPH - providing **C4** and **C5**, respectively, which on condensation with malonic acid in the presence of dry pyridine and piperidine¹⁴⁵ yielded **C6** and **C7** respectively (Scheme 30).



Scheme 30 Synthesis of cinnamic acid derivatives bearing mesogens. *Reagents and conditions:* (i) K_2CO_3 , 18-crown-6, acetone, reflux, (ii) malonic acid, pyridine, piperidine, $90^\circ C$

Unfortunately none of them exhibited liquid crystalline properties and for that reason no further optical measurements were carried out.

1.3 Results and discussion - Characterization

1.3.1 *Characterization by Nuclear Magnetic Resonance spectroscopy*

Nuclear Magnetic Resonance (NMR) spectroscopy is essential to characterize and to determine the structure of a compound as well as to follow the path or extent of a reaction. In the dendrimers described in this work, the characteristics of the focal points and the ratio of the functional groups are changed by increasing the generation.

In the following some representative NMR spectra for various compounds will be given as examples. The aromatic rings in all functional groups (**AZB**, **OCB** and **BPH**) are p-disubstituted benzenes and present AA'BB' patterns which resemble, in case of AZB and BPH, a two AB doublet or in case of OCB, an AB quartet (Figure 23) and will be thereafter described as doublets or quartets.

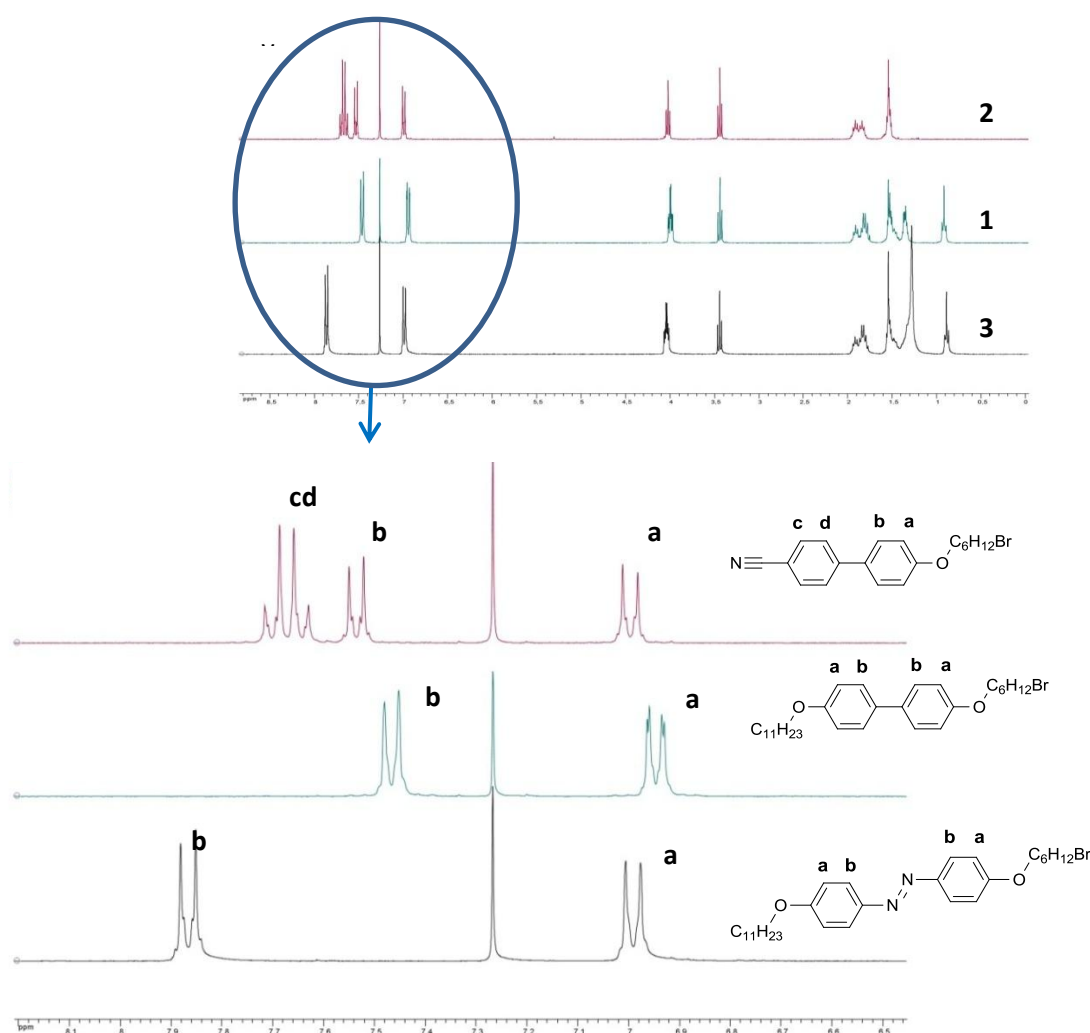


Figure 23 Characteristic of ^1H -NMR spectra of bromoalkylated functional groups

Characterization

In the case of the AZB functional group the ratio of *cis-trans* isomers can be well determined by $^1\text{H-NMR}$ spectra (Figure 24). The *trans* form can be easily switched to the *cis* form by irradiation with ultraviolet light that relaxes back to the *trans* via *cis-to-trans* isomerization without irradiation or if the material is not heated. In most cases, when azobenzene containing molecules were characterized by NMR spectroscopy only the *trans* isomer was present but in some cases the *cis* isomer occurred as well. This is not mentioned except for only one particular case when the ratio of the *cis* isomer was significant.

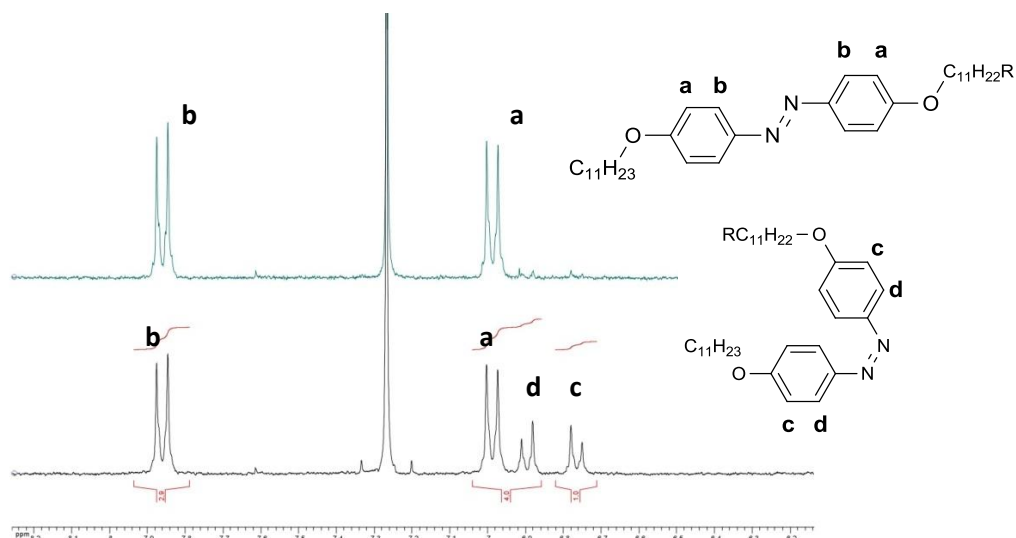
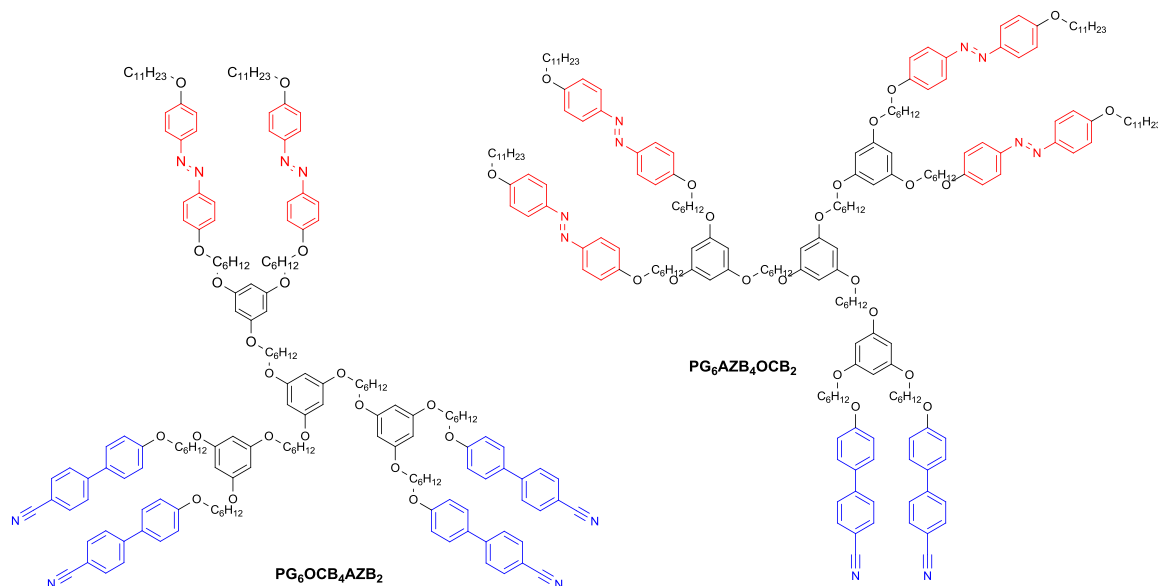


Figure 24 $^1\text{H-NMR}$ spectra of *trans* (top) and *cis-trans* (bottom) azobenzene moiety

For conjugated molecules, in which the branching points, core, linker and functional groups are the same but only differ in the proportion of the functional groups, the integral ratio of these peaks is varied accordingly as shown for $\text{PG}_6\text{AZB}_4\text{OCB}_2$ (**Pg9**) and $\text{PG}_6\text{OCB}_4\text{AZB}_2$ (**Pg11**) as representative examples (Figure 25 and Figure 26).



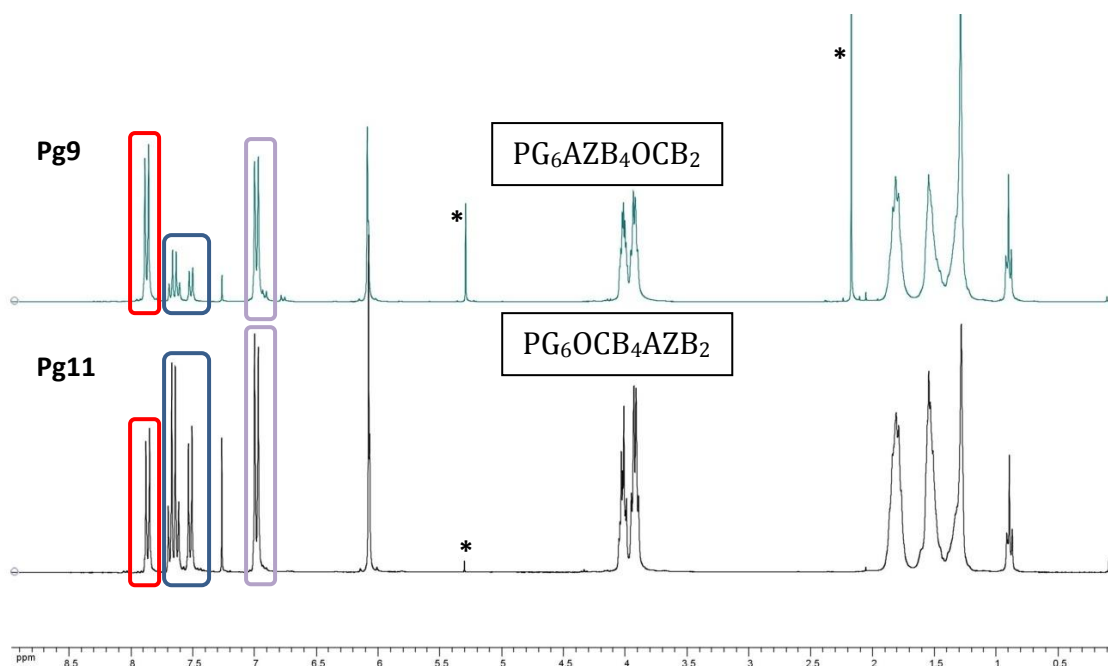


Figure 25 ^1H -NMR spectra of conjugated heterolithic dendrimers ($\text{PG}_6\text{AZB}_4\text{OCB}_2$ and $\text{PG}_6\text{OCB}_4\text{AZB}_2$)

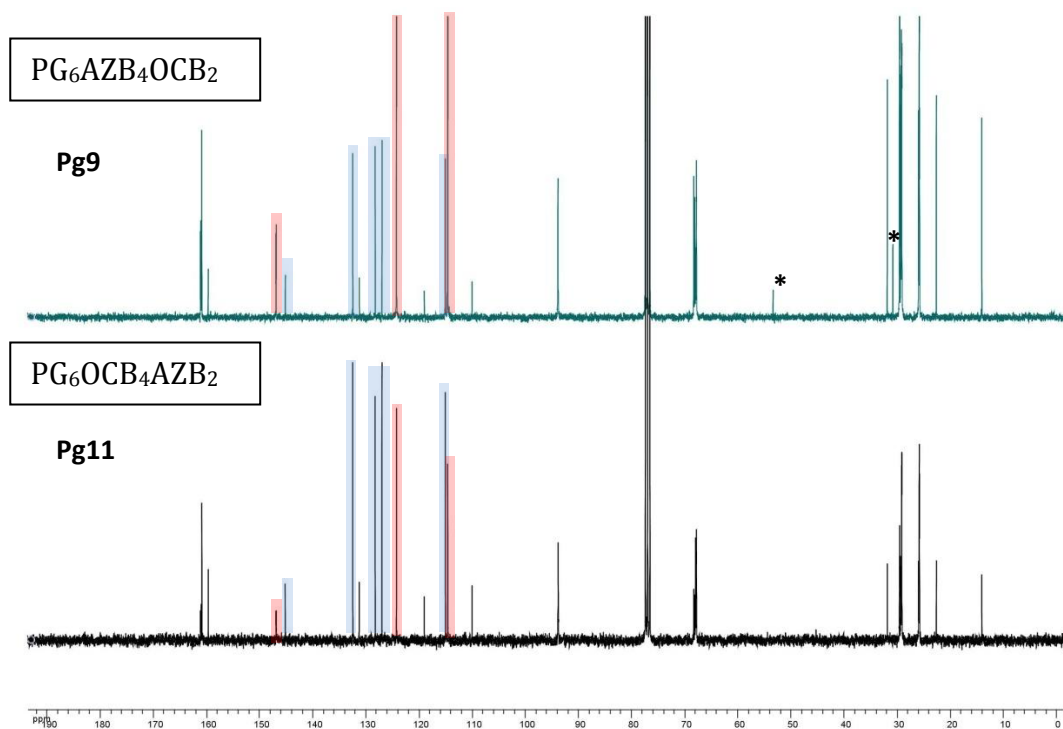


Figure 26 ^{13}C -NMR spectra of conjugated heterolithic dendrimers ($\text{PG}_6\text{AZB}_4\text{OCB}_2$ and $\text{PG}_6\text{OCB}_4\text{AZB}_2$)

By changing the focal point or increasing the generation number the feature of the branching points will be altered. This will be presented through the BPH-PG and OCB-BA based dendrons. The successful ether couplings on the two hydroxyl groups of the branching point (PG) are shown by ^1H -NMR by appearance of the signal of a triplet at 6.09ppm (*b*) with coupling: $J=2.1\text{Hz}$, corresponding to 1H, and of a doublet at 6.01ppm (*a*) with coupling: $J=2.2\text{Hz}$, correspond to two identical protons (Figure 27). When the remaining phenolic OH (*c*) of two

Characterization

branching points are successfully further functionalized and the generation number increased the protons of the branching points become identical and replaced by a singlet at 6.1ppm (*d*) – correspond to six identical protons – and the aromatic protons of the focal points remain the same as at the first generation (Figure 28) (* signals of CH₂Cl₂, EtOAc or acetone).

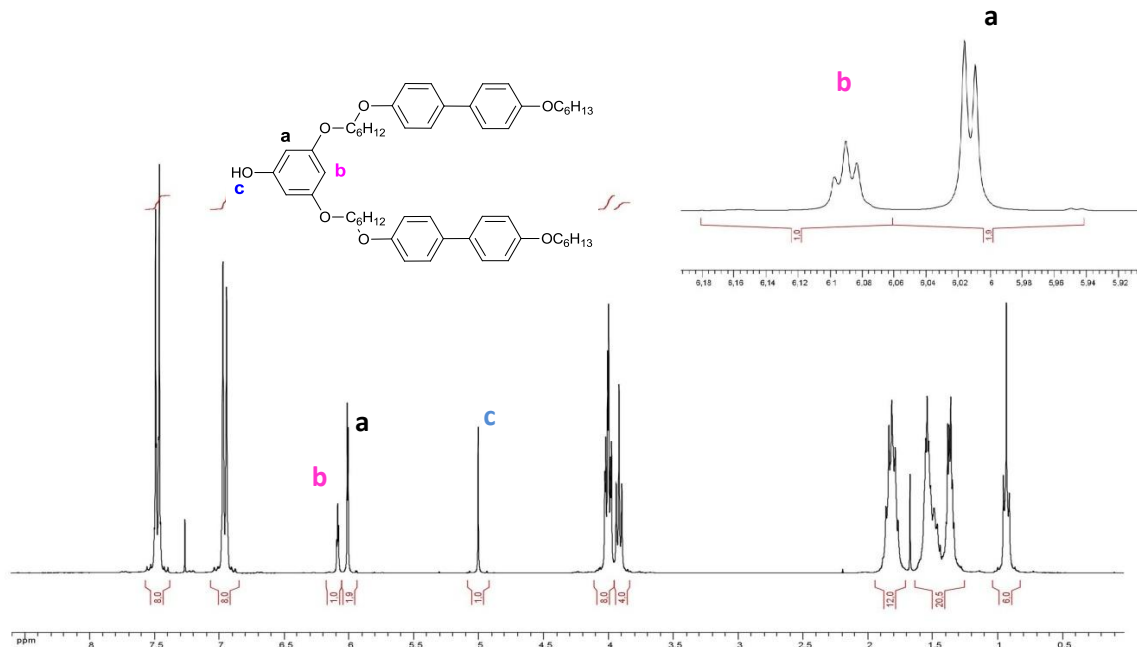


Figure 27 ¹H-NMR spectra of HO-PG₆BPH₂ (Pg1)

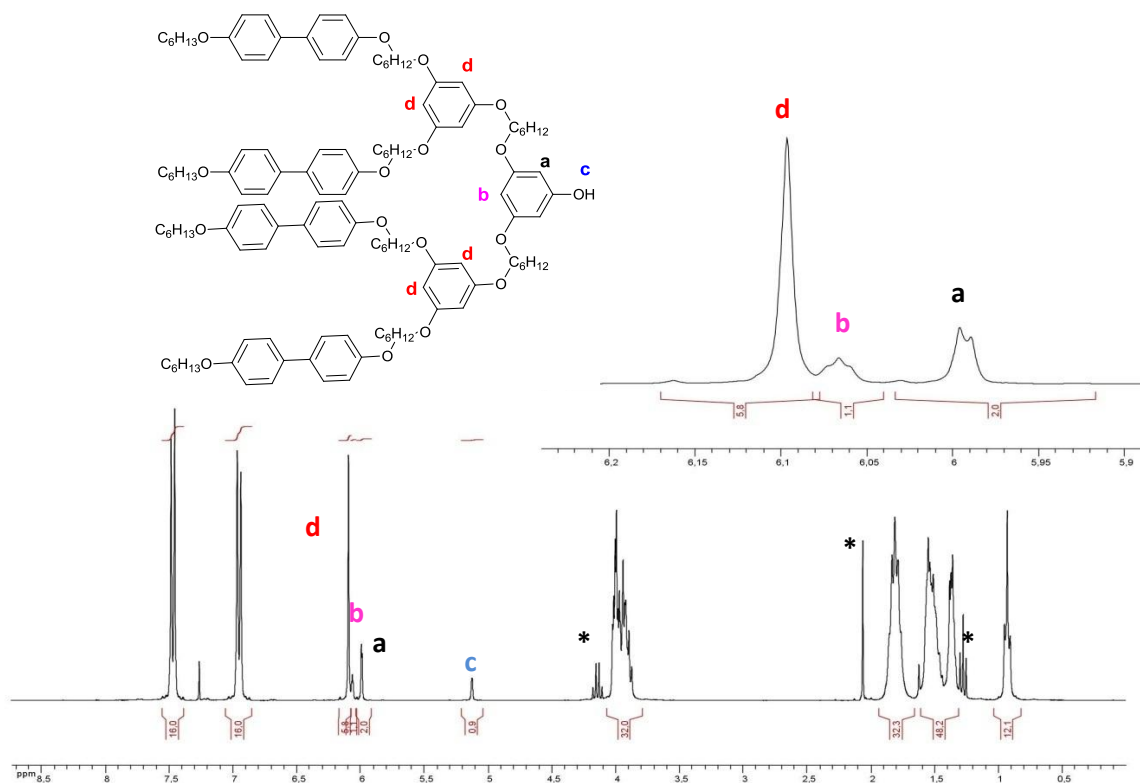


Figure 28 ¹H-NMR spectra of HO-PG₆BPH₄ (Pg3)

In case of benzyl alcohol based dendrons and dendrimers, difunctionalized benzyl alcohol has been successfully brominated as shown by the ^1H NMR, upon replacement of the methylene signal (*e*) next to the alcohol at 4.63ppm (*d*, $J=6.0\text{Hz}$) by the methylene signal next to the bromide at 4.50ppm as a singlet. One of the aromatic proton at the branching point (*b*), which emerge at 6.41ppm as a triplet ($J=2.2\text{Hz}$), is not identical with the further two protons (*a*) which show as a doublet at 6.55ppm with coupling constant $J=2.1\text{Hz}$. When the dendrons with a bromide focal point successfully further reacted with a phloroglucinol resulting in a second generation dendron, the singlet corresponds to the methylenes (*e*) shifts and appears at 4.91ppm. The aromatic protons of the phloroglucinol appear at 6.22ppm as a triplet and at 6.11ppm as a doublet and the ratio of the protons in the branching points will be 6:2:1:2 (*a*:*b*:*c*:*d*) (Figure 29)

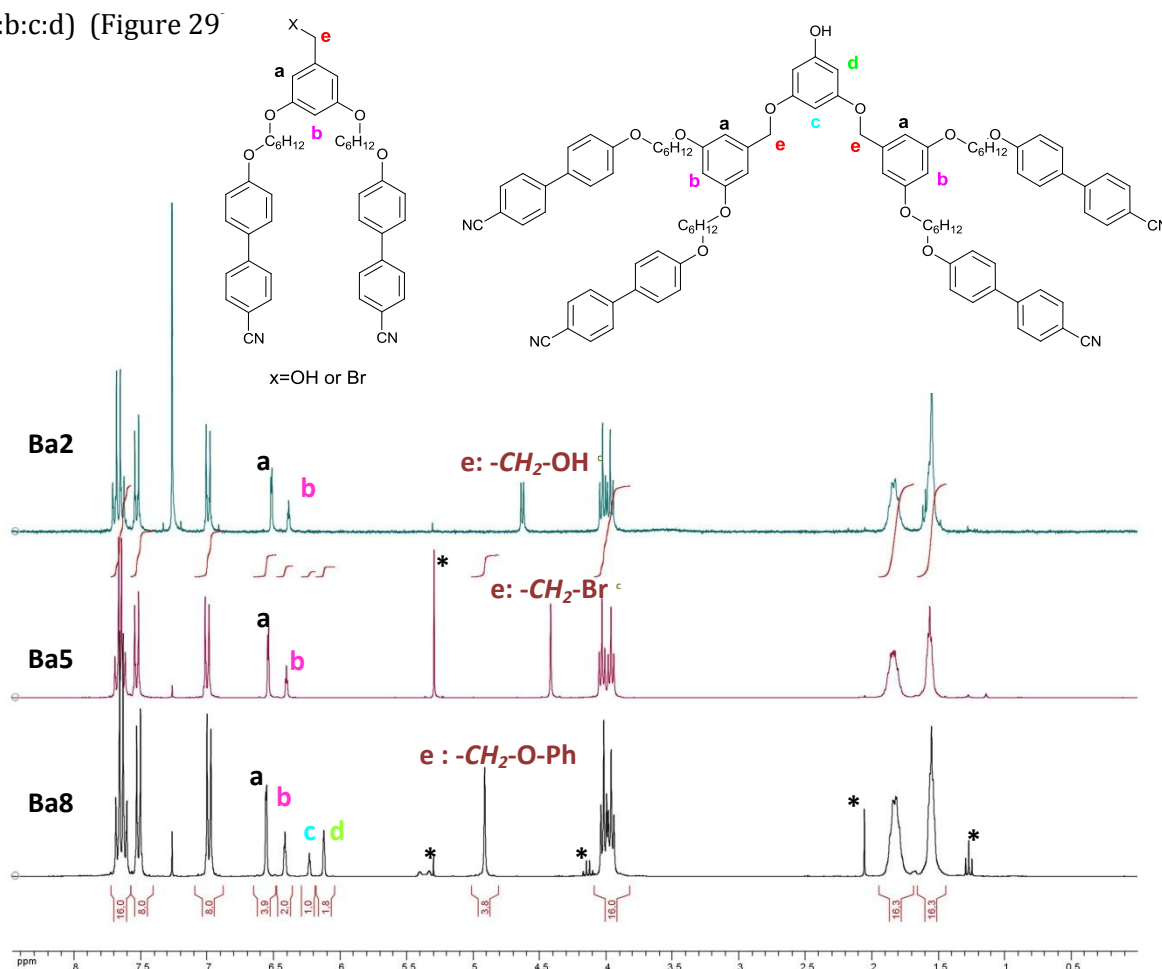


Figure 29 ^1H -NMR spectra of HO-BA₆OCB₂ (**Ba2**), Br-BA₆OCB₂ (**Ba5**) and HO-BA₆OCB₄ (**Ba8**)

In the case of homolithic (BA₆BPH₆ (**Ba14**) and BA₆OCB₆ (**Ba15**)) and heterolithic benzyl alcohol based dendrimers where the AZB is present in lower ratios (BA₆BPH₄AZB₂ (**Ba10**) and BA₆OCB₄AZB₂ (**Ba11**)), the corresponding aromatic protons of the branching points and the core are identical, as expected. As shown by the ^1H -NMR spectra the signal of three aromatic protons

Characterization

of the phloroglucinol core appear as a singlet at 6.3 ppm, the protons of the branching points' benzene rings at 6.6 ppm as a doublet (3x2H) and at 6.4 ppm as a triplet (3x1H) and the methylene signals, adjacent to the benzene ring in the benzyl, at 5.0 ppm as a singlet (3x2H) (Figure 30).

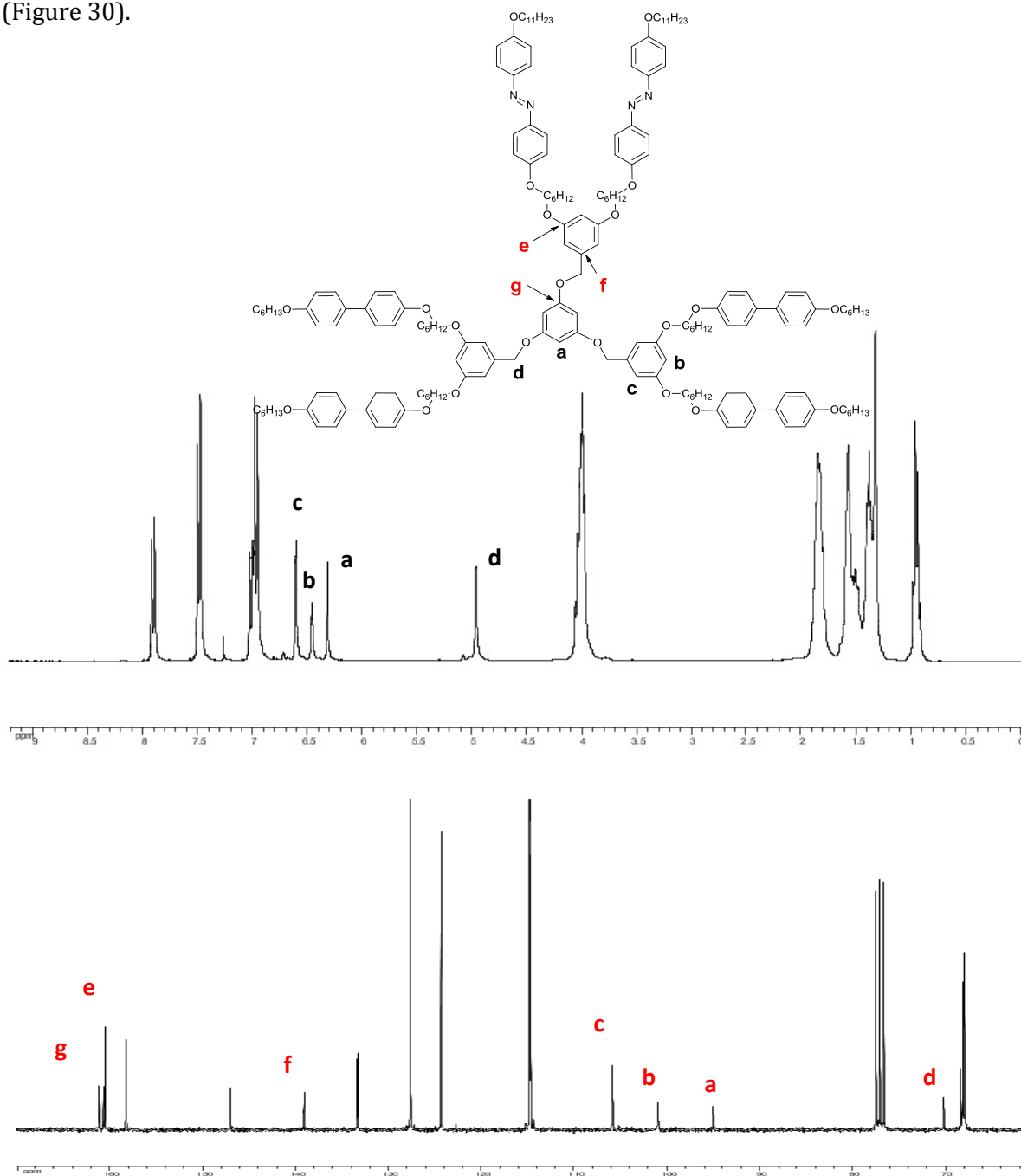


Figure 30 ^1H -NMR and ^{13}C -NMR spectra of $\text{Ba}_6\text{BPH}_4\text{AZB}_2$ (**Ba10**)

But in case of heterolithic dendrimers where the AZB present in higher ratios ($\text{Ba}_6\text{AZB}_4\text{BPH}_2$ (**Ba12**) and $\text{Ba}_6\text{AZB}_4\text{OCB}_2$ (**Ba13**)), the broadened and shifted signals (Figure 31) indicate that the corresponding protons and carbons of the core and branching points are not identical

any more, possibly due to the different chemical environment. This asymmetry was present in the ^{13}C -NMR spectra as well, by additional signals at the corresponding carbons.

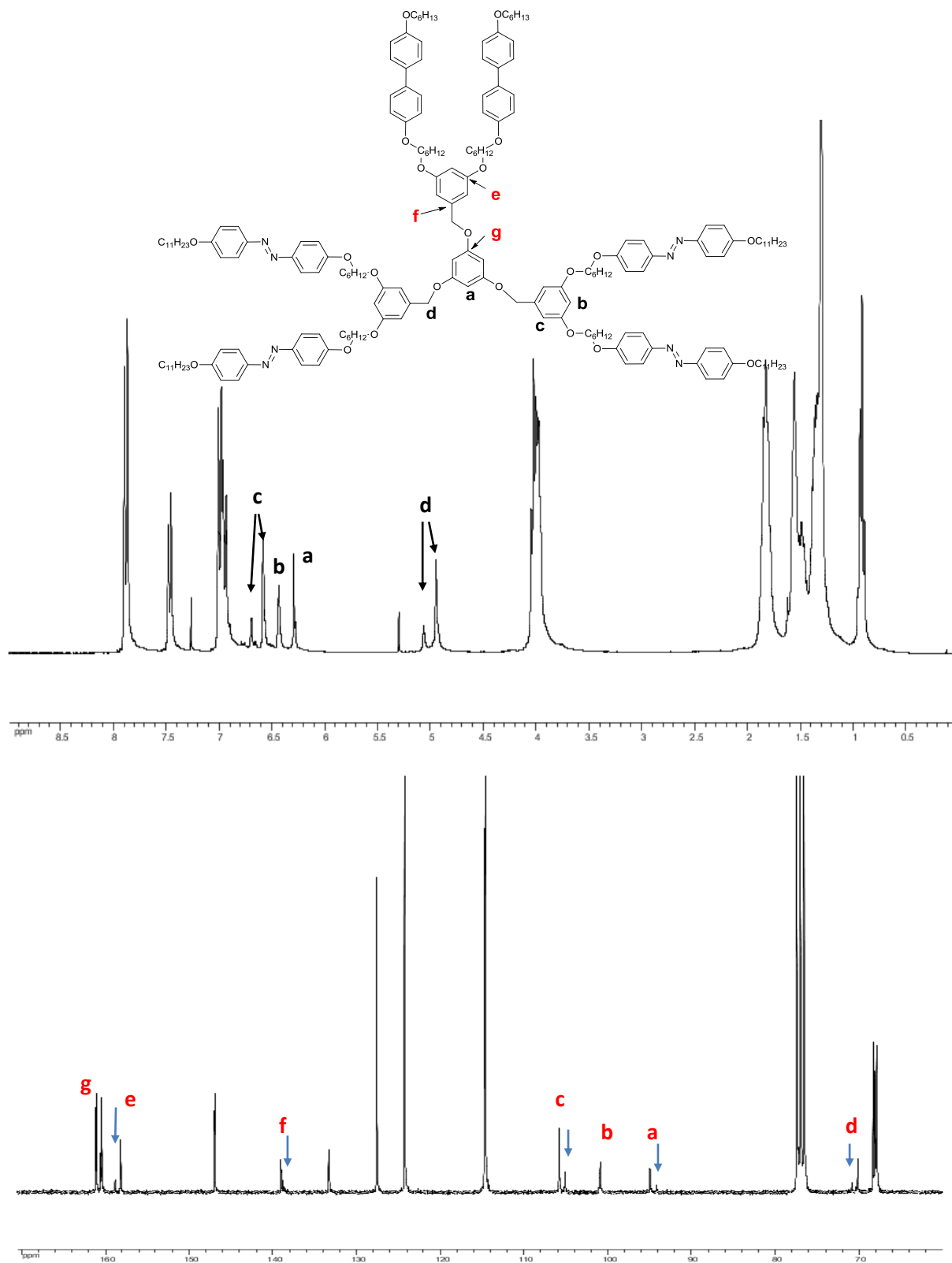


Figure 31 ^1H -NMR and ^{13}C -NMR spectra of $\text{Ba}_6\text{AZB}_4\text{BPH}_2$ (Ba12)

1.3.2 Characterization by Mass Spectroscopy

We used MALDI-ToF (Matrix-assisted Laser Desorption/Ionization - Time of Flight) mass spectroscopy to further characterize the final materials by determining the molecular weight. This spectrometry uses a soft ionization technique which allows the analysis of fragile molecules such as large organic molecules (polymers, dendrimers, biomolecules *etc.*). The analyses of MALDI-ToF spectroscopy were performed at the Institut Pluridisciplinaire Hubert Curien (IPHC), Département Sciences Analytiques (DSA) Laboratoire de Spectrométrie de Masse Bio-Organique (LSMBO), Strasbourg, France.

In MALDI-ToF MS technique the molecule is precipitated on an UV-light absorbing matrix and, as the first step, irradiated by a nanosecond laser pulse. The unwanted fragmentation of the molecule is prevented in this way as most of the laser energy is absorbed by the matrix. The second step is ionization which takes place in the hot plume which was generated by the ablation of the upper layer of the matrix material during UV irradiation. The ionized (protonated or deprotonated) molecules are accelerated in an electric field and enter to the flight tube where they are separated according to their mass to charge ratio during their flight and reach the detector at different time providing a distinct signal. The matrix used does not contain Na⁺, thus we obtained the direct mass spectrogram of the analysed products.

Figure 32 shows an example of the spectrogram made by MALDI-ToF MS method. The mass spectrum is showing two abundant groups of peaks: the isotopic distribution of the product PG₆BPH₄AZB₂ (**Pg12**) (Mol. Wt: 3062.22 g/mol) calculated for C₁₉₆H₂₆₆N₄O₂₄: 3059.97 (M) mono-isotopic molecular mass, where the atomic masses of each atom are based on the most common isotope for the element by definition, and its fragment 2799.60 (M- C₁₇H₂₇NO). The first peak of the isotopic distribution of the product at m/z = 3060.87 correspond to the singly protonated form (M+1) which is consistent to the theoretical values. The mass spectrum of the product PG₆OCB₄AZB₂ (**Pg11**) (Mol. Wt: 2761.62 g/mol) calculated for C₁₇₆H₂₁₄N₈O₂₀: 2759.60 (M) resemble of the previous one. The first peak of the isotopic distribution of the product at m/z = 2760.56 corresponds to the singly protonated form (M+1). Beside the isotopic distribution of the product, two fragments are present ((2499.30: M- C₁₇H₂₇NO, 2240.12: M- 2xC₁₇H₂₇NO) (Figure 33).

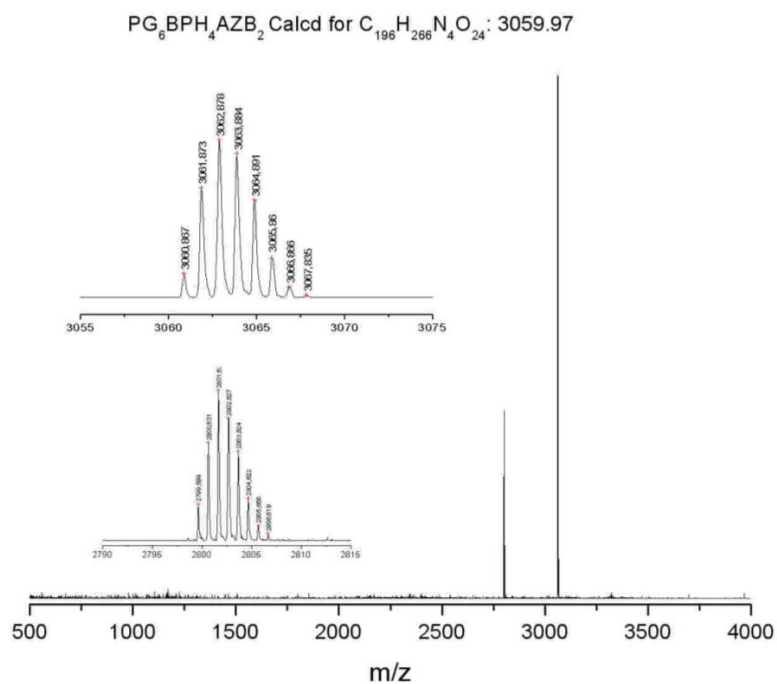


Figure 32 MALDI-ToF spectra of PG₆BPH₄AZB₂ (**Pg12**) calculated for C₁₉₆H₂₆₆N₄O₂₄: m/z = 3059.97 and its fragment 2799.60 (M- C₁₇H₂₇NO)

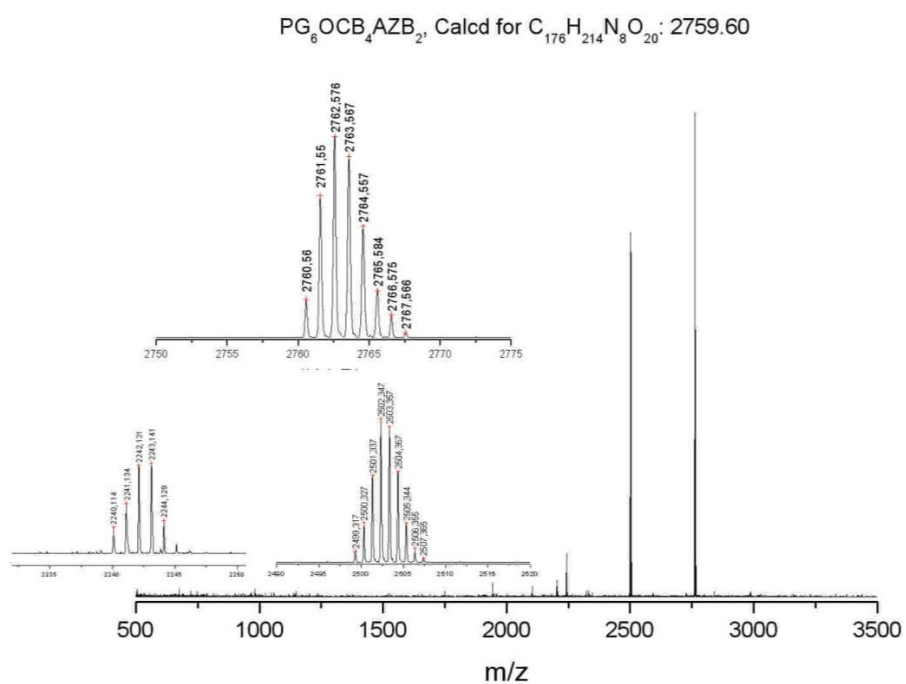


Figure 33 MALDI-ToF spectra of PG₆OCB₄AZB₂ (**Pg11**) (Mol. Wt: 2761.62 g/mol) calculated for C₁₇₆H₂₁₄N₈O₂₀: 2759.60 and its fragments

1.3.3 Characterization by Elemental analysis

We used quantitative elemental analysis (EA): carbon, hydrogen, and nitrogen (CHN analysis) to further characterize our trimers. EA determines the amount (in this case weight percent) of an element in a compound. However EA is not perfectly accurate and generally not appropriate for the characterization of molecules with large masses, but in the case of trimers – presented below – it was effective.

1.3.4 Mesomorphic properties and self-assembly

In this paragraph we will describe the liquid crystalline properties of the final materials and the effects of the structural modifications on the mesomorphism (mesophase structures, temperature ranges, and thermodynamic stability) but first we will discuss the techniques that are used for their characterization.

To determine the mesomorphic behaviour of the synthesised trimers and dendrimers, first thermogravimetric analysis (TGA) was used to determine their thermal stability as it is usually required before using differential scanning calorimetry, which contains several heating and cooling cycles. **TGA** is a technique in which the loss of mass of a substance is monitored as a function of temperature or time under a controlled temperature program in a controlled atmosphere, and the degradation temperature is determined from the onset of weight loss temperature curve. As an example, TG curves of the trimers are presented (Figure 34). All trimers are stable above 300°C and exhibit similar decomposition behaviour, except PG₁₁AZB₃ (**T1**), which starts degrading just around 200°C. The degradation temperature of the first generation PG dendrimers and the BA dendrimers varied between 280-350°C. The TGA measurements were carried out on a SDT 600 apparatus at a scanning rate of 10°C/min under air flow (by Mr. D. Burger).

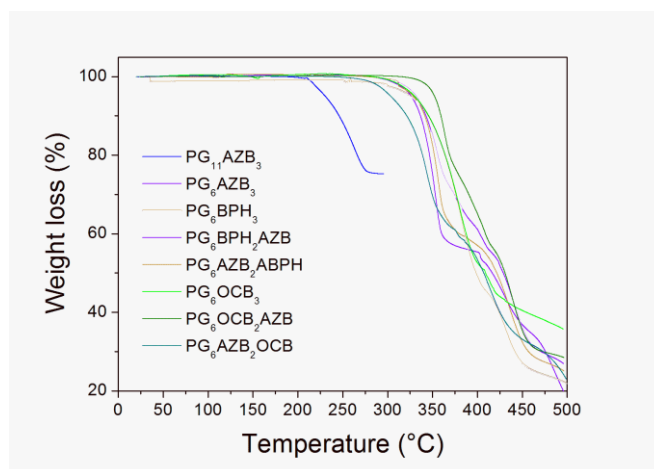


Figure 34 TGA curves of the trimers

Polarized optical microscopy - POM

Light with transverse wave vibrations that possesses direction, is called polarized light. Light from an ordinary light source (natural light) that vibrates in random directions is called non-polarized light. In contrast, while light with vertical vibration that travels within a single plane is called linearly polarized light; circularly polarized light and elliptically polarized light are types of light in which the vibration plane rotates with time. Liquid crystals are birefringent or in other words they have a double refraction which can be observed if irradiated with polarized light. When plane-polarized light enters a birefringent material, it is refracted into two individual rays: extraordinary (slow) and ordinary (fast) rays each polarized in mutually perpendicular planes. These light components travel at different velocities, which vary with the propagation direction through the sample. When the rays exit the material and pass through the analyser they recombine with constructive and destructive interference (due to the phase difference) and image contrast will be created.

A polarized light microscope (Figure 35) is designed to observe samples that are visible primarily due to their optically anisotropic character. These microscopes are equipped with both a polarizer, positioned in the light path before the sample, and an analyzer (a second polarizer) placed in the optical pathway between the objective rear aperture and the observation tubes or camera port. In the absence of liquid crystal material, if the polarizer and analyser are parallel the light passes through but if they are perpendicular to each other no light can be observed.

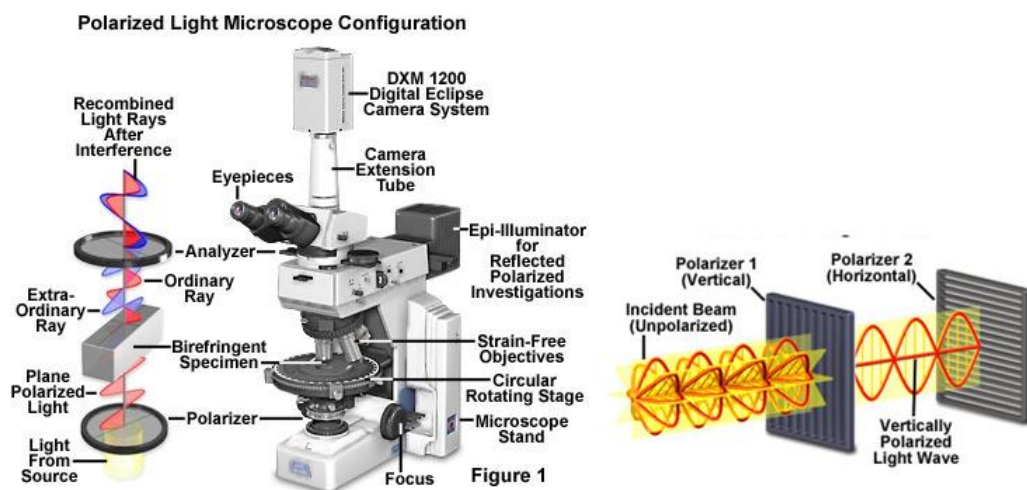


Figure 35 Configuration of polarized light microscope

All the samples were observed with a Leitz Orthoplan polarizing microscopy equipped with a Mettler FP82 hot stage and a FP80 central processor.

Differential scanning calorimetry (DSC) is used as a complimentary technique to POM and to X-ray diffraction. DSC is used to confirm whether the changes observed by POM, arise from phase transitions. This is a technique which allows studying the thermal transition of a material by measuring the amount of energy (heat), which is proportional to the enthalpy of the transition (ΔH), absorbed or released by a sample as it is heated, cooled or held at a constant temperature¹⁴⁶. The sample measured against a reference sample of which heat capacity is well defined. During a phase transition the sample needs less or more heat to be applied, to maintain the sample at the same temperature of the reference compound, depending on whether the reaction is exothermic (e.g. melting) or endothermic (e.g. crystallization). The transition is defined by the free energy which can be expressed as:

$$\Delta G = \Delta H - T\Delta S$$

where ΔH is the change of enthalpy of the system, ΔS is the change of the entropy and T is the absolute transition temperature (usually the onset temperature). At the transition $\Delta G = 0$, so ΔS can be determined and a peak will be present on the DSC profile which is represented by curves of heat flux versus temperature or versus time. The enthalpy can be calculated by integrating the peak. When phase transitions occur without a change in entropy they are referred to as second order and are accompanied by a discontinuity in heat capacity (ΔC_p) which is the second derivative of G with respect to T at constant pressure. *Glass Transition* (T_g) temperature is associated with a change in the baseline. (In liquid crystals the temperature where a phase is frozen also called T_g but it is different from the term used for polymers.) In liquid crystals, transitions between phases are referred to as weakly first order, however second order transitions are not uncommon (e.g. SmC-to-SmA). Large enthalpies correspond to first order transitions e.g. *melting transition* (crystal-to-mesophase or to-isotropic liquid), transition between two mesophases and in some cases at the *clearing transition* (mesophase-to-isotropic liquid). When a crystal melts to an isotropic liquid at T_i , but on cooling crystallises at lower temperature T_K , ($T_K < T_i$) the liquid is called *supercooled* and is the result of kinetic stabilization. If a material exhibits a mesophase during the heating process, when the entropy of the system increases due to loss of positional and orientational ordering, and also on cooling, then this phase is thermodynamically stable. Such a phase is described as *enantiotropic* and the enthalpies are reproducible. If a mesophase only appears on cooling (thermally less stable), due to the hysteresis at the crystallization temperature, which is the product of kinetic stabilization, it is described as *monotropic* (Figure 36). In this case the clearing point is reversible. When materials exhibit a number of different mesophases, involving an increase of entropy of the

system, they are called *polymorphic*. Except for the first phase transition temperature, which might be supercooled, the transitions are reversible.

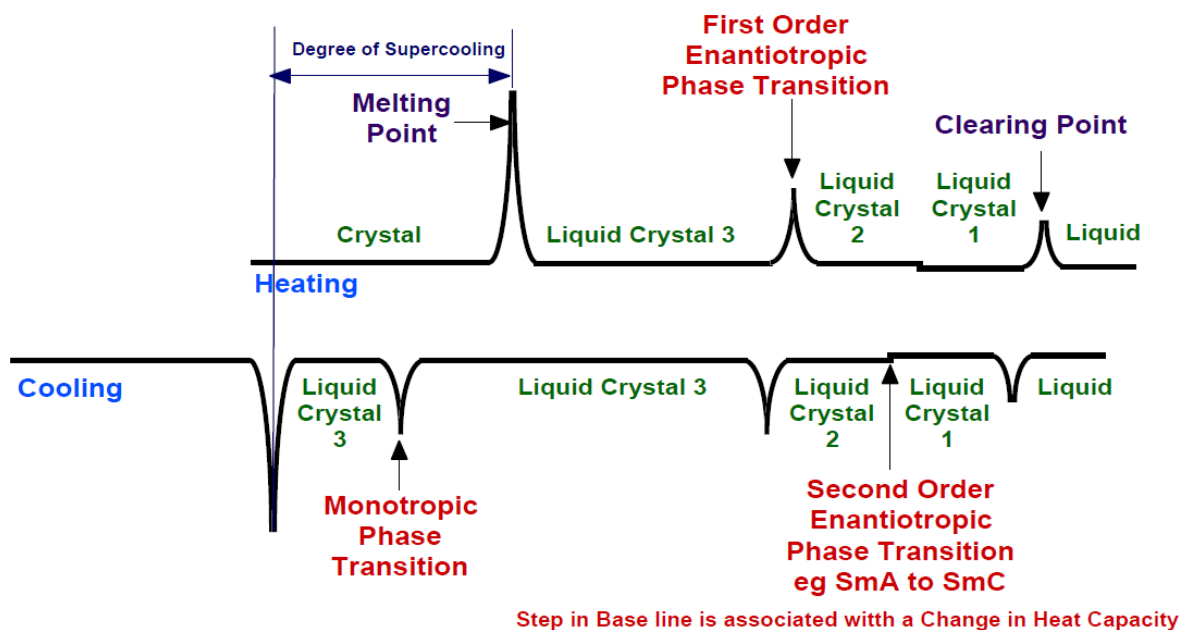


Figure 36 An example DSC trace of Liquid Crystalline Phases

When information is collected from a DSC trace, the transition temperature is indicated at the onset temperature and the T_g is taken as the mid-point of the change. DSC curves were obtained with a Q1000 DSC of TA Instrument at speeds of $2^\circ\text{C}/\text{min}$ and $5^\circ\text{C}/\text{min}$, samples were sealed in an aluminium capsule in air. In most cases the DSC traces, which are recorded on the first and second heating rates, are different but the traces on the cooling and on the 2nd and 3rd heating, are reproducible. The DSC traces of the trimers and dendrimers are presented on the 1st heating / 1st cooling and the 2nd heating.

Small Angle X-ray Scattering (SAXS)

X-rays are a form of electromagnetic radiations, with typical wavelength $\lambda < 1\text{nm}$. The X-ray scattering power of atoms is proportional to the atomic number Z . X-ray diffraction picks out any periodically repeating features of a structure, e.g. if a lamellar liquid crystal was positioned with its layers roughly parallel to the incident beam, a series of spots would be observed¹⁴⁷. These result from Bragg reflections of the smectic layers. Bragg's law for X-ray diffraction, which is anticipated from crystal structures, can be used to determine the supramolecular arrangement of the liquid crystals, but not the atomic position because the mesophase exhibits some disorder. Small angle X-ray diffraction ($2\theta < 30^\circ$) can be used to determine mesophase ordering (low order reflections, large distances). The Bragg's law indicates that constructive interference between rays reflected by successive planes will only

occur when the path difference, $2d\sin\theta$, equals an integral number of wavelengths³⁷ of the radiation:

$$2d\sin\theta = n\lambda$$

where d is the spacing between planes, θ is the angle of incidence, n is an integer and λ is the wavelength (=0.154 nm in our experiment). The reciprocal relationship between scattering angle and spacing allows us to interpret the X-ray diffraction from LCs as the following: small distances result in a large scattering angle and large distances result in small scattering angle; long range (crystal-like) order results in intense, sharp peaks and short range (liquid-like) order results in diffuse peaks (halo), e.g. the diffuse maxima of the molten and/or rigid disordered aliphatic chains are generally observed at 4.5 Å. For a nematic phase, diffuse maxima are seen at both small scattering angle and large scattering angle. For smectic phases, a number of equally-spaced small angle ($00l$) pseudo-Bragg peaks can be observed, but generally only the first one or two have observable intensity. The wide angle diffusion peak is similar to that observed for the nematic phase. Distinguishing a SmA from a SmC phase is difficult as the only difference is that the layer distance is smaller in SmC but the variation of the d -spacing can be observed during a temperature change due to the tilt angle variation. For the hexatic phases (SmB^h and the tilted versions: SmF and SmI), the small angle patterns are similar to those from SmA and SmC, but the wide angle peak becomes much sharper due to long range lattice orientational order of the hexatic phases. Most commonly, columnar phases are typical for the molecular arrangement of discotic liquid crystals and the phases are ordered in at least two dimensions. The positional order along the columns can be short range or long range. In case of hexagonal columnar phase in the small angle region the Bragg reflections are present in the ratio: 1, $\sqrt{3}$, $\sqrt{4}$, leading to the indexation $(hk) = (10), (11), (20)$. However, it was shown that polycatenar mesogens also exhibit columnar phases.

The XRD patterns were obtained with two different experimental set-ups. In all cases, a linear monochromatic Cu-K α 1 beam ($\lambda = 0.154$ nm) was obtained using a sealed-tube generator (900W) equipped with a bent quartz monochromator. In all cases, the crude powder was filled in Lindemann capillaries of 1 mm diameter and 10 μ m wall thickness. An initial set of diffraction patterns was recorded with a curved Inel CPS 120 counter gas-filled detector linked to a data acquisition computer; periodicities up to 40 Å can be measured, and the sample temperature controlled to within ± 0.01 °C from 20 to 200°C. Alternatively, patterns were also recorded on an image plate (scanned by STORM 820 from Molecular Dynamics with 50 μ m resolution); periodicities up to 70 Å can be measured. In each case, exposure times were varied from 1 to 24h.

1.3.4.1 Mesomorphism of Trimers

In this section we will describe the mesomorphic behaviour of the trimers through representative samples. Models describing the various supramolecular organizations of these tripedes into multilayered structures are proposed and discussed.

The two homolitic azobenzene derivatives (PG₆AZB₃ (**T6**) and PG₁₁AZB₃ (**T1**)) are mesomorphic, although the phase domain is strongly reduced when the spacer chain-length is shortened: PG₁₁AZB₃ (**T1**) shows a mesophase between ca. 100 and 120°C, whereas the phase becomes monotropic for the shortest homologue (PG₆AZB₃ (**T6**)) (Figure 37). This is the result of the decrease of the melting temperature for the longer spacer, the mesophase-to-isotropic phase transition temperatures remaining unchanged for both compounds. The texture of the enantiotropic phase, shown in Figure 37, is characteristic of a tilted disordered SmC phase as identified by the presence of Schlieren features and striated domains¹⁴⁸.

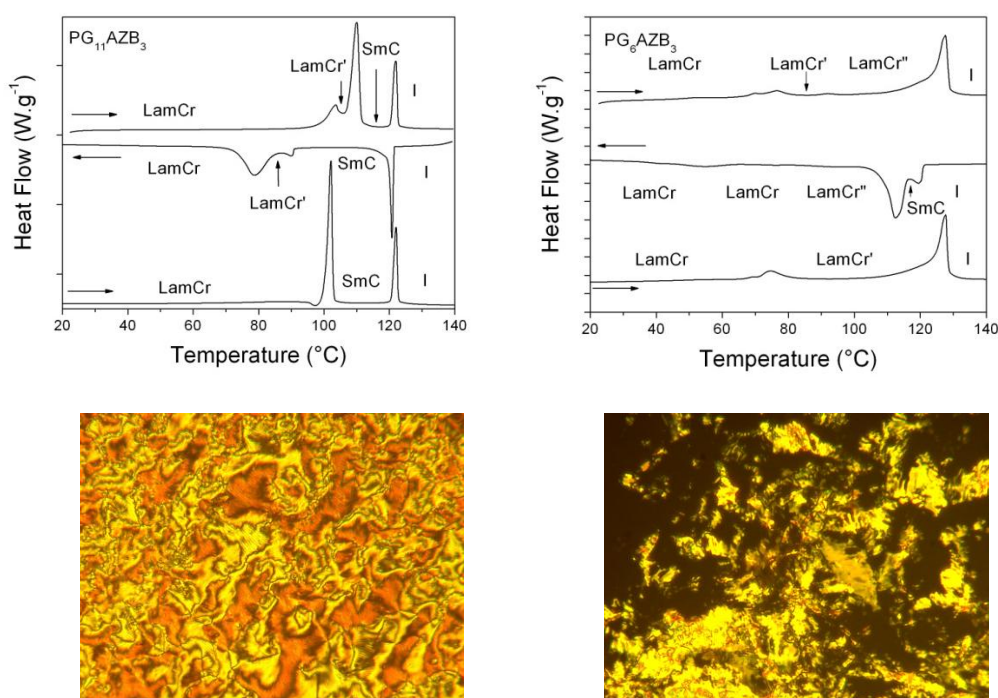


Figure 37 DSC traces (first heating, first cooling and second heating cycle) and POM texture of PG₁₁AZB₃ (**T1**) (left; SmC, T = 116°C) and PG₆AZB₃ (**T6**) (right; SmC, T = 120°C)

The monotropic phase was harder to detect due to its short temperature range (about 3°C only on cooling), and could not be unequivocally assigned. At the isotropic-to-mesophase temperature transition, the formation of small focal conics was sufficient to assign the formation of a SmC phase too. Diffraction patterns of PG₁₁AZB₃ (**T1**) recorded between 105 and 120°C confirmed the LC nature of the mesophase. The diffractogram registered at 110°C, described as

a representative example (Figure 39), shows a sharp and intense small-angle reflection whose position gives a periodicity of 37.25 Å (d_{001}), along with the presence of a large and diffuse signal at ca 4.5 Å associated with the liquid-like lateral ordering of the molten chains and mesogenic cores ($h_{ch}+h_c$). This, along with the POM observation, permits the unequivocal assignment of the mesophase as SmC. Despite its narrow domain of existence, a diffraction pattern of the monotropic mesophase (PG₆AZB₃ (**T6**)) could be obtained at 120°C, in the vicinity of the isotropic liquid: it revealed a single small-angle reflection corresponding to the lamellar periodicity ($d_{001} \approx 60.9$ Å). For both compounds, the SmC mesophase transforms on further cooling into crystalline phases with a highly pronounced layered character and sharp interfaces as testified by XRD, thereafter labelled as LamCr phases (Figure 37). Patterns measured down to room temperature systematically revealed up to four sharp small-angle reflections in the ratio 1:2:3:4, and the occurrence of several sharp large-angle peaks (three to five) indicative of the chain crystallization and 3D crystalline packing.

The sequential exchange of azobenzene by biphenylene groups along the series PG₆AZB₃ (**T6**) → PG₆AZB₂BPH (**T13**) → PG₆BPH₂AZB (**T11**) → PG₆BPH₃ (**T8**) does not significantly modify the liquid crystalline properties, and in particular the SmC-to-I transition temperature is almost constant for all AZB-containing compounds (Table 1). However, for both heterolithic systems, the melting temperatures are depressed by 23 and 20°C with respect to ideal mixtures of similar composition for PG₆AZB₂BPH (**T13**) and PG₆BPH₂AZB (**T11**), respectively,

$$(e.g. \Delta T = \frac{2x T_m(PG_6AZB_3) + T_m(PG_6BPH_3)}{3} - T_m(PG_6AZB_2BPH) = 23^\circ C)$$

where T_m is the melting temperature of the compound (Table 1)). Such a thermal behaviour (of the heterolithic compounds) resembles that associated to microsegregation of eutectic solid phases in mixtures¹⁴⁹, although here the two components can only microsegregate at the molecular level in alternating sub-layers since they are chemically connected. As for technically used liquid crystal mixtures, this melting point depression, conjugated to a quite ideal clearing temperature variation (here between 116 and 124°C, Table 1), logically leads to mesophase induction at intermediate compositions. Thus, both heterolithic tripedes show the SmC phase on a broader range than PG₆AZB₃ (**T6**), whereas mesomorphism is not observed in the homolithic biphenylene-containing compound (PG₆BPH₃ (**T8**)). PG₆AZB₂BPH (**T13**) exhibits an enantiotropic domain (ca. 10°C on heating) which can be supercooled (e.g. down to ca 80°C), whilst the mesophase is monotropic by only 1°C for the conjugate homolog (Figure 38). The SmC phase was confirmed by the observation of typical Schlieren textures (Figure 38) and by XRD (Figure 39).

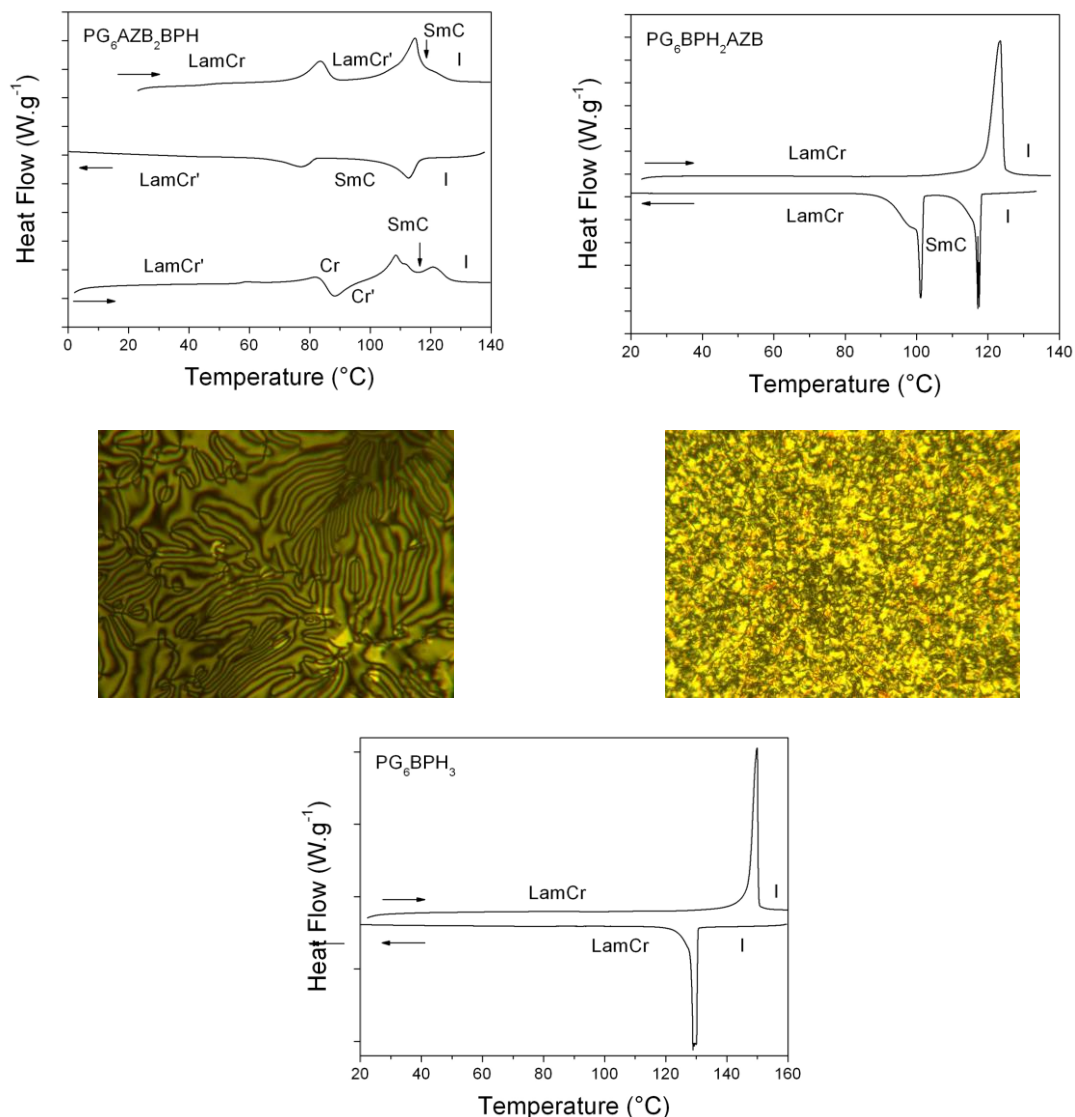


Figure 38 DSC traces (first heating, first cooling and second heating cycle) and POM texture of PG_6AZB_2BPH (**T13**) (left; SmC, $T = 112^\circ C$) and PG_6BPH_2AZB (**T11**) (right; SmC, $T = 117^\circ C$), PG_6BPH_3 (**T8**) (bottom)

Diffraction patterns recorded for PG_6AZB_2BPH (**T13**) (Figure 39) between $115^\circ C$ down to $85^\circ C$ are all identical: they display two intense, sharp, small-angle reflections in the ratio 1:2, indexed as d_{001} (55.1 \AA) for the most intense, and d_{002} for the second order, characteristic of the layering of the molecular arrangement, and the diffuse scattering corresponding to the molten chains and mesogenic cores (Table 2). The abnormal intensity profile in the reflection series, with a relatively intense (002) reflection with respect to the (001) (Figure 39), indicates segregation at the molecular level, with alternation of several high-electronic density sub-layers, associated with the two different mesogens, with low-electronic density sublayers, associated with the aliphatic tails and with the alkyl spacers, respectively (Figure 42).

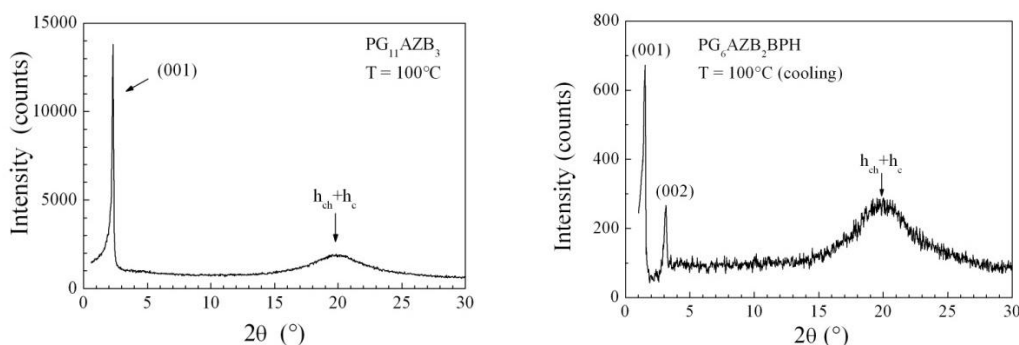


Figure 39 Representative small-angle X-ray patterns of PG₁₁AZB₃ (**T1**) (SmC, 100°C) and PG₆AZB₂BPH (**T13**) (SmC, 100°C).

The respective intensities of first and second order reflections then depend subtly on the respective thickness ratios of these sub-layers, from the electronic density increase within the aliphatic sub-layers due to PG nodes and from the sharpness of their interfaces, *i.e.* the quality of the segregation between mesogens and aliphatic parts. A different intensity ratio may thus be expected for PG₆BPH₂AZB (**T11**), having an opposite number of undecyl and hexyl terminal chains, and therefore a different sub-layer thickness ratio. Unfortunately, such a quantitative comparison (first-to-second order intensity-ratio) could not be performed since only one reflection of low intensity was detected ($d_{001} = 51.2 \text{ \AA}$) during the substantially shortened acquisition, due to the mesophase metastability (monotropic SmC). As for the pure azobenzene derivatives, both heterolithic compounds form low-temperature crystalline phases with a pronounced layering, as evidenced by XRD (LamCr).

The same melting temperature decrease is also observed when the azobenzene units are sequentially exchanged by the stronger cyanobiphenyl mesomorphic promoter along the series PG₆AZB₃ (**T6**) → PG₆AZB₂OCB (**T14**) → PG₆OCB₂AZB (**T12**) → PG₆OCB₃ (**T10**). However, the discrepancy from ideality is much larger here, because of the different chemical structures of both constitutive mesogens (AZB and OCB). Consequently, the induction of mesomorphism is also larger in this series. For instance, the depression is around 11°C for the low OCB-content trimer PG₆AZB₂OCB (**T14**) and reaches even 40°C for PG₆OCB₂AZB (**T12**), giving rise to enantiotropic mesophases domains of 7 and 25°C respectively. In contrast, mesophases of both homolithic compounds are monotropic. Nevertheless, for all the OCB-containing compounds, the mesophases can be supercooled and frozen into a glassy state close to room-temperature (Figure 40). It should be noted that the thermal behaviour of the low OCB-content trimer is however not fully reversible on subsequent heating and exhibits a complicated thermal behaviour with a succession of crystallization and melting events. In contrast to the previous system, PG_zAZB_xBPH_{3-x}, the mesophase exhibited by both heterolithic compounds is different from that of both homolithic compounds: thus, at both extremes, a SmC (for PG₆AZB₃ (**T6**)) and

a N (for PG₆OCB₃ (**T10**), Figure 40) phases are present, whilst a SmA mesophase was induced in both intermediate compounds, readily identified by POM (Figure 40). Noteworthy, the behaviour exhibited in this series reproduced the typical behaviour of classical calamitic mesogens within a homologous series, with the N phase observed at short chain-lengths, SmC phase at longer chain-lengths, and SmA phase at intermediate chain-lengths¹⁵⁰.

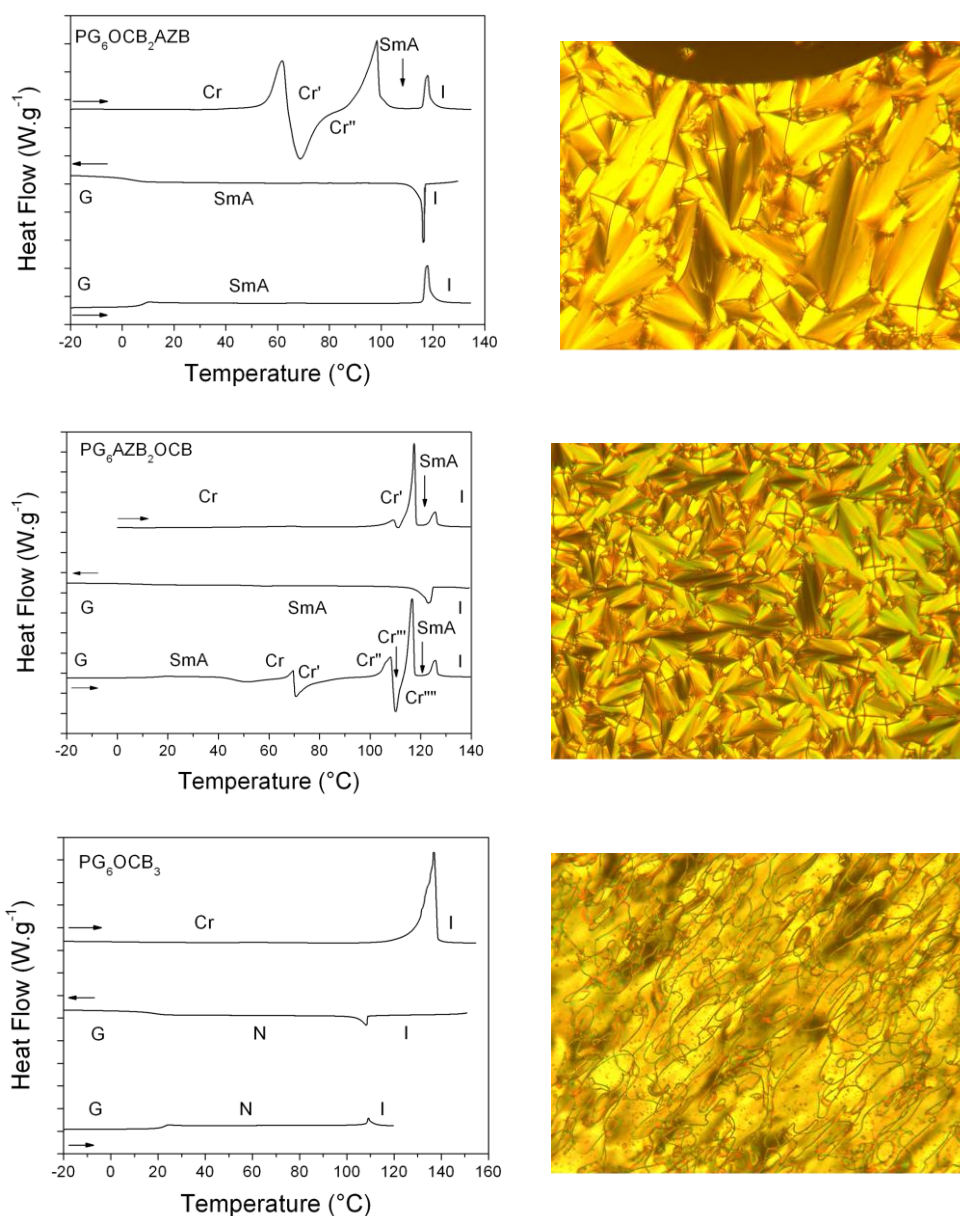


Figure 40 DSC traces (first heating, first cooling and second heating cycle) and POM texture of PG₆OCB₂AZB (**T12**) (top; SmC, T = 115°C), PG₆AZB₂OCB (**T14**) (middle; SmC, T = 117°C) and, PG₆OCB₃ (**T10**) (bottom; N, T = 70°C)

X-ray patterns of both heterolithic samples confirm the smectic nature of the mesophase, and show only one sharp small-angle reflection along the broad and diffuse scattering in the wide-angle range ($h_{ch}+h_c$, Figure 41): layer periodicities are of the order of 30 Å (Table 2) and no

significant variation of the d-spacing with temperature, signifies the absence of significant tilt angle variations. Phase transition temperatures and corresponding enthalpies are calculated from DSC data collected in Table 1. The structural parameters of the mesophases are shown in Table 2.

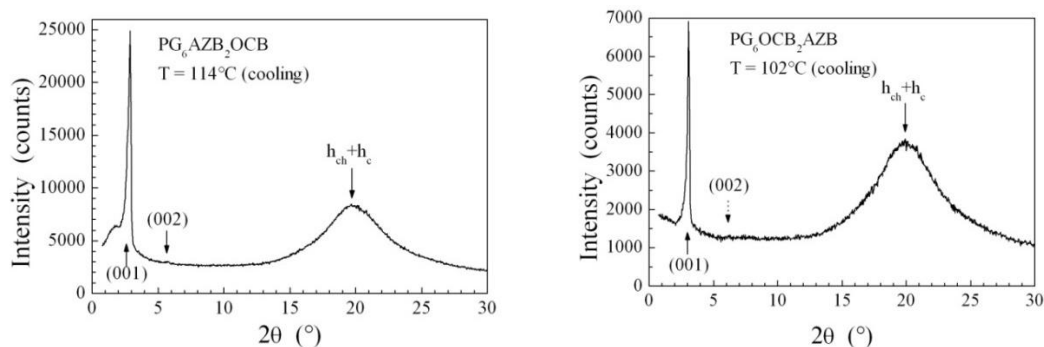


Figure 41 Representative small-angle X-ray patterns of PG₆AZB₂OCB (**T14**) (SmA, 114°C) and PG₆OCB₂AZB (**T12**) (SmA, 102°C).

Table 1. Phase transition temperatures (°C) and corresponding enthalpy ΔH (J.g⁻¹) or specific heat variation ΔC_p (J.g⁻¹.°C⁻¹)^{a,b} in bracket

PG₁₁AZB₃ (T1)	
<i>h</i> ¹	LamCr 100.3 (-) LamCr' 107.2 (83.9) ^c SmC 120.5 (21.2) I
<i>c</i> ¹	I 121.4 (-25.4) SmC 90.8 (-) LamCr' 78.5 (-48.4) ^c LamCr
<i>h</i> ²	LamCr 100.4 (50.9) SmC 120.7 (22.1) I
PG₆AZB₃ (T6)	
<i>h</i> ¹	LamCr 66.0 (8.5) LamCr' 87.9 (1.01) LamCr'' 123.7 (48.0) I
<i>c</i> ¹	I 121.0 (-) SmC 118.0 (-58.7) ^c LamCr'' 79.5 (-0.4) LamCr' 63.3 (-2.5) LamCr
<i>h</i> ²	LamCr 70.6 (10.2) LamCr' 123.9 (55.6) I
PG₆AZB₂BPH (T13)	
<i>h</i> ¹	LamCr 76.6 (14.6) LamCr' 108.3 (37.0) ^c SmC 116.0 (-) I
<i>c</i> ¹	I 115.8 (-13.9) SmC 81.8 (-8.0) LamCr'
<i>h</i> ²	LamCr 75.3 (3.2) Cr 84.6 (-9.8) Cr' 108.6 (37.4) ^c SmC 118 (-) I
PG₆BPH₂AZB (T11)	
<i>h</i> ¹	LamCr 119.3 (64.7) I
<i>c</i> ¹	I 118 (-31.3) SmC 101.9 (-31.1) LamCr
PG₆BPH₃ (T8)	
<i>h</i> ¹	LamCr 147.3 (76.7) I
<i>c</i> ¹	I 130.3 (-76.0) LamCr
PG₆AZB₂OCB (T14)	
<i>h</i> ¹	Cr 105.0 (6.4) Cr' 116.0 (57.8) SmA 122.8 (12.8) I
<i>c</i> ¹	I 124.8 (-12.9) SmA 9.8 (0.25) G
<i>h</i> ²	G 17.4 (0.28) SmA 42.5 (-4.4) Cr 66.8 (4.6) Cr' 70.0 (-24.0) Cr'' 103.7 (19.3) Cr''' 108.0 (-24.9) Cr'''' 114.2 (26.6) SmA 123.5 (11.42) I
PG₆OCB₂AZB (T12)	
<i>h</i> ¹	Cr 55.9 (24.8) Cr' 62.0 (-28.3) Cr'' 91.2 (37.4) SmA 116.0 (9.2) I
<i>c</i> ¹	I 117.1 (-9.2) SmA 3.6 (0.43) G
<i>h</i> ²	G 7.4 (0.45) SmA 116.2 (9.8) I
PG₆OCB₃ (T10)	
<i>h</i> ¹	Cr 133.6 (67.0) I
<i>c</i> ¹	I 108.8 (-3.9) N 18.2 (0.4) G
<i>h</i> ²	G 21.8 (0.4) N 108.4 (2.7) I

^aOnset temperature (DSC), Cr-Cr''''': crystalline, LamCr-LamCr'': lamellar crystalline, SmA/C: smectic A/C, N: nematic phase; G: glassy state; I: isotropic liquid; ^bFirst heating (*h*¹), first cooling (*c*¹), second heating (*h*²); ^cCumulated enthalpy.

Self-organization

The mesogens involved in these compound series are typical calamitic mesogens and therefore smectic mesomorphism was expected. However, due to the specific tripodal architecture and nodes, the conformational freedom is reduced, and thus the layering is substantially constrained. Indeed, the homolothic tripedes are not liquid-crystalline or show only monotropic behaviour, but quite remarkably mesomorphism was promoted in the heterolithic tripedes. As shown above, this promotion is actually due to the depression of the melting points associated to the co-crystallization of segregating mesogens in separated layers, and not to the clearing point variation. Despite the complexity introduced by the additional segregation between mesogens due to 2:1 stoichiometry in heterolithic systems, the accommodation of the different sub-layers areas can take place according to different processes as listed below (Figure 42):

- i) intimate mixing of incompatible mesogens within one single sub-layer alternating with either sub-layers of mixed tails, spacers and nodes (case a), or with differentiated aliphatic sub-layers (case b),
- ii) micro-segregation of the mesogens in alternated layers (AB-type bilayer) either with a large tilt within the sub-layers of the mesogens in minority (case a), or with a strong curvature of the sub-layers interfaces, and a possible evolution toward alternative type of packing (case b),
- iii) and finally a segregation of the mesogens into a three-layer arrangement of the ABB-type.

The latter ABB arrangement (iii) is excluded by X-ray data: the layer periodicities and the intensity modulation of the lamellar reflection series are compatible with either single or bilayer structures only (Table 2). Since the mesogens are all identical, the mixture of mesogens in one layer occurs for PG₁₁AZB₃ (**T1**) only, likely because the length of the terminal chains and spacer are identical, allowing inter-lamellar exchange without affecting aliphatic sub-layers thickness (Figure 42, ia). The threefold nodes randomly distributed in those sub-layers: the supramolecular arrangement results in the simple alternation of mesogenic (AZB moieties are slightly tilted) and aliphatic (tails and spacers undifferentiated) layers (Figure 42, ia). This was clearly proven by the absence of a double periodicity in long-time acquisition X-ray patterns and the resulting molecular areas. However, this arrangement is not valid for the smaller homolithic azobenzene-based compound (**T6**), as the d-spacing corresponds to a periodicity of two mesogenic layers, very likely since tails and spacers, which have different lengths, are forced into identifiable layers of different thicknesses, with an average antiparallel orientation of the nodes (Figure 42, ib). In contrast, the embedding mesogenic sub-layers are undifferentiated.

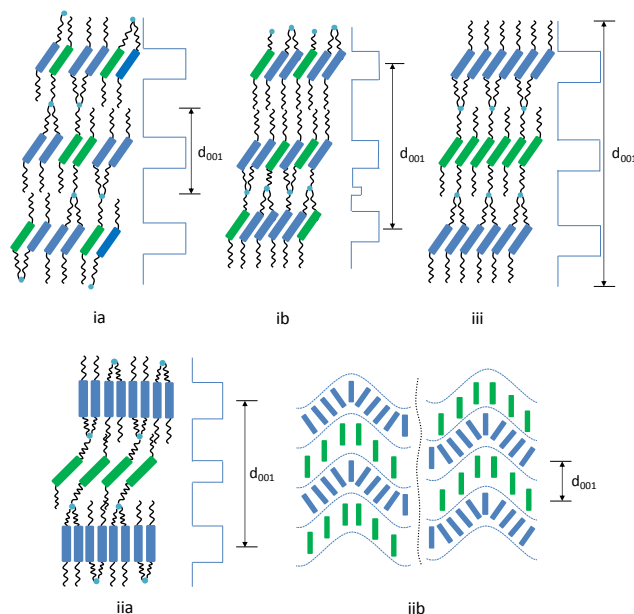


Figure 42 Possible processes of trimers packing in smectic phases (d_{001} : smectic phase periodicity and the blue line is the corresponding schematic electronic density variation). Top row (from left to right): cases ia, ib, iii (not observed here). Bottom row (from left to right): cases iia and iib. For the homolitic systems $PG_{11}AZB_3$ and PG_6AZB_3 , one-colour brick for ia and ib (see text).

For the heterolithic BPH-containing systems, segregation between the two types of mesogens occurs, leading to a more intricate organization as for the latter, with an additional differentiation between two mesogenic sub-layers (Figure 42, iia). Both conjugates give rise to bi-layered organizations with a very high tilt-angle of the low-content component, segregating into a SmC-like sub-layer from non-tilted SmA-like sub-layers of the high-content component. Indeed, the molecular area, identical for both systems, is imposed by the cross-section sum of the high-content mesogen (Table 2). Nevertheless, the slight loss in the molecular area values (10% smaller compared to the estimated cross-section, $\approx \sigma_{CH_2} \approx 22.5 \text{ \AA}^2$, Table 2) suggests that a restricted amount of inter-layer diffusion occurs, simultaneously reducing the tilt angle to 55° (instead of 60° in the ideal case of perfectly segregated mesogens of identical cross-sections).

Unexpectedly, un-differentiation of the layers is total for the OCB-containing materials, as evidenced by the monolayer SmA phase (see d and A_{mol} values, Table 2, and also POM Figure 40), composed of apparently untilted mesogens mixed in the same layer, instead of the bilayer SmC phase formed by the BPH-containing systems just described. Yet, a good segregation between the two different mesogens in separated individual layers is a priori expected because of their strong structural difference. In reality, this result is not in contradiction with the occurrence of segregation on the local scale between the mesogens, but the substitution of the alkyl chain by a cyano group reduces the segregation within the aliphatic medium. This

hypothesis being supported by the fact that PG₆OCB₃ shows the N and not a smectic phase. Therefore, the compensation of the various areas is promoted by a layer undulation process (Figure 42, iib) which facilitates permutation between the mesogens sub-layers. At a larger scale-length, this permutation leads to an average apparent sub-layer made of untilted mixed mesogens similarly to classical SmA-SmC phases found in calamitic compounds.¹⁵¹ In the particular cases of the OCB-containing systems, the suppression of the terminal chains gives the possibility of monolayer packing (SmA1) similar to the mesogens with terminal chains, but also to a bi-layer packing (SmA2) through cyano pairing, or to a mixture of both (SmAd) ¹⁵². The molecular area of the low-OCB content trimer is fully compatible with a SmA1 type, whilst the smaller molecular area of the high-OCB content compound is consistent with a SmAd type, with 30 to 40% of pairing.

Table 2 Structural parameters of the mesophases^a

Compounds		d/Å	V _{mol} /Å ³	a _{AZB} /Å ²	d _{AZB} /Å	ψ _{AZB} /°
		N _L	A _{mol} /Å ²	(a _{BPH} /	(d _{BPH} /	ψ _{BPH} /
		n _{Lmes<i>i</i>}	n _{Ames<i>i</i>}	a _{OCB})	d _{OCB})	ψ _{OCB})
PG ₁₁ AZB ₃	T1	37.2	2820	25.2	10.95	≈ 25
SmC		1	75.7	(-)	(-)	(-)
(T = 110°C)		1	3			
PG ₆ AZB ₃	T6	60.9	2405	26.3	10.6	≈ 30
SmC		2	39.5	(-)	(-)	(-)
(T = 120°C)		2	1.5			
PG ₆ AZB ₂ BPH	T13	55.1	2196	20.0	13.8	0
SmC		2	39.9	(40.0)	6.1	(≈ 55)
(T = 100°C)		1:1	2:1			
PG ₆ BPH ₂ AZB	T11	51.2	2043	40.0	6.95	≈ 55
SmC		2	39.9	(20.0)	(12.3)	(0)
(T = 115°C)		1:1	1:2			
PG ₆ AZB ₂ OCB	T14	30.8	2062	22.5	[12.2]	0
SmA		1	67.1	(22.5)		(0)
(T = 114°C)		1:1	[2+1]			
PG ₆ OCB ₂ AZB	T12	28.8	1715	22.5	[13.3]	0
SmA		1	59.7	(18.5)*		(0)*
(T = 102°C)		1:1	[1+2]			

^ad is the smectic periodicity, N_L is the number of mesogenic layers per smectic period (N_L = 1 for a monolayer and N_L = 2 for a bilayer), n_{Lmes*i*} is the number of sub-layers containing the mesogenic groups of type *i* (*i* = AZB, BPH or OCB) in a smectic layer, V_{mol} is the molecular volume, A_{mol} is the molecular area (A_{mol} = V_{mol}/d), n_{Ames*i*} is the number of mesogenic groups of type *i* covering the area A_{mol} in sub-layers [for OCB-containing trimers, mesogen sublayers are not differentiated and thus appear constituted by both mesogens, see text], a_{*i*} is the mesogenic area, a_{*i*} = A_{mol}/n_{Ames*i*} (*calculated for a monolayer OCB packing, but the small value reveals a change of the packing type, see text), d_{*i*} is the sub-layer thickness d_{*i*} = f_{*i*} × d/n_{Lmes*i*} [average thickness deduced from the sum of both mesogens' volume fractions, f_{*i*}, Table 3], ψ is the tilt angle, ψ = arcos(σ/a_{*i*}) = arcos(d_{*i*}/l_{*i*}) with σ ≈ V_{CH₂}/1.27 and l_{AZB} ≈ 12.2, l_{BPH} ≈ 10.8, l_{OCB} ≈ 11.5 Å.

Table 3 Partial volume fractions (f_i) of chains and mesogens

Code	chains	PG	AllAl	-OCB	-AZB	-	BPH	AllMes
PG ₁₁ AZB ₃	0.6738	0.0321	0.7059	0	0.2941		0	0.2941
PG ₆ AZB ₃	0.6148	0.0379	0.6527	0	0.3473	0	0	0.3473
PG ₆ AZB ₂ BPH	0.5986	0.0409	0.6395	0	0.2500		0.1106	0.3606
PG ₆ BPH ₂ AZB	0.5796	0.0445	0.6241	0	0.1358		0.2402	0.376
PG ₆ BPH ₃	0.5570	0.0487	0.6057	0	0		0.3943	0.3943
PG ₆ AZB ₂ OCB	0.5599	0.0440	0.6039	0.1272	0.2689		0	0.3961
PG ₆ OCB ₂ AZB	0.4840	0.0525	0.5365	0.3033	0.1603		0	0.4636
PG ₆ OCB ₃	0.3719	0.0650	0.4369	0.5631	0		0	0.5631

1.3.4.2 Mesomorphism of PG Dendrimers

In this section we will describe the mesomorphic behaviour of the PG based first generation dendrimers (Figure 43) in comparison to the homologous trimers. The liquid crystalline properties have been characterized by DSC, POM and SAXS, in a similar way as it was presented for the trimers. Finally models of their self-organization will be proposed.

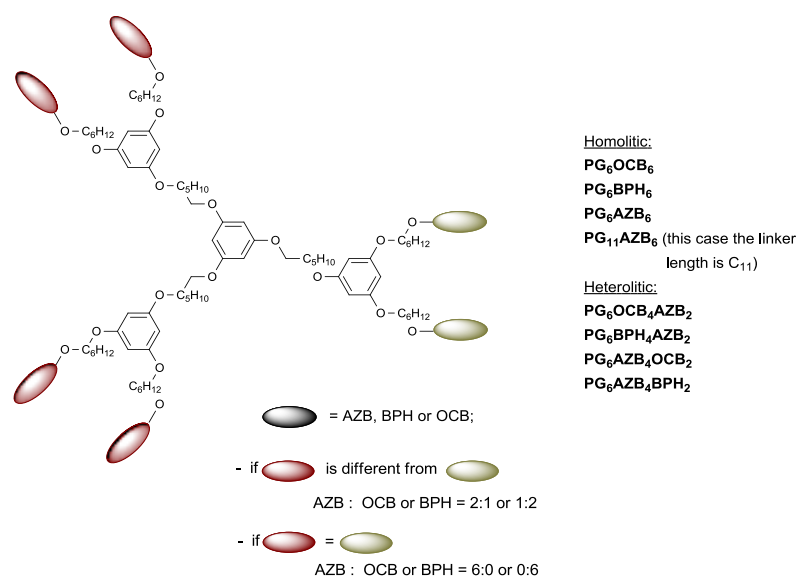


Figure 43 General structure of first generation PG dendrimers

An increase of the generation number strongly stabilized the mesomorphic behaviour with respect to trimers. The first generation dendrimers exhibit mesophases in all cases, including both homolitic and heterolitic structures (Figure 44). The heterolitic PG dendrimers have stable, enantiotropic and in most cases exhibit more than one phase (except of PG₆OCB₄AZB₂ (**Pg11**)) and T_g is increased to above room temperature. The mesophases depend on the structure of the mesogenic components and are different from the trimers as *e.g.* both

tilted phases (SmC) and non-tilted phases (SmA, SmB, SmB^h) are present in AZB/BPH dendrimers but similarly only non-tilted phases are typical for the AZB/OCB dendrimers. Mesomorphism was also induced in the homolithic BPH and AZB dendrimers. Compared to the trimers the temperature range of the mesophases of the PG dendrimers is broadened, essentially, due to the strong depression of the melting point, in most cases, beside a general decrease of the clearing points (Figure 44).

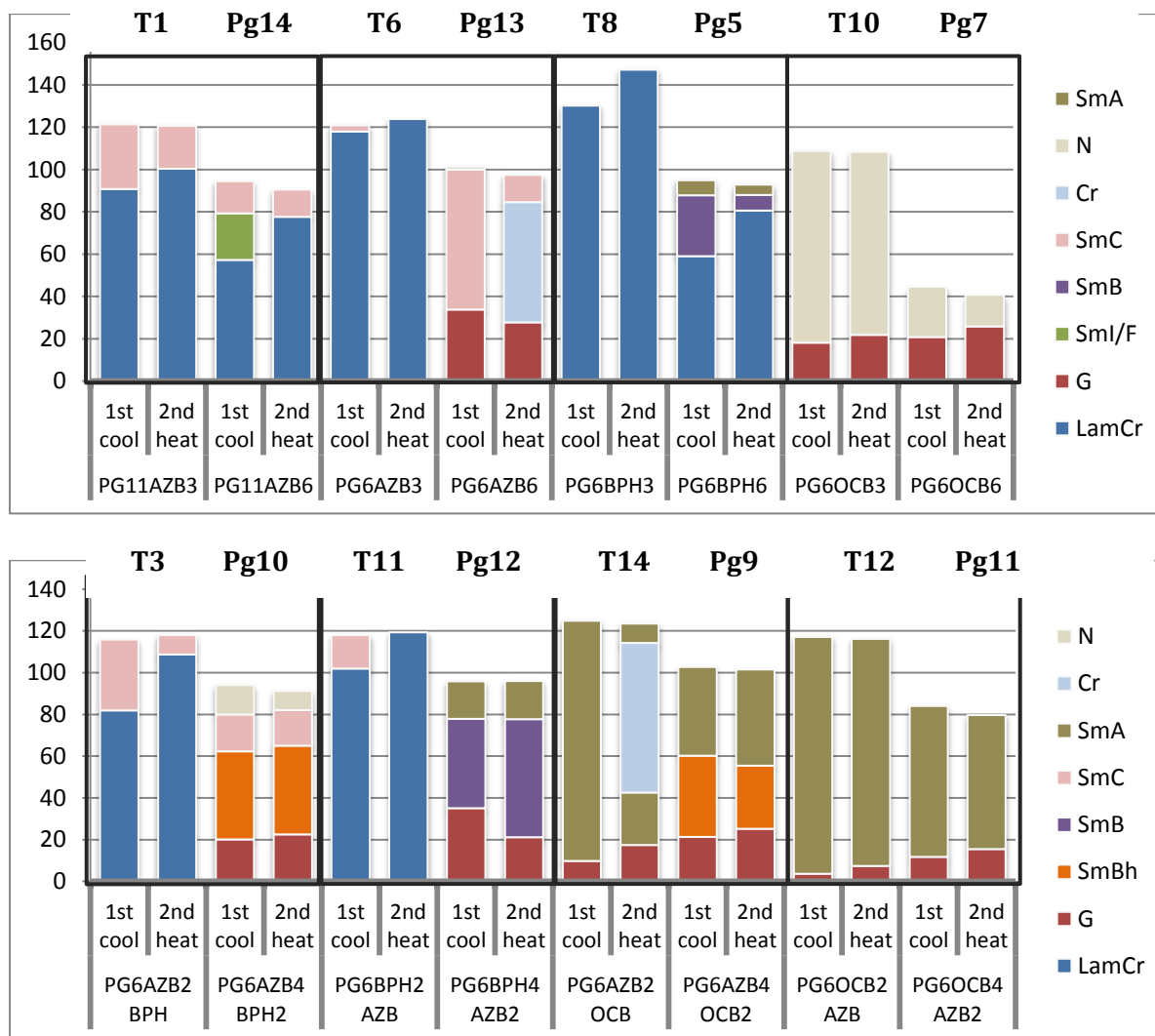


Figure 44 Comparative phase transition diagram of homolithic (top) and heterolithic (bottom) PG trimers and dendrimers; N-Nematic, Sm-Smectic, Cr-Crytsal, LamCr-Lamellar crystal phase, G – glassy state; in each case the first cooling and the second heating cycle is indicated

One of the most drastic improvement in the mesophase temperature range occurred in the shortest homologue of the homolithic azobenzene trimer as a result of increasing the generation number. An enantiotropic SmC phase is induced in the PG₆AZB₆ (**Pg13**). However, on heating the mesophase still occurs only over a short temperature range (about 10°C) but can

be supercooled and frozen into the glassy state at around 34°C. This is not reversible on subsequent heating due to a succession of crystallization and melting events (Figure 45). A nematic phase between SmC phase and isotropic liquid occurs (Table 4) and has been confirmed by POM during cooling from Schlieren textures with Maltese crosses “popping up” indicating the phase change which is in agreement with the DSC trace. The nematic phase is enantiotropic as well but cannot be observed during heating. The phase domain of the homolithic dendrimer with the longer spacer, PG₁₁AZB₆ (**Pg14**), is not increased on heating when compared to the corresponding trimer but also can be supercooled (down to 79°C) and followed by another phase transition into a monotropic SmI/F phase. The POM texture is not very characteristic as mainly small domains and nucleations can be seen (Figure 45).

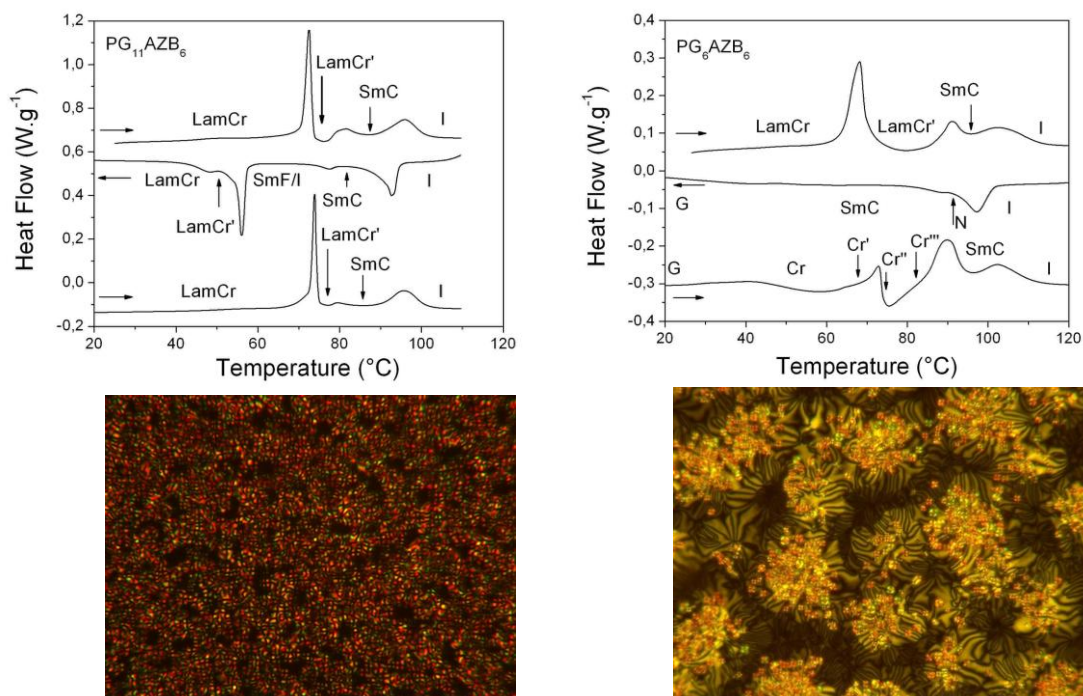


Figure 45 DSC traces (first heating, first cooling and second heating cycle) and POM texture of PG₁₁AZB₆ (**Pg14**) (left; SmC, T = 96°C) and PG₆AZB₆ (**Pg13**) (right; SmC+N, T = 102°C)

In both homolithic dendrimers, PG₁₁AZB₆ and PG₆AZB₆, both clearing (~30°C) and melting temperatures are depressed when compared to the relevant trimers (Table 4). The thermal behaviour of the homolithic dendrimer of the OCB mesogen (PG₆OCB₆ (**Pg7**)) is not very different from the corresponding trimer, showing a nematic phase, easily recognized by POM with typical nematic threads, but there is no melting and the clearing temperature is significantly reduced down to 40°C (Figure 46). As a result the temperature range of the mesophase is reduced but the phase can be frozen into the glassy state, similarly to the trimer. The thermal behaviour of the homolithic BPH dendrimer (PG₆BPH₆ (**Pg5**)) is quite different

from that of its corresponding trimer, since the latter has no liquid crystalline property. Mesomorphism is induced in the (PG₆BPH₆ (**Pg5**)); namely two enantiotropic non-tilted phases, a SmB on a short 6°C range on heating, which can be supercooled down to 59°C, and a high temperature SmA phase, with similar range at 88°C. The liquid crystal phase was observed by POM showing small “Maltese crosses” during nucleation on cooling from the isotropic liquid (Figure 46).

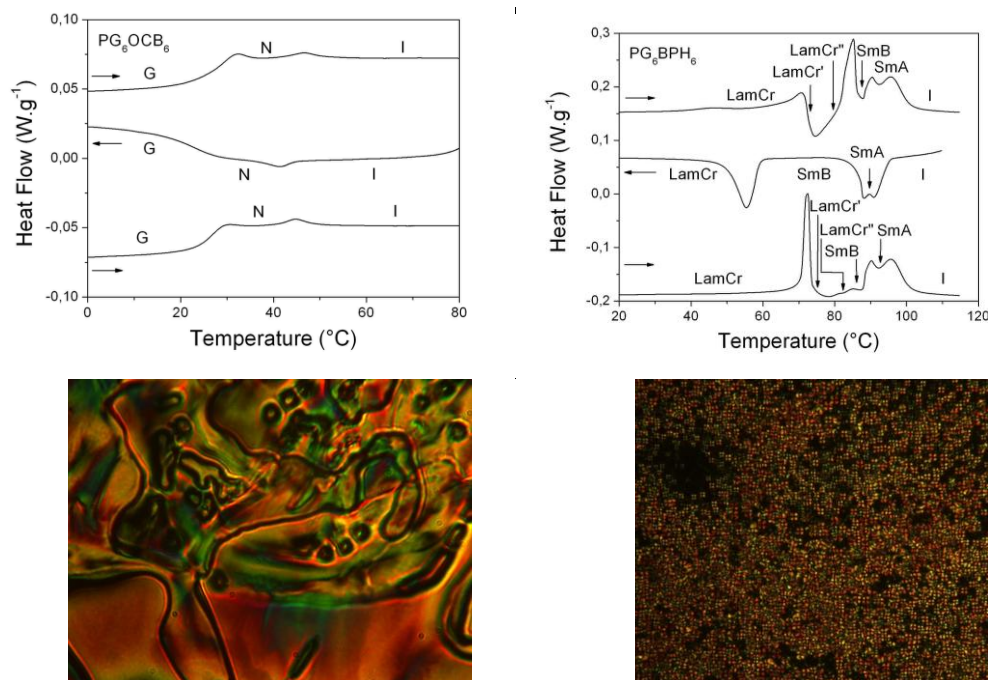


Figure 46 DSC traces (first heating, first cooling and second heating cycle) and POM texture of PG₆OCB₆ (left; N, T = 36°C) and PG₆BPH₆ (right; SmA, T = 95°C)

The phase identities were confirmed by SAXS (Figure 47). The diffractogram of PG₁₁AZB₆ (**Pg14**) recorded at 85°C reveal two sharp small-angle reflections, one intense (001, smectic periodicity 60 Å) and one less intense (002): the typical intensities of the first and second order reflections of smectic phases, and a large diffuse signal at ca 4.5Å, which when combined with POM observations confirms the SmC phase. The diffractogram recorded at 75°C confirms the SmI/F phase. It reveals a sharp relatively intense peak in the diffuse wide-angle signal (typical for hexatic smectic phases), which corresponds to the lateral distances (4.3Å) of the mesogens, whereas the smectic periodicity remains similar to the one of SmC. The diffractogram of PG₆AZB₆ (**Pg13**) also confirms the SmC mesophase and the pattern at 96°C is presented in Figure 47. The diffraction patterns recorded in the mesomorphic temperature range (46-98°C) are all identical and show three small-angle reflections in the ratio 1:2:3 (smectic periodicity 72Å) and a large diffuse peak at a wide-angle associated with molten chains

and mesogens ($h_{ch}+h_{mes}$). The nematic phase between SmC and isotropic liquid can be not confirmed by SAXS but only by POM and DSC (Figure 45). The two enantiotropic phases of PG_6BPH_6 (**Pg5**) (SmA and SmB) were confirmed by a small-angle reflection series with 1:2 ratios (smectic periodicity 42\AA) but with an abnormal intensity profile, where the intensity of the first periodicity (001) is significantly reduced and the 002 reflection is intense. Whereas only one broad diffuse signal is observed for the upper case (SmA), a sharp and broad signal is seen in the lower temperature range, and since periodicity remains similar the signals is attributed to SmB.

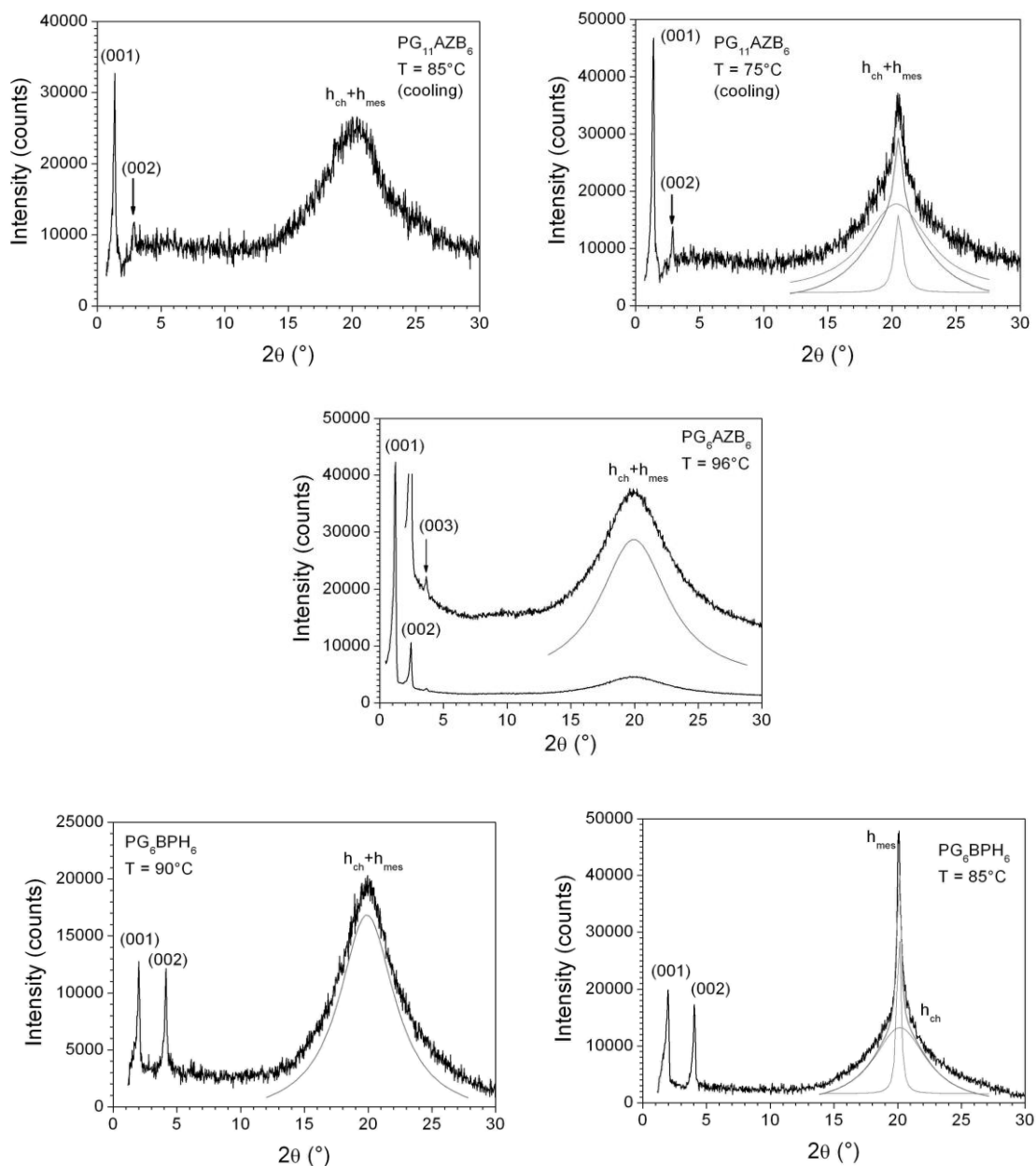


Figure 47 Representative small-angle X-ray patterns of $PG_{11}AZB_6$ (**Pg14**) (SmC, 85°C ; SmI/F, 75°C), PG_6AZB_6 (**Pg13**) (SmC, 96°C) and PG_6BPH_6 (**Pg5**) (SmA, 90°C ; SmB, 85°C)

In the heterolithic dendrimers, T_g was induced in the AZB/BPH systems and in the case of AZB/OCB systems, where T_g was already present in the trimers, this transition temperature was increased by increasing the generation number. The $PG_6AZB_4BPH_2$ (**Pg10**) dendrimer has the richest mesophase of all the PG dendrimers. Three stable enantiotropic phases are present, from hexatic SmB (SmB^h) (non-tilted) through SmC (tilted) to nematic before the transition to an isotropic liquid (Figure 48), where the clearing temperature is decreased by about $15^\circ C$ compared to the corresponding trimer. The mesophase range in the conjugate dendrimer ($PG_6BPH_4AZB_2$ (**Pg12**)) is also increased according to the generation effect, where in the corresponding trimer only a monotropic tilted phase arises over a relatively short temperature range ($16^\circ C$). In this dendrimer two non-tilted mesophase occur: SmA and SmB , which can be frozen into a glassy state at around $35^\circ C$ (Figure 48 and Table 4). For both AZB/BPH heterolithic systems, the melting temperatures are depressed, similarly to the corresponding trimers, by $25^\circ C$ for the higher and $23^\circ C$ for the lower AZB containing dendrimers with respect to the ideal mixtures.

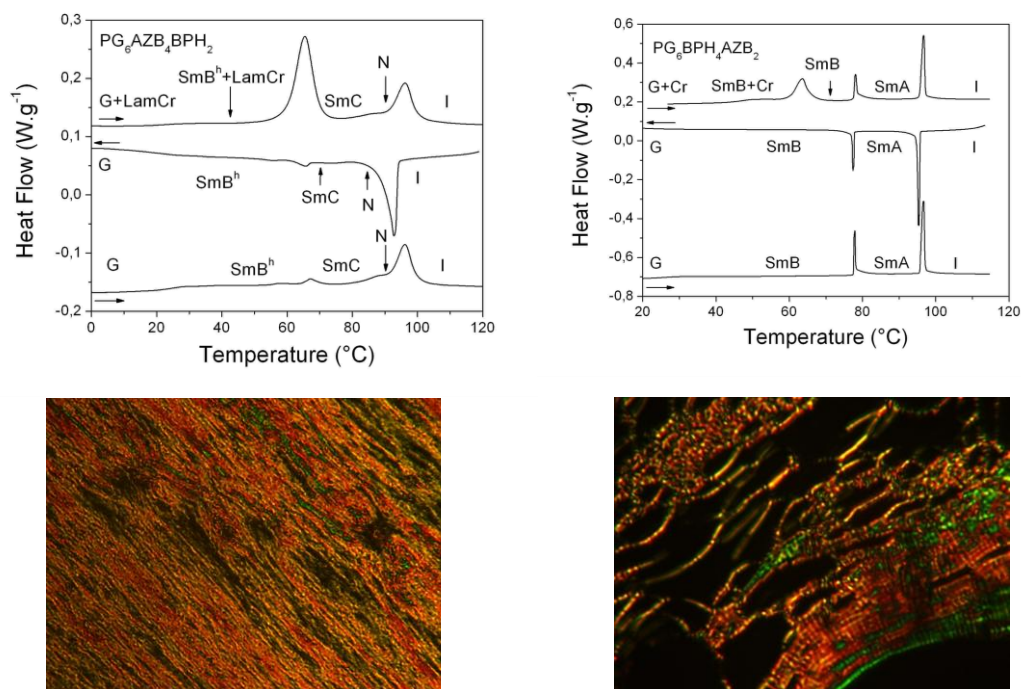


Figure 48 DSC traces and POM texture of $PG_6AZB_4BPH_2$ (**Pg10**) (left; SmC , $T = 77^\circ C$) and $PG_6BPH_4AZB_2$ (**Pg12**) (right; SmA , $T = 95^\circ C$)

The representative diffraction patterns of AZB/BPH dendrimers are shown in Figure 49. The diffractogram of $PG_6AZB_4BPH_2$ (**Pg10**) recorded at $70^\circ C$ shows three sharp small-angle reflections in the ratio 1:2:3 with first order periodicity 68.8 \AA (001) along with a large and diffuse signal at the wide-angle associated with molten chains, confirming the smectic phase.

Only the first order has high intensity. The diffraction pattern at 60°C reveals an additional sharp and intense peak at 4.35 Å (Table 5) which corresponds to the lateral distance of the mesogens in the SmB^h phase. The small-angle reflections did not change. The type of smectic phases is confirmed by the calculated structural parameters (I.3.4.4). The diffraction pattern recorded for PG₆BPH₄AZB₂ (**Pg12**) at 80°C displays two sharp small-angle reflections in the ratio of 1:2 with an abnormal intensity profile - the second order reflection has the same intensity as the (001) reflection - and a large and diffuse signal at ca. 4.5 Å which corresponds to the molten chains and the mesogens. The pattern recorded at 60°C shows a very sharp and intense peak at 4.33 Å (similar to that was observed at the SmB phase of PG₆BPH₆ (**Pg5**)) along with a large and diffuse signal which corresponds to the molten chains which remains the same. This pattern, along with the mesogenic area calculation and POM observation allows the determination of the SmA and SmB phases.

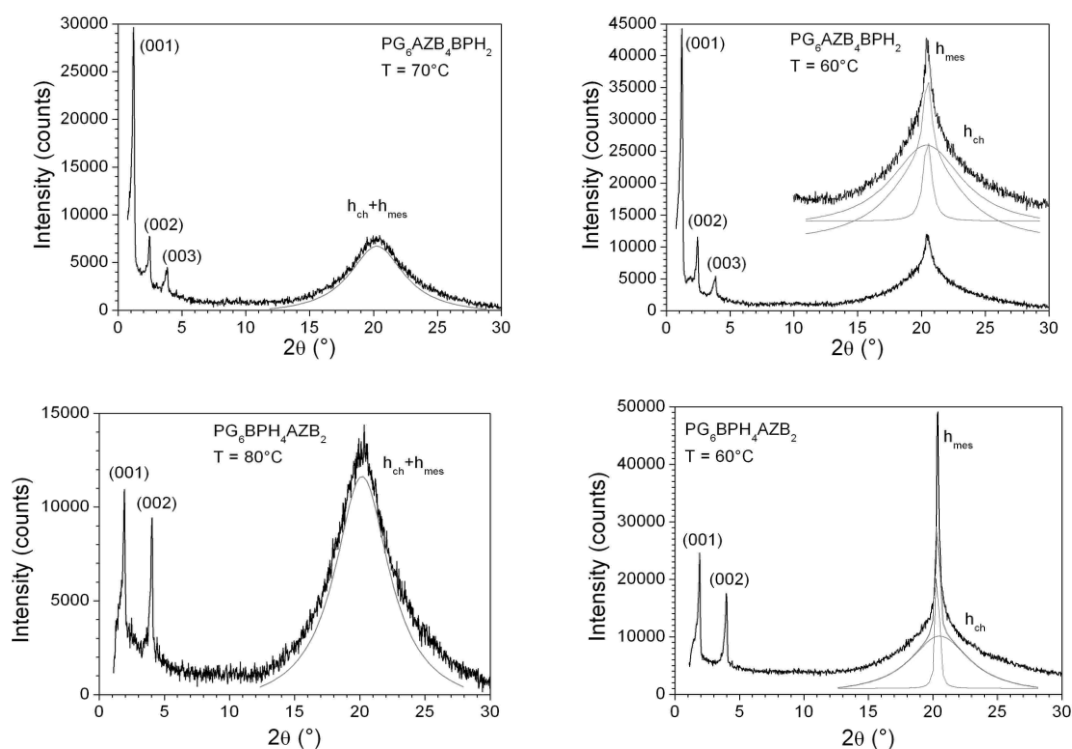


Figure 49 Representative small-angle X-ray patterns of PG₆AZB₄BPH₂ (**Pg10**) (SmC, 70°C; SmB^h, 60°C), PG₆BPH₄AZB₂ (**Pg12**) (SmA, 80°C, SmB, 60°C)

For the OCB/AZB dendrimers, the generation number increase favours the increase of the basic T_g by ~8°C in both PG₆AZB₄OCB₂ (**Pg9**) and PG₆OCB₄AZB₂ (**Pg11**) and the type of the phase is not changed, remaining non-tilted smectic (Figure 44). In both dendrimers the temperature range of the mesophases are shortened due to the decrease in the clearing temperature but for PG₆AZB₄OCB₂ (**Pg9**) the smectic phase is stabilized. In the low OCB

containing dendrimer (**Pg9**) the SmA phase which arises in the first heating cycle, can be supercooled and a further decrease in the temperature results in a transition to the SmB^h phase. Both phases are stable and fully reversible on subsequent heating. The conjugate dendrimer (**Pg11**) has only one mesophase and has a very similar thermal behaviour to the relevant trimer (Figure 50), with increased T_g and depressed clearing temperature, as it was already mentioned. The focal conic textures seen on POM observations (Figure 50) and X-ray patterns (see later) confirmed the mesophase identify.

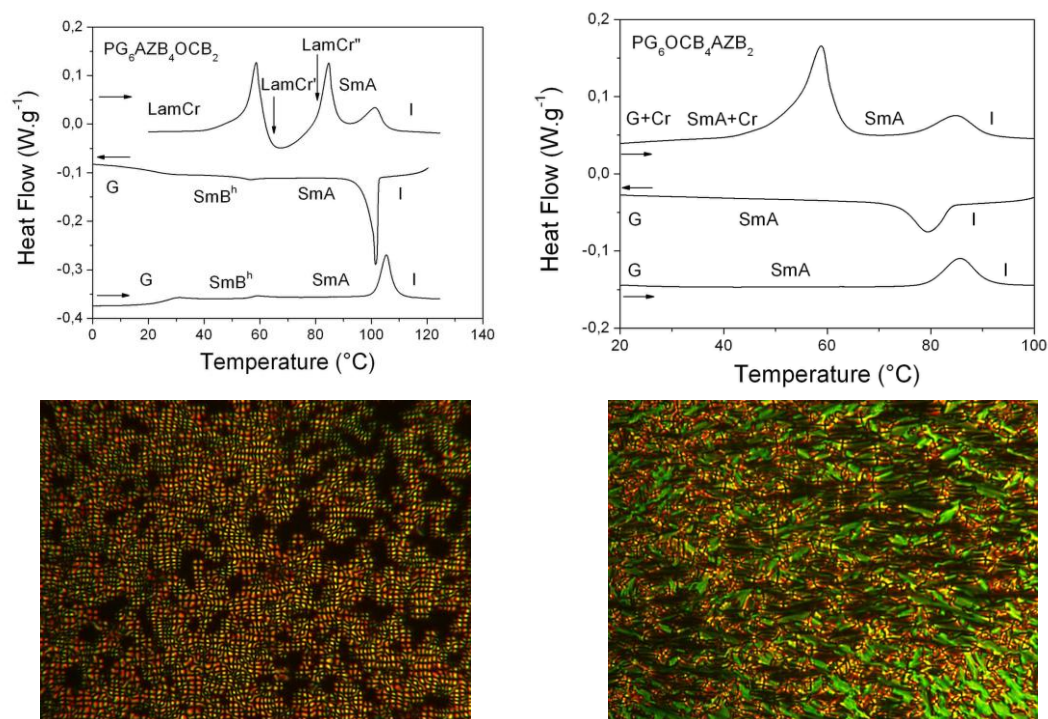


Figure 50 DSC traces and POM texture of PG₆AZB₄OCB₂ (**Pg9**) (left; SmB^h, T = 46°C) and PG₆OCB₄AZB₂ (**Pg11**) (right; SmA, T = 79°C)

The diffraction patterns of AZB/OCB dendrimers are shown in Figure 51. At 90°C, at small-angle two sharp reflections are displayed in the diffraction pattern of PG₆AZB₄OCB₂ (**Pg9**). The $d_{001} = 41.8 \text{ \AA}$ with large intensity and $d_{002} = 20.9$ with low intensity and a large and diffuse signal at the wide-angle area is present, which confirms the SmA phase (along with calculated values (I.3.4.4) and POM observations). With a decreasing in temperature the signal sharpens at the wide-angle region at $h_{mes} = 4.35 \text{ \AA}$, which corresponds to the mesogens in the SmB^h phase, similarly to PG₆AZB₄BPH₂ (**Pg10**). X-ray patterns of PG₆OCB₄AZB₂ (**Pg11**) confirm the smectic phase as shown by two sharp small-angle reflections in the ratio 1:2, along with the broad and diffuse scattering in the wide-angle range which remains the same in the temperature range between 30°C to 80°C. The LC behaviours of all PG systems and X-ray characterization are summarized in Table 5.

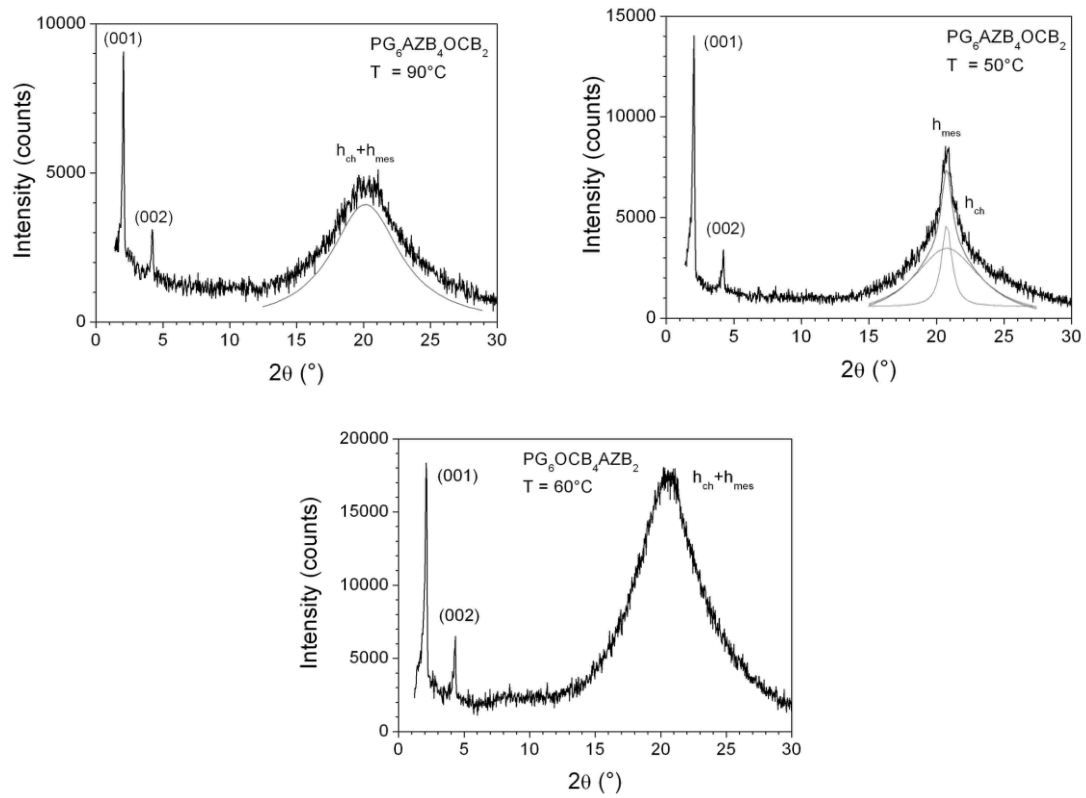


Figure 51 Representative small-angle X-ray patterns of $\text{PG}_6\text{AZB}_4\text{OCB}_2$ (**Pg9**) (SmA, 90°C ; SmB^h, 60°C), $\text{PG}_6\text{OCB}_4\text{AZB}_2$ (**Pg11**) (SmA, 60°C)

Table 4 Phase transition temperatures (°C) and corresponding enthalpy ΔH (J.g⁻¹) or specific heat variation ΔC_p (J.g⁻¹.°C⁻¹)^{a,b} in bracket

PG₁₁AZB₆ (Pg14)	
<i>h1</i>	LamCr 71.0 (28.3) LamCr' 77.3 (7.0) SmC 89.8 (14.2) I
<i>c1</i>	I 94.5 (-15.7) SmC 79.3 (-1.3) SmF/I 57.3 (-31.0) ^c LamCr' 47.5 (-) LamCr
<i>h2</i>	LamCr 72.8 (23.5) LamCr' 77.7 (1.4) SmC 90.5 (15.0) I
PG₆AZB₆ (Pg13)	
<i>h1</i>	LamCr 64.0 (32.1) LamCr' 86.7 (32.0) ^c SmC 96.9 (-) I
<i>c1</i>	I 101.4 (-15.3) N 100 (-) ^c SmC ~ 34 (-) ^d G
<i>h2</i>	G 28 (-) Cr 49.5 (-4.6) Cr' 70.0 (2.6) Cr'' 73.5 (-8.6) Cr''' 84.6 (18.2) SmC 97.5 (8.7) I
PG₆AZB₄BPH₂ (Pg10)	
<i>h1</i>	G + LamCr 22.3 (0.4) SmB^h + LamCr 60.1 (28.6) SmC 79.8 (13.3) ^c N 90.8 (-) I
<i>c1</i>	I 94.0 (-15.5) N ~ 80.0 (-) ^c SmC 62.3 (-0.9) SmB^h 20.1 (0.2) G
<i>h2</i>	G 22.4 (0.3) SmB^h 65.0 (2.0) SmC 82.0 (14.5) ^c N 91.2 (-) I
PG₆BPH₄AZB₂ (Pg12)	
<i>h1</i>	G + Cr 46.6 (0.5) SmB + Cr 60.4 (12.8) SmB 77.6 (4.7) SmA 95.6 (11.1) I
<i>c1</i>	I 95.8 (-12.0) SmA 77.8 (-3.9) SmB 35.0 (-0.4) G
<i>h2</i>	G 21.2 (0.4) SmB 77.5 (4.8) SmA 95.7 (11.9) I
PG₆BPH₆ (Pg5)	
<i>h1</i>	LamCr 64.7 (6.4) LamCr' 74.7 (-7.2) LamCr'' 81.8 (9.6) SmB 88.1 (14.0) ^c 93.0 SmA (-) I
<i>c1</i>	I 95.0 (-15.5) ^c SmA (-) 87.8 SmB 59.0 (-16.0) LamCr
<i>h2</i>	LamCr 70.7 (13.3) LamCr' 80.6 (1.4) ^c LamCr'' 82 (-) SmB 88.0 (16.3) ^c SmA (92.9 (-) I
PG₆AZB₄OCB₂ (Pg9)	
<i>h1</i>	LamCr 54.2 (28.0) LamCr' 62.7 (-15.3) LamCr'' 80.7 (15.0) SmA 94.8 (7.8) I
<i>c1</i>	I 102.6 (-17.4) SmA 60.2 (-0.5) SmB^h 21.3 (0.4) G
<i>h2</i>	G 25.2 (0.4) SmB^h 55.4.0 (1.0) SmA 101.5 (12.5) I
PG₆OCB₄AZB₂ (Pg11)	
<i>h1</i>	G + Cr 16.2 (0.3) SmA + Cr 52.9 (25.4) SmA 77.0 (7.0) I
<i>c1</i>	I 84.0 (-6.9) SmA 11.7 (0.27) G
<i>h2</i>	G 15.4 (0.5) SmA 79.7 (7.1) I
PG₆OCB₆ (Pg7)	
<i>h1</i>	G 24.9 (0.68) N 41.5 (0.6) I
<i>c1</i>	I 44.6 (-0.4) N 20.8 (0.6) G
<i>h2</i>	G 25.9 (0.6) N 40.7 (0.6) I

^aOnset temperature (DSC), Cr: crystalline phase, LamCr-LamCr'': lamellar crystalline phases, SmA/B/C/F/I phases, N: nematic phase, I: isotropic liquid; ^bFirst heating (*h1*), first cooling (*c1*), second heating (*h2*); ^cCumulated enthalpy (unresolved peaks).

Table 5 X-ray characterization of the mesophases

Compounds	$d_{\text{meas.}}/\text{\AA}$	hkl	I (L)	$d_{\text{theor.}}/\text{\AA}$	Phase and parameters	
PG ₁₁ AZB ₆ (T = 85°C)	(Pg14)	60.35	001	VS (sh)	60.4	d = 60.4 Å
		30.2	002	M (sh)	30.2	SmC
		4.5	-	VS (br)	$h_{\text{ch}}+h_{\text{mes}}$	
	(T = 75°C)	60.0	001	VS (sh)	60.0	d = 60.0 Å
		29.9	002	M (sh)	30.0	SmF/I
		4.5	-	VS (br)	h_{ch}	
PG ₆ AZB ₆ (T = 96°C)	(Pg13)	71.9	001	VS (sh)	71.9	d = 71.9 Å
		35.85	002	M (sh)	35.95	SmC
		24.0	003	W (sh)	23.95	
		4.5	-	VS (br)	$h_{\text{ch}}+h_{\text{mes}}$	
PG ₆ AZB ₄ BPH ₂ (T = 70°C)	(Pg10)	68.8	001	VS (sh)	68.8	d = 68.8 Å
		34.3	002	M (sh)	34.4	SmC
		23.0	003	W (sh)	22.95	
		4.5	-	VS (br)	$h_{\text{ch}}+h_{\text{mes}}$	
	(T = 60°C)	72.7	001	VS (sh)	72.65	d = 72.65 Å
		36.2	002	M (sh)	36.3	SmB ^h
		24.3	003	W (sh)	24.2	
		4.5	-	VS (br)	h_{ch}	
PG ₆ BPH ₄ AZB ₂ (T = 80°C)	(Pg12)	43.5	001	M (sh)	43.35	d = 43.35 Å
		21.6	002	M (sh)	21.7	SmA
		4.5	-	VS (br)	$h_{\text{ch}}+h_{\text{mes}}$	
	(T = 60°C)	43.7	001	M (sh)	43.55	d = 43.55 Å
		21.7	002	M (sh)	21.8	SmB
		4.5	-	VS (br)	h_{ch}	
PG ₆ BPH ₆ (T = 90°C)	(Pg5)	42.3	001	M (sh)	42.35	d = 42.35 Å
		21.2	002	M (sh)	21.15	SmA
		4.5	-	VS (br)	$h_{\text{ch}}+h_{\text{mes}}$	
	(T = 85°C)	43.2	001	M (sh)	43.1	d = 43.1 Å
		21.5	002	M (sh)	21.55	SmB
PG ₆ AZB ₄ OCB ₂ (T = 90°C)	(Pg9)	41.8	001	VS (sh)	41.8	d = 41.8 Å
		20.9	002	M (sh)	20.9	SmA
		4.5	-	VS (br)	$h_{\text{ch}}+h_{\text{mes}}$	
	(T = 50°C)	41.35	001	VS (sh)	41.3	d = 41.3 Å
		20.65	002	M (sh)	20.65	SmB ^h
PG ₆ OCB ₄ AZB ₂ (T = 80°C)	(Pg11)	41.6	001	VS (sh)	41.5	d = 41.5 Å
		20.7	002	M (sh)	20.75	SmA
		4.5	-	VS (br)	h_{ch}	
		4.35	-	S (sh)	h_{mes}	
PG ₆ OCB ₄ AZB ₂ (T = 80°C)	(Pg11)	41.6	001	VS (sh)	41.5	d = 41.5 Å
		20.7	002	M (sh)	20.75	SmA
		4.5	-	VS (br)	$h_{\text{ch}}+h_{\text{mes}}$	

1.3.4.3 Mesomorphism of BA Dendrimers

In this section we will describe the mesomorphic behaviour of the BA based dendrimers (Figure 52). Analogous to the previous section (I.3.4.2), the liquid crystalline properties have been characterized by DSC, POM and SAXS but here the mesophases of the BA dendrimers will be compared with the first generation PG dendrimers in order to focus on the impact of branching points on the mesomorphic behaviour (Figure 53).

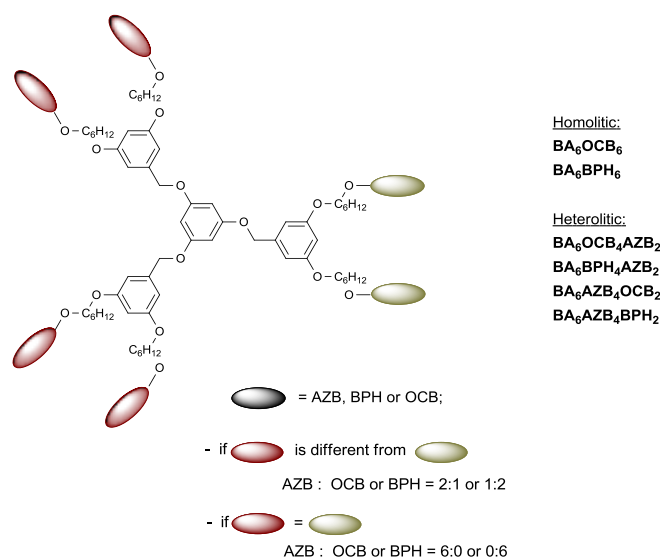


Figure 52 General structure of BA dendrimers

Changing the branching points from phloroglucinol to 3,5-dihydroxybenzyl alcohol (and as a result, shortening the linker between the core and the branching points) increased both the temperature range of the mesophase, due to the increase of the clearing temperature, and the glass transition temperature (Figure 53). In all cases the abundance of the mesophases, which were characteristic of the PG dendrimers, are reduced only in one enantiotropic mesophase in the BA dendrimers. The mesophases similarly depend on the structure. Tilted smectic phases are typical for BPH/AZB dendrimers ($BA_6BPH_4AZB_2$ and $BA_6AZB_4BPH_2$) but a non-tilted smectic phase and lamellar columnar phase are present in the AZB/OCB dendrimers.

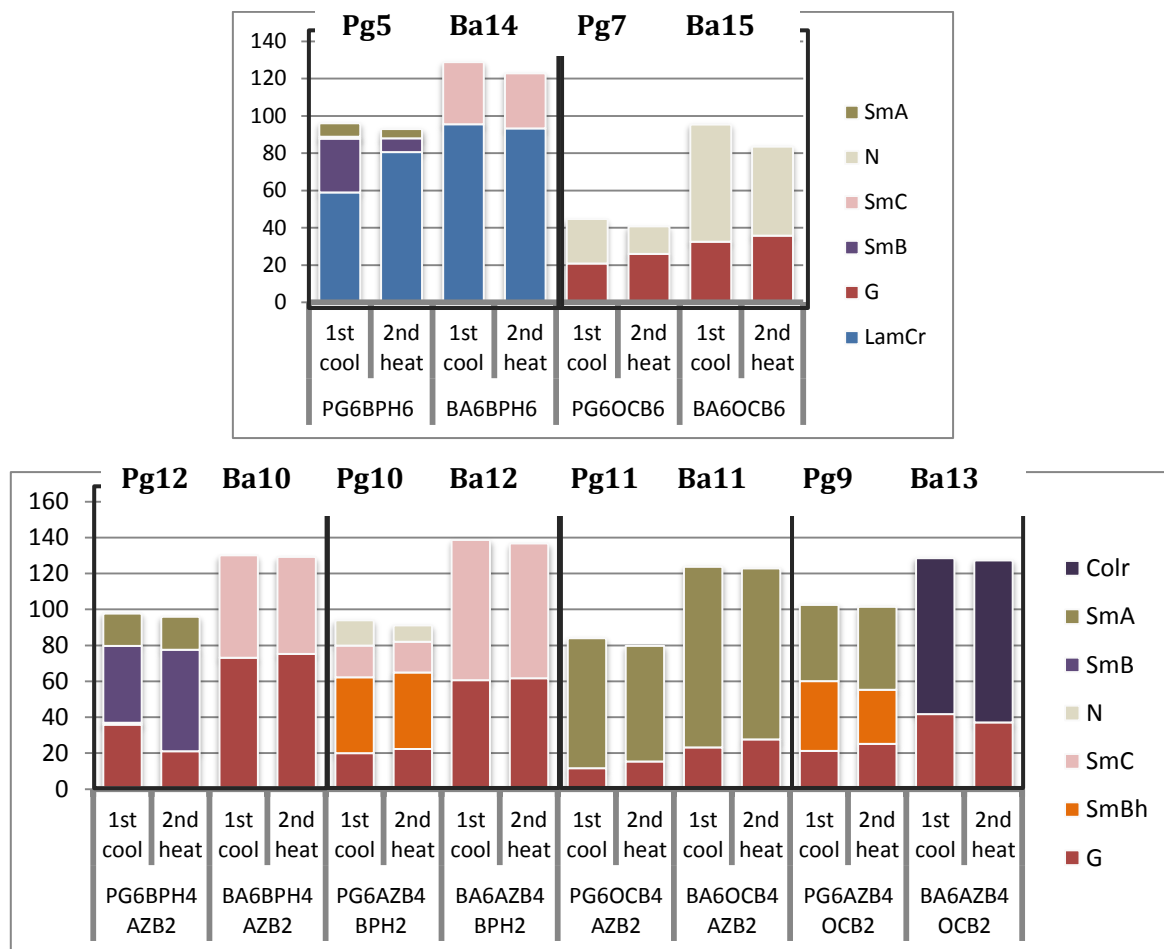


Figure 53 Comparative phase transition diagram of homolithic (top) and heterolithic (bottom) PG and BA dendrimers; N-Nematic, Sm-Smectic, Cr-Crytsal, Colr – Columnar rectangular, LamCr-Lamellar crystal phase, G – glassy state; in each case the 1st cooling and the 2nd heating cycle is indicated

The homolithic BA₆BPH₆ (**Ba14**) dendrimer exhibits tilted smectic liquid-crystalline behaviour contrary to the non-tilted phases of the relevant PG dendrimer. The SmC phase is present with a 16°C range which can be supercooled down to 95°C and remains stable on further heating (Figure 54). The melting temperature on cooling and second heating matches the clearing temperature of the PG₆BPH₆ dendrimer and no T_g is induced in the BA dendrimer either. The mesophase of the PG₆OCB₆ is monotropic but remains stable on the following heating and remains nematic as of the relevant PG dendrimer. The temperature range of the nematic phase is significantly extended and confirmed by POM where textures of the phase were observed (Figure 54). The T_g is increased by about 10°C.

The smectic phase of the BA₆BPH₆ (**Ba14**) dendrimer was clearly confirmed by POM and SAXS as well as the nematic phase of the BA₆OCB₆ (**Ba15**). The diffraction pattern of BA₆BPH₆ recorded at 110°C reveals three sharp small-angle reflections in the ratio 1:2:3 with typical

intensity profiles, with smectic periodicity of 54 Å (001) and a large diffuse signal at 4.5 Å (h_{ch} and h_{mes}) (Figure 54).

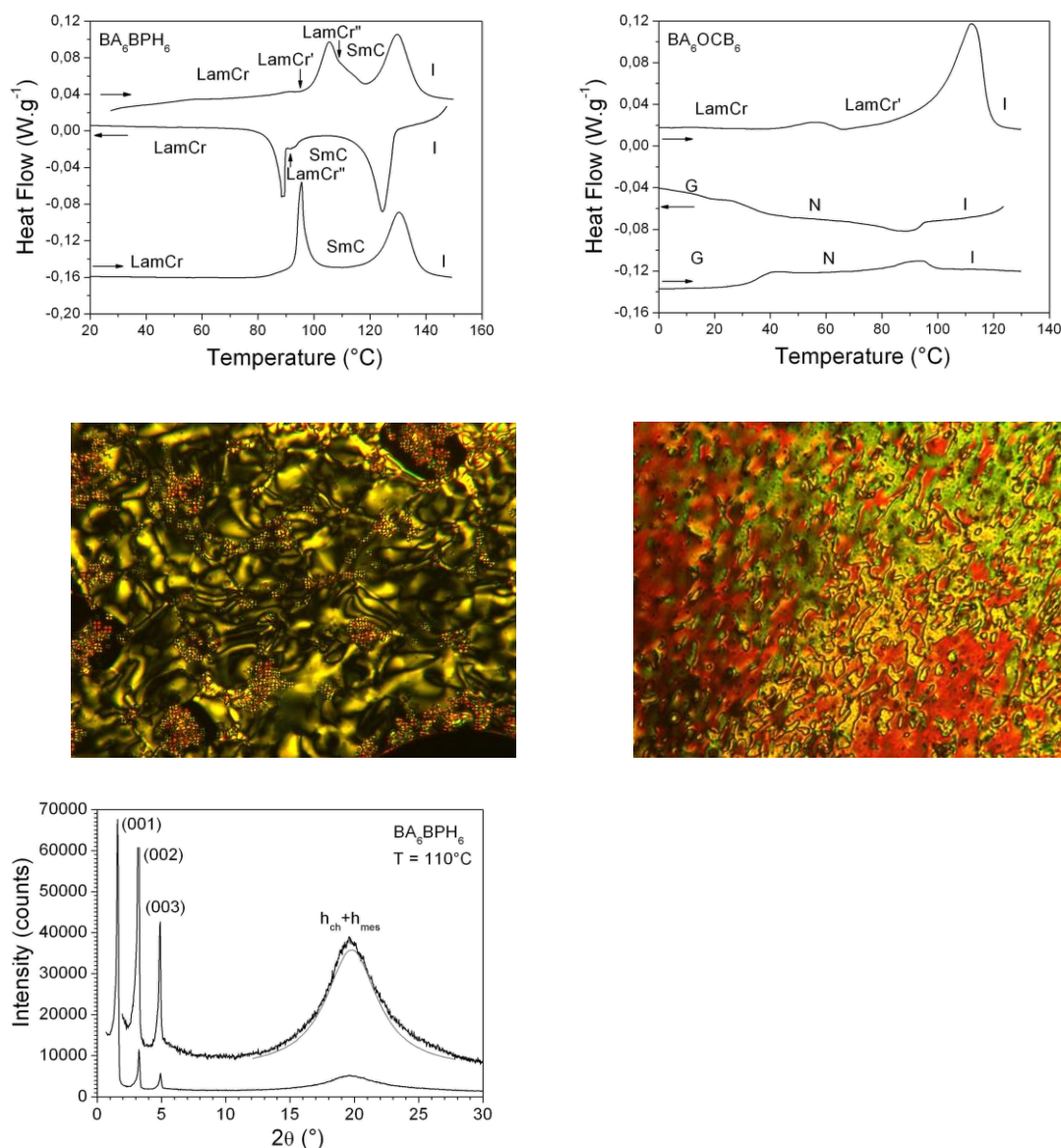


Figure 54 DSC traces (first heating, first cooling and second heating cycle) and POM texture of BA₆BPH₆ (**Ba14**) (left; SmC, T = 123°C) and BA₆OCB₆ (**Ba15**) (right; N, T = 65°C), and a representative small-angle X-ray patterns of BA₆BPH₆ (**Ba14**) (SmC, 110°C)

In both heterolithic AZB/BPH dendrimers the T_g and the clearing temperature are significantly increased (more than 40°C and 35°C, respectively, Table 6, Figure 53) and only one tilted SmC mesophase occurs (identified by the presence of Schlieren features, Figure 55) contrary to the PG₆BPH₄AZB₂ (**Pg12**) dendrimer where two non-tilted phases are present (SmB on lower range and SmA on higher temperature range) and to the conjugate one where three phases occur (SmB^h, SmC, N (Figure 53)). There is no melting temperature but a T_g, increased

far above room temperature (75°C), in the BA₆BPH₄AZB₂ (**Ba10**), which is interestingly at the temperature of the mesophase-to-mesophase transition of the relevant PG dendrimer (Figure 55). In the BA₆AZB₄BPH₂ (**Ba12**) dendrimer the melting temperature, on the first heating, remained about the same (64°C) when compared to the corresponding PG dendrimer but the clearing temperature increased by ~40°C resulting in the increase of the temperature range of the mesophase. The phase can be frozen into the glassy state and is fully reversible on consequent heating. The T_g, similar is to the conjugate, occurs at the mesophase-to-mesophase (SmB^h to SmC) transition of the relevant PG dendrimer (Figure 55).

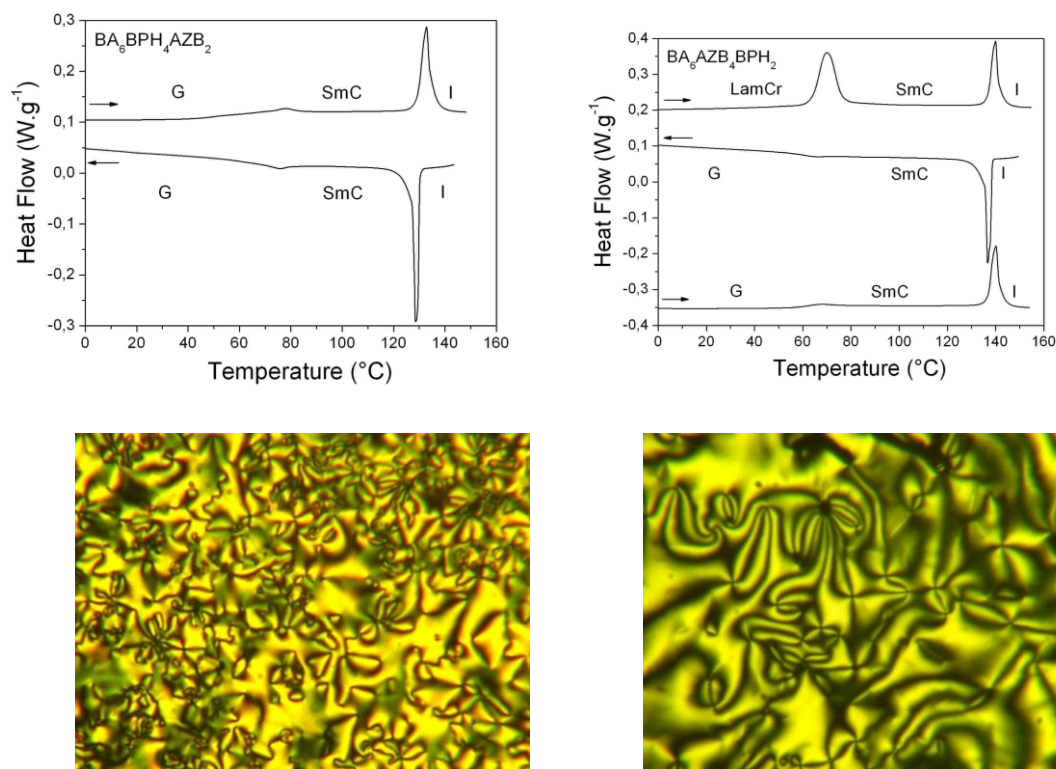


Figure 55 DSC traces (first heating, first cooling and second heating cycle) and POM texture of BA₆BPH₄AZB₂ (**Ba10**) (left; SmC, T = 119°C) and BA₆AZB₄BPH₂ (**Ba12**) (right; SmC, T = 130°C)

In both heterolithic AZB/OCB dendrimers T_g was increased by 12°C and the clearing temperatures were increased by 26°C in the low OCB-content dendrimer (**Ba13**) and by 43°C in the conjugate (**Ba11**), resulting in the increase of phase domains, when compared to the corresponding PG dendrimers (Table 6, Figure 56). The mesophases of both dendrimers can be frozen into the glassy states and remain fully reversible on consequent heating. There is no change in the phase type of the BA₆OCB₄AZB₂ (**Ba11**) when compared to the relevant PG dendrimers and the phase remains SmA, unlike the conjugate (**Ba13**) where a phase with a 2D

rectangular symmetry was detected by SAXS. Based on the molecular structure, the phase is likely lamellar columnar.

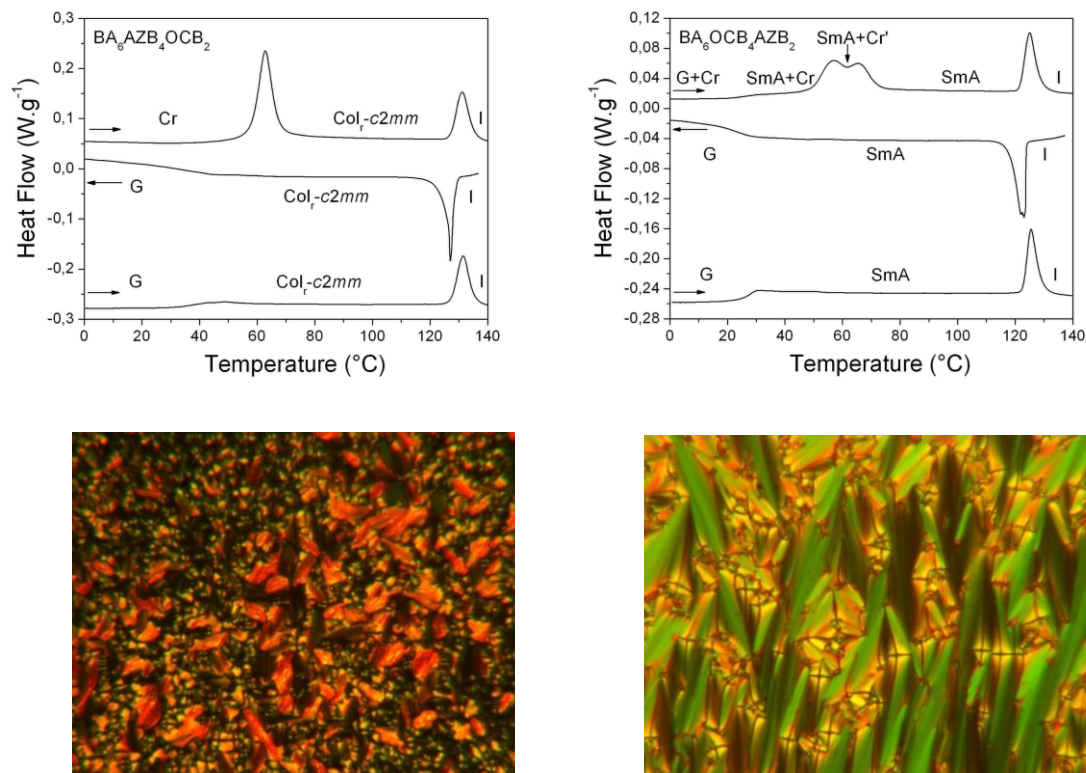


Figure 56 DSC traces (first heating, first cooling and second heating cycle) and POM texture of $BA_6AZB_4OCB_2$ (**Ba13**) (left; Col_r-c2mm , $T = 75^\circ C$) and $BA_6OCB_4AZB_2$ (**Ba11**) (right; SmA , $T = 119^\circ C$)

Table 6 Phase transition temperatures ($^\circ C$) and corresponding enthalpy ΔH ($J.g^{-1}$) or specific heat variation ΔC_p ($J.g^{-1}.^\circ C^{-1}$)^{a,b} in bracket

$BA_6AZB_4BPH_2$ (Ba12)	
<i>h1</i>	LamCr 63.9 (33.5) SmC 136.8 (20.3) I
<i>c1</i>	I 138.7 (-25.0) SmC 60.7 (-0.2) G
<i>h2</i>	G 61.8 (0.4) SmC 136.8 (19.7) I
$BA_6BPH_4AZB_2$ (Ba10)	
<i>h1</i>	G 75.3 (0.2) SmC 129.3 (21.3) I
<i>c1</i>	I 130.1 (-23.4) SmC 73.1 (-0.2) G
<i>h2</i>	G 75.3 (0.2) SmC 129.3 (21.2) I
BA_6BPH_6 (Ba14)	
<i>h1</i>	LamCr 85.0 (-) LamCr' 99.4 (13.7) ^c LamCr'' 107 (-) SmC 122.6 (15.7) I
<i>c1</i>	I 128.8 (-18.2) SmC 95.4 (-) LamCr'' 89.8 (-11.0) ^c LamCr
<i>h2</i>	LamCr 93.2 (11.4) SmC 122.7 (17.5) I
$BA_6AZB_4OCB_2$ (Ba13)	
<i>h1</i>	Cr 58.0 (33.4) Lam - Col_r (<i>c2mm</i>) 127.2 (14.8) I
<i>c1</i>	I 128.5 (-14.1) Lam - Col_r (<i>c2mm</i>) 41.8 (0.2) G
<i>h2</i>	G 37.2 (0.3) Lam - Col_r (<i>c2mm</i>) 127.4 (15.1) I
$BA_6OCB_4AZB_2$ (Ba11)	
<i>h1</i>	G +Cr 28.8 (0.2) SmA+Cr 49.7 (17.0) ^c SmA+Cr' (-) 62.0 SmA 121.7 (11.0) I

c^1 I 123.8 (-12.0) **SmA** 23.2 (0.3) **G**

h^2 **G** 27.8 (0.4) **SmA** 122.8 (11.0) **I**

BA₆OCB₆ (Ba15)

h^1 LamCr 46.3 (2.4) LamCr' 98.9 (37.6) **I**

c^1 I 95.3 (-1.5) **N** 32.5 (0.3) **G**

h^2 **G** 35.8 (0.4) **N** 83.4 (2.0) **I**

^aOnset temperature (DSC), Cr: crystalline phase, LamCr-LamCr': lamellar crystalline phases, SmA/C: smectic A/C phases, N: nematic phase, Col_r: rectangular columnar phase, I: isotropic liquid; ^bFirst heating (h^1), first cooling (c^1), second heating (h^2); ^cCumulated enthalpy.

The phase identities were confirmed by SAXS, in the case of heterolithic dendrimers as well (Figure 57). The diffractograms of the two heterolithic AZB/BPH dendrimers reveal reflections which are typical of smectic phases: four sharp small-angle reflections with 1:2:3:4 ratios and a large and diffuse signal at 4.5 Å. The layer periodicity of BA₆BPH₄AZB₂ (**Ba10**) and BA₆AZB₄BPH₂ (**Ba12**) is 57 Å and 60 Å, respectively (Table 7). This, along with the observation of Schlieren textures (Figure 55), confirms the SmC phase. The diffractogram of BA₆OCB₄AZB₂ (**Ba11**) is also characteristic of a smectic phase, displaying two sharp, small-angle reflection with a layer periodicity of 33.2 Å (001), where the second periodicity is also relatively intense. The SAXS pattern and the focal conic fan textures observed by POM (Figure 56) identify the SmA phase.

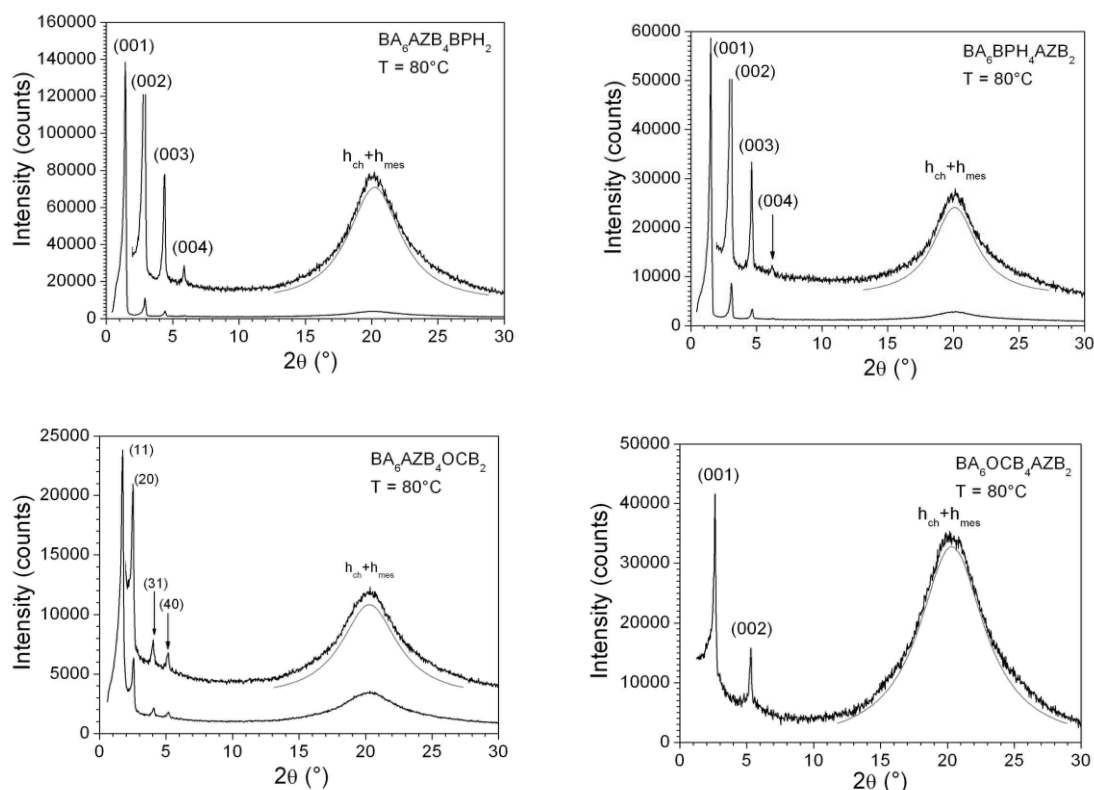


Figure 57 Representative small-angle X-ray patterns of BA₆AZB₄BPH₂ (**Ba12**) (SmC, 80°C), BA₆BPH₄AZB₂ (**Ba10**) (SmC, 80°C), BA₆AZB₄OCB₂ (**Ba13**) (LamCol_r-*c2mm*, 80°C), BA₆OCB₄AZB₂ (**Ba11**) (SmA, 80°C),

The pattern of BA₆AZB₄OCB₂ (**Ba13**) seen at 80°C is characteristic of columnar phase with *c2mm* symmetry, which formed by the breakage of the undulated lamellar phase: Lam-Col-*c2mm*. In the small-angle region, it is possible to identify four sharp diffraction peaks associated with the (11, 11 \cdot), (20), (31, 31 \cdot) and (40) reflections, and a diffuse reflection in the wide-angle region (Figure 57). The lattice parameters of the rectangular cell are a=68 Å and b=74 Å (Table 7).

Table 7 X-ray characterization of the mesophases

Compounds	<i>d</i> _{meas.} /Å	<i>hkl</i>	I (L)	<i>d</i> _{theor.} /Å	Phase and parameters	<i>d</i> /Å	$V_{\text{mol}}/\text{Å}^3$ $A_{\text{mol}}/\text{Å}^2$
BA ₆ AZB ₄ BPH ₂ (T = 80°C) (Ba12)	59.9	001	VS (sh)	59.8	d = 59.8 Å	59.8	4577 76.5
	29.9	002	M (sh)	29.9	SmC		
	19.9	003	W (sh)	19.95			
	14.95	004	W (sh)	14.95			
	4.5	-	VS (br)	<i>h</i> _{ch} + <i>h</i> _{mes}			
BA ₆ BPH ₄ AZB ₂ (T = 80°C) (Ba10)	56.8	001	VS (sh)	56.7	d = 56.7 Å	56.7	4233 74.7
	28.3	002	M (sh)	28.35	SmC		
	18.85	003	W (sh)	18.9			
	14.2	004	W (sh)	14.15			
	4.5	-	VS (br)	<i>h</i> _{ch} + <i>h</i> _{mes}			
BA ₆ BPH ₆ (T = 110°C) (Ba14)	53.8	001	VS (sh)	53.7	d = 53.7 Å	53.7	3973 74.0
	26.8	002	M (sh)	26.85	SmC		
	17.9	003	W (sh)	17.9			
	4.5	-	VS (br)	<i>h</i> _{ch} + <i>h</i> _{mes}			
BA ₆ AZB ₄ OCB ₂ (T = 80°C) (Ba13)	49.9	11	VS (sh)	-	a = 67.8 Å	67.8 /73.8	4272
	33.9	20	M (sh)	-	b = 73.8 Å		
	21.8	31	W (sh)	21.6	S = 5002 Å ²		
	17.0	40	W (sh)	16.95	LamCol- <i>c2mm</i>		
	4.5	-	VS (br)	<i>h</i> _{ch} + <i>h</i> _{mes}			
BA ₆ OCB ₄ AZB ₂ (T = 80°C) (Ba11)	33.2	001	VS (sh)	33.2	d = 33.2 Å	33.2	3623 109.1
	16.6	002	M (sh)	16.6	SmA		
	4.5	-	VS (br)	<i>h</i> _{ch} + <i>h</i> _{mes}			

1.3.4.4 Self-organization of PG and BA dendrimers

In trimers, the PG nodes are drawn within aliphatic sublayers, without expressing any marked micro-segregation ability as compared to the mesogen moieties tendency. In contrast, due to the much voluminous dendritic parts of the dendritic structures (PG and BA dendrimers), the PG and BA node cores behave almost as mesogens whose micro-segregation enters in competition with that of the true calamitic mesogens. Indeed, one may imagine a structure with 4 mesogenic sublayers (BAAB stacking) allowing the total segregation of mesogens, dendrons and aliphatic parts in separated, sublayers, but as pointed out for trimers, more compact structures are observed instead, leading to this competition. Thus, two types of phases with two mesogens' sublayers per layer are observed, depending upon the micro-segregation of the PG/BA, or the micro-segregation of the mesogens dominates.

The phase type 1 (Figure 58) corresponds to the **ia** type of trimers and realizes the micro-segregation of the mesogens, whilst the PG/BA distribute among two sublayers. In patterns, the intensity of the first order is reduced and the one of the second order is enhanced; molecular areas, in the order of 100-110 Å², are determined, in consistency with the cross section of 4 mesogenic units, which are thus distributed between a densely packed sublayers with 4 four mesogens and a loosely packed with the mesogens of the third dendritic branch (the mesogens are tilted with or without correlation of the tilt angle).

This phase type occurs for all OCB containing dendrimers (because of their enhanced micro-segregation in combination with AZB), for none other BA dendrimers (BA should micro-segregate from aliphatic parts more easily than PG), and for the PG dendrimers whose spacer has the same length than the tail of the major mesogen (mixing becomes the easier). Remarkably, among these compounds, the molecular area is maximum for BA₆AZB₄OCB₂ (**Ba12**), leading to the disruption into ribbons of the sublayer of the mesogens in minority. This then result in the apparition of columns over structure and to an overall mesophase organization of the lamello-columnar type with c2mm symmetry (Figure 59).

In the phase type 2 (Figure 60), occurring for all non-OCB containing BA-dendrimers and for the PG dendrimers whose spacer length is different from the tail length of the major mesogen, the dendritic part micro-segregate in a single sublayer, whilst the mesogens equally distribute in two undifferentiated sublayers. Molecular areas in the order of 70-75 Å² are logically found, corresponding to the cross-sections of 3 mesogens. The layers thus contain 3 high electronic density sublayers in consistency with the enhanced third order in patterns. Indeed, up to four orders are visible whilst only two could be seen in the phase type 1, revealing the enhanced confinement in alternating high and low electronic density sublayers.

Table 8 Structural parameters of PG and BA dendrimers

Compounds Phase type (Temperature)	$d/\text{\AA}$ N_L $n_{L\text{mesi}}$	$V_{\text{mol}}/\text{\AA}^3$ $A_{\text{mol}}/\text{\AA}^2$ n_{Amesi}	$a_{\text{AZB}}/\text{\AA}^2$ ($a_{\text{BPH}}/$ a_{OCB})	$n_{\text{LPG/BA}}$ $a_{\text{PG/BA}}/\text{\AA}^2$ $a_{\text{CH}}/\text{\AA}^2$
PG ₁₁ AZB ₆ (Pg14)	60.4	6652	27.5-55*	2
1 (SmC) (85°C)	2 2	110.1 4-2*	-	- 27.5
1 (SmF/SmI) (75°C)	60.0 2 2	6604 110.0 4-2	27.5-55*	2 - 27.5
PG ₆ AZB ₆ (Pg13)	71.9	5422	25.1	1
2 (SmC) (96°C)	2 2	75.4 3	-	75.4 25.1
PG ₆ AZB ₄ BPH ₂ (Pg10)	68.8	4980	24.1	1
2 (SmC) (70°C)	2 2:2	72.4 [2+1]	(24.1)	72.4 24.1
2 (SmB _h) (60°C)	72.65 2 2:2	4944 68.0 [2+1]	22.7 (22.7)	1 68.0 22.7
BA ₆ AZB ₄ BPH ₂ (Ba12)	59.8	4577	25.5	1
2 (SmC) (80°C)	2 2:2	76.5 [2+1]	(25.5)	76.5 25.5
PG ₆ BPH ₄ AZB ₂ (Pg12)	43.35	4671	53.9	2
1 (SmA) (80°C)	2 1:1	107.8 2:4	(26.95)	- 26.95
1 (SmB) (60°C)	43.55 2 1:1	4604 105.7 2:4	52.9 (26.4)	2 - 26.4
BA ₆ BPH ₄ AZB ₂ (Ba10)	56.7	4233	24.9	1
2 (SmC) (80°C)	2 2:2	74.7 [1+2]	(24.9)	74.7 24.9
PG ₆ BPH ₆ (Pg5)	42.35	4358	25.7-51.4*	2
1 (SmA) (90°C)	2 2	102.9 4-2	-	- 25.7
1 (SmB) (85°C)	43.1 2 2	4343 100.8 4-2	25.2-50.4* -	2 - 25.2
BA ₆ BPH ₆ (Ba14)	53.7	3973	24.7	1
2 (SmC) (110°C)	2 2	74.0 3	-	74.0 24.7

Compounds Phase type (Temperature)	$d/\text{\AA}$ N_L n_{L,mes_i}	$V_{mol} / \text{\AA}^3$ $A_{mol} / \text{\AA}^2$ n_{A,mes_i}	$a_{AZB} / \text{\AA}^2$ ($a_{BPH}/$ a_{OCB})	$n_{LPG/BA}$ $a_{PG/BA} / \text{\AA}^2$ $a_{CH} / \text{\AA}^2$
$PG_6AZB_4OCB_2$ (Pg9) 1b (SmA) (90°C)	41.8 2 1:1	4745 113.5 4:2	28.4 (56.8)	2 - 28.4
1b (SmB _h) (50°C)	41.3 2 1:1	4609 111.6 4:2	27.9 (55.8)	2 - 27.9
$BA_6AZB_4OCB_2$ (Ba13) 1b*** (LamCol _R) (80°C)	33.9** 2*** 1:1***	4272 126 4:2***	31.5 (63.0)***	2 - 31.5
$PG_6OCB_4AZB_2$ (Pg11) 1a (SmA) (60°C)	41.54 2 1:1	4003 96.4 4:2	48.2 (24.1)	2 - -
$BA_6OCB_4AZB_2$ (Ba11) 1a (SmA) (80°C)	33.2 2 1:1	3623 109.1 4:2	54.6 (27.3)	2 - -

^a d is the smectic periodicity, N_L is the number of mesogenic layers per smectic period ($N_L = 1$ for a monolayer and $N_L = 2$ for a bilayer), n_{L,mes_i} is the number of sub-layers containing the mesogenic groups of type i ($i = AZB, BPH$ or OCB) in a smectic layer, V_{mol} is the molecular volume, A_{mol} is the molecular area ($A_{mol} = V_{mol}/d$), n_{A,mes_i} is the number of mesogenic groups of type i covering the area A_{mol} in sub-layers [for OCB -containing trimers, mesogen sublayers are not differentiated and thus appear constituted by both mesogens, see text], a_i is the mesogenic or core area, $a_i = A_{mol}/n_{A,mes_i}$,

* internal sublayer with 3rd branches of hexamers

** based on the reflection $d_{lam}=d_{20}$

*** interrupted sublayers of the mesogen in minority

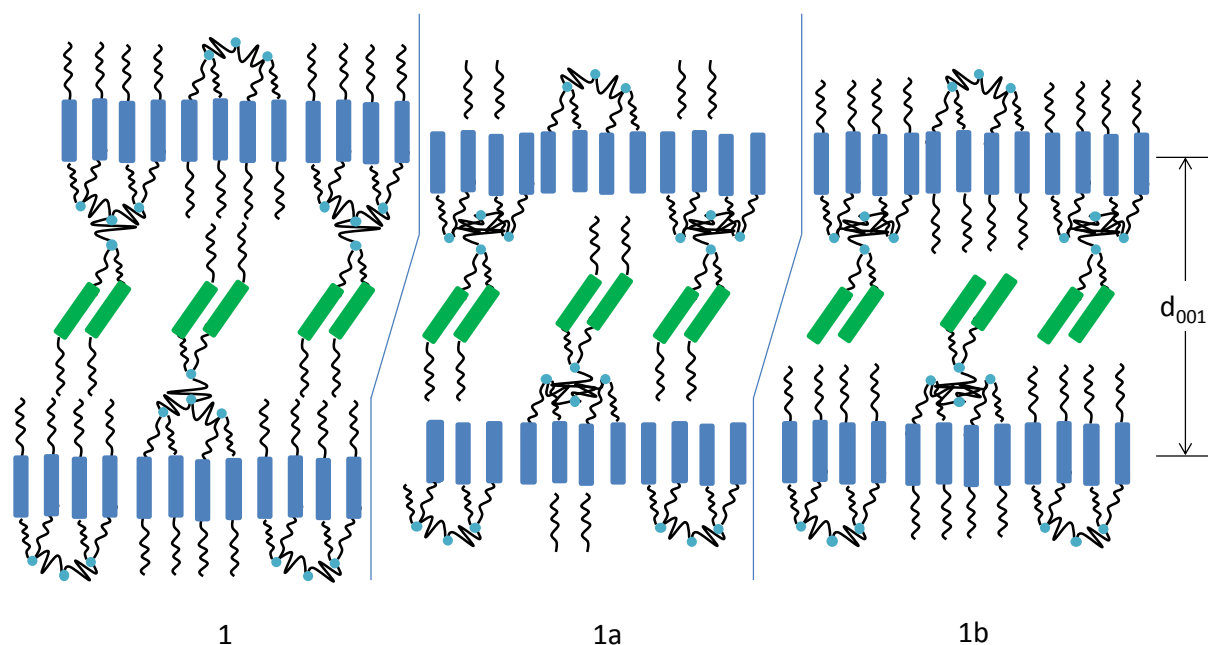


Figure 58 Schematic representation of the structure of phases type 1 (PG_6BPH_6 , $PG_{11}AZB_6$, $PG_6BPH_4AZB_2$), type 1a ($PG_6OCB_4AZB_2$, $BA_6OCB_4AZB_2$) and type 1b ($PG_6AZB_4OCB_2$)

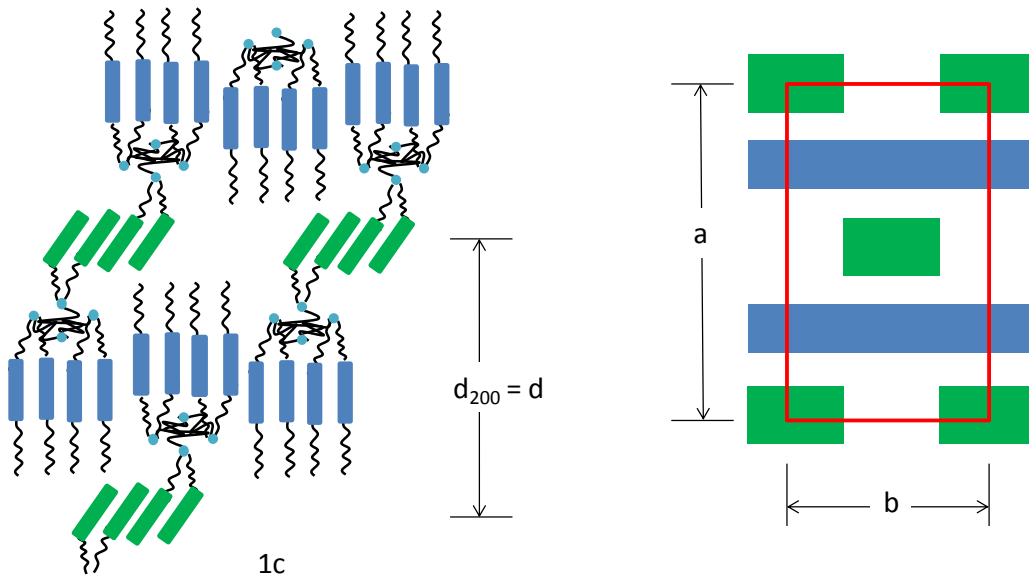


Figure 59 Schematic representation of the structure of the lamella-columnar phase (type 1c) of $(BA_6AZB_4OCB_2)$

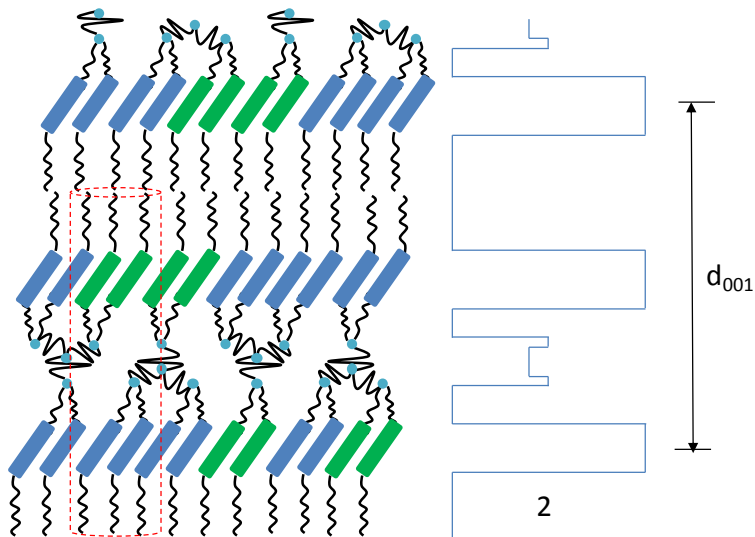


Figure 60 Schematic representation of the structure of phase type 2 (PG_6AZB_6 , $PG_6AZB_4BPH_2$, $BA_6AZB_4BPH_2$, $BA_6BPH_4AZB_2$ and BA_6BPH_6)

1.3.5 Photochemical behaviour

Isomerization of azobenzenes can be tracked by UV/Vis spectroscopy. *Trans* isomers show an intense $\pi\pi^*$ band at $\lambda_{\max}=360$ nm and a weak $n\pi^*$ band in the visible region at $\lambda_{\max}=450$ nm. Azobenzene-type units are the only chromophores in the AZB/BPH trimers and dendrimers. Therefore, in the absence of intra- or intermolecular interactions, the wavelengths of the absorption maxima should not change, while the molar absorption coefficient should increase linearly with increasing the number of azobenzene-type units in the dendrimers. The absorption band of the AZB and the mesogens are separated from each other. This is in agreement with the measured data which are presented on Figure 61 - with AZB/BPH trimers and dendrimers as representative samples. The $\pi\pi$ band of the alkoxy-biphenyl (BPH) is located at $\lambda_{\max}=268$ nm and the aromatic branching points and/or core is below 260 nm.

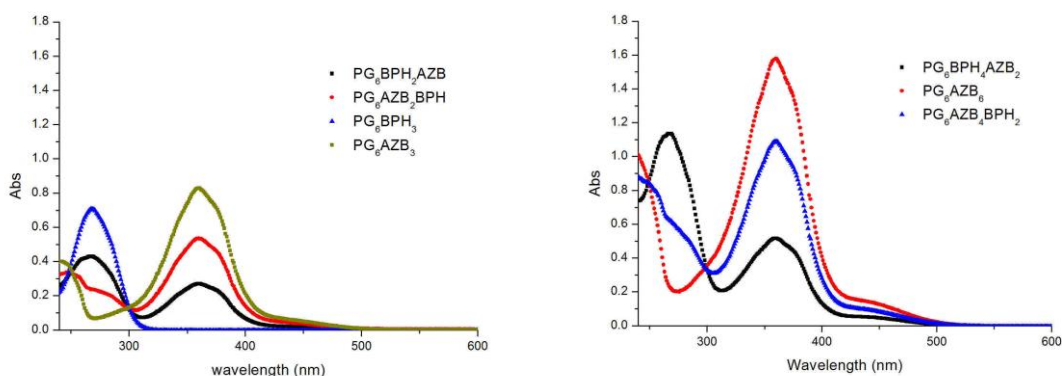


Figure 61 Absorption spectra of PG based AZB/BPH trimers (left) with 0 (only BPH), 1, 2 or 3 AZB units and dendrimers (right) with 2, 4, 6 AZB units, at concentration of 10^{-8} mol/ml in CH_2Cl_2

Comparing the absorption spectra of AZB/BPH and AZB/OCB dendrimers with both a PG and a BA based interior reveals that the $\pi\pi$ band of the alkoxy-cyanobiphenyl (OCB), which is located at $\lambda_{\max}=298$ nm, is red-shifted compared to the BPH due to its electron acceptor group (Figure 62), which is in agreement with the so called push-pull effect¹⁵³. A slight difference in the intensity maxima of $\pi\pi^*$ band of AZB between PG and BA based dendrimers, at same concentration and number of chromophore, is also present. The linear increase of the absorption coefficient with number of azobenzene units is satisfactory if the experimental uncertainty is taken into account. The absorption data for azobenzene trimers and dendrimers, in solution is collected in Table 9.

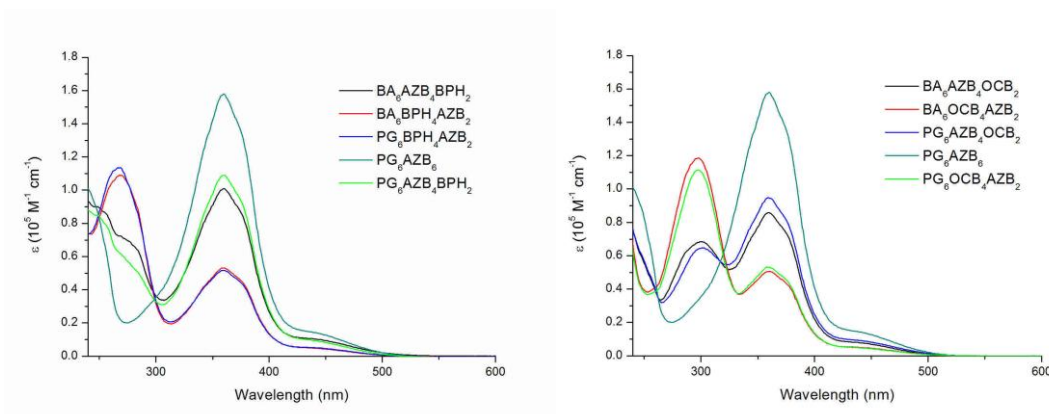


Figure 62 Absorption spectra of PG and BA based AZB/BPH dendrimers (left) and AZB/OCB dendrimers (right), at concentration of 10^{-8} mol/ml in CH_2Cl_2

Absorption, λ_{max} , nm ($\epsilon, 10^4 \text{ M}^{-1} \text{ cm}^{-1}$)			
	$\pi \rightarrow \pi^*$ (AZB)	$\pi \rightarrow \pi$ (BPH)	$\pi \rightarrow \pi$ (OCB)
PG ₁₁ AZB ₃	360 (7.30)		
PG ₆ AZB ₃	360 (8.30)		
PG ₆ AZB ₂ BPH ₁	360 (5.35)	268 (2.38)	
PG ₆ BPH ₂ AZB ₁	360 (2.71)	268 (4.29)	
PG ₆ AZB ₂ OCB ₁	360 (5.15)		298 (3.59)
PG ₆ OCB ₂ AZB ₁	360 (2.32)		298 (5.89)
PG ₁₁ AZB ₆	360 (18.41)		
PG ₆ AZB ₆	360 (15.80)		
PG ₆ AZB ₄ BPH ₂	360 (10.90)	268 (6.22)	
PG ₆ BPH ₄ AZB ₂	360 (5.16)	268 (11.35)	
PG ₆ AZB ₄ OCB ₂	360 (9.46)		298 (6.42)
PG ₆ OCB ₄ AZB ₂	360 (5.31)		298 (11.14)
BA ₆ AZB ₄ BPH ₂	360 (10.09)	268 (7.24)	
BA ₆ BPH ₄ AZB ₂	360 (5.30)	268 (10.91)	
BA ₆ AZB ₄ OCB ₂	360 (8.57)		298 (6.81)
BA ₆ OCB ₄ AZB ₂	360 (5.06)		298 (11.85)

Table 9 Absorption data (Abs maxima, λ_{max} , and molar absorption coefficients, ϵ) of trimers and dendrimers with different proportion of AZB/BPH or OCB with different dendrimer interior (PG or BA) in CH_2Cl_2 at room temperature

1.3.5.1 Photochemical behaviour of trimers

The photochemical behaviour of the trimers containing 1 to 3 photochromic azobenzene groups (PG₁₁AZB₃ (**T1**), PG₆AZB₃ (**T6**), PG₆BPH₂AZB (**T11**), PG₆AZB₂BPH (**T13**), PG₆AZB₂OCB (**T14**), PG₆OCB₂AZB (**T12**)) and higher generation dendrimers (PG₆BPH₄AZB₂ (**Pg12**), BA₆BPH₄AZB₂ (**Ba10**), BA₆OCB₄AZB₂ (**Ba11**)) was measured and investigated by the Fraunhofer Institute for Applied Polymer Research group (Prof. J. Stumpe, Potsdam, Germany) in the frame of Marie Curie Network, "Dendreamers" project.

The photoisomerization process of azobenzenes moieties was studied in solution and, based on these results, the light-induced anisotropy was investigated in thin films as the next step. A Lambda 2 spectrometer (Perkin-Elmer) was used to collect the UV-Vis spectra in chloroform (HPLC grade). Photoisomerization investigations in solution were performed with two different light sources of light: UV lamp at 366 nm (950 μW/cm², Carl Roth) and DPSS laser at 532 nm. The UV-Vis spectra of initial and irradiated solutions were recorded. The Photoisomerization process of the azobenzene moiety of PG₆AZB₂BPH and PG₆AZB₂OCB in chloroform under UV exposure is shown in Figure 63 at different elapsed times.

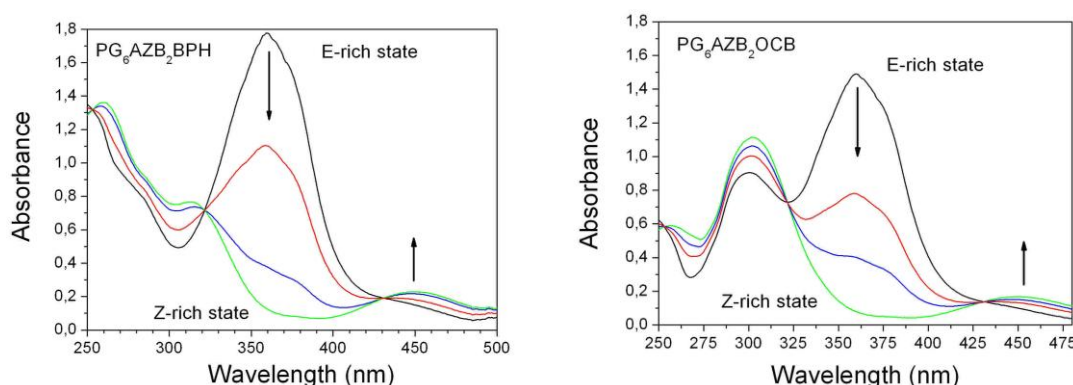


Figure 63 UV-Vis spectra of PG₆AZB₂BPH (**T13**) (left, C=2.1×10⁻⁵ mol.dm⁻³) and PG₆AZB₂OCB (**T14**) (right, C=2.4×10⁻⁵ mol.dm⁻³) in CHCl₃. Arrows indicate the absorption spectra change after UV (366 nm) light exposure.

UV irradiation at 366 nm results in the photoisomerisation establishing a steady state between the thermodynamically stable *trans* (E) isomeric form of azobenzene and its meta-stable *cis* (Z) form. A decrease in the absorption maxima (λ_{\max}) of the $\pi \rightarrow \pi^*$ band between the two isobestic points (322 and 431 nm) and the simultaneous increase in the λ_{\max} of the $n \rightarrow \pi^*$ band is observed (Figure 63). Subsequent Vis exposure (532 nm) results in the establishment of a new steady state rich with *trans* isomers. The UV-Vis spectra of the other trimeric compounds in solution were similar and varied due to different proportions of the AZB to the BPH or OCB

groups.

Films without scattering have to be prepared to be able to measure photoisomerization and photo-orientation properties. Many different films were prepared using solvents in which the material was able to fully dissolve. Most of the materials are very soluble in THF, CHCl_3 , or CH_2Cl_2 (see synthesis part) but in order to prepare spin coated films less volatile solvents are preferred. The following commercially available solvents were tested: 1,1,2-trichloroethane, THF, toluene, DMF, cyclohexane, butanone, chloroform, CH_2Cl_2 and *n*-hexane. Not surprisingly, most of the materials were not soluble in cyclohexane, DMF, butanone and *n*-hexane, but in the remaining solvents as expected. Finally, thin films were prepared using a THF/chloroform mixture (3:2) or chloroform on glass substrates by spin coating (2000 rpm, 2 minutes) and a dynamic method was used providing films with good properties in case of PG_6AZB_3 , $\text{PG}_6\text{AZB}_2\text{OCB}$ and $\text{PG}_6\text{OCB}_2\text{AZB}$.

The self-association of dyes in solution or in thin films is a frequently encountered phenomenon in dye chemistry owing to strong intermolecular van der Waals-like attractive forces between the molecules¹⁵⁴. From the spectral shifts, various aggregation patterns of the dyes in different media have been proposed. The bathochromically shifted J-bands (J for Jelly, one of the first workers who investigated these shifts) and hypsochromically shifted H-bands (H for hypsochromic) of the aggregates have been explained in terms of molecular exciton coupling theory¹⁵⁵. The aggregates according to the shifts in their absorption spectrum are called J or H aggregates. For $\text{PG}_6\text{AZB}_2\text{BPH}$ (**T13**) the absorption maximum of the $\pi \rightarrow \pi^*$ transition of spin-coated film is significant blue shifted up to 336 nm compared to the spectrum recorded in solvent (chloroform) (Figure 64) and the band has an asymmetric shape which indicates H-aggregates of AZBs¹⁵⁶.

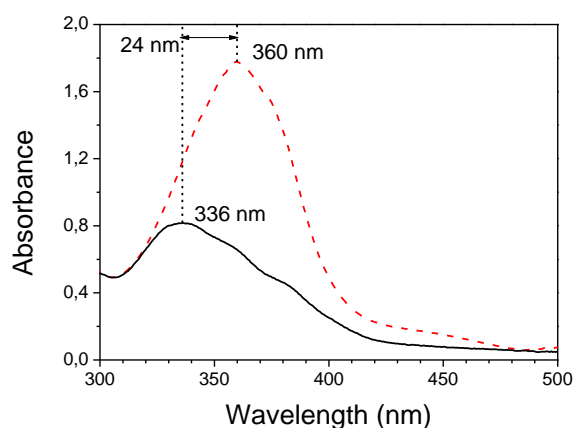


Figure 64 Absorption spectra of $\text{PG}_6\text{AZB}_2\text{BPH}$ in chloroform solution (red-dashed) and in the film (black-solid) with the shift of $\pi \rightarrow \pi^*$ band

The AZBs aggregate in a parallel way (plane-to plane stacking) and is probably promoted by further intra-/intermolecular interactions. A transition to the upper state in parallel aggregates having parallel transition moments and to a lower state in a head-to-tail arrangement with perpendicular transition moments leads to hypsochromic (blue) and bathochromic (red) shifts, respectively (Figure 65). In contrast to PG₆AZB₂BPH (**T13**), PG₆AZB₂OCB (**T14**) and PG₆OCB₂AZB (**T12**) show a much smaller blue shift of only 5 nm.

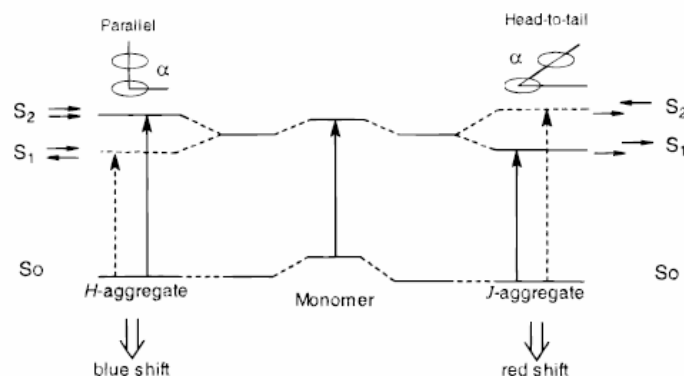


Figure 65 Schematic representation of the relationship between chromophore arrangement and spectral shift based on the molecular exciton theory

Based on the results of photoisomerisation of the compounds in solution the suitable wavelength of the light was selected for induction of optical anisotropy in film. The photoisomerisation and photo-orientation of two of the trimers (PG₆AZB₂BPH (**T13**) and PG₆OCB₂AZB (**T12**)) occur also in films. The optical anisotropy in the films was induced by irradiation with a linearly polarized light at $\lambda=488$ nm of an Argon ion laser (160 mW/cm², Coherent, Innova 90-4). Subsequently, the angular-dependent UV-Vis absorbance spectra were measured using a diode array XDAP Spectrometer (Polytec) equipped with a polarizer (the spectra were collected every 5°). The dichroism was calculated from the angular-dependent absorbance spectra for the maximum of the transition band according to

$$D = \frac{(A_{\max} - A_{\min})}{(A_{\max} + A_{\min})}$$

where D is dichroism at the defined wavelength, A_{\max} (\parallel) and A_{\min} (\perp) are the absorbances parallel and perpendicular to the polarization direction of the irradiation light, respectively.

In case of PG₆AZB₂BPH (**T13**) a much lower ratio of *cis* isomers occurred in the steady state of the aggregated films compared to solution. The azobenzene chromophores oriented parallel to the electric field vector (E) are activated for isomerization cycles by the rotation of their molecular long axis until they are perpendicular to the direction E and became inactive (see section I.1.4), thus optical anisotropy is induced in the film. The absorption spectra of the initial and irradiated PG₆AZB₂BPH films are depicted in Figure 66. During irradiation of the

sample, the chromophores oriented parallel to the electric field vector decreases while no increase is observed in perpendicular direction, resulting in larger absorbance in the direction perpendicular than the absorbance parallel to the polarized incident beam. This results in a weak anisotropy, dichroism of about 0.13, with the absorption maximum perpendicular to the electric field vector of the incident light (Figure 67).

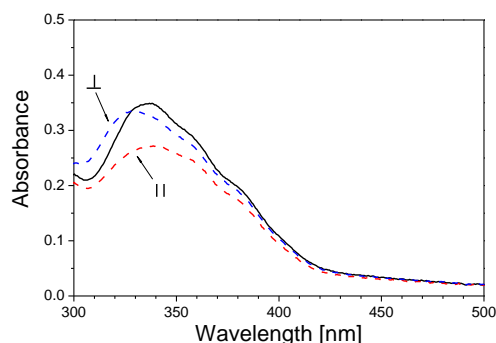


Figure 66 Polarized UV-Vis absorption spectra of the PG₆AZB₂BPH film measured with a beam polarized parallel (red-dashed) and perpendicular (blue-dashed) to the polarization direction of the incident beam of an Ar⁺ laser (488 nm, 160 mW/cm², 43 mins) compared with the initial spectrum (black-solid).

Such changes suggest that the orientation process is more complex and contains probably an out-of-plane orientation¹⁵⁷ component of the mobile non-aggregated molecules in the film. The $\pi \rightarrow \pi^*$ maximum at 336 nm is not shifted by the exposure indicating that the film is still strongly aggregated. The anisotropy did not increase due to subsequent annealing of films of the LC derivatives.

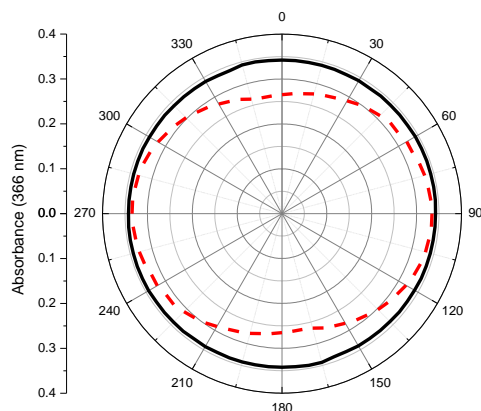


Figure 67 Absorption polar diagram plotted for 366 nm for PG₆AZB₂BPH film before (black-solid) and after irradiation (red-dashed) with linear polarized laser light (488 nm, 160 mW/cm², 43 minutes).
D=0.13

In contrast, the PG₆OCB₂AZB (**T12**) leads to very promising results (Figure 68): after a multi-step irradiation procedure a dichroism of about 0.77 (366nm) was generated. This value is also very high compared to polymeric LC systems.

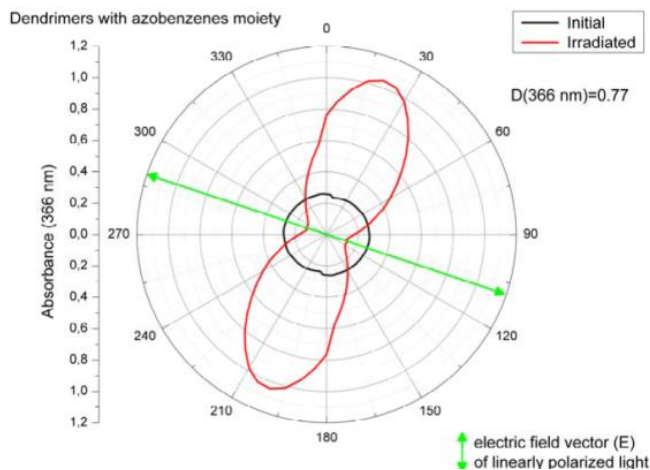


Figure 68 Polar plots of the absorbance of the PG₆OCB₂AZB at 366 nm in the initial state and after irradiation.

In this case, a decrease of the absorption in the direction parallel and a dramatic increase of the absorption in the direction perpendicular to the electric field vector (E) of linearly polarized light occur. The difference of global absorbance of the initial and the irradiated film reveals an out-of-plane orientation of the azobenzenes in the initial film. The sequence of irradiation processes causes a de-aggregation and decreases of the out-of-plane order by the intermediate UV exposure step resulting in high in-plane anisotropy and preferred (perpendicular) alignment of the chromophores in the plane of the film.

With this sample, PG₆OCB₂AZB (**T12**), the ability of the polarization grating and surface relief grating formation have also been studied. The films were illuminated by a polarization interference pattern using a holographic grating recording technique ($\lambda=488$ nm, Argon ion). The gratings were recorded after prior UV exposure and the measurements were performed at room temperature (RT) and at temperatures of the LC phase. The diffraction efficiency reached the value of ~ 13 % after around 25 minutes of the irradiation. In the next step of the investigation, the grating recording process was performed at the temperature of the LC phase in order to check the possible enhancement of the diffracted signal due to alignment of the mesogens, but no enhancement of diffraction was observed. The formed grating starts to be slowly erased with increasing temperature. The film surface of the PG₆OCB₂AZB was examined by AFM before (Figure 69) and after (Figure 70) the grating recording process. The surface of the material before illumination was rather rough which was later reflected in the quality of formed SRG. After the grating the sample surface diverges from sinusoidal shape.

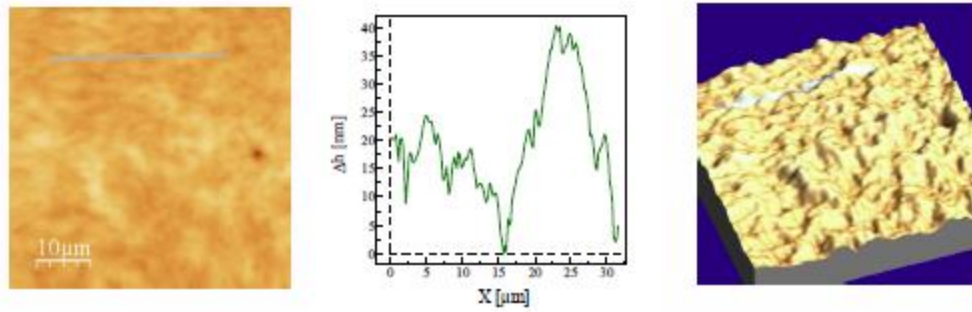


Figure 69 Views 2D (left) and 3D (right) of AFM scans (50x50 μm), and the surface profile (middle) of the film surface of the PG₆OCB₂AZB before diffraction grating recording process.

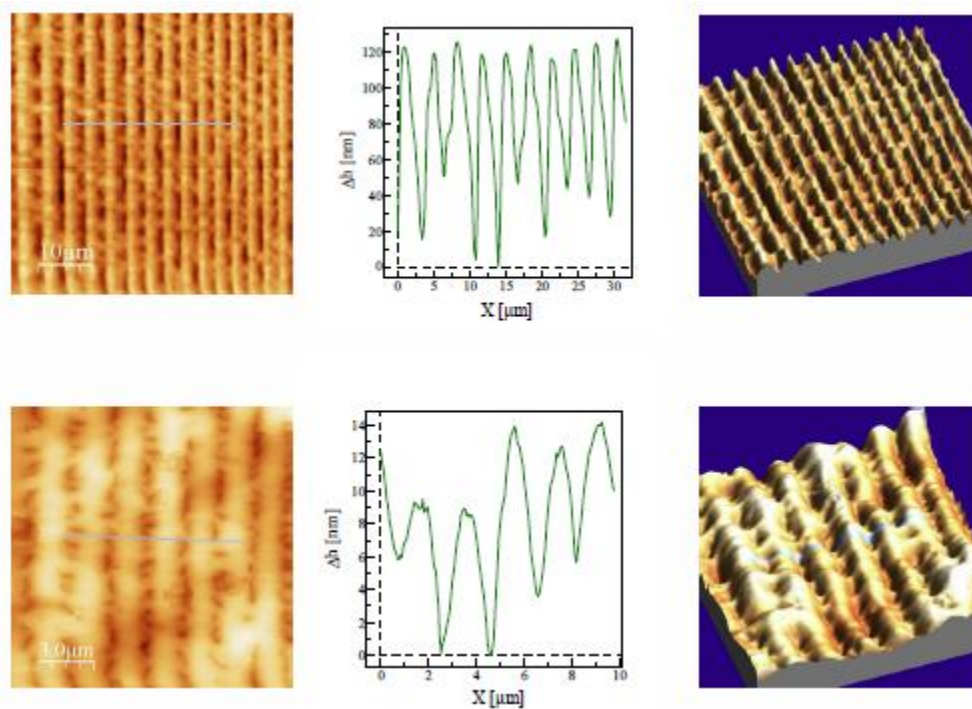


Figure 70 Views 2D (left) and 3D (right) AFM scans, and the surface profile (middle) of the film surface of the PG₆OCB₂AZB after the diffraction grating formation process. Different scans size: 50x50 μm (above) and 15x15 μm (below).

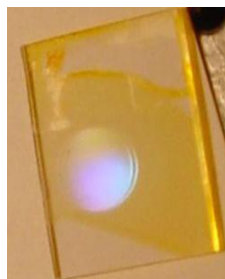


Figure 71 SRG on the film

1.4 Conclusions and Outlooks

A large part of this work is based on the design and synthesis of polyether dendrimers to introduce multifunctional properties e.g. combining liquid crystalline and photoresponsive properties. In order to achieve this goal, new sets of homo- and heterolithic liquid crystal polyether trimers (zero generation) and dendrimers (first generation) bearing chromophores have been synthesized successfully. The mesomorphic behaviour and transition temperatures are finely tuneable via changing structural parameters and their effects were studied. Their optical properties were also investigated.

Typical calamitic mesogens - alkoxy-azobenzene (AZB) based chromophore, alkoxy-biphenyl (BPH) and cyanobiphenyl (OCB) - were used as building blocks. Trimers were built up using phloroglucinol as the core and long linear alkyl chains to connect the functional groups on the periphery to the core. In order to carry out a detailed study of the mesomorphic and optical behaviour, several structural parameters were modified. This included changing the relative molar proportion of the chromophore, which was varied by exchanging it with the other calamitic mesogens, the dendritic generation number, in the case of the first generation, the branching points (changing from the phloroglucinol (PG) based dendrons to benzyl ether type (BA)) and the length of the linker in the case of the homolithic AZB trimers and dendrimers.

Combination of divergent and convergent methods were used for the syntheses of dendrimers but the divergent method in many cases was not good enough due to the low reactivity of the hydroxylated mesogen precursors (BPH, OCB) toward etherification; a convergent method was successful in most cases. In order to incorporate the chromophores in different proportions within the molecular structure and/or to increase the generations number of the phloroglucinol based dendrimers, benzoic acid ester (Bz) was found to be the most efficient protective group, in the given reaction conditions, for the selective protection of one of the hydroxyl group of the phloroglucinol. Using mild conditions during the deprotection step, such as 1-octylamine, turned out to be essential in the success of the reaction and improved the yield. Using benzyl alcohol type branching points simplified the reactions by eliminating the selective protection and deprotection of a hydroxyl group at the branching point. Consequently, use of an iterative sequence of reaction steps such as bromo alkylation or bromination, etherification (Williamson-etherification) and deprotection (hydrolysis), allowed us to increase the generation number in a precise and controlled way and to obtain monodisperse well determined dendrimers. The characterization techniques such as NMR spectroscopy, mass spectroscopy and elemental analysis confirmed the success of the reactions and the purity of the products which is essential for investigating the mesomorphic behaviour and to find

relationship with the structure of the materials. In order to investigate optical properties of other photoresponsive groups, cinnamic acid ester containing materials were also synthesized but no liquid crystalline behaviour was seen and they were not further investigated.

Studies were carried out to identify the mesomorphic behaviour, revealed smectic mesophases in most compounds as expected since the building blocks are typical calamitic mesogens.

In the case of homolithic trimers, very limited mesomorphic behaviour (or even no mesophase) occurs. In the heterolithic systems, segregation between the two types of mesogens occurs, leading to more intricate organizations than for homolithic ones, with a good differentiation between the two mesogenic sub-layers: tilted SmC phases with bilayer structures were induced in the BPH containing trimers and non-tilted, SmA phases with monolayer structure were formed in the OCB containing ones. In AZB/BPH trimers the mesophase occurs only in a short temperature range but the mesophase of the AZB/OCB occur over a wide range and a T_g below room temperature was induced. Clearing temperatures in all smectic systems occur around 120°C.

Increasing the generations number induced and stabilized the mesomorphic behaviour. Both homolithic and heterolithic dendrimers exhibit smectic mesophases. Enantiotropic polymorphism was induced in most of the PG dendrimers beside the decrease of the clearing temperature by at least 20°C, when compared to the trimers (Figure 44), due to the increased flexibility of the dendrimer interior. In addition, all systems exhibit glass transition and the mesophases are frozen at room temperature.

Changing the branching points from phloroglucinol to 3,5-dihydroxybenzyl alcohol drastically increased the temperature range of the mesophases as a result of the increase of the clearing temperature by more than 20°C (in some case even 40°C), likely due to the decreased flexibility and the more compact structure of the dendrimer interior. In all cases the abundance of the mesophases which were characteristic of the PG dendrimers, are reduced to only one enantiotropic mesophase in the BA dendrimers due to the “exchange” of the polymorphism by a glassy state (glass transition temperature above room temperature, up to 75°C) (Figure 53). The mesophases similarly depend on the molecular construction of morphology. In the heterolithic systems (except the high AZB content AZB/OCB dendrimer) segregated lamellar phases with sharp interfaces between the sublayers are formed and display from first to fourth order small-angle reflections in SAXS. The smectic mesophases of both BA and PG first generation dendrimers, similarly to the trimers, exhibit well differentiated segregation of the different mesogens within the layers too.

The photochemical behaviour of the trimers containing 1 to 3 photochromic azobenzene groups was measured and investigated by a collaborative partner (Fraunhofer group), in order to know whether photoinduced optical anisotropy or SRG can be generated. Measurements of further three AZB containing PG and BA dendrimers is still in progress. There were several parameters that the materials had to fulfil in order for these experiments to be conducted e.g. mesomorphic behaviour, good film forming property, high solubility and T_g above room temperature.

Fast crystallization of the photosensitive groups occurred in most of the spin coated films of the trimers except for PG₆AZB₂BPH and PG₆OCB₂AZB. A comparison of the UV-Vis spectra of PG₆AZB₂BPH in the solution and in spin-coated films revealed a strong “blue” shift of the maximum absorption band indicating the formation of H-aggregates. The aggregated azobenzenes do not undergo photo-isomerisation or photo-orientation upon linearly polarized light exposure. Consequently, only a small dichroism was induced by light (0.13 in PG₆AZB₂BPH). The PG₆OCB₂AZB showed much smaller blue shift. When trimers were processed with a multi-step irradiation procedure, which caused de-aggregation, it led to very good results, especially for PG₆OCB₂AZB where a strong dichroism (D=0.77) was generated, which is a very high value even if compared to polymeric LC systems. Formation of diffraction gratings were also investigated. Diffraction gratings with a diffraction efficiency of ~13 % were recorded. AFM investigations revealed a sinusoidal shaped surface relief grating but not-well-defined with an amplitude varying between 60 and 110 nm. Further investigations are in progress.

As the trimers have already showed very promising results, the first generation heterolithic dendrimers can be of great interest as we successfully fulfilled the requirements of the material properties, such as a T_g above room temperature (some of them have a T_g above 60°C), improved solubility and a stable mesophase on a very wide temperature range.

Outlook

According to the structural variety provided by dendrimers, many parameters could be changed (*e.g.* variety of the mesogens in one molecule, type of the mesogens, connectivity of the central core, connectivity of the branching points, spacer length) in order to investigate their effect on mesomorphic behaviour. Preserving the basic structural design of the dendrimers that were presented in this work, the parameters which could have strong influence on the LC properties - and therefore their effects are the main interest of the investigation - are on the one hand the increase of the generations number, and on the other hand the variations of the

branching points. It would be interesting to change the 3,5-dihydroxybenzyl alcohol branching points to 3,5-di(hydroxymethyl)phenol (**11**), which is already synthesized, and by this change, the position of the long linkers between the core and the branching points, would allow the construction of a flexible dendrimer interior but with a bulkier inter layer (Figure 72). This could complete our study in order to allow a better control of the mesomorphic behavior. The variation of the chromophore is also interest using e.g. cinnamic acids, diaryl ethers.

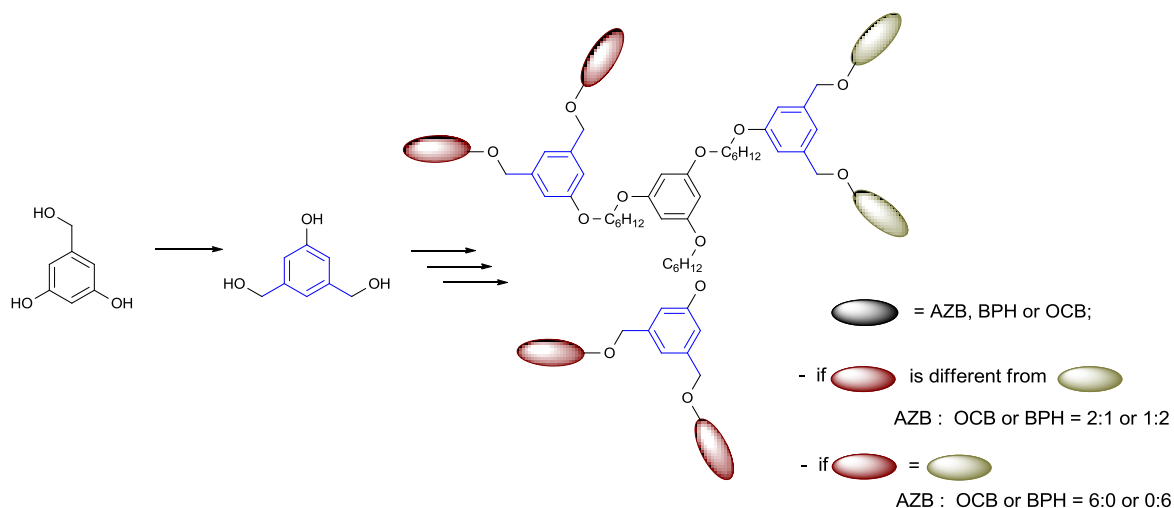


Figure 72 New dendritic structures

The optical measurements of the first generation dendrimers, which are good candidates because of their properties, are important and would allow a better understanding between photoinduced isomerization tendency and structure. It could be also interesting to investigate the mixtures of the heterolithic and homolithic trimers in different proportions, which could induce or increase T_g and change the temperature range of the mesophases.

1.5 Experimental part

Analytical thin layer chromatography was performed on silica plates. All solvents were dried before use. Solvent THF and CH₂Cl₂ was dried using Dry solvent station GT S100, the DMF and acetone was stored over 3Å molecular sieves. Chemicals were purchased from Acros, Alfa Aesar and Aldrich and used without further purification unless otherwise stated. All reaction was carried out under argon atmosphere

1.5.1 Synthesis of mesogenic units and branching points

General procedure for bromoalkylation:

A large excess (5-8 equiv.) of 1,6-dibromohexane was added to a mixture of phenolic alcohol (1 equiv.) and anhydrous K₂CO₃ (2 – 3 equiv.) in acetone and was refluxed under argon for 48 h. The cooled reaction mixture was filtered. The residue was dissolved in CHCl₃ and washed sequentially with water and sat. aq. NaCl. The organic layer was dried over Mg₂SO₄, filtered and concentrated.

AZB: 4-Hydroxy-4'-(undecyloxy)azobenzene (Scheme 1): To a solution of 4-acetamidophenol (12.073 g, 79.9 mmol) and K₂CO₃ (27.880 g, 201.7 mmol) in 100 ml DMF, 1-bromoundecane (19.815 g, 84.2 mmol) was added and stirred for 48 h at 95 °C. Once cooled, the mixture was concentrated under reduced pressure and poured into water. The precipitate was filtered off and washed with 5 wt. % aqueous NaOH and water, the crude 4-(undecyloxy)phenyl acetamide was heated with 150 ml of 40 wt. % sulphuric acid at 101 °C for 4 h. Once the reaction mixture was cooled to room temperature, the amine salt was filtered off and repeatedly washed with water. The salt was suspended in 140 ml of water at 80 °C, a solution of NaOH (6.0 g, 150 mmol, in 12 ml of water) and 120 ml of toluene were added and the reaction mixture was refluxed overnight. After cooling to room temperature, the toluene layer was separated and the aqueous layer was extracted three times with 20 ml of toluene. The toluene solution was dried over anhydrous Na₂SO₄ and molecular sieves. The filtrate was concentrated in vacuum. After cooling the 4-(undecyloxy)aniline crystallized. The mixture of 4-(undecyloxy)aniline (20.111 g, 76.3 mmol) and 40 ml of 18 wt. % HCl was heated until the amine dissolved. The solution was cooled and kept at 0–5 °C. NaNO₂ (7.901 g, 114.5 mmol) was dissolved in 46 ml of water, added dropwise to the amine solution. The solution of diazonium salt was kept at 0–5 °C and added dropwise to a solution of phenol (15.806 g, 168 mmol) and NaOH (13.284 g, 332 mmol) in 166 ml of water. The reaction temperature was maintained below 5 °C. Finally the reaction mixture was put to pH = 3 with HCl. The precipitate was filtered off, washed with ice water, dissolved in

dichloromethane and washed sequentially with water and sat. aq. NaCl. The organic layer was dried over anhydrous MgSO₄, filtrated and concentrated. The crude product was recrystallized from chloroform. The product was isolated as blood red crystals 14.365 g, 49% (Mol. Wt: 368.51 g/mol). The reaction was repeated several times with similar yield.

¹H NMR (CDCl₃): δ 7.87 (d, J=9.0Hz, 2H), 7.84 (d, J=9.0Hz, 2H), 7.00 (d, J=8.8Hz, 2H), 6.94 (d, J=8.8Hz, 2H), 4.04 (t, J=6.5Hz, 2H), 1.82 (quintet, J=7.0Hz, 2H), 1.58-1.2 (m, 16H), 0.89 (t, J=6.9Hz, 3H); ¹³C NMR (CDCl₃): δ 161.30, 157.63, 147.29, 146.81, 124.55, 124.37, 115.73, 114.70, 68.37, 31.91, 29.61, 29.60, 29.57, 29.39, 29.34, 29.22, 26.02, 22.68, 14.11.

BPH: 4'-(Hexyloxy)biphenyl-4-ol (Scheme 1), To a mixture of 4,4'-dihydroxybiphenyl (23.012 g, 120 mmol), K₂CO₃ (16.387 g, 119 mmol) and potassium iodide (catalytic amount) in DMF (75 ml) 1-bromohexane (15.4 ml, 108 mmol) was added dropwise. The reaction mixture was stirred for 18 h at 80 °C then allowed to cool to room temperature. The reaction mixture was poured into distilled water (700 ml) and was acidified with 2M HCl solution. The precipitate was isolated by filtration, washed thoroughly with distilled water and dried. The solids were dissolved in ethyl acetate (200 ml) and the insoluble solids (r0) were removed by filtration and the filtrate (f0) was concentrated. The residue (r0) was recrystallized from EtOAc the residue (r1) was rejected and the filtrate (f1) was concentrated under reduced pressure. The concentrated filtrate (f0) was recrystallized from ethanol and the filtrate (f2) was rejected. The residue (r1) was combined with f0 and was further purified by silica gel column chromatography using CH₂Cl₂:ethyl acetate (4:1) as eluent. The product was isolated as a white solid, 12.293g, 42% (Mol. Wt: 270.37 g/mol). The reaction was repeated once more with similar yield.

¹H NMR (d₆-acetone): δ 8.32 (s, 1H), 7.48 (d, J=8.8Hz, 2H), 7.42 (d, J=8.7Hz, 2H), 6.96 (d, J=8.8Hz, 2H), 6.88 (d, J=8.8Hz, 2H), 4.01 (t, J=6.5Hz, 2H), 1.77 (quintet, J=7.0Hz 2H), 1.56-1.26 (m, 6H), 0.90 (t, J=7.0Hz, 3H); ¹³C NMR (d₆-acetone):158.26, 156.53, 133.33, 132.16, 127.42, 127.22, 115.57, 114.70, 67.70, 31.44, 28.53, 25.58, 22.38, 13.38.

(1) 4-(6-Bromohexyloxy)-4'-hexyloxybiphenyl (Scheme 2): The product was prepared according to the general procedure of "bromoalkylation" from **BPH** (4.056 g 15.0 mmol) and 1,6-dibromohexane (19 ml, 118.6 mmol) using acetone (100 ml) as solvent. Once cooled, the reaction mixture was concentrated and suspended in ethanol. The precipitate was separated by filtration, the residue was dissolved in CHCl₃ and washed sequentially with water and sat. aq. NaCl. The organic layer was dried over Mg₂SO₄, filtrated and concentrated. The product was

Experimental

dried under vacuum to give 5.867 g, 90%, white solid (Mol. Wt: 433.42 g/mol). The synthesis was carried out two more times with good yields (4.454 g, 91.78% and 9.065 g, 80% yield).

¹H NMR (CDCl₃): δ 7.47 (d, J=8.5Hz, 4H), 6.95 (d, J=8.7Hz, 4H), 4.0 (t, J=6.4 Hz, 2H), 3.99 (t, J=6.6Hz, 2H), 3.44 (t, J=6.8Hz, 2H), 1.74–1.98 (m, 6H), 1.26–1.52 (m, 10H), 0.92 (t, J=7.0Hz, 3H); **¹³C NMR** (CDCl₃): δ 158.28, 158.13, 133.48, 133.30, 127.67, 127.65, 114.77, 114.75, 68.13, 67.82, 33.76, 32.71, 31.61, 29.30, 29.15, 27.95, 25.75, 25.34, 22.62, 14.03.

(2) 4'-(6-Bromohexyloxy)biphenyl-4-carbonitrile (Scheme 2): The product was prepared according to the general procedure of “bromoalkylation” from 4'-hydroxy-4-biphenylcarbonitrile (OCB, 4.0 g, 20.5 mmol) and 1,6-dibromohexane (26 ml, 169.0 mmol) using acetone (140 ml) as solvent. The cooled reaction mixture was filtered. The filtrate was concentrated on rotary evaporator and suspended in petroleum ether and refrigerated. The crystallized part separated by filtration and dried under vacuum to give 7.0 g, 95%, white solid (Mol. Wt: 357.07 g/mol). The synthesis was carried out more times with similar yields.

¹H-NMR (CDCl₃): δ 7.67 (#q, J=8.5Hz, 4H), 7.54 (#d, J=8.9Hz, 2H), 7.0 (#d, J=8.8Hz, 2H), 4.02 (t, J=6.4Hz, 2H), 3.44 (t, J=6.8Hz, 2H), 2.0-1.76 (m, 4H), 1.54 (quintet, J=3.58Hz, 4H); **¹³C NMR** (CDCl₃): δ 159.72, 145.27, 132.55, 131.40, 128.34, 127.09, 119.07, 115.10, 110.12, 67.91, 33.71, 32.67, 29.04, 27.90, 25.29.

(3) 4-(6-Bromohexyloxy)-4'-undecaneoxyazobenzene (Scheme 2): The product was prepared according to the general procedure of “bromoalkylation” from **AZB** (3.01 g, 8.2 mmol) and 1,6-dibromohexane (11.0 ml, 68.6 mmol) using acetone (60 ml) as solvent. The product was isolated as yellow solid, 3.696 g, 85%, (Mol. Wt: 531.57 g/mol). The synthesis was carried out once more with similar yield (2.537 g, 88%)

¹H NMR (CDCl₃) of *trans*-azo: δ 7.87 (d, J=8.8Hz, 4H), 6.99 (d, J=8.8Hz, 4H), 4.05 (t, J=6.6 Hz, 2H), 4.04 (t, J=6.6 Hz, 2H), 3.44 (t, J=6.8 Hz, 2H), 1.74–1.98 (m, 6H), 1.22–1.58 (m, 16H), 0.89 (t, J=6.8 Hz, 3H); **¹H NMR** (CDCl₃) of *cis*-azo: δ 6.90 (d, J=8.9Hz, 4H), 6.77 (d, J=8.9Hz, 4H), 3.94 (t, J=6.4 Hz, 2H), 3.93 (t, J=6.5 Hz, 2H), 3.44 (t, J=6.8 Hz, 2H), 1.74–1.98 (m, 6H), 1.22–1.58 (m, 16H), 0.89 (t, J=6.8 Hz, 3H); **¹³C NMR** (CDCl₃): δ 161.21, 161.03, 147.04, 146.95, 124.29, 114.68, 114.66, 68.35, 68.04, 33.71, 32.67, 31.91, 29.61, 29.60, 29.57, 29.39, 29.34, 29.23, 29.06, 27.92, 26.03, 25.29, 22.68, 14.11.

(4) 1,3,5-Tris-(11-bromoundecaneoxy)benzene (Scheme 4): A solution of DIAD (3.70 ml, 18.8 mmol) in 20 ml of THF was added dropwise to triphenylphosphine (4.916 g, 18.7 mmol) in THF

(30 ml) at 0 °C. Phloroglucinol (0.641 g, 5.1 mmol) was added to this solution which was followed by 11-bromo-1-undecanol (4.935 g, 19.6 mmol) in 25 ml THF. The temperature was raised slowly and the mixture refluxed for 58 h. The crude product was purified by silica gel chromatography using chloroform: cyclohexane (5:1) as the eluent. The product was isolated as a white solid, 2.126 g, 51% (Mol. Wt: 825.68 g/mol).

¹H NMR (CDCl₃): δ 6.06 (s, 3H), 3.91 (t, J=6.5Hz, 6H), 3.42 (t, J=6.9Hz, 6H), 1.86 (quintet, J=7.2Hz, 6H), 1.76 (quintet, J=7.0Hz, 6H), 1.52–1.2 (m, 42H); ¹³C NMR (CDCl₃): δ 160.97, 93.84, 68.00, 33.98, 32.85, 29.50, 29.44, 29.40, 29.34, 29.26, 28.75, 28.17, 26.04.

(5) 1,3,5-Tris-(6-bromohexeneoxy)benzene (Scheme 4): of 1,6-dibromohexane Excess (9.00 ml, 56.2 mmol) was added to a mixture of phloroglucinol (0.649 g, 5.1 mmol), 18-crown-6 (0.175 g, 0.7 mmol) and anhydrous K₂CO₃ (2.87 g, 20.8 mmol) in acetone and was refluxed under argon for 48 h. Then the reaction mixture was cooled to room temperature and the solvent was evaporated under reduced pressure. The residue was dissolved in CH₂Cl₂ and washed sequentially with water and sat. aq. NaCl. The organic layer was dried over Mg₂SO₄, filtrated and concentrated. The crude product was precipitated and further purified by silica gel column using CH₂Cl₂: cyclohexane (3:1) as eluent. Product was isolated as yellowish viscous liquid 1.722 g, 54% (Mol. Wt: 615.28 g/mol).

¹H NMR (CDCl₃): δ 6.06 (s, 3H), 3.92 (t, J=6.4 Hz, 6H), 3.43 (t, J=6.8 Hz, 6H), 1.90 (quintet, J=7.2Hz, 6H), 1.78 (quintet, J=7.0Hz, 6H), 1.38–1.32 (m, 12H)

(6a) TBDMS protected phloroglucinol (Scheme 6): To a mixture of phloroglucinol (5.013 g, 39.8 mmol) and imidazole (2.705 g, 39.8 mmol) in DMF (150 ml) TBDMSCl (5.994 g, 39.8 mmol) in DMF (30 ml) was added and stirred at room temperature for 24 hours. Then the mixture was concentrated under reduced pressure and poured into water. The precipitate was removed by filtration, the residue was dissolved in Et₂O and washed sequentially with water and sat. aq. NaCl. The organic layer was dried over Mg₂SO₄, filtrated and concentrated. The crude product was further purified by a silica gel column using DCM: EtOAc (5:1) as eluent. The product was isolated as a white solid 3.800 g, 40% (Mol. Wt: 240.37 g/mol). The diprotected by-product was also isolated as a white solid 2.819g, 20% (Mol. Wt: 354.63 g/mol).

(6a) Monoprotected: ¹H NMR (CDCl₃): δ 5.98 (t, J=2.1Hz, 1H), 5.95 (d, J=2.1Hz, 2H), 4.76 (s, 2H), 0.97 (s, 9H), 0.20 (s, 6H)

(6b) Diprotected: ¹H NMR (CDCl₃): δ 6.02-6.97 (m, 2H), 5.95 (t, J=2.1Hz, 1H), 0.97 (s, 18H), 0.20 (s, 12H)

(7a) 3,5-dihydroxyphenyl benzoate (Scheme 7): To a mixture of anhydrous phloroglucinol (19.279 g, 152 mmol) and pyridine (25 ml, 310 mmol) in 250 ml THF under argon atmosphere, benzoyl chloride (17 ml, 146.5 mmol) in 80 ml of THF was added dropwise over 2 h and the reaction mixture was refluxed for 48 h. Once cooled, the solvent was removed and the residue was dissolved in CHCl_3 and 2M HCl was added until precipitate occurred. The white precipitate was filtered off and put aside (crude product). The filtrate was dried under reduced pressure then dissolved in hot chloroform/EtOAc. After cooling, the resultant precipitate was filtered and the residue was added to the previous precipitate. It was dissolved in ethyl acetate and washed with water and sat. aq. NaCl. The organic layer was dried over anhydrous MgSO_4 , filtrated and concentrated. The crude products were further purified by silica gel column chromatography using CH_2Cl_2 :ethyl acetate (5:1) as the eluent. The product was isolated as white crystalline solid, 14.165 g, 42% (Mol. Wt: 230.22 g/mol).

(7a) Monoprotected: $^1\text{H NMR}$ (d_6 -acetone): δ 8.53 (s, 2H), 8.13 (dd, $J=8.7\text{Hz}$, 1.3Hz, 2H), 7.71 (t, $J=7.6\text{Hz}$, 1H), 7.58 (t, $J=7.6\text{Hz}$, 2H), 6.30 (t, $J=2.1\text{Hz}$, 1H), 6.27 (d, $J=2.2\text{Hz}$, 2H).

(7b) Diprotected (5-hydroxy-1,3-phenylene dibenzoate): $^1\text{H NMR}$ δ 8.13 (dd, $J=8.7\text{Hz}$, 1.3Hz, 4H), 7.71 (t, $J=7.6\text{Hz}$, 2H), 7.58 (t, $J=7.6\text{Hz}$, 4H), 6.30 (t, $J=2.1\text{Hz}$, 1H), 6.27 (d, $J=2.2\text{Hz}$, 2H).

(8) 3,5-Bis(6-bromohexyloxy)-phenyl benzoate (Scheme 8): A solution of DIAD (13.0 ml, 66.0 mmol) in THF (25 ml) was added dropwise to triphenylphosphine (17.109g, 65.2 mmol) in THF (30 ml) at 0 °C. After 3,5-dihydroxyphenyl benzoate (6.008 g, 26.1 mmol) in 30 ml THF was added which was followed by 6-bromo-1-hexanol (7.8 ml, 59.6 mmol). The temperature was raised slowly and the solution was refluxed for 48 h. The crude product was purified by silica gel chromatography using CH_2Cl_2 :cyclohexane (3:1 to 9:1) as the eluent. The product was isolated as viscous liquid, 10.323g, 71% (Mol. Wt: 556.33 g/mol).

$^1\text{H NMR}$ (CDCl_3): δ 8.2 (dd, $J=8.2\text{Hz}$, 1.2Hz, 2H), 7.65 (tt, $J=7.5\text{Hz}$, 1.8Hz, 1H), 7.52 (t, $J=7.5\text{Hz}$, 2H), 6.375 (s, 3H), 3.95 (t, $J=6.4\text{Hz}$, 4H), 3.43 (t, $J=6.7\text{Hz}$, 4H), 1.9 (quintet, $J=6.8\text{Hz}$, 4H), 1.8 (quintet, $J=6.8\text{Hz}$, 4H), 1.6-1.42 (m, 8H); $^{13}\text{C NMR}$ (CDCl_3): 165.00, 160.63, 152.45, 133.57, 130.15, 129.59, 128.57, 100.73, 99.30, 68.00, 33.76, 32.70, 28.99, 27.91, 25.29

(9) 3,5-Bis(6-bromoundecyloxy)-phenyl benzoate (Scheme 8): According to the procedure above for (8): from DIAD (7.5 ml, 38.1 mmol) in THF (15 ml), triphenylphosphine (9.961 g, 15.0 mmol) in THF (30 ml), 3,5-dihydroxyphenyl benzoate (3.457 g, 26.1 mmol) in 30 ml THF, 6-bromo-1-undecanol (9.780 g, 39.0 mmol), using CHCl_3 :cyclohexane (9:1) as the eluent for silica

gel chromatography, the product was isolated as a white solid, 9.698g, 92% (Mol. Wt: 696.59 g/mol)

$^1\text{H NMR}$ (CDCl_3): δ 8.2 (dd, $J=8.1\text{Hz}, 1.4\text{Hz}, 2\text{H}$), 7.65 (tt, $J=7.5\text{Hz}, 1.8\text{Hz}, 1\text{H}$), 7.52 (t, $J=7.5\text{Hz}, 2\text{H}$), 6.35 (s, 3H), 3.93 (t, $J=6.4\text{Hz}, 4\text{H}$), 3.42 (t, $J=6.7\text{Hz}, 4\text{H}$), 1.86 (quintet, $J=7.1\text{Hz}, 4\text{H}$), 1.77 (quintet, $J=6.8\text{Hz}, 4\text{H}$), 1.6-1.42 (m, 28H); $^{13}\text{C NMR}$ (CDCl_3): 165.01, 160.71, 152.42, 133.53, 130.15, 129.65, 128.54, 100.64, 99.31, 68.25, 33.99, 32.85, 29.48, 29.43, 29.39, 29.31, 29.16, 28.75, 28.17, 26.00

(10) TBDMS protected dimethyl 5-hydroxyisophthalate (Scheme 9): To a mixture of dimethyl 5-hydroxyisophthalate (6.00 g, 28.5 mmol) and imidazole (4.032g, 59.2 mmol) in CH_2Cl_2 (90 ml) TBDMSCl (4.746 g, 31.5 mmol) was added dropwise and stirred at room temperature. After 3h the resulting precipitate was removed by filtration and washed with CH_2Cl_2 . The filtrate was washed with H_2O and sat. aq. NaCl. The organic layer was dried over MgSO_4 , filtered and evaporated providing the product 9.120 g, 99% (Mol. Wt: 324.44 g/mol).

$^1\text{H NMR}$ (CDCl_3): δ 8.30 (t, $J=1.5\text{Hz}, 1\text{H}$), 7.68 (s, $J=1.5\text{Hz}, 2\text{H}$), 3.94 (s, 6H), 1.01 (s, 9H), 0.24 (s, 6H)

(11) TBDMS protected 3,5-Di(hydroxymethyl)phenol (Scheme 9): To a solution **10** (7.015 g, 21.6 mmol) in THF (120 ml) LiAlH_4 (1M solution in THF, 35.0 ml, 35.0 mmol) was added dropwise at 0°C and stirred at 25°C . After 4h the reaction was quenched with MeOH. The solvent was removed by evaporation, the residue was dissolved in Et_2O and washed with H_2O and sat. aq. NaCl. The organic layer was dried over MgSO_4 , filtered and evaporated, providing the product 2.832 g, 49% (Mol. Wt: 268.42 g/mol).

$^1\text{H NMR}$ (CDCl_3): δ 6.97 (brs, 1H), 6.78 (brs, 2H), 4.65 (d, $J=6.0\text{Hz}, 4\text{H}$), 1.64 (t, $J=6.0\text{Hz}, 2\text{H}$), 0.99 (s, 9H), 0.21 (s, 6H)

(12) 3,5-bis(bromomethyl)benzoate (Scheme 10): A solution of methyl 3,5-dimethylbenzoate (6.005g, 36.6 mmol), N-bromosuccinimide (13.677 g, 76.8 mmol) and a catalytic amount of AIBN in CCl_4 was stirred at 80°C . After 48 hours the mixture was cooled at room temperature, the resulting precipitate was removed by filtration (succinimide) and washed with CCl_4 . The filtrate was washed with sat. aq. NaHCO_3 and sat. aq. NaCl. The organic layer was dried over anhydrous Na_2SO_4 , filtrated, concentrated, suspended in petroleum ether and refrigerated. The crystalized part (mainly product) was further purified by silica gel column chromatography

using cyclohexane:EtOAc (5:1) as the eluent and the product was isolated as white crystals (2.894 g).

The filtrate (containing mono- and gem-dibrominated mixture) was concentrated dissolved in THF and diethyl phosphite (10.5 ml, 81.9 mmol) and DIPEA (14.3 ml, 81.9 mmol) was added to it at 0°C under Ar. The mixture was stirred at room temperature. After 24h, most of the THF was removed by evaporation and the mixture was poured into ice-water and extracted with Et₂O. The organic layer was washed with 1N HCl and brine, dried over MgSO₄, filtered and evaporated. The crude product was further purified by column chromatography using cyclohexane:EtOAc (9:1) as eluent. The product was isolated as white crystals (1.740 g). 4.634 g 39% (Mol. Wt: 321.99 g/mol).

¹H NMR (CDCl₃): δ 8.01 (d, J=1.7Hz, 2H), 7.63 (t, J=1.8Hz, 1H), 4.51 (s, 4H), 3.95 (s, 3H); ¹³C NMR (CDCl₃): δ 165.91, 131.46, 138.96, 133.81, 130.01, 52.37, 31.79

1.5.2 *Synthesis of Dendrons and Trimers*

General procedure for bromoalkylation:

A large excess (5-8 equiv.) of dibromoalkene (1,6-dibromohexane or 1,11-dibromoundecane) was added to a mixture of phenolic alcohol (1 equiv.), anhydrous K₂CO₃ (2 – 3 equiv.) and 18-crown-6 (0.2 equiv.) in THF and was refluxed under argon for 48 h. Then the reaction mixture was cooled to room temperature and the solvent was evaporated under reduced pressure. The residue was dissolved in CH₂Cl₂ and washed sequentially with water and sat. aq. NaCl. The organic layer was dried over anh. Mg₂SO₄, filtrated and concentrated. The crude product was precipitated and/or further purified by silica gel column when necessary.

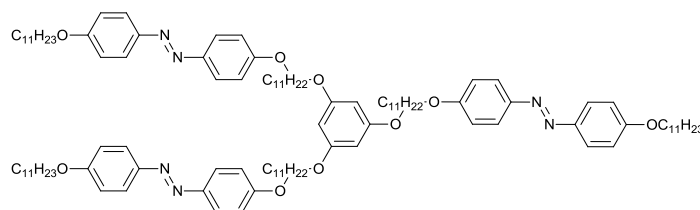
General procedure of etherification

Method A: A mixture of 3,5-dihydroxyphenyl benzoate (1 equiv.), bromide derivative (2.0-2.5 equiv.), K₂CO₃ (3-4 equiv.), 18-crown-6 (0.2 equiv.) and KI (catalytic amount) in solvent was refluxed under argon for 24 - 72 h. The reaction mixture was cooled to room temperature and the solvent was evaporated under reduced pressure or poured into water and the precipitate filtrated. The residue was dissolved in dichloromethane and washed sequentially with water and sat. aq. NaCl. The organic layer was concentrated by rotary evaporator. The crude intermediate was further treated by refluxing with KOH (4-5 equiv.) in THF/H₂O overnight. The reaction mixture was cooled to room temperature again, acidified and the solvent was evaporated under reduced pressure or if precipitate occurred filtrated. The residue was

dissolved in dichloromethane and washed sequentially with water and sat. aq. NaCl. The organic layer was dried over anhydrous MgSO_4 , filtrated and concentrated. The crude product was recrystallized or purified by silica gel column chromatography.

Method B: A mixture of phenolic derivative (1 equiv.), and bromide the derivative (small excess), K_2CO_3 (3-4 equiv.), 18-crown-6 (0.2 equiv.) and KI (catalytic amount) in solvent was refluxed under argon for 24 - 72 hours. Then the reaction mixture was cooled to room temperature and the solvent evaporated under reduced pressure or the mixture poured into water and the precipitate filtered. The residue was dissolved in dichloromethane and washed sequentially with water and sat. aq. NaCl. The organic layer was dried over anhydrous MgSO_4 , filtrated and concentrated. The crude product was recrystallized or purified by silica gel column chromatography.

(T1) $\text{PG}_{11}\text{AZB}_3$

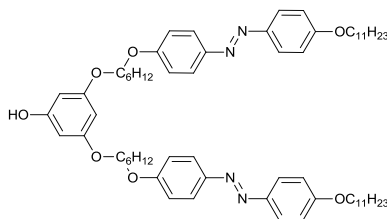


T1 was prepared according to the “Method B” from 1,3,5-Tris-(11-bromoundecaneoxy)benzene **4** (0.809 g, 1.0 mmol), **AZB** (1.302 g, 3.5 mmol) using DMF (50 ml) as solvent. The crude product was recrystallized from acetone. The product was isolated as yellow solid 0.724 g, 44% (Mol. Wt: 1688.48 g/mol). (Scheme 12)

$^1\text{H NMR}$ (CDCl_3): δ 7.88 (d, $J=8.9\text{Hz}$, 12H), 6.99 (d, $J=78.\text{Hz}$, 12H), 6.07 (s, 3H), 4.03 (t, $J=6.6\text{Hz}$, 12H), 3.91 (t, $J=6.7\text{Hz}$, 6H), 1.9-1.7 (m, 18H), 1.55-1.21 (m, 90H), 0.89 (t, $J=6.7\text{Hz}$, 9H); $^{13}\text{C NMR}$ (CDCl_3): δ 161.16, 160.98, 146.97, 124.28, 114.66, 93.84, 68.35, 68.02, 31.91, 29.61, 29.60, 29.57, 29.53, 29.50, 29.38, 29.33, 29.30, 29.26, 29.23, 26.05, 26.03, 22.68, 14.10.

MALDI-ToF: Calcd for $\text{C}_{108}\text{H}_{162}\text{N}_6\text{O}_9$: 1687.24, m/z : found: 1688.32 (M+1), 1689.32 (M+2), 1690.32 (M+3), 1691.32 (M+4); fragments: 1427.08 (M- $\text{C}_{17}\text{H}_{27}\text{NO}$) **EA** calcd: C 76.82, H 9.67, N 4.98; found: C 76.69, H 9.65, N 4.92.

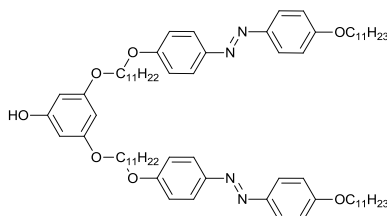
(T2) HO-PG₆AZB₂



T2 was prepared according to the “Method A” from 3,5-Bis(6-bromohexyloxy)-phenyl benzoate (**8**) (2.992 g, 5.4 mmol) and **AZB** (5.001 g, 13.6 mmol) using DMF (30mL) as solvent. After washing the crude reaction mixture, it was further treated with KOH (1.6 g, 28.5 mmol) in THF/H₂O (1:1) 50mL under reflux. The residue was recrystallized from acetone. The product (**T2**) was isolated as yellow solid, 4.895 g, 89% (Mol. Wt: 1027.42 g/mol). (Scheme 13)

¹H NMR (CDCl₃): δ 7.87 (d, J=8.7Hz, 8H), 6.99 (d, J=8.9Hz, 8H), 6.07 (t, J=2.3Hz, 1H), 5.99 (d, J=2.1Hz, 2H), 4.12-3.96 (m, 8H), 3.92 (t, J=6.5 Hz, 4H), 1.92-1.7 (m, 12H), 1.65-1.2 (m, 40H), 0.89 (t, J=6.5 Hz, 6H); ¹³C NMR (CDCl₃): δ 161.20, 161.11, 161.10, 157.30, 147.00, 146.95, 124.29, 114.69, 94.68, 94.18, 68.36, 68.14, 67.84, 31.90, 29.60, 29.56, 29.39, 29.33, 29.23, 29.12, 29.11, 26.03, 25.83, 25.79, 22.67, 14.09.

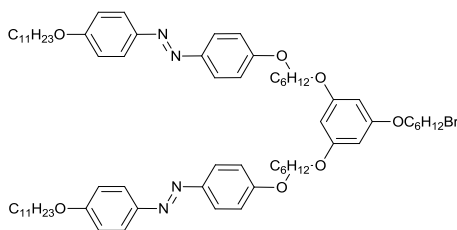
(T3) HO-PG₁₁AZB₂



T3 was prepared according to the “Method A” from 3,5-Bis(6-bromoundecyloxy)-phenyl benzoate (**9**) (2.268 g, 3.3 mmol) and **AZB** (2.905 g, 8.0 mmol) using acetone (30 ml) as solvent. After washing, the crude intermediate was further treated by KOH (0.913 g, 16.3 mmol) in THF/H₂O (1:1) 30ml under reflux. The residue was recrystallized from acetone giving product (**9**) 3.518 g, 92 % yellow solid (Mol. Wt: 1167.68 g/mol). (Scheme 13)

¹H NMR (CDCl₃): δ 7.86 (d, J=8.7Hz, 8H), 6.99 (d, J=8.9Hz, 8H), 6.08-6.04 (m, 1H), 6.02-5.99 (d, J=2.1Hz, 2H), 4.04 (t, J=6.4Hz 8H), 3.89 (t, J=6.7 Hz, 4H), 1.94-1.66 (m, 12H), 1.65-1.2 (m, 60H), 0.89 (t, J=6.5 Hz, 6H); ¹³C NMR (CDCl₃): 161.17, 157.22, 146.96, 124.29, 114.68, 94.58, 94.21, 68.35, 68.05, 31.91, 29.61, 29.60, 29.57, 29.50, 29.46, 29.39, 29.33, 29.23, 29.20, 26.03, 22.68, 14.10

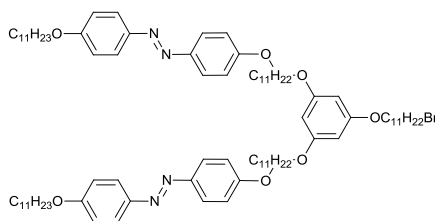
(T4) *Br-6-PG₆AZB₂*



T4 was prepared according to the “bromoalkylation” from **HO-PG₆AZB₂**, (**T2**) (1.192 g, 1.16 mmol), and 1,6-dibromohexane (1.5 ml, 9.75 mmol), using THF (15 ml) as solvent (refluxed for 72 hours). After workup, the organic layer was dried over anhydrous MgSO₄, filtrated and concentrated and the crude product was precipitated, in methanol. The product was further purified using CH₂Cl₂:petroleum ether:EtOAc (4:1:0.1) as the eluent for silica gel column chromatography and isolated as a yellow viscous solid 1.009 g, 73% (Mol. Wt: 1190,48 g/mol). The synthesis was carried out once more using DMF as a solvent, resulting in the product 0.995g, 43%. (Scheme 13)

¹H NMR (CDCl₃): δ 7.87 (d, J=8.8Hz, 8H), 6.99 (d, J=8.9Hz, 8H), 6.08 (s, 3H), 4.10-3.86 (m, 14H), 3.42 (t, J=6.8 Hz, 2H), 1.96-1.7 (m, 16H), 1.62-1.24 (m, 44H), 0.90 (t, J=6.8 Hz, 6H); ¹³C NMR (CDCl₃): δ 161.19, 161.09, 160.95, 160.92, 147.01, 146.96, 124.29, 114.67, 93.91, 68.35, 68.16, 67.84, 67.76, 33.73, 32.70, 31.91, 29.61, 29.56, 29.39, 29.33, 29.23, 29.17, 29.07, 27.92, 26.03, 25.88, 25.83, 25.32, 22.67, 14.09

(T5) *Br-11-PG₁₁AZB₂*



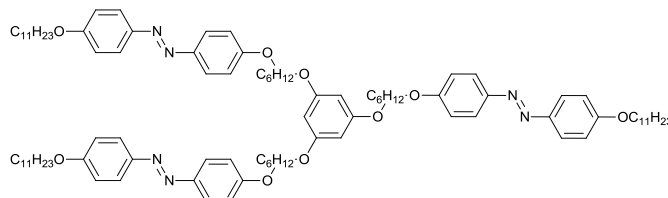
T5 was prepared according to the “bromoalkylation” from **HO-PG₁₁AZB₂** (**T3**) (1.611 g, 1.38 mmol) and 1,11-dibromoundecane (3.0 ml 12.75 mmol) using THF (20 ml) as the solvent. After work up the crude product was suspended in acetone, the precipitate was filtered and dried. The product (**Br-11-PG₁₁AZB₂**) was isolated as a yellow solid 1.678 g, 87% (Mol. Wt: 1400.88 g/mol). (Scheme 13)

¹H NMR (CDCl₃): δ 7.86 (d, J=8.9Hz, 8H), 6.99 (d, J=8.9Hz, 8H), 6.06 (s, 3H), 4.03 (t, J=6.6Hz, 8H), 3.90 (t, J=6.4Hz, 6H), 3.41 (t, J=6.8 Hz, 2H), 1.92-1.68 (m, 18H), 1.53-1.21 (m, 82H), 0.90 (t, J=6.8 Hz, 6H); ¹³C NMR (CDCl₃): δ 161.16, 160.97, 146.96, 124.28, 114.66, 93.83, 68.35, 68.01, 34.00,

Experimental

32.84, 31.91, 29.61, 29.60, 29.57, 29.54, 29.50, 29.44, 29.39, 29.34, 29.23, 28.75, 28.17, 26.03, 22.68, 14.11

(T6) PG₆AZB₃

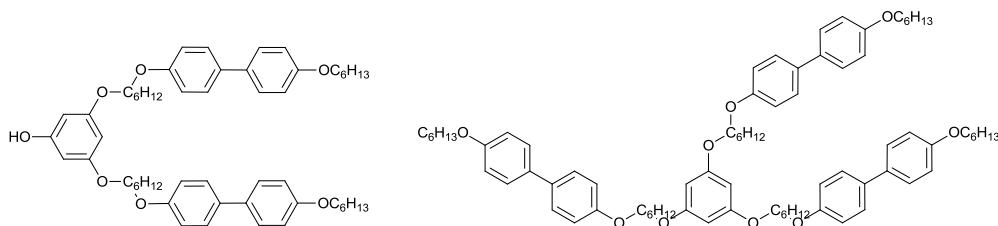


A mixture of **T4** (0.685 g, 0.58 mmol), **AZB** (0.236 g, 0.64 mmol) and K₂CO₃ (0.223 g, 1.61 mmol) in DMF (8 ml) was stirred under argon at 70 °C for 72 h. Once cooled, the reaction mixture was poured into distilled water and the precipitate was isolated by filtration. The residue was dissolved in chloroform and washed with water and sat. aq. NaCl. The organic layer was dried over anhydrous MgSO₄, filtrated and concentrated. The crude product was purified by silica gel column chromatography using CH₂Cl₂:EtOAc (30:1) as the eluent. **T6** was isolated as a yellow solid 0.353 g, 42% (Mol. Wt: 1478.08 g/mol). (Scheme 13)

¹H NMR (CDCl₃): δ 7.87 (d, J=8.8Hz, 12H), 6.99 (d, J=8.9Hz, 12H), 6.08 (s, 3H), 4.10-3.97 (m, 12H), 3.94 (t, J=6.5Hz, 6H), 1.92-1.74 (m, 18H), 1.62-1.22 (m, 60H), 0.89 (t, J=6.8 Hz, 9H); ¹³C NMR (CDCl₃): δ 161.19, 161.10, 160.95, 147.00, 146.96, 124.29, 114.67, 93.90, 68.35, 68.16, 67.84, 31.92, 29.62, 29.58, 29.40, 29.34, 29.23, 29.17, 26.03, 25.90, 25.84, 22.69, 14.11.

MALDI-ToF: Calcd for C₉₃H₁₃₂N₆O₉: 1477.01, m/z: found: 1478.00 (M+1), 1478.98 (M+2), 1480.01 (M+3), 1481 (M+4), fragments: 1216.80 (M-C₁₇H₂₇NO). **EA** calcd: C 75.57, H 9.00, N 5.69; found: C 75.48, H 9.00, N 5.57.

(T7) HO-PG₆BPH₂ and (T8) PG₆BPH₃



T7 (and **T8**) was prepared according to the "Method A" from **1** (4.159 g, 9.6 mmol) and **7a** (1.001 g, 4.3 mmol), using DMF (54 ml) as solvent, stirred under argon at 80 °C for 72 h. It was concentrated by rotary evaporation, poured in water (250 ml) and washed with chloroform. The organic layer was dried over anhydrous MgSO₄, filtrated and concentrated. The crude protected dendron was purified by silica gel column chromatography using CH₂Cl₂:cyclohexane

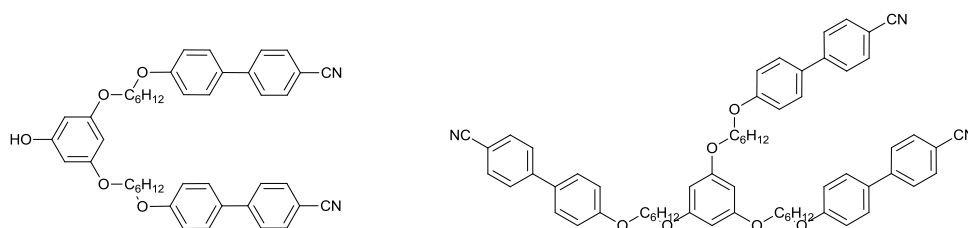
(5:1) as the eluent. 3,5-Bis(((6(4-(4'-hexyloxybiphenyl)oxy)hexyl)oxy)-phenyl benzoate was further treated by refluxing with KOH (1.906 g, 34.0 mmol) in THF/H₂O (1:1) 50 ml. After cooling at room temperature the reaction mixture was acidified with 1M HCl. The precipitate was filtered. The residue was dissolved in CH₂Cl₂ and washed with water and sat. aq. NaCl. The organic layer was dried over anhydrous MgSO₄, filtrated and concentrated. The crude product was purified by silica gel column chromatography using CH₂Cl₂ as the eluent. The product (**T7**) was isolated as a white solid 1.927 g, 53% (Mol. Wt: 831.13 g/mol) and **PG₆BPH₃** (**T8**) 0.365 g (Mol. Wt: 1183.64 g/mol) was obtained as a side product. (Scheme 14)

T7: ¹H NMR (CDCl₃): δ 7.48 (d, J=8.6Hz, 8H), 6.96(d, J=8.6Hz, 8H), 6.09 (t, J=2.1Hz, 1H), 6.01 (d, J=2.2Hz, 2H), 5.00 (s, 1H), 4.01 (t, J=6.4Hz, 4H), 4.00 (t, J=6.6Hz, 4H), 3.92 (t, J=6.4Hz, 4H), 1.94-1.70 (m, 12H), 1.6-1.2 (m, 20H), 0.92 (t, J=7.1Hz, 6H); ¹³C NMR (CDCl₃): δ 161.14, 158.26, 158.18, 157.19, 133.43, 133.32, 127.66, 127.65, 114.77, 94.62, 94.23, 68.13, 67.92, 67.89, 31.60, 29.29, 29.25, 29.14, 25.87, 22.61,14.03.

T8: ¹H NMR (CDCl₃) : δ 7.46 (d, J=8.8Hz, 12H), 6.94(d, J=8.8Hz, 12H), 6.079 (s, 3H), 4.05-3.95 (m, 12H), 3.92 (t, J=6.5Hz, 6H), 1.94-1.70 (m, 18H), 1.6-1.2 (m, 30H), 0.92 (t, J=7.1Hz, 9H); ¹³C NMR (CDCl₃): δ 160.95, 158.26, 158.18, 133.33, 127.65, 114.77, 93.90, 68.12, 67.94, 67.86, 31.60, 29.30, 29.26, 29.20, 25.89, 25.74, 22.61, 14.02.

T8: MALDI-ToF: Calcd for C₇₈H₁₀₂O₉: 1182.75; m/z: found: 1182.85 (M), 1183.87 (M+1), 1184.86 (M+2), 1185.86 (M+3). **EA** calcd: C 79.15, H 8.69; found: C 79.05, H 8.73.

(**T9**) HO-PG₆OCB₂ and (**T10**) PG₆OCB₃



T9 (and **T10**) was prepared according to the "Method A" from **2** (1.968 g, 5.5 mmol), **7a** (0.603 g, 2.6 mmol), using acetone (50 ml) as solvent refluxing for 72 h. The crude reaction mixture was further treated by refluxing with KOH (1.114 g, 19.9 mmol) in 30 ml THF/H₂O (1:1). The crude product was purified by silica gel column chromatography using CH₂Cl₂ as the eluent. The product (**T9**) was isolated as a white solid 0.994 g, 55% (Mol. Wt: 680.83 g/mol) and **PG₆OCB₃** (**T10**), 0.372 g, (Mol. Wt: 958.19 g/mol) was obtained as a side product. The reaction was carried out several times with similar yield. (Scheme 14)

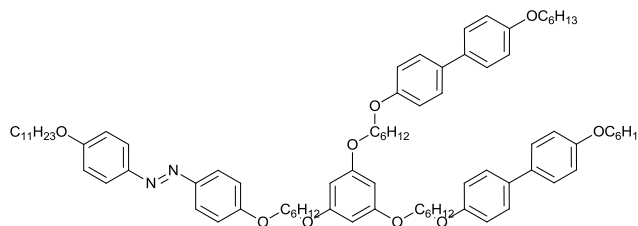
Experimental

T9: $^1\text{H-NMR}$ (CDCl_3): 7.67 (#q, $J=8.5\text{Hz}$, 8H), 7.53 (#d, $J=8.7\text{Hz}$, 4H), 7.00 (#d, $J=8.8\text{Hz}$, 4H), 6.07 (t, $J=2.1\text{Hz}$, 1H), 6.01 (d, $J=2.1\text{Hz}$, 2H), 4.69 (s, 1H), 4.03(t, $J=6.6$, 4H), 3.93(t, $J=6.4$, 4H), 1.94–1.72 (m, 8H), 1.64–1.44 (m, 8H); $^{13}\text{C NMR}$ (CDCl_3): 161.11, 159.74, 157.23, 145.26, 132.54, 131.34, 128.31, 127.06, 119.05, 115.10, 110.09, 94.60, 94.24, 67.99, 67.85, 29.13, 29.12, 25.84, 25.81.

T10: $^1\text{H-NMR}$ (CDCl_3): δ 7.67 (#q, $J=8.5\text{Hz}$, 12H), 7.53 (#d, $J=8.7\text{Hz}$, 6H), 7.00 (#d, $J=8.6\text{Hz}$, 6H), 6.11 (s, 3H), 4.02(t, $J=6.42\text{Hz}$, 6H), 3.95(t, $J=6.42\text{Hz}$, 6H), 1.94 – 1.72 (m, 12H), 1.64–1.44 (m, 12H); $^{13}\text{C NMR}$ (CDCl_3): δ 160.95, 159.75, 145.25, 132.55, 131.36, 128.33, 127.07, 119.06, 115.107, 110.12, 93.88, 68.01, 67.84, 29.19, 29.16, 25.89, 25.85.

T10: MALDI-ToF: Calcd for $\text{C}_{63}\text{H}_{63}\text{N}_3\text{O}_6$: 957.47; m/z : found: 958.43 (M+1), 959.45 (M+2), 960.45 (M+3). **EA** calcd: C 78.97, H 6.63, N 4.39; found: C 77.835, H 6.63, N 4.29

(T11) $\text{PG}_6\text{BPH}_2\text{AZB}$

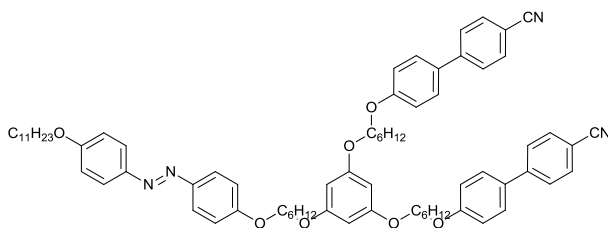


T11 was prepared according to the “Method B” from $\text{PG}_6\text{BPH}_2\text{OH}$ (**T7**) (0.642 g, 0.8 mmol) and **3** (0.451 g, 0.8 mmol), using DMF/THF (3:1, 12 ml) as solvent and CHCl_3 :cyclohexane (9:1) as the eluent for silica gel chromatography. The product was isolated as a yellow solid 0.859 g, 87% (Mol. Wt: 1281.79 g/mol). (Scheme 14)

$^1\text{H NMR}$ (CDCl_3): δ 7.87 (d, $J=8.8\text{Hz}$, 4H), 7.47 (d, $J=8.8\text{Hz}$, 8H), 6.99 (d, $J=8.8\text{Hz}$, 4H), 6.95 (d, $J=8.7\text{Hz}$, 8H), 6.09 (s, 3H), 4.12 – 3.86 (m, 18H), 1.94– 1.72 (m, 18H), 1.64 – 1.22 (m, 40H), 0.97 – 0.85 (m, 9H); $^{13}\text{C NMR}$ (CDCl_3): δ 161.19, 161.11, 160.97, 158.27, 158.19, 147.01, 146.97, 133.41, 133.33, 127.65, 124.30, 114.77, 114.68, 93.91, 68.35, 68.16, 68.12, 67.94, 67.90, 67.87, 67.84, 31.92, 31.61, 29.62, 29.58, 29.40, 29.34, 29.31, 29.26, 29.24, 29.20, 29.18, 26.03, 25.90, 25.84, 25.76, 22.69, 22.62, 14.11, 14.03.

MALDI-ToF: Calcd for $\text{C}_{83}\text{H}_{112}\text{N}_2\text{O}_9$: 1280.84, m/z : found: 1281.85 (M+1), 1282.85 (M+2), 1283.87 (M+3), 1284.88 (M+4), fragments: 1020.67 (M- $\text{C}_{17}\text{H}_{27}\text{NO}$). **EA** calcd: C 77.77, H 8.81, N 2.19; found: C 77.78, H 8.88, N 2.19.

(T12) PG₆OCB₂AZB

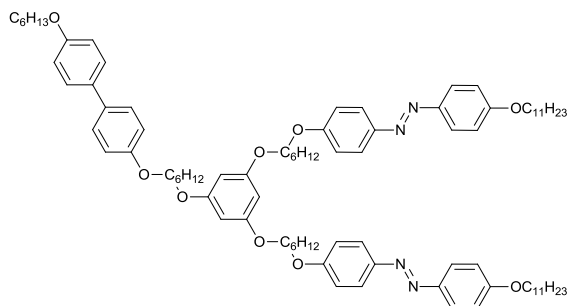


T12 was prepared according to the “Method B” from **PG₆OCB₂OH (T9)** (0.391 g, 0.6 mmol) and **3** (0.331 g, 0.6 mmol), using THF (6 ml) as solvent and CH₂Cl₂ as the eluent for silica gel chromatography. The product was isolated as a yellow solid 0.558 g, 86% (Mol. Wt: 1131.49 g/mol). (Scheme 14)

¹H NMR (CDCl₃): δ 7.9 (d, J=8.9Hz, 4H), 7.67 (#q, J=8.5Hz, 8H), 7.53 (d, J=8.8Hz, 4H), 7.08–6.9 (m, 8H), 6.14 (s, 3H), 4.1–3.90 (m, 14H), 1.92–1.74 (m, 14H), 1.66–1.2 (m, 28H), 0.93 (t, J=6.8Hz, 3H); ¹³C NMR (CDCl₃): δ 161.27, 161.15, 161.03, 159.81, 147.01, 146.95, 145.16, 132.53, 131.20, 128.31, 127.01, 124.37, 119.09, 115.14, 114.71, 110.05, 94.01, 93.97, 68.37, 68.17, 68.03, 67.87, 31.98, 29.68, 29.64, 29.47, 29.41, 29.29, 29.26, 29.22, 26.08, 25.95, 25.90, 22.75, 14.22.

MALDI-ToF: Calcd for C₇₃H₈₆N₄O₇: 1130.65, m/z: found: 1131.67 (M+1), 1132.68 (M+2), 1133.68 (M+3), 1134.70 (M+4). **EA** calcd: C 77.49, H 7.66, N 4.95; found: C 77.42, H 7.71, N 4.95.

(T13) PG₆AZB₂BPH:



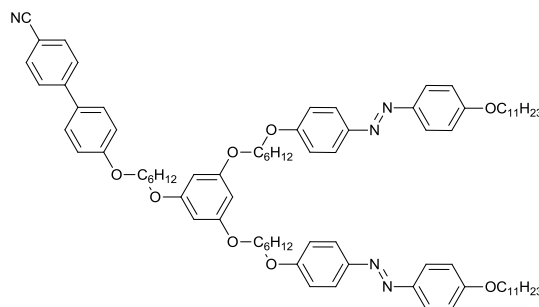
T13 was prepared according to the “Method B” from **T2** (0.997 g, 1.0 mmol) and **1** (0.465 g, 2.2 mmol), using DMF/THF 3:1 (12 ml) as solvent and CHCl₃:cyclohexane (9:1) as the eluent for silica gel chromatography. The product was isolated as a yellow solid 0.751 g, 56% (Mol. Wt: 1379.93 g/mol). (Scheme 15)

¹H NMR (CDCl₃): δ 7.86 (d, J=8.8Hz, 8H), 7.46 (d, J=8.8Hz, 4H), 6.99 (d, J=8.8Hz, 8H), 6.95 (d, J=8.7Hz, 4H), 6.08 (s, 3H), 4.12 – 3.86 (m, 18H), 1.94- 1.72 (m, 18H), 1.64 – 1.22 (m, 50H), 0.97 – 0.85 (m, 9H); ¹³C NMR (CDCl₃): δ 161.19, 161.10, 160.95, 158.26, 158.18, 147.00, 146.96, 133.41, 133.32, 127.65, 114.77, 114.67, 93.90, 124.29, 68.35, 68.16, 68.12, 67.94, 67.87, 67.83,

31.91, 31.60, 29.61, 29.60, 29.57, 29.39, 29.34, 29.30, 29.23, 29.17, 26.03, 25.89, 25.84, 25.75, 22.68, 22.61, 14.10, 14.02.

MALDI-ToF: Calcd for $C_{88}H_{122}N_4O_9$: 1378.92, m/z: found: 1379.86 (M+1), 1380.85 (M+2), 1381.88 (M+3), 1382.88 (M+4). **EA** calcd: C 76.59, H 8.91, N 4.06; found: C 76.40, H 8.86, N 4.16.

(T14) PG₆AZB₂OCB:



T14 was prepared according to the “Method B” from **T2** (0.702 g, 0.7 mmol) and **2** (0.0256 g, 0.7 mmol) using THF (7 ml) as solvent and CH_2Cl_2 as the eluent for silica gel chromatography. The product was isolated as yellow solid 0.391 g, 44 % (Mol. Wt: 1304.78 g/mol). (Scheme 15)

¹H NMR ($CDCl_3$): δ 7.87 (d, J=8.9Hz, 8H), 7.67 (#q, J=8.5Hz, 4H), 7.53 (d, J=8.8Hz, 2H), 6.99 (d, J=8.8Hz, 10H), 6.09 (s, 3H), 4.1 – 3.97 (m, 10H), 3.94 (t, J=6.3Hz, 6H), 1.92–1.74 (m, 16H), 1.65–1.17 (m, 44H), 0.9 (t, J=6.7Hz, 6H); **¹³C NMR** ($CDCl_3$): δ 161.22, 161.11, 160.98, 159.78, 147.02, 146.96, 145.26, 132.54, 131.30, 128.31, 127.06, 124.31, 119.07, 115.12, 114.69, 110.08, 93.94, 93.92, 68.36, 68.16, 68.03, 67.84, 31.93, 29.62, 29.59, 29.42, 29.35, 29.25, 29.18, 26.04, 25.90, 25.84, 22.70, 14.13.

MALDI-ToF: Calcd for $C_{83}H_{109}N_5O_8$: 1303.83, m/z: found: 1304.89 (M+1), 1305.89 (M+2), 1306.89 (M+3), 1307.91 (M+4), 1308.91 (M+5), fragments: 1043.67 (M-C₁₇H₂₇NO). **EA** calcd: C 76.40, H 8.42, N 5.37; found: C 76.31, H 8.49, N 5.33.

1.5.3 Synthesis of PG dendrimers

General procedures for etherification:

Method A: A mixture of the phenolic alcohol (1 equiv.), the bromide derivative (1.1-1.4 equiv.), K_2CO_3 (2-3 equiv.), 18-crown-6 (0.2 equiv.) and KI (catalytic amount) in solvent was refluxed under argon for 24 - 72 hours. The reaction mixture was cooled to room temperature and the solvent was evaporated under reduced pressure. The residue was dissolved in dichloromethane and washed sequentially with 0.1M aq. HCl, water and sat. aq. NaCl. The organic layer was dried

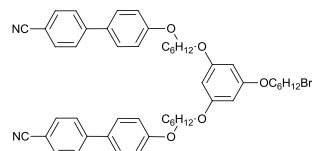
over anhydrous MgSO_4 , filtrated and concentrated. The crude product was purified by silica gel column chromatography.

Method B: A mixture of 3,5-dihydroxyphenyl benzoate (1 equiv.), first generation bromide derivative (2.0-2.5 equiv.), K_2CO_3 (3-4 equiv.), 18-crown-6 (0.2 equiv.) and KI (catalytic amount) in solvent was refluxed under argon for 24 - 72 hours. The reaction mixture was cooled to room temperature and the solvent evaporated under reduced pressure. The residue was dissolved in dichloromethane and washed sequentially with water and sat. aq. NaCl. The organic layer was dried over anhydrous MgSO_4 , filtrated and concentrated. The crude intermediate was dissolved in THF and alarge excess of 1-butylamine (8-10 equiv.) was added then refluxed for 18 - 24 hours. The reaction mixture was cooled to room temperature again and the solvent evaporated under reduced pressure. The residue was dissolved in dichloromethane and washed sequentially with 0.1M aq. HCl, water and sat. aq. NaCl. The organic layer was dried over anhydrous MgSO_4 , filtrated and concentrated. The crude product was purified by silica gel column chromatography.

General procedure for bromoalkylation:

A large excess (5-8 equiv.) of 1,6-dibromohexane was added to a mixture of phenolic alcohol (1 equiv.) and anhydrous K_2CO_3 (2 - 3 equiv.) in THF or acetone and was refluxed under argon for 48 h. The reaction mixture was cool to room temperature and the solvent was evaporated under reduced pressure. The residue was dissolved in CH_2Cl_2 and washed sequentially with water and sat. aq. NaCl. The organic layer was dried over Mg_2SO_4 , filtrated and concentrated by rotary evaporator. The crude product was precipitated and/or further purified using a silica gel column if was necessary.

(Pg1), *Br-6-PG₆OCB₂*



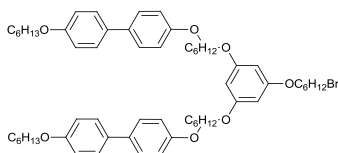
Pg1 was prepared by “bromoalkylation” from HO-PG₆OCB₂, (**T9**) (0.751g, 1.10 mmol), and 1,6-dibromohexane (1.5 ml, 9.75 mmol), using THF:acetone (1:2, 15 ml) as solvent (refluxed for 72 hours), CH_2Cl_2 as the eluent for silica gel chromatography and isolated as a white solid 0.929 g, 99% (Mol. Wt: 843.89 g/mol).(Scheme 17)

$^1\text{H NMR}$ (CDCl_3): δ : 7.74-7.58 (m, J=8H), 7.53 (d, J=8.7Hz, 4H), 7.00 (d, J=8.8Hz, 4H), 6.09 (s, 3H), 4.03(t, J=6.6, 4H), 3.98 - 3.84(m, 6H), 3.42 (t, J=6.9Hz, 2H), 1.94 - 1.72 (m, 12H), 1.64-1.44 (m, 12H); $^{13}\text{C NMR}$ (CDCl_3): δ : 160.95, 160.93, 159.76, 145.27, 132.55, 131.36, 128.32, 127.07,

Experimental

119.04, 115.12, 110.13, 93.97, 93.91, 68.03, 67.84, 67.76, 33.69, 32.68, 29.18, 29.16, 29.06, 27.90, 25.88, 25.84, 25.31

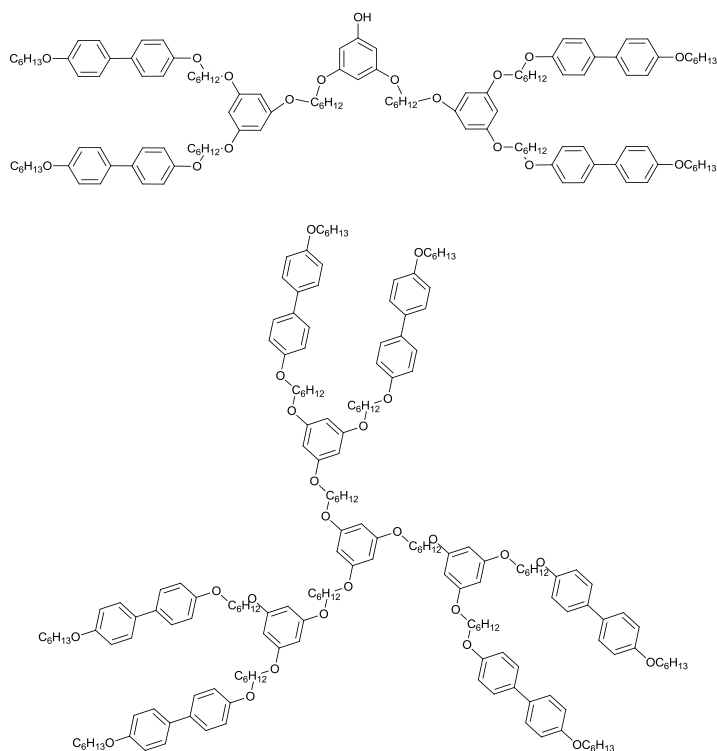
(Pg2), *Br-6-PG₆BPH₂*



Pg2 was prepared by “bromoalkylation” from HO-PG₆BPH₂, (**T7**) (1.004 g, 1.21 mmol), and 1,6-dibromohexane (1.5 ml, 9.75 mmol), using THF (15 ml) as solvent (refluxed for 72 hours). After workup the organic layer was dried over anhydrous MgSO₄, filtrated, concentrated and the crude product was precipitated, in methanol. The product was further purified using CH₂Cl₂ : cyclohexane (3:1) as the eluent for silica gel column chromatography and isolated as a white solid 1.126g 94% (Mol. Wt: 994.18 g/mol). The synthesis was carried out once more with a similar yield. (Scheme 17)

¹H NMR (CDCl₃): δ 7.46 (d, J=8.8Hz, 8H), 6.95 (d, J=8.6Hz, 8H), 6.07 (s, 3H), 4.06-3.88 (m, 14H), 3.43 (t, J=6.8 Hz, 2H), 1.95-1.70 (m, 16H), 1.60-1.28 (m, 24H), 0.92 (t, J=7Hz, 6H); ¹³C NMR (CDCl₃): δ 160.95, 160.90, 158.26, 158.18, 133.42, 133.32, 127.65, 114.77, 93.89, 68.13, 67.94, 67.87, 67.75, 33.74, 32.70, 31.60, 29.30, 29.26, 29.20, 29.07, 27.92, 25.89, 25.75, 25.32, 22.61, 14.02

(Pg3) HO-PG₆BPH₄ and (Pg5) PG₆BPH₆



The synthesis of **HO-PG₆BPH₄** was carried out three times, according to the following methods: **TBDMS protected phloroglucinol**: A mixture of Br-6-PG₆BPH_{2 (**Pg2**) (0.152 g, 0.15 mmol), TBDMS protected phloroglucinol (**6a**, 0.018 g, 0.07mmol), 18-crown-6 (0.005 g, 0.02 mmol), KI (catalytic amount) and K₂CO₃ (0.03 g, 0.22mmol) in THF (2 ml) was refluxed for 48 hours. The reaction mixture was cooled at room temperature and 0.1 ml TBAF (1M solution in THF) was added and stirred for further 16h at room temperature. The solvent was evaporated under reduced pressure, the residue dissolved in CHCl₃ and washed sequentially with 0.1M aq. HCl, water and sat. aq. NaCl. The organic layer was dried over anhydrous MgSO₄, filtrated and concentrated. The crude product was purified by silica gel column chromatography using CH₂Cl₂ to CH₂Cl₂:EtAc (40:1) as the eluent. This method produced mainly the first generation homolithic dendrimer **PG₆BPH₆** 0.076 g (Mol. Wt: 2865,93g/mol) instead of the desired product. (Scheme 18)}

Modified "Method B" using KOH for deprotection: A mixture of Br-6-PG₆BPH₂ (**Pg2**) (0.273 g, 0.27 mmol), and 3,5-dihydroxyphenyl benzoate (**7a**, 0.029 g, 0.13 mmol), K₂CO₃ (0.082 g, 0.59 mmol), 18-crown-6 (0.009 g, 0.03 mmol) and KI (catalytic amount) in DMF (3ml) was stirred at 80°C for 72 hours. Once cooled, the reaction mixture was poured into distilled water and the precipitate was isolated by filtration. The crude reaction mixture was further treated with KOH (0.118 g, 0.21 mmol) and refluxed in 4mL of THF/H₂O (1:1). After cooling at room temperature

Experimental

the reaction mixture was acidified with 2M HCl solution. The precipitate was filtered off and washed with distilled water. The residue was dissolved in CH₂Cl₂ and washed with sat. aq. NaCl. The organic layer was dried over anhydrous MgSO₄, filtrated and concentrated. The crude product was purified by silica gel column chromatography using CH₂Cl₂:EtAc (50:1 to 20:1) as the eluent. The product **HO-PG₆BPH₄** was isolated as white solid 0.052 g, 21% (overall yield) (Mol. Wt: 1952.66 g/mol).

Modified "Method B": A mixture of Br-6-PG₆BPH₂ (**Pg2**) (0.552 g, 0.68 mmol), and 3,5-dihydroxyphenyl benzoate (**7a**, 0.060 g, 0.26 mmol), K₂CO₃ (0.151 g, 1.09 mmol), 18-crown-6 (0.016 g, 0.06 mmol) and KI (catalytic amount) in THF:acetone (1:1, 4 ml) was refluxed under argon for 72 hours. The reaction mixture was cooled to room temperature and the solvent evaporated under reduced pressure. The residue was dissolved in dichloromethane and washed sequentially with 0.1M HCl aq, water and sat. aq. NaCl. The organic layer was dried over anhydrous MgSO₄, filtrated and concentrated. The crude protected product was purified by silica gel column chromatography using CH₂Cl₂:petroleum ether (20:1 to) as the eluent. The protected product **Bz-COO-PG₆BPH₄** (**Pg4**) was isolated as a white solid 0.439 g, 82% (Mol. Wt: 1652.06 g/mol).

¹H-NMR (CDCl₃): δ 8.20 (dd, J=8.4Hz, 1.4Hz, 2H), 7.64 (t, J=7.5Hz, 1H), 7.58 (t, J=7.6Hz, 2H), 7.47 (d, J=8.7Hz, 16H), 6.95 (d, J=8.4Hz, 16H), 6.39 (s, 3H), 6.09 (s, 6H), 4.06-3.84 (m, 32H), 1.92-1.68 (m, 32H), 1.62 – 1.32 (m, 48H), 0.93 (t, J=6.8Hz, 12H)

Due to the in-situ simultaneous deprotection of the 3,5-dihydroxyphenyl benzoate during the etherification the first generation homolithic dendrimer **PG₆BPH₆**, as by-product was generated and isolated as a white solid, 0.037 g PG₆BPH₆ (Mol. Wt: 2865,93g/mol).

PG₆BPH₆ (**Pg5**)

¹H-NMR (CDCl₃): 7.47 (d, J=8.7Hz, 24H), 6.95 (d, J=8.4Hz, 24H), 6.08 (s, 9H), 6.07 (s, 3H), 4.06-3.84 (m, 48H), 1.92-1.68 (m, 48H), 1.64 – 1.28 (m, 72H), 0.93 (t, J=6.8Hz, 18H); ¹³C NMR (CDCl₃): δ 160.95, 158.26, 158.19, 133.41, 133.33, 127.63, 114.77, 93.92, 68.13, 67.95, 67.87, 31.60, 29.30, 29.26, 29.21, 25.90, 25.74, 22.60, 14.01

MALDI-ToF: Calcd for C₁₈₆H₂₄₆O₂₄ : 2863.80; m/z: found: 2864.94 (M+1), 2865.93 (m+2), 2866.95 (M+3), 2867.94 (M+4), 2868.93 (M+5), fragment: 1034.83 (M- 2xC₆₀H₈₁O₇)

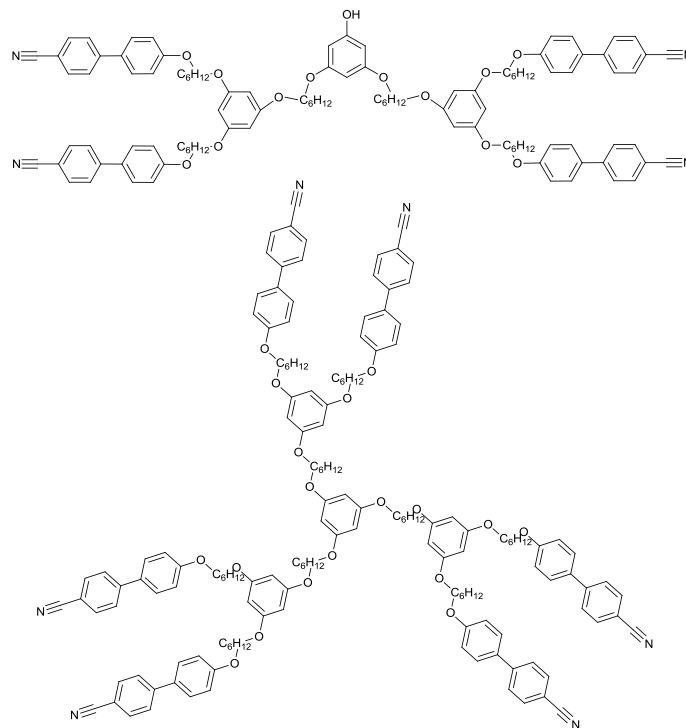
The intermediate (**Bz-PG₆BPH₄**) was dissolved in THF (2.5 ml), a large excess of 1-butylamine (0.24 ml, 2.43 mmol) was added and refluxed for 18 hours. Then the reaction mixture was cooled to room temperature and the solvent was evaporated under reduced pressure. The

residue was dissolved in CH₂Cl₂ and washed sequentially with 0.1M aq. HCl, water and sat. aq. NaCl. The organic layer was dried over anhydrous MgSO₄, filtrated and concentrated. The crude product was purified by silica gel column chromatography using CH₂Cl₂:EtAc (50:1 to 20:1) as the eluent. The product **HO-PG₆BPH₄** was isolated as a white solid 0.345 g, 68% (overall yield) (Mol. Wt: 1952.66 g/mol).

HO-PG₆BPH₄ (Pg3)

¹H-NMR (CDCl₃): δ 7.47 (d, J=8.7Hz, 16H), 6.95 (d, J=8.4Hz, 16H), 6.10 (s, 6H), 6.07 (t, J=2.0Hz, 1H), 5.99 (d, J=2.1Hz, 2H), 5.13 (s, 1H), 4.06-3.84 (m, 32H), 1.92-1.68 (m, 32H), 1.62 – 1.32 (m, 48H), 0.93 (t, J=6.8Hz, 12H); ¹³C NMR (CDCl₃): δ 161.13, 160.95, 158.26, 158.18, 157.27, 133.43, 133.33, 127.64, 114.78, 94.66, 94.21, 93.98, 68.14, 67.96, 67.89, 67.84, 31.60, 29.29, 29.25, 29.19, 29.15, 29.10, 25.88, 25.82, 25.81, 25.74, 22.59, 14.01

(Pg6) HO-PG₆OCB₄ and (Pg7) PG₆OCB₆



Pg6 was prepared according to the “Method B” from Br-6-PG₆OCB₂ (**PG2**) (0.574 g, 0.68 mmol), and 3,5-dihydroxyphenyl benzoate (**7a**, 0.068 g, 0.30 mmol), using THF:acetone (1:1, 6ml) as solvent (refluxed for 72 hours).), using 1-butylamine (0.3 ml, 3.04 mmol) in THF (4ml) for deprotection, CH₂Cl₂:EtAc (100:1 to 30:1) as the eluent for silica gel column chromatography and isolated as a white sticky solid 0.136 g, 28% (Mol. Wt: 1652.06 g/mol).

Due to the in-situ simultaneous deprotection of the 3,5-dihydroxyphenyl benzoate during the etherification, the first generation homolithic dendrimer **PG₆OCB₆**, as by-product was generated and isolated as a white viscous solid, 0.057 g (Mol. Wt: 2415,03 g/mol). (Scheme 19)

HO-PG₆OCB₄ (Pg6)

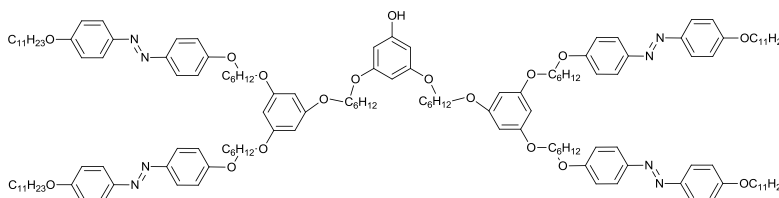
¹H-NMR (CDCl₃): δ 7.66 (q, J=8.2Hz, 16H), 7.53 (d, J=8.3Hz, 8H), 6.99 (d, J=8.7Hz, 8H), 6.08 (s, 6H), 6.05 (t, J=2.1Hz, 1H), 6.00 (d, J=2.2Hz, 2H), 5.09 (s, 1H), 4.02 (t, J=6.4Hz, 8H), 3.98-3.82 (m, 16H), 1.92-1.68 (m, 24H), 1.66 – 1.40 (m, 24H); ¹³C NMR (CDCl₃): δ 161.11, 160.98, 160.94, 159.76, 157.41, 145.27, 132.54, 131.35, 128.31, 127.06, 119.06, 115.13, 110.10, 94.69, 94.16, 93.97, 68.03, 67.86, 29.15, 25.87, 25.83,

PG₆OCB₆ (Pg7)

¹H-NMR (CDCl₃): δ 7.66 (q, J=8.2Hz, 24H), 7.53 (d, J=8.3Hz, 12H), 6.99 (d, J=8.7Hz, 12H), 6.07 (s, 9H), 6.06 (s, 3H), 4.02 (t, J=6.4Hz, 12H), 3.98-3.82 (m, 24H), 1.92-1.68 (m, 36H), 1.66 – 1.40 (m, 36H); ¹³C NMR (CDCl₃): δ 160.95, 159.75, 145.24, 132.54, 131.35, 128.31, 127.06, 119.04, 115.11, 110.12, 93.90, 68.02, 67.89, 67.84, 29.22, 29.19, 29.16, 25.92, 25.88, 25.84

MALDI-ToF: Calcd for C₁₅₆H₁₆₈N₆O₁₈ : 2413,24; m/z: found: 2414.48 (M+1), 2415.49 (M+2), 2416.42 (M+3), 2417.43 (M+4)

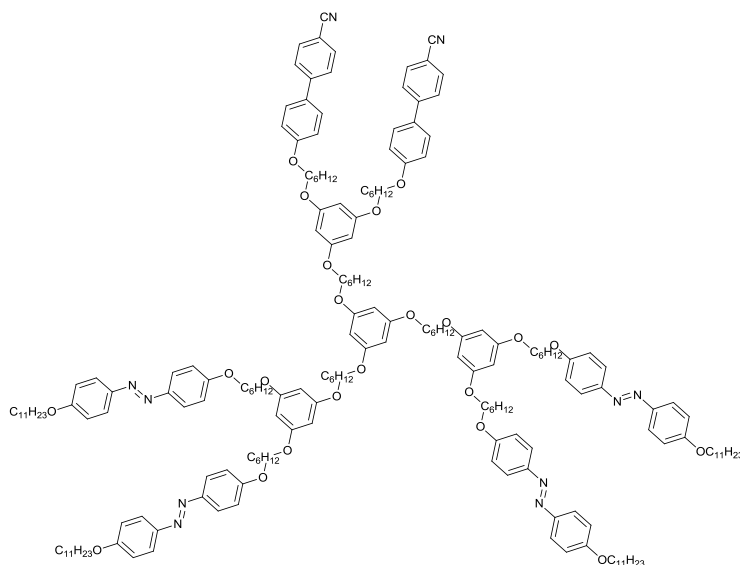
(Pg8), HO-PG₆AZB₄



Pg8 was prepared according to the “Method B” from Br-6-PG₆AZB₂, (**T4**) (0.571 g, 0.48 mmol), 3,5-dihydroxyphenyl benzoate (**7a**, 0.050 g, 0.22 mmol), acetone/THF (1:2, 6ml) as solvent (refluxed for 48 hours), using 1-butylamine (0.3 ml, 3.04 mmol) in THF (3ml) for deprotection, CH₂Cl₂:EtAc (100:1) as the eluent for silica gel column chromatography and isolated as a yellow viscous solid 0.355 g, 70% (Mol. Wt: 2345.24 g/mol). (Scheme 19)

¹H-NMR (CDCl₃): δ 7.87 (d, J=8.9Hz, 16H), 7.00 (d, J=8.7Hz, 16H), 6.10 (s, 6H), 6.06 (t, J=2.1Hz, 1H), 5.98 (d, J=2.0Hz, 2H), 4.12-3.90 (m, 28H), 3.87 (t, J=6.8H, 4H), 1.96-1.68 (m, 32H), 1.62 – 1.20 (m, 88H), 0.92 (t, J=6.6Hz, 12H); ¹³C NMR (CDCl₃): δ 161.22, 161.14, 160.97, 157.54, 147.01, 146.97, 124.33, 114.71, 94.70, 94.16, 94.00, 68.37, 68.18, 67.87, 31.94, 29.63, 29.60, 29.43, 29.36, 29.26, 29.19, 26.06, 25.91, 25.85, 22.71, 14.14

(Pg9) PG₆AZB₄OCB₂

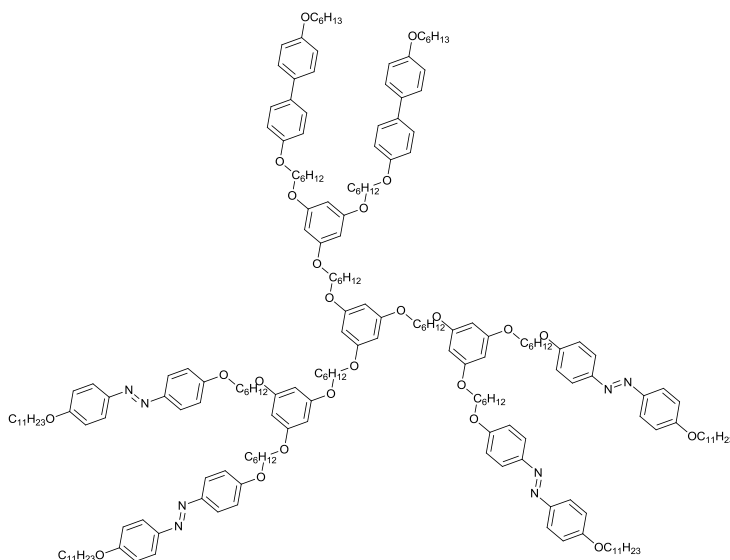


Pg9 was prepared according to the “Method A” from Br-6-PG₆OCB₂ (**Pg2**) (0.0653 g, 0.08 mmol), and HO-PG₆AZB₄ (**Pg8**) (0.1352 g, 0.06 mmol) using THF (2ml) as solvent (refluxed for 72 hours). The crude product was purified twice by silica gel column chromatography using CH₂Cl₂:EtAc (100:1) as the eluent. Product **PG₆AZB₄OCB₂** was isolated as yellow viscous solid 0.123 g, 51% (Mol. Wt: 3108.22 g/mol). (Scheme 20)

¹H-NMR (CDCl₃): δ 7.88 (d, J=8.9Hz, 16H), 7.65 (q, J=8.7Hz, 8H), 7.52 (d, J=8.7Hz, 4H), 6.99 (d, J=8.8Hz, 20H), 6.09 (s, 9H), 6.08 (s, 3H), 4.10-3.86 (m, 44H), 1.92-1.72 (m, 44H), 1.64 – 1.20 (m, 100H), 0.91 (t, J=6.7Hz, 12H); **¹³C NMR** (CDCl₃): δ 161.22, 161.12, 160.97, 159.77, 147.00, 146.95, 145.23, 132.53, 131.30, 128.31, 127.04, 124.31, 119.06, 115.11, 114.68, 110.09, 93.92, 68.35, 68.16, 68.01, 67.88, 67.84, 31.92, 30.88, 29.62, 29.59, 29.42, 29.35, 29.25, 29.20, 29.18, 26.04, 25.91, 25.86, 22.70, 14.13

MALDI-ToF: Calcd for C₁₉₆H₂₆₀N₁₀O₂₂: 3105.95; m/z: found: 3106.84 (M+1); fragments: 2845.62 (M- C₁₇H₂₇NO), 2586.45 (M- 2x C₁₇H₂₇NO), 2327.27 (M- 3x C₁₇H₂₇NO)

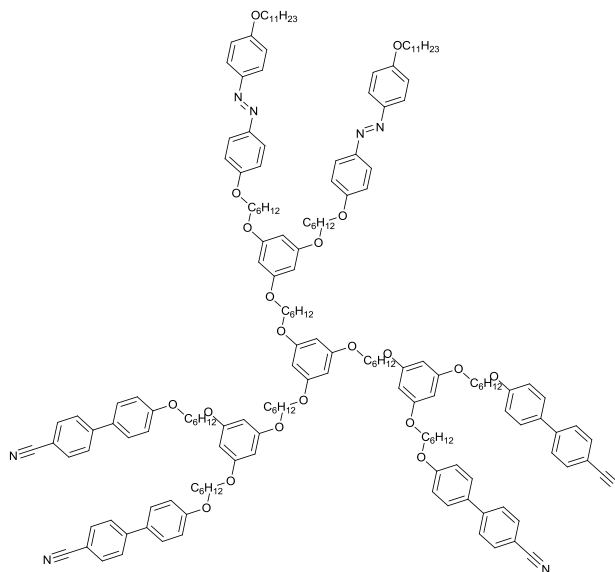
(Pg10) PG₆AZB₄BPH₂



Pg10 was prepared according to the “Method A” from 6-Br-PG₆BPH₂ (**Pg1**) (0.0768 g, 0.08 mmol), and HO-PG₆AZB₄ (**Pg8**) (0.1482 g, 0.06 mmol), using THF (3ml) as solvent (refluxed for 72 hours). The crude product was purified three times by silica gel column chromatography using CH₂Cl₂:EtAc (100:1) as the eluent and further by Bio-Beads SX-1 gel permeation chromatography swollen in CH₂Cl₂. Product **PG₆AZB₄BPH₂** was isolated as a yellow sticky solid 0.026 g, 10% (Mol. Wt: 3258.51 g/mol). (Scheme 20)

¹H-NMR (CDCl₃): δ 7.87 (d, J=8.9Hz, 16H), 7.46 (d, J=8.7Hz, 8H), 6.98 (d, J=8.7Hz, 16H), 6.94 (d, J=8.7Hz, 8H), 6.08 (s, 9H), 6.07 (s, 3H), 4.10-3.84 (m, 48H), 1.92-1.72 (m, 48H), 1.64 – 1.20 (m, 112H), 0.96-0.84 (m, 18H); ¹³C NMR (CDCl₃): δ 161.20, 161.11, 160.95, 158.26, 158.19, 146.98, 146.95, 133.40, 133.32, 127.64, 124.30, 114.77, 114.67, 93.90, 68.35, 68.16, 68.12, 67.94, 67.87, 67.84, 31.92, 31.61, 29.60, 29.58, 29.40, 29.34, 29.31, 29.23, 29.19, 26.03, 25.90, 25.84, 25.75, 22.68, 22.61, 14.11, 14.03

MALDI-ToF: Calcd for C₂₀₆H₂₈₆N₈O₂₄: 3256.14; m/z: found: 3258.09 (M+1); fragments: 2997.86 (M- C₁₇H₂₇NO), 2738.65 (M- 2x C₁₇H₂₇NO), 2481.46 (M- 3x C₁₇H₂₇NO)

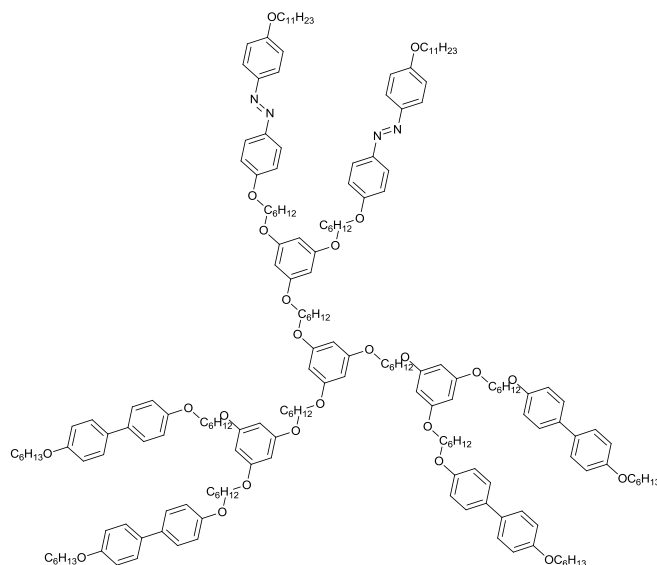
(Pg11) PG₆OCB₄AZB₂

Pg11 was prepared according to the “Method A” from Br-6-PG₆AZB₂ (**T4**) (0.0873 g, 0.07 mmol), and HO-PG₆OCB₄ (**Pg6**) (0.100 g, 0.06 mmol), using THF (3ml) as solvent (refluxed for 72 hours). The crude product was purified twice by silica gel column chromatography using CH₂Cl₂:EtAc (100:1 and 60:1 to 10:1). Product **PG₆OCB₄AZB₂** was isolated as a yellow sticky solid 0.096 g, 47% (Mol. Wt: 2761.62 g/mol). (Scheme 20)

¹H-NMR (CDCl₃): δ 7.87 (d, J=8.8Hz, 8H), 7.66 (q, J=8.6Hz, 16H), 7.52 (d, J=8.7Hz, 8H), 6.99 (d, J=8.8Hz, 16H), 6.08 (s, 9H), 6.07 (s, 3H), 4.10-3.86 (m, 40H), 1.92-1.72 (m, 40H), 1.64 – 1.20 (m, 68H), 0.90 (t, J=6.7Hz, 6H); **¹³C NMR** (CDCl₃): δ 161.21, 161.10, 160.95, 159.75, 146.99, 146.93, 145.24, 132.55, 131.33, 128.31, 127.06, 124.30, 119.07, 115.11, 114.67, 110.09, 93.86, 68.36, 68.16, 68.01, 67.87, 67.83, 31.92, 29.62, 29.58, 29.40, 29.34, 29.23, 29.20, 29.18, 26.03, 25.90, 25.86, 22.69, 14.11

MALDI-ToF: Calcd for C₁₇₆H₂₁₄N₈O₂₀: 2759.60; m/z: found: 2760.56 (M+1), 2761.55 (M+2), 2762.58 (M+3), 2763.57 (M+4), 2764.56 (M+5), 2765.58 (M+6), 2766.58 (M+7), 2767.57 (M+8); fragments: 2499.30 (M- C₁₇H₂₇NO), 2240.12 (M- 2x C₁₇H₂₇NO)

(Pg12) PG₆BPH₄AZB₂

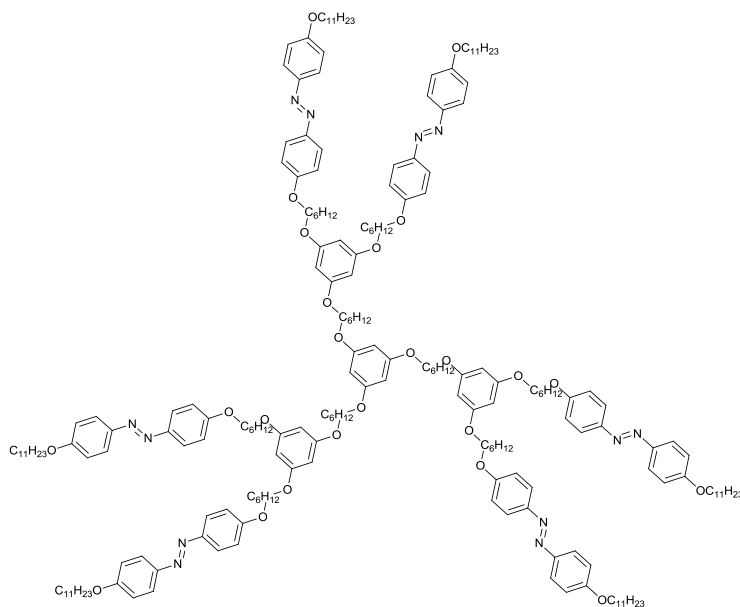


Pg12 was prepared according to the “Method A” from Br-6-PG₆AZB₂ (**T4**) (0.1498 g, 0.13 mmol), and HO-PG₆BPH₄ (**Pg3**) (0.1923 g, 0.10 mmol), using THF (3ml) as solvent (refluxed for 72 h). The crude product was purified twice by silica gel column chromatography using CH₂Cl₂:EtAc (100:1 and 1:0). Product **PG₆BPH₄AZB₂** was isolated as yellow viscous solid 0.147 g, 38% (Mol. Wt: 3062.22 g/mol). (Scheme 20)

¹H-NMR (CDCl₃): δ 7.87 (d, J=8.8Hz, 8H), 7.46 (d, J=8.7Hz, 16H), 6.98 (d, J=8.7Hz, 8H), 6.94 (d, J=8.7Hz, 16H), 6.08 (s, 9H), 6.07 (s, 3H), 4.08-3.84 (m, 48H), 1.92-1.70 (m, 48H), 1.64 – 1.20 (m, 92H), 0.98-0.84 (m, 18H); **¹³C NMR** (CDCl₃): δ 161.22, 161.12, 160.96, 158.27, 158.20, 146.99, 146.95, 133.41, 133.33, 127.63, 124.31, 114.78, 114.69, 93.92, 68.36, 68.16, 68.13, 67.95, 67.87, 31.91, 31.60, 29.60, 29.57, 29.39, 29.33, 29.31, 29.27, 29.23, 26.03, 25.90, 25.84, 25.75, 22.67, 22.60, 14.09, 14.01

MALDI-ToF: Calcd for C₁₉₆H₂₆₆N₄O₂₄: 3059.97; m/z: found: 3060.87 (M+1), 3061.87 (M+2), 3062.88 (M+3), 3063.88(M+4), 3064.89 (M+5), 3065.86 (M+6), 3066.87 (M+7), 3067.84 (M+8); fragments: 2799.60 (M- C₁₇H₂₇NO)

(Pg13) **PG₆AZB₆**

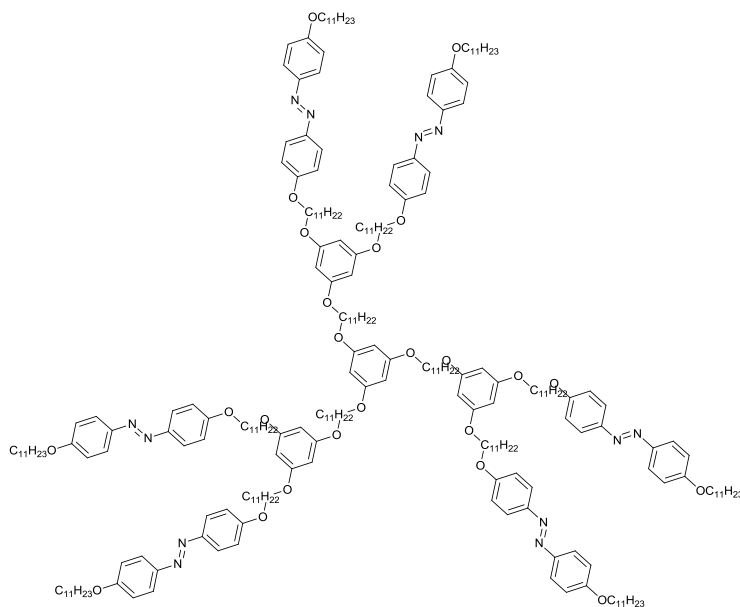


A mixture of HO-PG₆AZB₂ (**T2**) (0.316 g, 0.31 mmol), and 1,3,5-tris((6-bromohexyl)oxy)benzene (**5**) (0.062 g, 0.10 mmol), K₂CO₃ (0.081 g, 0.59 mmol), 18-crown-6 (0.016 g, 0.06 mmol) and KI (catalytic amount) in DMF (4 ml) was stirred at 80°C for 72 hours. Once cooled, the reaction mixture was poured into distilled water and the precipitate was isolated by filtration. The residue was dissolved in CH₂Cl₂ and washed with sat. aq. NaCl. The organic layer was dried over anhydrous MgSO₄, filtrated and concentrated. The crude product was purified by silica gel column chromatography using CH₂Cl₂:petroleum ether (5:1) as the eluent. The product **PG₆AZB₆** was isolated as a yellow solid 0.093 g, 27% (Mol. Wt: 34554.81 g/mol). (Scheme 21)

¹H-NMR (CDCl₃): δ 7.87 (d, J=8.8Hz, 24H), 7.00 (d, J=8.7Hz, 24H), 6.09 (s, 9H), 6.08 (s, 3H), 4.10-3.86 (m, 48H), 1.92-1.72 (m, 48H), 1.62 – 1.20 (m, 132H), 0.90 (t, J=6.7Hz, 18H); **¹³C NMR** (CDCl₃): δ 161.20, 161.11, 160.96, 147.02, 146.98, 124.30, 114.68, 93.93, 68.36, 68.16, 67.89, 67.84, 31.92, 29.61, 29.58, 29.41, 29.34, 29.24, 29.19, 29.18, 26.04, 25.91, 25.85, 22.69, 14.11

MALDI-ToF: Calcd for C₂₁₆H₃₀₆N₁₂O₂₄ : 3452.31; m/z: found: 3453.46 (M+1) fragments: 3193.12 (M- C₁₇H₂₇NO), 2427.49 (M- C₆₄H₈₉N₄O₇)

(Pg14) PG₁₁AZB₆



A mixture of HO-PG₁₁AZB₂ (**T3**) (0.774 g, 0.66 mmol), and 1,3,5-tris((11-bromoundecyl)oxy)benzene (**4**) (0.149 g, 0.18 mmol), K₂CO₃ (0.211 g, 1.53 mmol), and KI (catalytic amount) in DMF (6 ml) was stirred at 80°C for 72 hours. Once cooled, the reaction mixture was poured into distilled water and the precipitate was isolated by filtration. The residue was dissolved in CH₂Cl₂ and washed with sat. aq. NaCl. The organic layer was dried over anhydrous MgSO₄, filtrated and concentrated. The crude product was purified by silica gel column chromatography using CH₂Cl₂:cyclohexane (3:1 to 9:1) as the eluent. The product **PG₁₁AZB₆** was isolated as a yellow solid 0.159 g, 22% (Mol. Wt: 4086.00 g/mol). (Scheme 21)

¹H-NMR (CDCl₃): δ 7.88 (d, J=8.8Hz, 24H), 7.00 (d, J=8.7Hz, 24H), 6.09 (s, 12H), 4.03 (t, J=6.5Hz, 24H), 3.92 (t, J=6.7Hz, 24H), 1.92-1.64 (m, 48H), 1.56 – 1.20 (m, 222H), 0.90 (t, J=6.7Hz, 18H);
¹³C NMR (CDCl₃): δ 161.16, 160.98, 146.97, 124.28, 114.66, 93.85, 68.34, 68.02, 31.91, 29.61, 29.60, 29.57, 29.54, 29.52, 29.39, 29.33, 29.27, 29.23, 26.06, 26.03, 22.67, 14.09,

MALDI-ToF: Calcd for C₂₆₁H₃₉₆N₁₂O₂₄ : 4083.01; m/z: found: 4088.40; fragments: 3829.50 (M - C₁₇H₂₇NO), 3569.66 (M - 2xC₆₄H₈₉N₄O₇), 3310.26 (M - 3xC₆₄H₈₉N₄O₇),

1.5.4 Synthesis of BA dendrimers

General procedures for etherifications:

Method A: A mixture of phenolic alcohol (1 equiv.), benzyl bromide (small excess), K_2CO_3 (1.0 – 2.2 equiv.), 18-crown-6 (0.2 equiv.) and KI (catalytic amount) in solvent was refluxed under argon for 24 - 72 hours. Then the reaction mixture was cooled to room temperature and the solvent evaporated under reduced pressure. The residue was dissolved in dichloromethane and washed sequentially with 0.1M aq.HCl, water and sat. aq. NaCl. The organic layer was dried over anhydrous $MgSO_4$, filtrated and concentrated. The crude product was purified by silica gel column chromatography.

Method B: A mixture of 3,5-dihydroxyphenyl benzoate (1 equiv.), benzyl bromide (2.0-2.5 equiv.), K_2CO_3 (2.0 – 3.5 equiv.), 18-crown-6 (0.2 equiv.) and KI (catalytic amount) in solvent was refluxed under argon for 24 - 72 hours. Then the reaction mixture was cooled to room temperature and a large excess of 1-butylamine (8-10 equiv.) was added and refluxed once more for 18 - 24 hours. Then the reaction mixture was cooled to room temperature again and the solvent was evaporated under reduced pressure. The residue was dissolved in dichloromethane and washed sequentially with 0.1M aq. HCl, water and sat. aq. NaCl. The organic layer was dried over anhydrous $MgSO_4$, filtrated and concentrated. The crude product was purified by silica gel column chromatography.

Method E: A mixture of 3,5-dihydroxybenzyl-alcohol (1 equiv.), bromide derivative of the functional group (**Br-6-M**, 2.0-2.2 equiv.), K_2CO_3 (3-4 equiv.), 18-crown-6 (0.1-0.2 equiv.) and KI (catalytic amount) in solvent was refluxed under argon for 24 - 72 hours. The reaction mixture was cooled to room temperature and the solvent evaporated under reduced pressure. The residue was dissolved in dichloromethane and washed sequentially with 0.1M HCl aq., water and sat. aq. NaCl. The organic layer was dried over anhydrous $MgSO_4$, filtrated and concentrated. The crude product was purified by silica gel column chromatography.

General procedures for bromination of benzyl alcohol:

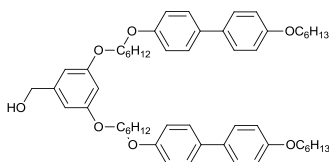
Method C: A mixture of benzyl alcohol (1 equiv.), PPh_3 (2 equiv.) and CBr_4 (2 equiv.) in dry THF, was stirred for 1 hour under argon at room temperature and then added to water. The mixture was extracted with CH_2Cl_2 and the organic layer was dried over anhydrous $MgSO_4$, filtrated and concentrated. The crude product was purified by silica gel column chromatography.

Method D: To a solution of benzyl alcohol (1 equiv.) in CH_2Cl_2 , PBr_3 (1M solution in CH_2Cl_2 , 0.8 - 1 equiv.) was added dropwise at $0^\circ C$ and was stirred for 1h at the same temperature. The

Experimental

mixture was diluted with CH_2Cl_2 and washed with sat. aq. NaHCO_3 , and sat. aq. NaCl . If the extraction led to micelle formation (it was cloudy), then the collected water layer was extracted with ethyl acetate as well. The combined organic layers were dried over anhydrous Na_2SO_4 , filtrated and concentrated. The crude product was filtered through a silica plug.

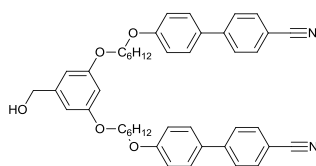
(Ba1) *HO-BA₆BPH₂*



Ba1 was prepared according to the “Method E” from 4-(6-Bromohexyloxy)-4'-hexyloxybiphenyl (**1**, 3.000g, 6.93 mmol) and 3,5-dihydroxybenzyl alcohol (0.452 g, 3.23 mmol) using acetone:THF (2:1, 40 ml) as solvent (refluxed for 48 hours), CH_2Cl_2 :EtAc (100:1 to 25:1) as the eluent for silica gel chromatography and isolated as white solid 1.735 g, 64% (Mol.Wt: 845.16 g/mol). The synthesis was repeated one more time (0.402 g, 83%) (Scheme 23)

$^1\text{H NMR}$ (CDCl_3) : δ 7.47 (d, $J=8.8\text{Hz}$, 8H), 6.96(d, $J=8.8\text{Hz}$, 8H), 6.54 (d, $J=2.1\text{Hz}$, 2H), 6.4 (t, $J=2.1\text{Hz}$, 1H), 4.63 (d, $J=5.9\text{Hz}$, 2H), 4.12-3.88 (m, 12H), 1.96-1.73 (m, 12H), 1.7-1.2 (m, 20H), 0.93 (t, $J=6.8\text{Hz}$, 6H); $^{13}\text{C NMR}$ (CDCl_3): δ 160.41, 158.29, 158.19, 143.25, 133.446, 133.33, 127.668, 114.785, 105.14, 100.642, 68.13, 67.94, 67.92, 65.46, 33.745, 31.622, 29.302, 29.185, 25.895, 25.764, 22.629, 14.044

(Ba2) *HO-BA₆OCB₂*

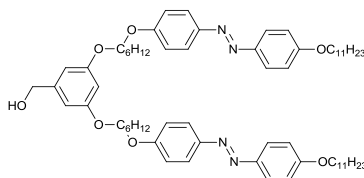


Ba2 was prepared according to the “Method E” from 6-bromo-(4-cyanobiphenyl-4'-oxy)hexane (**2**, 4.400 g, 12.28 mmol) and 3,5-dihydroxybenzyl alcohol (0.780 g, 5.69 mmol) using acetone:THF (2:1, 60 ml) as solvent (refluxed for 72 hours), CH_2Cl_2 :EtAc (50:1 to 20:1) as the eluent for silica gel chromatography and isolated as a white solid 3.321 g 84% (Mol.Wt: 694.86 g/mol). The synthesis was repeated more times with similar yield (0.273g 78% and 1.740 g, 72%, no 18-crown-6). (Scheme 23)

$^1\text{H NMR}$ (CDCl_3) : δ 7.67 (q, $J=8.2\text{Hz}$, 8H), 7.53 (d, $J=8.7\text{Hz}$, 4H), 7.00 (d, $J=8.8\text{Hz}$, 4H), 6.52 (d, $J=2.3\text{Hz}$, 2H), 6.39 (t, $J=2.3\text{Hz}$, 1H), 4.63 (d, $J=4.3\text{Hz}$, 2H), 4.03 (t, $J=6.5\text{Hz}$, 4H), 3.97(t, $J=6.5$, 4H),

1.94 – 1.72 (m, 8H), 1.62 (t, J=6.2Hz, 1H), 1.58-1.46 (m, 8H); ^{13}C NMR (CDCl_3): δ 160.50, 159.75, 145.27, 143.28, 132.55, 131.36, 128.33, 127.08, 119.08, 115.11, 110.10, 105.09, 100.66, 68.01, 67.88, 65.44, 29.20, 29.17, 25.88, 25.85

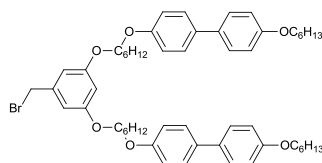
(Ba3) HO-BA₆AZB₂



Ba3 was prepared according to the “Method E” from **3** (Br-6-AZB, 2.260g, 4.25 mmol), and 3,5-dihydroxybenzyl alcohol (0.277g, 1.98 mmol) using THF:acetone (1:1, 30 ml) as solvent (refluxed for 72 hours), CH_2Cl_2 :EtAc (50:1 to 20:1) as the eluent for silica gel chromatography and isolated as a yellow solid 1.760 g, 86% (Mol.Wt: 1041.45 g/mol). The synthesis was repeated one more time with a similar yield (0.946g 84%). (Scheme 23)

^1H NMR (CDCl_3) : δ 7.86 (d, J=8.6Hz, 8H), 6.99(d, J=8.8Hz, 8H), 6.51 (d, J=2.1Hz, 2H), 6.39 (t, J=2.2Hz, 1H), 4.63 (d, J=5.9Hz 2H), 4.1-4.0 (m, 8H), 3.97 (t, J=6.4Hz, 4H), 1.93-1.73 (m, 12H), 1.65 (t, J=6.1Hz, 1H), 1.60-1.16 (m, 40H), 0.89 (t, J=6.5Hz, 6H); ^{13}C NMR (CDCl_3): δ 161.19, 161.09, 160.51, 147.00, 146.95, 143.27, 124.29, 114.68, 105.13, 100.62, 68.35, 68.14, 67.87, 65.44, 31.90, 29.60, 29.56, 29.39, 29.33, 29.23, 29.18, 29.15, 26.03, 25.86, 25.82, 22.67, 14.09

(Ba4) Br-BA₆BPH₂



Ba4 was prepared according to three methods (Scheme 23):

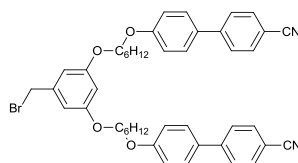
- i. according to “Method C” from **Ba1** (HO-BA₆BPH₂, 0.191 g, 0.23 mmol), PPh_3 (0.125 g, 0.48 mmol) and CBr_4 (0.167 g, 0.50 mmol) using THF as solvent (5ml) and CH_2Cl_2 as the eluent for silica gel column chromatography and isolated as a white solid 0.160 g, which contained 30% of benzyl chloride by- product which was not possible to separate.
- ii. according to “Method D” from **Ba1** (HO-BA₆BPH₂, 1.380 g, 1.63 mmol) and PBr_3 (1.60 ml, 1.60 mmol, 1M solution in CH_2Cl_2), using CH_2Cl_2 (20ml) as a solvent and was isolated as a white solid 1.030 g, 71% (Mol.Wt: 908.05 g/mol).

Experimental

iii. To a solution **Ba1** (HO-BA₆BPH₂ (0.186g, 0.22mmol)) in dry CH₂Cl₂ (3ml) trimethylsilyl bromide (TMSBr, 0.142g, 0.93mmol) was added at room temperature. After 6 days the the solvent was evaporated under reduced pressure. The crude product was purified by silica gel column chromatography using CH₂Cl₂ as the eluent. The product was isolated as a white solid, 0.07g, 35.03%.

¹H NMR (CDCl₃) : δ 7.51 (d, J=8.6Hz, 8H), 6.99 (d, J=8.6Hz, 8H), 6.57 (d, J=1.9Hz, 2H), 6.47-6.42 (m, 1H), 4.44 (s, 2H), 4.12-3.88 (m, 12H), 1.98-1.74 (m, 12H), 1.68-1.30 (m, 20H), 0.97 (t, J=6.7Hz, 6H); ¹³C NMR (CDCl₃): δ 160.41, 158.29, 158.19, 139.61, 133.45, 133.33, 127.67, 114.79, 107.49, 101.51, 68.14, 67.95, 33.75, 31.62, 29.30, 29.19, 25.90, 25.76, 22.63, 14.04

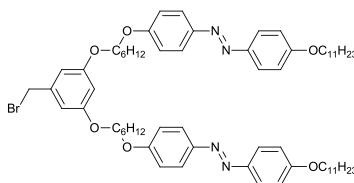
(Ba5) Br-BA₆OCB₂



Ba5 was prepared according to “**Method D**” from **Ba2** (HO-BA₆OCB₂, 2.673, 3.85 mmol) and PBr₃ (4.0 ml, 4.00 mmol), using CH₂Cl₂ (11ml) as a solvent and was isolated as a white solid 2.300 g, 76% (Mol.Wt: 757.75 g/mol). The synthesis was repeated one more time with a similar yield (0.595g 78%). (Scheme 23)

¹H NMR (CDCl₃) : δ 7.74-7.58 (m, J=8H), 7.53 (d, J=8.7Hz, 4H), 7.00 (d, J=8.8Hz, 4H), 6.52 (d, J=2.3Hz, 2H), 6.39 (t, J=2.3Hz, 1H), 4.41 (s, 2H), 4.03 (t, J=6.5Hz, 4H), 3.97(t, J=6.5, 4H), 1.94 – 1.72 (m, 8H), 1.64-1.44 (m, 8H); ¹³C NMR (CDCl₃): δ 160.38, 159.75, 145.26, 139.63, 132.56, 131.35, 128.34, 127.08, 119.08, 115.11, 110.10, 107.44, 101.53, 68.00, 67.93, 33.72, 29.16, 25.87, 25.85

(Ba6) Br-BA₆AZB₂



Ba6 was prepared according to two methods (Scheme 23):

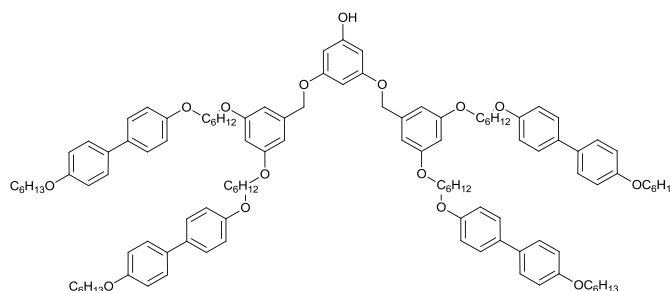
- according to “**Method C**” from **Ba3** (HO-BA₆AZB₂, 0.200 g, 0.19 mmol), PPh₃ (0.080 g, 0.31 mmol) and CBr₄ (0.105 g, 0.32 mmol) using THF as solvent (3ml) and CH₂Cl₂ as the

eluent for silica gel column chromatography and isolated as a white solid 0.156 g, which contained 10% of benzyl chloride byproduct which was not possible to separate.

- ii. according to “**Method D**” from **Ba3 (HO-BA₆AZB₂**, 1.660 g, 1.59 mmol) and PBr₃ (1.70 ml, 1.70 mmol, 1M solution in CH₂Cl₂), using CH₂Cl₂ (35ml) as a solvent and was isolated as a yellow powder 1.044 g, 56% (Mol.Wt: 1104.35 g/mol).

¹H NMR (CDCl₃) : δ 7.87 (d, J=8.8Hz, 8H), 6.99 (d, J=8.9Hz, 8H), 6.53 (d, J=2.2Hz, 2H), 6.4 (t, J=2.3Hz, 1H), 4.42 (s, 2H), 4.13-3.99 (m, 8H), 3.96 (t, J=6.3Hz, 4H), 1.96-1.70 (m, 12H), 1.66-1.16 (m, 40H), 0.9 (t, J=6.7Hz, 6H); ¹³C NMR (CDCl₃): δ 161.21, 161.10, 160.39, 146.99, 146.95, 139.61, 124.30, 114.68, 107.48, 101.49, 68.35, 68.13, 67.93, 33.72, 31.91, 29.61, 29.58, 29.39, 29.34, 29.23, 29.15, 26.03, 25.86, 25.84, 22.68, 14.11

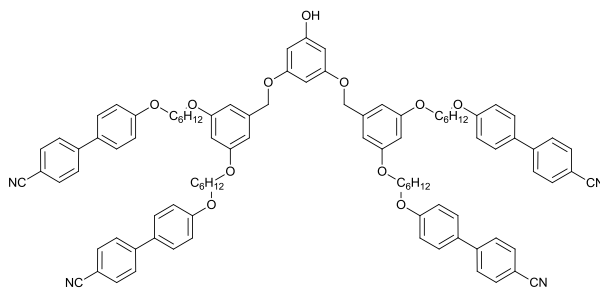
(Ba7) HO-PG(BA₆BPH₂)₂



Ba7 was prepared according to the “Method B” from **Ba4** (0.700 g, 0.77 mmol) and 3,5-dihydroxyphenyl benzoate (**7a**, 0.083 g, 0.36 mmol), using 1-butylamine (0.35ml, 3.54mmol) for deprotection, acetone/THF (1:2, 6ml) as solvent (refluxed for 64 hours), CH₂Cl₂ as the eluent for silica gel column chromatography and isolated as a white solid 0.325 g, 51% (Mol. Wt: 1780.39 g/mol). (Scheme 24)

¹H-NMR (CDCl₃): δ 7.52 (d, J=8.6Hz, 16H), 7.00 (d, J=8.6Hz, 16H), 6.61 (d, J=2.0Hz, 4H), 6.49 (t, J=2.1Hz, 2H), 6.30 (t, J=1.9Hz, 1H), 6.15 (d, J=2.1Hz, 2H), 6.85 (s, 1H), 4.94 (s, 4H), 4.12-3.82 (m, 24H), 1.98-1.72 (m, 24H), 1.68 - 1.34 (m, 40H), 0.99 (t, J=6.8Hz, 12H); ¹³C NMR (CDCl₃): δ 160.83, 160.53, 158.31, 158.23, 157.72, 139.19, 133.43, 133.34, 127.67, 114.87, 105.82, 100.99, 95.49, 95.00, 70.12, 68.19, 68.01, 67.84, 31.70, 29.39, 29.34, 29.27, 29.12, 25.96, 25.83, 22.70, 14.14

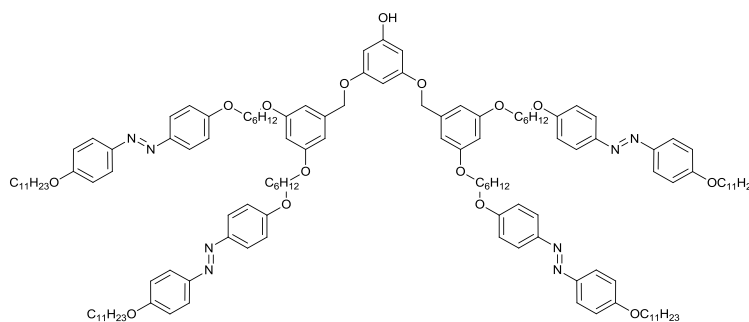
(Ba8) HO-PG(BA₆OCB₂)₂,



Ba8 was prepared according to the “Method B” from **Ba5** (0.513 g, 0.68 mmol), and 3,5-dihydroxyphenyl benzoate (**7a**, 0.0703 g, 0.30 mmol), using 1-butylamine (0.30ml, 3.04mmol) for deprotection, acetone/THF (1:2, 6ml) as solvent (refluxed for 64 hours), CH₂Cl₂:EtAc (30:1) as the eluent for silica gel column chromatography and isolated as a white solid 0.231 g, 51% (Mol. Wt: 1479.79 g/mol). (Scheme 24)

¹H-NMR (CDCl₃): δ 7.65 (q#, J=8.5Hz, 16H), 7.52 (d#, J=8.7Hz, 8H), 6.99 (d#, J=8.7Hz, 8H), 6.55 (d, J=2.2Hz, 4H), 6.41 (t, J=2.2Hz, 2H), 6.22 (t, J=2.0Hz, 1H), 6.11 (d, J=2.0Hz, 2H), 4.91 (s, 4H), 4.02 (t, J=6.4Hz, 8H) 3.96 (t, J=6.4Hz, 8H)), 1.94-1.72 (m, 16H), 1.64 – 1.45 (m, 17H); ¹³C NMR (CDCl₃): δ 160.79, 160.48, 159.75, 157.59, 145.24, 139.08, 132.55, 131.33, 128.32, 127.05, 119.07, 115.14, 110.05, 105.80, 100.93, 95.44, 94.91, 70.12, 68.03, 67.91, 29.17, 29.15, 25.87, 25.84, 21.04

(Ba9) HO-PG(Ba₆AZB₂)₂

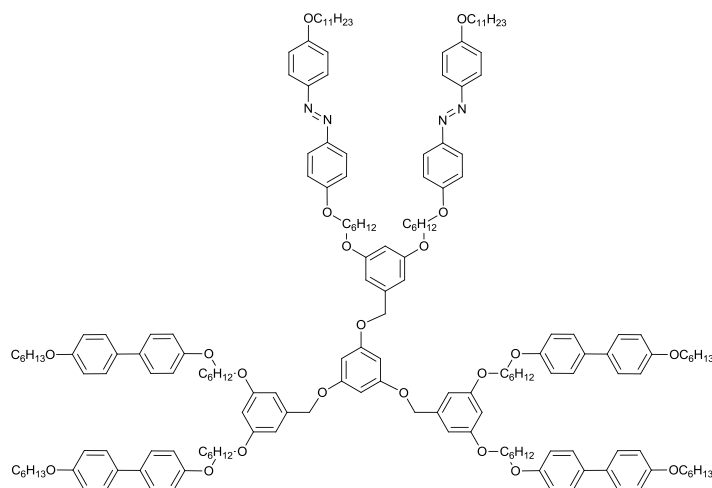


Ba9 was prepared according to “Method B” from **Ba6** (0.600 g, 0.54 mmol), and 3,5-dihydroxyphenyl benzoate (**7a**, 0.058 g, 0.25 mmol), using 1-butylamine (0.30ml, 3.04mmol) for deprotection, acetone/THF (1:4, 10ml) as solvent (refluxed for 48 hours), CH₂Cl₂:EtAc (100:1) as the eluent for silica gel column chromatography and isolated as a white solid 0.319 g, 58% (Mol. Wt: 2172.98 g/mol). (Scheme 24)

¹H-NMR (CDCl₃): δ 7.89 (d, J=8.3Hz, 16H), 6.99 (dd, J=8.9Hz, 1.9Hz, 16H), 6.56 (d, J=2.2Hz, 4H), 6.42 (t, J=2.2Hz, 2H), 6.24 (t, J=2.1Hz, 1H), 6.09 (d, J=2.1Hz, 2H), 4.90 (s, 4H), 4.02 (t, J=6.6Hz,

16H), 3.96 (t, J=6.3Hz, 8H), 1.82 (quintet, J=6.8Hz, 24H), 1.63-1.16 (m, 80H), 0.92 (t, J=6.8Hz, 12H); ^{13}C NMR (CDCl_3): δ 161.23, 161.14, 160.76, 160.47, 157.60, 146.99, 146.95, 139.14, 124.34, 114.71, 105.76, 100.93, 95.49, 94.97, 70.08, 68.37, 68.18, 67.91, 53.43, 31.95, 29.65, 29.61, 29.44, 29.37, 29.27, 29.17, 26.06, 25.89, 25.84, 22.72, 14.15

(Ba10) BA₆BPH₄AZB₂

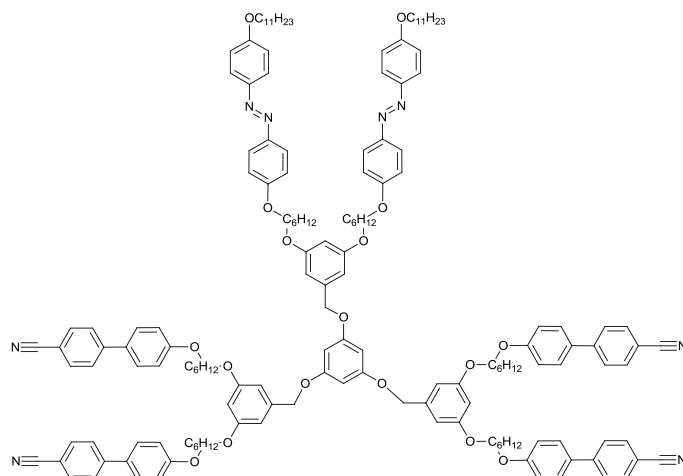


According to the "Method A" **Ba10** was isolated as a yellow solid 0.288 g, 66% (Mol. Wt: 2803.82 g/mol) from **Ba7** (HO-PG(Ba₆BPH₂)₂, 0.246 g, 0.14 mmol) and **Ba6** (Br-BA₆AZB₂, 0.171 g, 0.15 mmol), using THF (5ml) as solvent and CH₂Cl₂:petroleum ether (20:1) to CH₂Cl₂:Ethyl acetate (40:1) as the eluent for silica gel column chromatography. (Scheme 25)

$^1\text{H-NMR}$ (CDCl_3): δ 7.91 (d, J=8.8Hz, 8H), 7.49 (d, J=8.6Hz, 16H), 7.01 (d, J=8.8Hz, 8H), 6.97 (d, J=8.8Hz, 16H), 6.61 (d, J=2.3Hz, 6H), 6.46 (t, J=2.1Hz, 3H), 6.32(s, 3H), 4.97 (s, 6H), 4.15 – 3.85 (m, 36H), 2.00-1.70 (m, 36H), 1.68 – 1.22 (m, 80H), 1.05-0.85(m, 18H); ^{13}C NMR (CDCl_3): δ 161.24, 161.15, 160.71, 160.54, 158.31, 158.23, 147.04, 147.00, 139.09, 133.41, 133.32, 127.65, 124.35, 114.81, 114.71, 105.86, 100.97, 95.05, 70.21, 68.37, 68.18, 68.13, 67.95, 31.97, 31.66, 29.66, 29.63, 29.46, 29.39, 29.36, 29.32, 29.29, 29.26, 26.08, 25.95, 25.90, 25.80, 22.73, 22.66, 14.17, 14.09

MALDI-ToF: Calcd for C₁₈₁H₂₃₆N₄O₂₁: 2801.75; m/z: found: 2802.69 (M+1), 2803.68 (M+2), 2804.67 (M+3), 2805.66 (M+4), 2806.67 (M+5), 2808.66 (M+6); fragments: 2541.46 (M-C₁₇H₂₇NO), 1023.68 (M-C₁₁₆H₁₄₅O₁₅)

(Ba11) BA₆OCB₄AZB₂

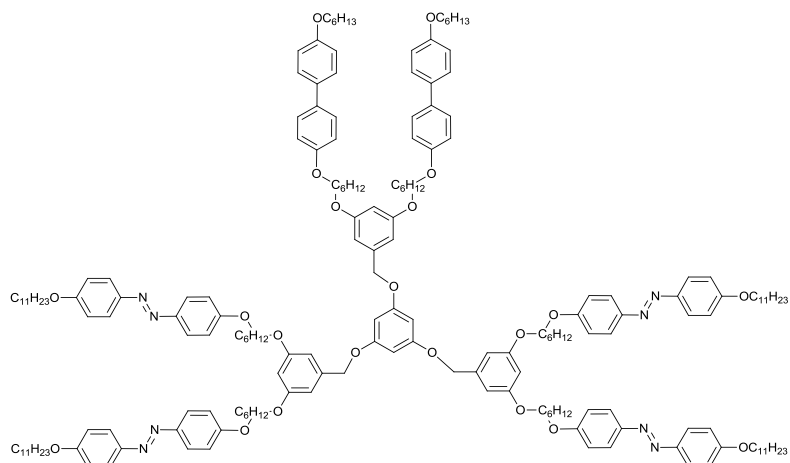


Ba11 was prepared according to the “Method A” from **Ba6** (Br-BA₆AZB₂, 0.164 g, 0.15 mmol) and **Ba8** (HO-PG(Ba₆OCB₂)₂, 0.200 g, 0.14 mmol), using THF (5ml) as solvent (refluxed for 48 hours), CH₂Cl₂:EtAc (60:1) as the eluent for silica gel column chromatography and isolated as a yellow solid 0.216 g, 58% (Mol. Wt: 2503.23 g/mol). (Scheme 25)

¹H-NMR (CDCl₃): δ 7.87 (d, J=8.8Hz, 8H), 7.67 (#q, J=8.6Hz, 16H), 7.51 (d, J=8.6Hz, 8H), 6.98 (#d, J=8.6Hz, 16H), 6.64-6.52 (m, 6H), 6.46-6.38 (m, 3H), 6.28 (s, 3H), 4.93 (s, 6H), 4.10-3.86 (m, 28H), 1.95-1.71 (m, 28H), 1.65 – 1.20 (m, 56H), 0.90 (t, J=6.7Hz, 6H); ¹³C NMR (CDCl₃): δ 161.24, 161.10, 160.67, 160.50, 159.76, 147.00, 146.93, 145.21, 139.04, 132.54, 131.30, 128.31, 127.03, 124.32, 119.07, 115.11, 114.69, 114.68, 110.08, 105.87, 100.93, 100.88, 94.98, 70.19, 68.37, 68.16, 68.01, 67.91, 31.92, 29.62, 29.59, 29.42, 29.35, 29.25, 29.20, 29.18, 26.05, 25.90, 25.87, 22.70, 14.14

MALDI-ToF: Calcd for C₁₆₁H₁₈₄N₈O₁₇: 2501.38; m/z: found: 2502.38 (M+1); fragments: 2242.18 (M- C₁₇H₂₇NO), 1024.71 (A=M- C₉₆H₉₃N₄O₁₁), 763.41 (A- C₁₇H₂₇NO),

(Ba12) BA₆AZB₄BPH₂

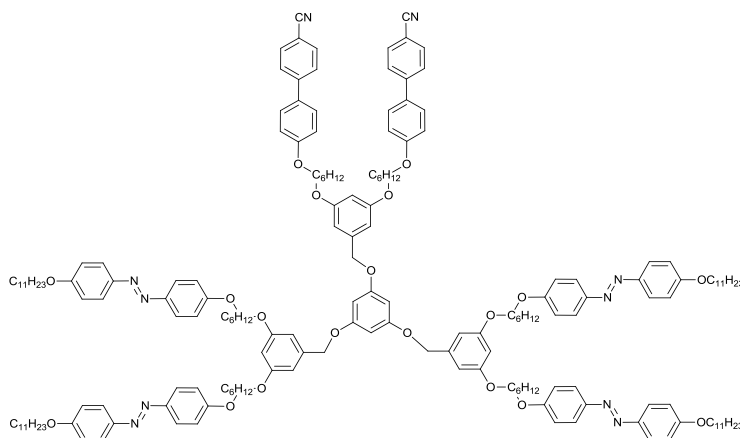


Ba12 was prepared according to the “MethodA” from **Ba4** (Br-BA₆BPH₂, 0.06 g, 0.07 mmol) and **Ba9** (HO-PG(Ba₆AZB₂)₂ 0.121 g, 0.06 mmol), using THF (4ml) as solvent (refluxed for 64 hours), CH₂Cl₂ to CH₂Cl₂:acetone (100:1) as the eluent for silica gel column chromatography and isolated as yellow solid 0.130 g, 78% (Mol. Wt: 3000.12 g/mol). (Scheme 26)

¹H-NMR (CDCl₃): δ 7.88 (d, J=9.0Hz, 16H), 7.47 (d, J=8.6Hz, 8H), 7.00 (d, J=8.9Hz, 16H), 6.95 (d, J=8.6Hz, 8H), 6.72-6.64 (m, 2H), 6.62-6.54 (m, 4H), 6.44 (t, J=2.2Hz, 3H), 6.32-6.26 (m, 3H), 5.07 (brs, 2H), 4.95 (s, 4H), 4.14-3.86 (m, 36H), 1.94-1.70 (m, 36H), 1.68 – 1.14 (m, 100H), 1.02-0.82 (m, 18H); **¹³C NMR** (CDCl₃): δ 161.20, 161.11, 160.66, 160.57, 160.50, 160.45, 158.89, 158.27, 158.20, 147.00, 146.97, 139.07, 139.04, 138.84, 138.81, 138.66, 133.39, 133.30, 127.63, 124.31, 114.77, 114.67, 105.84, 105.13, 100.93, 95.01, 94.21, 70.88, 70.18, 68.35, 68.16, 68.11, 67.93, 31.93, 31.63, 29.63, 29.59, 29.42, 29.36, 29.32, 29.28, 29.26, 29.19, 26.05, 25.91, 25.87, 25.76, 22.70, 22.63, 14.13, 14.05

MALDI-ToF: Calcd for C₁₉₁H₂₅₆N₈O₂₁: 2997.92; m/z: found: 2998.75 (M+1), 2999.74 (M+2), 3000.73 (M+3), 3001.76 (M+4), 3002.78 (M+5), 3003.70 (M+6); fragments: 2589.48 (M-C₁₇H₂₇NO), 1023.68 (A=M-C₁₂₆H₁₆₅N₄O₁₅), 763.04 (A- C₁₇H₂₇NO)

(Ba13) BA₆AZB₄OCB₂

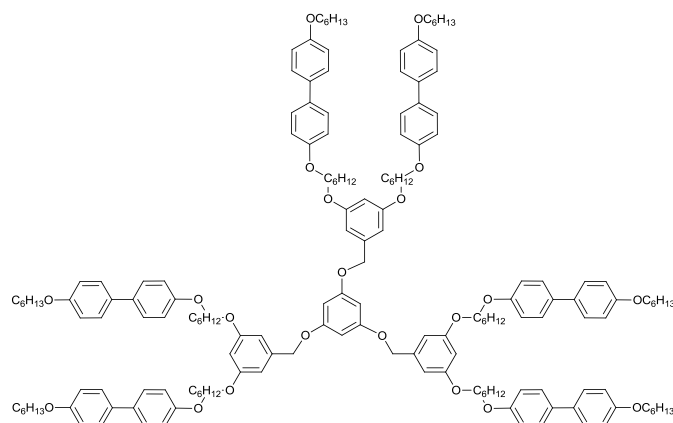


Ba13 was prepared according to the “Method A” from **Ba5** (Br-BA₆OCB₂, 0.045 g, 0.06 mmol) and **Ba9** (HO-PG(Ba₆AZB₂)₂, 0.100 g, 0.05 mmol), using THF (4ml) as solvent (refluxed for 72 hours), CH₂Cl₂:acetone (200:1) was used as the eluent for silica gel column chromatography and further by Bio-Beads SX-1 gel permeation chromatography swollen in CH₂Cl₂ and isolated as a yellow solid 0.088 g, 67% (Mol. Wt: 2849.82 g/mol). (Scheme 26))

¹H-NMR (CDCl₃): δ 7.87 (d, J=8.8Hz, 16H), 7.74-7.56 (m, 8H), 7.56-7.44 (m, 4H), 7.08-6.88 (m, 20H), 6.73-6.64 (m, 2H), 6.62-6.52 (m, 4H), 6.46-6.38 (m, 3H), 6.32-6.26 (m, 3H), 5.09-5.01 (brs, 2H), 4.94 (s, 4H), 4.14-3.86 (m, 32H), 1.94-1.70 (m, 32H), 1.68 – 1.14 (m, 88H), 0.91 (t, J=6.7Hz, 12H); **¹³C NMR** (CDCl₃): δ 161.20, 161.08, 160.66, 160.56, 160.49, 160.44, 159.75, 158.88, 147.00, 146.94, 145.22, 139.06, 139.02, 138.82, 138.79, 138.61, 132.53, 131.29, 128.31, 127.03, 124.30, 119.08, 115.09, 114.66, 110.07, 105.84, 105.12, 100.94, 100.88, 94.98, 94.20, 70.87, 70.17, 68.35, 68.15, 68.00, 67.89, 31.92, 29.61, 29.58, 29.41, 29.34, 29.24, 29.18, 26.03, 25.90, 25.86, 22.69, 14.11

MALDI-ToF: Calcd for C₁₈₁H₂₃₀N₁₀O₁₉: 2847.73; m/z: found: 2848.68 (M+1), 2849.68 (M+2), 2850.70 (M+3), 2851.69 (M+4), 2852.69 (M+5), 2853.68 (M+6); fragments: 2589.48 (M-C₁₇H₂₇NO), 2589.48 (M- 2x C₁₇H₂₇NO), 1023.68 (A = M-C₁₁₆H₁₃₉N₆O₁₃), 763.04 (A- C₁₇H₂₇NO)

(Ba14) BA₆BPH₆

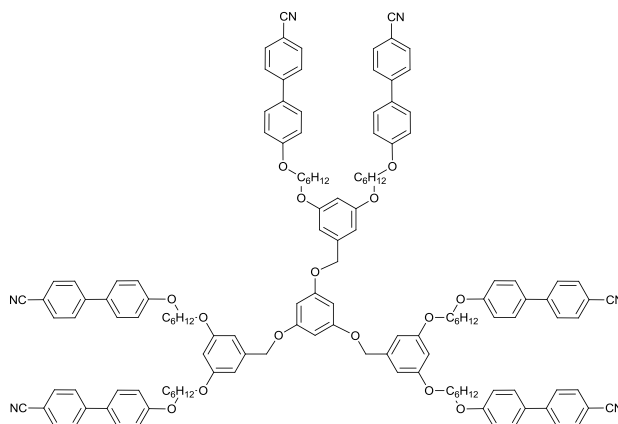


Ba14 was prepared according to the “Method A” from **Ba4** (Br-BA₆BPH₂, 0.267 g, 0.29 mmol) and phloroglucinol (0.010 g, 0.08 mmol) using THF (5ml) as solvent (refluxed for 48 hours). CH₂Cl₂:Petroleum ether (30:1) to CH₂Cl₂:Ethyl acetate (60:1) as the eluent for silica gel chromatography and isolated as a white solid 0.046 g, 22% (Mol. Wt: 2607.53 g/mol). (Scheme 27)

¹H-NMR (CDCl₃): δ 7.47 (d, J=8.7Hz, 24H), 6.95 (d, J=8.7Hz, 24H), 6.58 (d, J=2.1Hz 6H), 6.43 (t, J=2.2Hz, 3H), 6.30 (s, 3H), 4.99 (s, 6H), 4.17 -3.82 (m, 36H), 1.93 - 1.69 (m, 36H), 1.65 - 1.22 (m, 60H), 0.93 (t, J=6.9Hz, 18H); ¹³C NMR (CDCl₃): δ 160.66, 160.50, 160.43, 158.27, 158.20, 139.04, 133.40, 133.31, 127.64, 114.77, 105.85, 100.93, 94.99, 70.19, 68.12, 67.94, 31.63, 29.32, 29.28, 29.23, 25.92, 25.76, 22.62, 14.04

MALDI-ToF: Calcd for C₁₇₁H₂₁₆O₂₁: 2605.58; m/z: found: 2605.53 (M), 2606.56 (M+1), 2607.55 (M+2), 2607.55 (M+3), 2608.57 (M+4), 2609.57 (M+5); fragments: 827.53 (A = M- C₁₁₆H₁₄₅O₁₅), 1654.05 (2xA)

(Ba15) PG(BA₆OCB₂)₃



According to the “Method A” the **Ba15** was isolated as white solid 0.048 g, 20% (Mol. Wt: 2156.54 g/mol) from **Ba5** (Br-BA₆OCB₂, 0.300 g, 0.40 mmol) and phloroglucinol (0.014 g, 0.11

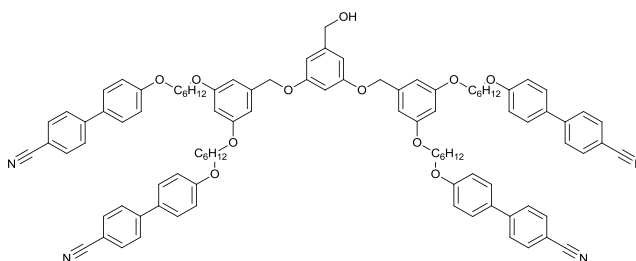
Experimental

mmol), using acetone:THF (1:2, 6ml) as solvent and CH₂Cl₂:Ethyl acetate (60:1) to CH₂Cl₂:ethyl acetate (20:1) as the eluent for silica gel column chromatography. (Scheme 27)

¹H-NMR (CDCl₃): δ 7.65 (#q, J=8.4Hz, 24H), 7.52 (#d, J=8.6Hz, 12H), 6.98 (#d, J=8.6Hz, 12H), 6.56 (d, J=2.2Hz, 6H), 6.42 (t, J=2.2Hz, 3H), 6.27 (s, 3H), 4.91 (s, 6H), 4.01 (t, J=6.5Hz, 12H), 3.96 (t, J=6.5Hz, 12H), 1.94-1.71 (m, 24H), 1.64-1.44 (m, 24H); **¹³C NMR** (CDCl₃): δ 160.67, 160.50, 159.74, 145.20, 138.95, 132.55, 131.33, 128.31, 127.04, 119.06, 115.10, 110.10, 105.90, 100.88, 94.90, 70.18, 68.00, 67.89, 29.18, 29.15, 25.88 25.85

MALDI-ToF: Calcd for C₁₄₁H₁₃₈N₆O₁₅: 2155.02; m/z: found: 2155.08 (M), 2156.04 (M+1), 2157.07 (M+2), 2158.05 (M+3), 2159.06 (M+4), 2160.08 (M+5); 2161.08 (M+6) fragments: 677.34 (A = M- C₉₆H₉₃N₄O₁₁), 663.43 (M- C₉₇H₉₅N₄O₁₁) 1353.74 (2xA)

(Ba16) HO-BA₆OCB₄

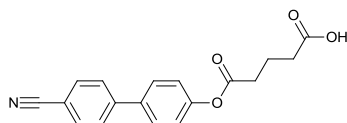


Ba16 was prepared according to the "Method E" from **Ba4** (Br-BA₆OCB₂, 0.290 g, 0.38 mmol) and 3,5-dihydroxybenzyl alcohol (0.0237 g, 0.17 mmol) using acetone:THF (1:2, 3 ml) as solvent (refluxed for 48 hours), CH₂Cl₂:EtAc (20:1) as the eluent for silica gel chromatography and isolated as a white solid 0.198 g, 78% (Mol.Wt: 1493.82 g/mol). (Scheme 28)

¹H NMR (CDCl₃): δ 7.65 (q, J=8.5Hz, 16H), 7.52 (d, J=8.2Hz, 8H), 6.99 (d, J=8.8Hz, 8H), 6.62 (d, J=1.9Hz, 2H), 6.58-6.52 (m, 5H), 6.41 (t, J=2.0Hz, 2H), 4.96 (s, 4H), 4.63 (d, J=5.9Hz, 2H), 4.02 (t, J=6.3Hz, 8H), 3.97 (t, J=6.3Hz, 8H), 1.94 - 1.73 (m, 16H), 1.64 (t, J=6.3Hz, 1H), 1.60-1.48 (m, 16H); **¹³C NMR** (CDCl₃): δ 160.50, 160.18, 159.75, 145.23, 143.44, 139.08, 132.54, 131.36, 128.31, 127.05, 119.03, 115.11, 110.13, 105.79, 105.74, 101.43, 100.90, 70.14, 68.01, 67.90, 65.29, 29.18, 29.15, 25.87, 25.84

1.4.4 Synthesis of Cinnamic acid esters

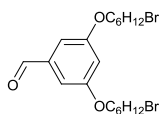
(C1), 4'-cyanobiphenyl hydrogen glutarate



N,N-Diisopropylethylamine (3.5 ml, 20.1 mmol) was added to a mixture of 4'-Hydroxy-4-biphenylcarbonitrile (3.900 g, 19.98 mmol) and glutaric anhydride (2.280 g, 19.98 mmol) in THF (10 ml) and refluxed for 24 hours. The cooled reaction mixture was poured into 1 M HCl (150 ml), the precipitate was filtered off and recrystallized from toluene. The product was isolated as white needles 4.766 g, 77% yield (Mol. Wt: 309.32 g/mol) (Scheme 29)

$^1\text{H NMR}$ (CDCl_3): δ 7.73, 7.66 (ABq, $J_{\text{AB}}=8.4\text{Hz}$, 4H), 7.60 (d, $J=8.4\text{Hz}$, 2H), 7.22 (d, $J=8.4\text{Hz}$, 2H), 2.72 (t, $J=7.2\text{Hz}$, 2H), 2.57 (t, $J=7.2\text{Hz}$, 2H), 2.12 (t, $J=7.2\text{Hz}$, 2H); $^{13}\text{C NMR}$ (CDCl_3): δ 177.47, 171.21, 151.01, 144.71, 136.91, 132.62, 128.33, 127.66, 122.23, 118.77, 111.11, 33.21, 32.59, 19.72

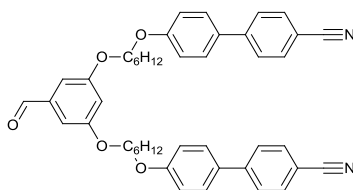
(C3)



1,6-dibromohexane (10 ml, 62.4 mmol) was added to a mixture of 3,5-dihydroxybenzaldehyde (0.991 g, 7.2 mmol) and K_2CO_3 (3.798 g, 27.5 mmol) in acetone (55 ml) and refluxed for 48 hours. Then the reaction mixture was cooled to room temperature and the solvent was evaporated under reduced pressure. The residue was dissolved in dichloromethane and washed sequentially with water and sat. aq. NaCl. The organic layer was dried over anhydrous MgSO_4 , filtered and concentrated. The crude product was purified by silica gel column chromatography using CH_2Cl_2 :petroleum ether (4:1) as the eluent. The product was isolated as a white solid 1.472 g, 44% yield (Mol. Wt: 464.23 g/mol) (Scheme 30)

$^1\text{H NMR}$ (CDCl_3): δ 9.90 (s, 1H), 6.99 (d, $J=2.4\text{Hz}$, 2H), 6.70 (t, $J=2.3\text{Hz}$, 1H), 4.01 (t, $J=6.3\text{Hz}$, 4H), 3.44 (t, $J=6.6\text{Hz}$, 4H), 1.98-1.76 (m, 8H), 1.58-1.44 (m, 8H) $^{13}\text{C NMR}$ (CDCl_3): 191.93, 160.70, 138.39, 108.05, 107.65, 68.19, 33.66, 32.65, 28.95, 27.88, 25.26

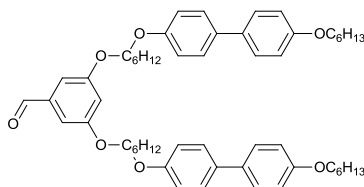
(C4)



A mixture of OCB (0.680 g, 3.5 mmol), **C3** (0.77, 1.7 mmol), K_2CO_3 (0.741 g, 5.4 mmol) and catalytic amount of KI in acetone (23 ml) was dissolved and refluxed for 48 hours. The reaction mixture was cooled to room temperature and the solvent was evaporated under reduced pressure. The residue was dissolved in dichloromethane and washed sequentially with water and sat. aq. NaCl. The organic layer was dried over anhydrous $MgSO_4$, filtrated and concentrated. The crude product was purified by silica gel column chromatography using $CH_2Cl_2:EtOAc$ (20:1) as the eluent. The product was isolated as a white solid 0.292 g, 12% yield (Mol. Wt: 692.84 g/mol) (Scheme 30)

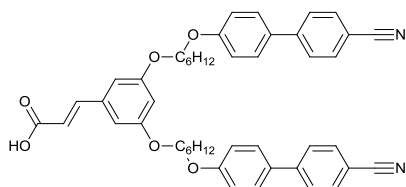
1H NMR ($CDCl_3$): δ 9.90 (s, 1H), 7.70, 7.64 (ABq, $J_{AB}=8.7Hz$, 8H), 7.60 (d, $J=8.4Hz$, 4H), 7.04-6.96 (m, 6H), 6.71 (t, $J=2.3Hz$, 1H), 4.10-3.95 (m, 8H), 1.94-1.78 (m, 8H), 1.64-1.52 (m, 8H) ^{13}C NMR ($CDCl_3$): 191.94, 160.73, 159.74, 145.25, 138.39, 132.55, 131.40, 128.33, 127.07, 119.04, 115.11, 110.14, 108.10, 107.62, 68.27, 67.97, 29.15, 29.07, 25.82

(C5)



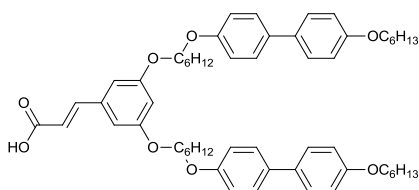
The reaction was carried out as described above using BPH (0.863 g, 3.2 mmol), **C3** (0.692, 1.5 mmol), K_2CO_3 (0.774 g, 5.6 mmol) and catalytic amount of KI, acetone (25 ml). The crude product was purified by silica gel column chromatography using CH_2Cl_2 :Petroleum ether (4:1) as the eluent. The product was isolated as a white solid 0.654 g, 52% yield (Mol. Wt: 843.14 g/mol) (Scheme 30)

1H NMR ($CDCl_3$): δ 9.90 (s, 1H), 7.46 (d, $J=8.4Hz$, 8H), 7.00 (d, $J=2.3Hz$, 2H), 6.95 (d, $J=8.6Hz$, 8H), 6.71(t, $J=2.3Hz$, 1H), 4.08-3.93 (m, 12H), 1.95-1.70 (m, 12H), 1.65-1.27 (m, 20H), 0.92(t, $J=7.1Hz$, 6H); ^{13}C NMR ($CDCl_3$): 191.99, 160.75, 158.28, 158.16, 138.38, 133.47, 133.31, 127.66, 127.64, 114.78, 114.77, 108.07, 107.66, 68.29, 68.13, 67.90, 31.60, 29.29, 29.24, 29.08, 25.87, 25.84, 25.74, 22.60, 14.01

(C6)

A mixture of malonic acid (0.179 g, 1.7 mmol), **C4** (0.292, 0.4 mmol), piperidine (0.17 ml, 1.7 mol) in pyridine (2 ml) was stirred at 90°C for 24 hours. The reaction mixture was cooled to room temperature, poured in 1M HCl (25 ml) and the solvent was decanted from the precipitate. The residue was dissolved in dichloromethane and washed sequentially with water and sat. aq. NaCl. The organic layer was dried over anhydrous MgSO₄, filtrated and concentrated. The crude product was purified by silica gel column chromatography using CH₂Cl₂:EtOAc (1:1 to 2:3) as the eluent. The product was isolated as a white solid 0.220 g, 69% yield (Mol. Wt: 734.88 g/mol) (Scheme 30)

¹H NMR (CDCl₃): δ 7.76-7.59 (m, 9H) 7.53 (d, J=8.7Hz, 4H), 7.00 (d, J=8.7Hz, 4H), 6.68 (d, J=2.1Hz, 2H), 6.52 (t, J=2.2Hz, 1H), 6.41 (d, J=15.8Hz, 1H), 4.12-3.90 (m, 8H), 1.96-1.76 (m, 8H), 1.66-1.48 (m, 8H) **¹³C NMR** (CDCl₃): 170.21, 160.55, 159.75, 147.06, 145.26, 135.85, 132.55, 131.38, 128.33, 127.07, 119.06, 117.30, 115.11, 110.12, 106.73, 104.00, 68.05, 67.99, 29.14, 29.12, 25.84,

(C7)

The reaction was carried out as described above using malonic acid (0.320 g, 3.1 mmol), **C5** (0.629, 0.7 mmol), piperidine (0.29 ml, 2.9 mol), pyridine (3.5 ml). The crude product was purified by silica gel column chromatography using CH₂Cl₂:acetone (3:2 to 2:1) as the eluent. The product was isolated as a white solid 0.526 g, 80% yield (Mol. Wt: 885.18 g/mol) (Scheme 30)

¹H NMR (CDCl₃): δ 7.68 (s, J=15.9Hz, 1H), 7.46 (d, J=8.6Hz, 8H), 6.94 (d, J=8.6Hz, 8H), 6.70-6.64 (m, 2H), 6.55-6.47 (m, 1H), 6.41 (d, J=15.6Hz, 1H), 4.08-3.93 (m, 12H), 1.95-1.70 (m, 12H), 1.65-1.27 (m, 20H), 0.92(t, J=7.1Hz, 6H); **¹³C NMR** (CDCl₃): 170.72, 160.55, 158.27, 158.17, 147.06, 135.85, 133.45, 133.31, 127.65, 127.64, 117.20, 114.77, 106.74, 103.97, 68.13, 68.08, 67.91, 31.60, 29.29, 29.26, 29.15, 25.88, 25.74, 22.60, 14.01

I.6 References

- ¹G. R. Newkome, C. N. Moorefield, F. Vögtle, *Dendrimers and Dendrons. Concepts, Syntheses, Applications*; Wiley-VCH: Weinheim, Germany, **2001**.
- ² J. M. J. Fréchet and D. A. Tomalia, *Dendrimers and Other Dendritic Polymers*, John Wiley & Sons, Chichester, **2001**, 3.
- ³ A. Carlmark, C. Hawker, A. Hult, M. Malkoch, *Chem. Soc. Rev.*, **2009**, *38*, 352–362
- ⁴ P.J. Flory, *J. Am. Chem. Soc.*, **1941**, *63*, 3083 ; 3091 ; 3096
- ⁵ P.J. Flory, *J. Am. Chem. Soc.*, **1942**, *63*, 132
- ⁶ E. Buhleier, W. Wehner and F. Vögtle, *Synthesis*, **1978**, 155.
- ⁷ D. A. Tomalia, H. Baker, J. Dewald, M. Hall, G. Kallos, S. Martin, J. Roeck, J. Ryder and P. Smith, *Polymer Journal*, **1985**, *17*, 117
- ⁸ D. A. Tomalia, J. M. J. Fréchet, *J. Polym. Sci., Part A: Polym. Chem.*, **2002**, *40*, 2719
- ⁹ G. R. Newkome, Z. Yao, G. R. Baker, V. K. Gupta . *J. Org. Chem.* **1985**, *50*, 2003.
- ¹⁰ C. J. Hawker, J. M. J. Fréchet, *J. Am. Chem. Soc.* **1990**, *112*, 7638
- ¹¹ Jansen, J. F. G. A.; de Brabander-van den Berg, E. M. M.; Meijer, E. W. *Science* **1994**, *266*, 1226-1229.
- ¹² S. M. Grayson J. M. J. Fréchet, *Chem. Rev.* **2001**, *101*, 3819.
- ¹³ A.W.Bosman, H.M.Janessen, E.W.Meijer, *Chem.Rev.*, **1999**, *99*, 1665
- ¹⁴ K. Inoue, *Prog. Polym. Sci.*, **2000**, *25*, 453-571
- ¹⁵ F. Vögtle, G. Richardt, N. Werner, *Dendrimer Chemistry Concepts, Syntheses, Properties, Applications*; Wiley: Weinheim, Germany, **2009**.
- ¹⁶ D. Astruc, E. Boisselier, C. Ornelas, *Chem. Rev.* **2010**, *110* , 1857–1959
- ¹⁷ G. R. Newkome, *Pure Appl. Chem.* **1998**, *70*, 2337
- ¹⁸ F. Zeng, S. C. Zimmermann, *Chem. Rev.* **1997**, *97*, 1681.
- ¹⁹ , D. A. Tomalia, *Mater. Today* **2005**, *8*, 34
- ²⁰ J.M.J. Fréchet, *PNAS*, **2002**, *99*, 4782-4787
- ²¹ V. Percec, J. G. Rudick, M. Peterca, M. E. Yurchenko, J. Smidrkal, P. A. Heiney, *Chem. Eur. J.* **2008**, *14*, 3355 – 3362
- ²² B. M. Rosen, C. J. Wilson, D. A. Wilson, M. Peterca, M. R. Imam and V. Percec, *Chem. Rev.*, **2009**, *109*, 6275–6540.
- ²³ V. Percec, B. C. Won, M. Peterca, P. A. Heiney, *J. Am. Chem. Soc.*, **2007**, *129*, 11265–11278
- ²⁴ P. Wu, A.K. Feldman, A. K. Nugent, C. J. Hawker, A. Scheel, B. Voit, J. Pyun, J. M. J. Fréchet, K.B. Sharpless, V. Fokin, *Angew. Chem. Int. Ed.* **2004**, *43*, 3928 –3932
- ²⁵ H. Ihre, A. Hult, J.M.J. Fréchet, I. Gitsov. *Macromolecules* **1998**, *31*, 4061.
- ²⁶ K.L. Wooley, C.J. Hawker, J.M.J. Fréchet, *Angew Chem, Int Ed Engl* **1994**, *33*, 82
- ²⁷ K.L. Wooley, C.J. Hawker, J.M.J. Fréchet, *J Am Chem Soc* **1991**, *113*, 4252.
- ²⁸ T. Kawaguchi, K.L. Walker, C.L. Wilkins, J.S. Moore, *J Am Chem Soc* **1995**, *117*, 2159

- ²⁹ P. Wu, A. K. Feldman, A. K. Nugent, C. J. Hawker, A. Scheel, B. Voit, J. Pyun, J. M. J. Fréchet, K. B. Sharpless, V. V. Fo-kin, M. J. Joralemon, R. K. O'Reilly, J. B. Matson, A. K. Nugent, C. J. Hawker, K.L. Wooley, *Macromolecules*, **2005**, *38*, 5436–5443
- ³⁰ F. Zeng, S.C. Zimmerman, *J Am Chem Soc*, **1996**, *118*, 5326
- ³¹ F. Reinitzer, *Monatsh.Chem.* **1888**, *9*, 421
- ³² O. Lehmann, *Z. Phys. Chem.* **1889**, *4*, 462, O. Lehmann, *Verhandl. d. Deutschen. Phys. Ges.*, **1900**, Sitzung V. **16**, 1
- ³³ Asia OLED – leaner and meaner, BNP Paribas, 21 March **2011**
- ³⁴ J.-M. Lehn, In *Supramolecular Chemistry: Concepts and Perspectives*, VCH, New York
- ³⁵ M. R. Wasielewski, *Acc. Chem. Res.*, **2009**, *42*, 1910-1921
- ³⁶ J. W. Steed and J. L. Atwood, In *Supramolecular Chemistry*, Wiley, Chichester, **2000**
- ³⁷ D. Demus, J. W. Goodby, G. W. Gray, H.-W. Spiess and V. Vill *Handbook of Liquid Crystals*, ed., Wiley-VCH: Weinheim, **1998**.
- ³⁸ S. Laschat, A. Baro, N. Steinke, F. Giesselmann, C. Hägele and G. Scalia, R. Judele, E. Kapatsina, S. Sauer, A. Schreivogel and M. Tosoni, *Angew. Chem., Int. Ed.*, **2007**, *46*, 4832–4887
- ³⁹ S. Sergeev, W. Pisula and Y. H. Geerts, *Chem. Soc. Rev.*, **2007**, *36*, 1902–1929
- ⁴⁰ S. Kumar, *Chem. Soc. Rev.*, **2006**, *35*, 83–109;
- ⁴¹ B. R. Kaafarani, *Chem. Mater.*, **2011**, *23*, 378–396
- ⁴² S. Kumar, *Liq. Cryst.*, **2009**, *36*, 607–638
- ⁴³ T. Kato, N. Mizoshita and K. Kishimoto, *Angew. Chem., Int. Ed.*, **2006**, *45*, 38–68
- ⁴⁴ T. Kato, T. Yasuda, Y. Kamikawa and M. Yoshio, *Chem. Commun.*, **2009**, 729–739
- ⁴⁵ J. W. Goodby, I. M. Saez, S. J. Cowling, V. Görtz, M. Draper, A. W. Hall, S. Sia, G. Cosquer, S. E. Lee and E. P. Raynes, *Angew. Chem., Int. Ed.*, **2009**, *47*, 2754–2787
- ⁴⁶ G. Friedel, *Ann. de Physique* **1922**, *18*, 273
- ⁴⁷ A. Skoulios and D. Guillon, *Mol. Cryst. Liq. Cryst.*, **1988**, *165*, 317-332;
- ⁴⁸ J. W. Goodby, I. M. Saez, S. J. Cowling, J. S. Gasowska, R. A. MacDonald, S. Sia, P. Watson, K. J. Toyne, M. Hird, R. A. Lewis, S.-E. Lee and V. Vaschenko, *Liq. Cryst.* **2009**, *36*, 567-605
- ⁴⁹ C. Tschierske *Nature*, **2002**, *419*, 681
- ⁵⁰ B. Donnio and D. Guillon, *Adv. Polym. Sci.*, **2006**, *201*, 45–155;
- ⁵¹ R. A. Reddy and C. Tschierske, *J. Mater. Chem.*, **2006**, *16*, 907–961;
- ⁵² C. Tschierske, *Chem. Soc. Rev.*, **2007**, *36*, 1930-1970
- ⁵³ G. Ungar, C. Tschierske, V. Abetz, R. Holyst, M. A. Bates, F. Liu, M. Prehm, R. Kieffer, X. Zeng, M. Walker, B. Glettner and A. Zywockinski, *Adv. Funct. Mater.*, **2011**, *21*, 1296–1323
- ⁵⁴ B. Glettner, F. Liu, X. Zeng, M. Prehm, U. Baumeister, M. Walker, M. A. Bates, P. Boesecke, G. Ungar and C. Tschierske, *Angew. Chem. Int. Ed.*, **2008**, *47*, 9063-9066;
- ⁵⁵ X. Zeng, R. Kieffer, B. Glettner, C. Nürnberger, F. Liu, K. Pelz, M. Prehm, U. Baumeister, H. Hahn, H. Lang, G. A. Gehring, C. H. M. Weber, J. K. Hobbs, C. Tschierske and G. Ungar, *Science*, **2011**, *331*, 1302-1306

- ⁵⁶ C. Tschierske, *Annu. Rep. Prog. Chem., Sect. C: Phys. Chem.*, **2001**, *97*, 191–267.
- ⁵⁷ V.N. Tsvetkov, *Acta Physicochimica U.R.S.S.* **1942**, *15*, 132
- ⁵⁸ G.W. Gray, J. W. Goodby, *Smectic Liquid Crystals*, L.Hill. **1984**
- ⁵⁹ B. Donnio, S. Buathong, I. Bury and D. Guillon, *Chem. Soc. Rev.* **2007**, *36*, 1495–1513
- ⁶⁰ H. T. Nguyen, C. Destrade, J. Malthête, *Adv. Mater.*, **1997**, *9*, 375
- ⁶¹ A.C. Ribeiro, B. Heinrich, C. Cruz, H.T. Nguyen, S. Diele, M.W. Schröder, D. Guillon, *Eur.Phys.J.E.*, **2003**, *10*, 143
- ⁶² J. Tang , R. Huang , H. Gao , X. Cheng , M. Prehm, C. Tschierske, *RSC Adv.*, **2012**, *2*, 2842-2847
- ⁶³ D. Guillon, B. Heinrich, A.C. Ribeiro, C. Cruz, H. T. Nguyen, *Mol. Cryst. Liq. Cryst.*, **1998**, *317*, 51-64
- ⁶⁴ V. S. K. Balagurusamy, G. Ungar, V. Percec, G. Johansson, *J. Am. Chem. Soc.*, **1997**, *119*, 1539.
- ⁶⁵ D. Felder, B. Heinrich, D. Guillon, J.-F. Nicoud, J.-F. Nierengarten, *Chem. Eur. J.*, **2000**, *6*, 3509.
- ⁶⁶ P. Fuchs, C. Tschierske, K. Raith, K. Das, S. Diele, *Angew. Chem. Int. Ed. Engl.*, **2002**, *41*, 628.
- ⁶⁷ J. W. Goodby, G. H. Mehl, I. M. Saez, R. P. Tuffin, G. Mackenzie, R. Auzély-Velty, T. Benvegnu and D. Plusquellec, *Chem. Commun.*, **1998**, 2057-2070
- ⁶⁸ I. M. Saez and J. W. Goodby, *J. Mater. Chem.* **2005**, *15*, 26-40;
- ⁶⁹ X. Zeng, G. Ungar, Y. Liu, V. Percec, A.E. Dulcey, J. K. Hobbs, *Nature*, **2004**, *428*, 157
- ⁷⁰ G. Ungar, Y. Liu, X. Zeng, V. Percec, W.-D. Cho, *Science*, **2003**, *299*, 1208
- ⁷¹ A. Belaisaoui, S. J. Cowling, I. M. Saez and J. W. Goodby, *Soft Matter*, **2010**, *6*, 1958-1963;
- ⁷² C. T. Imrie, P. A. Henderson and G.-Y. Yeap, *Liq. Cryst.*, 2009, **36**, 755- 777.
- ⁷³ B. Donnio, J. Barbera, R. Gimenez, D. Guillon, M. Marios, J. L. Serrano, *Macromolecules*, **2002**, *35*, 370-381
- ⁷⁴ J. Wolska, D. Mieczkowski, Pocięcha, S. Buathong, B. Donnio, D. Guillon and E. Gorecka, *Macromolecules*, **2009**, *42*, 6375-6384
- ⁷⁵ C. T. Imrie and P. A. Henderson, *Chem. Soc. Rev.* 2007, **36**, 2096–2124;
- ⁷⁶ A Yoshizawa, *J. Mater. Chem.*, 2008, **18**, 2877-2889;
- ⁷⁷ C. V. Yelamaggad, G. Shanker, U. S. Hiremath and S. K. Prasad, *J. Mater. Chem.* 2008, **18**, 2927–2949;
- ⁷⁸ I. M. Saez and J. W. Goodby, *Struct. Bond.* 2008, **128**, 1–62
- ⁷⁹ D.A. Tomalia, *Nat. Mater.*, **2003**, *2*, 711
- ⁸⁰ P. H. J. Kouwer and G. H. Mehl, *J. Mater. Chem.*, **2009**, *19*, 1564–1575
- ⁸¹ D. Felder-Flesch, L. Rupnicki, C. Bourgogne, B. Donnio and D. Guillon, *J. Mater. Chem.*, 2006, **16**, 304–309
- ⁸² Y.H. Kim, *J. Am. Chem. Soc.* **1992**, *114*, 4947
- ⁸³ V. Percec, P. W. Chu, G. Ungar, P.J. Zhou, *J. Am. Chem.* **1995**, *117*, 11441
- ⁸⁴ K. Lorentz, D. Holter, B. Stuhn, R. Mülhaupt, H. Frey, *Adv. Mater.* **1996**, *8*, 414
- ⁸⁵ S.A. Ponomarenko; E.A. Rebrov, N.I. Boiko, A.M. Muzafarov, V.P. Shibaev, *Polym. Sci. Ser. A.* **1998**, *40*, 763.

- ⁸⁶ S.A. Ponomarenko; E.A. Rebrov, N.I. Boiko, A.M. Muzafarov, V.P. Shibaev, E.V. Agina, R.M. Richardson, *Mol. Cryst. Liq. Cryst.* **2001**, *364*, 93
- ⁸⁷ E.V. Agina, S.A. Ponomarenko, N.I. Boiko, E.A. Rebrov, A.M. Muzafarov, V.P. Shibaev, *Polym. Sci. Ser. A.* **2001**, *43*, 1000
- ⁸⁸ S. A. Ponomarenko, N. I. Boiko, V. P. Shibaev, R. M. Richardson, I. J. Whitehouse, E. A. Rebrov, A. M. Muzafarov, *Macromolecules*, **2000**, *33*, 554
- ⁸⁹ A. Y. Bobrovsky, A. A. Pakhomov, X.M. Zhu, I.N. Boiko, V.P. Shibaev, J. Stumpe, *J. Phys. Chem. B*, **2002**, *106*, 540-546
- ⁹⁰ R. Elsaßer, G. H. Mehl, J. W. Goodby and M. Veith, *Angew. Chem., Int. Ed.*, **2001**, *40*, 2688
- ⁹¹ M. W. P. L. Baars, S. H. M. Söntjens, H. M. Fischer, H. W. I. Peerlings and E. W. Meijer, *Chem.–Eur. J.*, **1998**, *4*, 2456
- ⁹² J. H. Cameron, A. Facher, G. Lattermann and S. Diele, *Adv. Mater.*, **1997**, *9*, 398
- ⁹³ J. Barbera, B. Donnio, L. Gehringer, D. Guillon, M. Marcos, A. Omenat and J. L. Serrano, *J. Mater. Chem.*, **2005**, *15*, 4093
- ⁹⁴ L. Gehringer, C. Bourgoigne, D. Guillon, B. Donnio, *J. Am. Chem. Soc.*, **2004**, *126*, 3856
- ⁹⁵ D. J. Pesak and J. S. Moore, *Angew. Chem., Int. Ed. Engl.*, 1997, *36*, 1636.
- ⁹⁶ G. S. Kumar, D. C. Neckers, *Chem. Rev.*, **1989**, *89*, 1915-1925
- ⁹⁷ C. Cojocariu and P. Rochon, *Pure Appl. Chem.*, **2004**, *76*, 1479–1497
- ⁹⁸ T. Todorov, L. Nikolova, N. Tomova. *Appl. Opt.*, **1984**, *23*, 4309
- ⁹⁹ A. Natansohn, P. Rochon, J. Gosselin, S. Xie. *Macromolecules*, **1992**, *25*, 2268
- ¹⁰⁰ X. Meng, A. Natansohn, P. Rochon. *Supramol. Sci.* **1996**, *3*, 207
- ¹⁰¹ C. Maertens, P. Dubois, R. Jerome, P. A. Blanche, P. C. Lemaire. *J. Polym. Sci., Part B: Polym. Phys.* **2000**, *38*, 205
- ¹⁰² Fischer, T.; Laßker, L.; Rutloh, M.; Czaplá, S.; Stumpe, J., *Mol. Cryst. Liq. Cryst.*, **1997**, *299*, 293-299
- ¹⁰³ P. Rochon, J. Mao, A. Natansohn, E. Batalla, *Polym. Prep.*, **1994**, *35*, 154
- ¹⁰⁴ R. H. Berg, S. Hvilsted, P. S. Ramanujam, *Nature*, **1996**, *383*, 505 - 508
- ¹⁰⁵ K. Harada, M. Itoh, T. Yatagai and S. Kamemaru, *Opt. Rev.*, **2005**, *12*, 130
- ¹⁰⁶ P. C. Che, Y.N. He, X. G. Wang, *Macromolecules*, **2005**, *38*, 8657-8663
- ¹⁰⁷ A. Natansohn, P. Rochon, *Chem. Rev.*, **2002**, *102*, 4139
- ¹⁰⁸ D. J. Broer, J. A.M.M. van Haaren, P. van de Witte, C. Bastiaansen, *Macromol. Symp.*, **2000**, *154*, 1-14
- ¹⁰⁹ D.L. Jiang, T. Aida, *Nature (London)* **1997**, *388*, 454-456
- ¹¹⁰ R. Rosenhauer, J. Stumpe, R. Gimenez, M. Pinol, J. L. Serrano, A. Vinales, *Macromol. Rapid Commun.*, **2007**, *28*, 932-936
- ¹¹¹ R. Rosenhauer, J. Stumpe, R. Gimenez, M. Pinol, J. L. Serrano, A. Vinales, and D. Broer, *Macromolecules*, **2011**, *44*, 1438-1449
- ¹¹² A.I. Viñuales, J.L. Serrano, R. Giménez, M. Piñol, J. Tomczyk, J. Stumpe., *J Polym Sci Part A: Polym Chem*, **2011**, *49*, 3499

- ¹¹³ P.Gopalan, H. E.; Katz, D. J. McGee, C. Erben, T. Zielinski, D. Bousquet, D. Muller, J. Grazul, Y. Olsson, *J. Am. Chem. Soc.* **2004**, *126*, 1741-1747.
- ¹¹⁴ V. Shibaev, A. Bobrovsky, N. Boiko, *Prog PolymSci* , **2003**, *28*, 729–836
- ¹¹⁵ R. delonche, A.-M. Caminade, *J. Photochem Photobiol C-Photochem Rev*, **2010**, *11*, 25–45
- ¹¹⁶ H.B. Mekelburger, K. Rissanen, F. Vögtle, *Chem. Ber.*, **1993**, *126*, 1161
- ¹¹⁷ F. Vögtle, M. Gorka, R. Hesse, P. Ceroni, M. Maestri, V. Balzani, *Photochem. Photobiol. Sci*, **2002**, *1*, 45
- ¹¹⁸ J.W.Weener, E.W. Meijer, *Adv. Mater.*, **2000**, *12*, 741
- ¹¹⁹ J. Nithyanandhan, N. Jayaraman, R. Davis, S. Das, *Chem. Eur. J.*, **2004**, *10*, 689
- ¹²⁰ M. Uda, A. Momotake, T. Arai, *Photochem. Photobiol. Sci.*, **2003**, *2*, 845
- ¹²¹ D. Choi, J.H. Lee, K.H. Shin, E.J. Shin, *Bull. Kor. Chem. Soc.*, **2007**, *28*, 983
- ¹²² A. Ray, S. Bhattacharya, S. Ghorai, T. Ganguly, A. Bhattacharjya, *Tetrahedron Lett.*, **2007**, 48 8078.
- ¹²³ L.X. Liao, F. Stellaci, D.V. McGrath, *J. Am. Chem. Soc.*, **2004**, *126*, 2181
- ¹²⁴ D. Grebel-Koehler, D. Liu, S. De Feyter, V. Enkelmann, T. Weil, C. Engels, C.Samyn, K. Müllen, F.C. De Schryver, *Macromolecules*, **2003**, *36*, 578.
- ¹²⁵ D.M. Junge, D.V. McGrath, *J. Am. Chem. Soc.*, **1999**, *121*, 4912
- ¹²⁶ L.X. Liao, D.M. Junge, D.V. McGrath, *Macromolecules*, **2002**, *35*, 319
- ¹²⁷ T.-T.-T. Nguyen, D. Türp, D. P. Wang, B. Nölscher, F. Laquai, K. Müllen, *J. Am.Chem. Soc.*, **2011**, *133*, 11194–11204.
- ¹²⁸ L. Polakova, Z. Sedlakova, P. Latalova, *Polym. Bull.* **2010**, *64*, 315
- ¹²⁹ W. Li, S. Yin, J. Wang and L. Wu, *Chem. Mater.*, **2008**, *20*, 514–522
- ¹³⁰ C. Cordovilla, S. Coco, P. Espinet, B. Donnio, *J. Am. Chem.Soc.* **2010**, *132*, 1424–1431.
- ¹³¹ T. Itahara, T. Tsuchida, M. Morimoto *Polym Chem* **2010**, *1*,1062-1066
- ¹³² E. F. J.de Vries, J. Brussee, A. van der gen, *J. Org. Chem.* **1994**, *59*, 7133.
- ¹³³ P. G. M. Wuts, T. W. Greene, *Greene's Protective Groups in Organic Synthesis*,
- ¹³⁴ A. T. Khan, E. Mondal, B.M. Borah, S. Ghosh, *Eur. J. Org. Chem.* **2003**, *21*, 4113-4117
- ¹³⁵ W. Li, A. Zhang, A. D. Schlüter, *Macromolecules*, **2008** *41* 43-49
- ¹³⁶ L. Li, L. Zhu, X. Zhang, G. Zhang, G. Qu, *Can. J. Chem.* **2005**, *83*, 1120-1123
- ¹³⁷ S. V.Aathimanikandan, B. S.Sandanaraj, C. G.Arges, C. J Bardeen, S.Thayumanavan, *Org. Lett.* **2005**, *7*, 2809-2812.
- ¹³⁸ D. Felder, M. Gutiérrez-Nava, M. del Pilar Carreón, J.-F. Eckert, M. Luccisano, C. Schall, P. Masson, J.-L. Gallani, B. Heinrich, D. Guillon, J.-F. Nierengarten, *Helv. Chim. Acta* **2002**, *85*, 288–319.
- ¹³⁹ P. Liu, Y. Chen, J. Deng, J. Y. Tu, *Synthesis*, **2001**, *14*, 2078-2080
- ¹⁴⁰ H. Y. Kuchelmeister and C. Schmuck, *Eur. J. Org. Chem.*, **2009**, 4480
- ¹⁴¹ M. Takahashi, H. Morimoto, K. Miyake, H. Kawai, Y. Sei, K. Yamaguchi, T. Sengoku H. Yoda, *New J. Chem.*, **2008**, *32*, 547

- ¹⁴² A. K Roy, R. B. S. Batra, *Tetrahedron*, **2004**, *10*, 2301–2310
- ¹⁴³ Y. Rio, J.-F. Nicoud, J.-L. Rehspringer, J.-F. Nierengarten, *Tetrahedron Lett.* **2000**, *41*, 10207–10210.
- ¹⁴⁴ K. Suzuki, O. Haba, R. Nagahata, K. Yonetake, M. Ueda *High Perform. Polym.* **1998**, 10231
- ¹⁴⁵ R. Davis, N.S.S. Kumar, S. Abraham, C.H. Suresh, N.P. Rath, N.Tamaoki, S. Das., *J. Phys. Chem. C* **2008**, *112*, 2137.
- ¹⁴⁶ Differential Scanning Calorimetry and Liquid Crystals, Duncan W. Bruce, *Lecture on Liquid Crystal Workshop*, **2011**, Hull, UK
- ¹⁴⁷ X-ray Diffraction from Liquid Crystals, R. M; Richardson, *Lecture on Liquid Crystal Workshop*, **2011**, Hull, UK
- ¹⁴⁸ G. W. Gray and J. W. Goodby, *In Smectic Liquid Crystals; Textures and Structures*; Leonard Hill: Glasgow, **1984**.
- ¹⁴⁹ J. Szulc, Z. Witkiewicz and R. Dabrowski, *Mol. Cryst. Liq. Cryst.*, **1984**, *109*, 125-142.
- ¹⁵⁰ B. Heinrich and D. Guillon, *Mol. Cryst. Liq. Cryst.*, **1995**, *268*, 21-43.
- ¹⁵¹ A. J. Dianoux and F. Volino, *J. Phys. Fr.*, **1979**, *40*, 181-190.
- ¹⁵² D. Guillon, and A. Skoulios, *J. Phys. Fr.*, **1984**, *45*, 607-621.
- ¹⁵³ U. A. Hrozyk, S. V. Serak, N. V. Tabiryan, L. Hoke, D. M. Steeves, B. Kimball, and G. Kedziora, *Mol. Cryst. Liq. Cryst.* **2008**, *489*, 257
- ¹⁵⁴ O. Yazdani, M. Irandoust, Jahan B. Ghasemi, Sh. Hooshmand, *Dyes and Pigments*, **2012**, *92*, 1031
- ¹⁵⁵ M. Kasha, H. R. Rawls and M. Ashraf El-Bayoumi, *Pure Appl. Chem.*, **1965**, *11*, 371-392
- ¹⁵⁶ G. Narayan, N. S. S. Kumar, S. Paul, O. Srinivas, N. Jayaraman and S. Das, *J. Photochem. Photobiol. A: Chem.*, **2007**, *189*, 405-413.
- ¹⁵⁷ A. Bobrovsky, N. Boiko, V. Shibaev, J. Stumpe, *J. Photochem. Photobiol. A: Chem.*, **2004**, *163*, 347-358

Chapter II

Dendronized Gold Nanohybrids

II.1 Introduction

In this chapter we will discuss the synthesis and characterization of monodisperse gold nanoparticles (AuNPs) with well determined size, their functionalization with mesogenic and protodendritic ligands, to build up dendronized gold nanohybrids, and their self-assembly. The basic structure of the ligands which are used for this purpose have been partly described in Chapter I. This chapter has four main sections.

After a brief introduction of the history of gold nanoparticles (AuNPs), we will illustrate the synthesis of monolayer-protected AuNPs via direct reactions and how it is possible to control their size modification. This will be followed by the description of the ligand-exchange and coupling reactions, and how new functions can be introduced on the AuNPs. In the following part, liquid-crystalline dendronized gold nanohybrids will be discussed. First, the dendronized AuNPs will be presented through various examples from the literature, both the doped systems and the NP cored systems in more detail, with specific emphasis on ligand-exchange and coupling methods and their advantages and disadvantages. This will be followed by the introduction of the liquid crystalline gold nanohybrids, where the liquid crystallinity is the property of the hybrid and not that of mixture of hybrids and LCs.

In second section, the syntheses and the methods applied by us in order to gain dendronized gold nanohybrids will be shown. For the synthesis of monolayer protected, monodisperse AuNPs, the direct method has been adopted using a modified Brust's two phase synthesis. For the synthesis of dendronized gold nanohybrids, we have chosen a ligand-exchange reaction using thiolated ligands as strong binding agents. The synthesis of these ligands will be presented and our attempts to produce various types of dendronized gold nanohybrids with LC properties, will be detailed. In the next section their characterisation and the results will be discussed. Apart from general characterization (NMR, UV/Vis, etc.), both the self-assembly of the AuNPs and the hybrids and the mesomorphic behaviour of the hybrids will be discussed. Finally, in the last section, the conclusion will be drawn and the synthesis of both building blocks will be detailed.

II.1.1 Gold Nanoparticles

II.1.1.1 History of gold and gold nanoparticles

Gold is one of the most comprehensively investigated materials which can be followed back to 4000 B.C. when it was used to fashion decorative objects. The Sumer civilization used to create a wide range of jewellery using gold in 3000 B.C. The *Shekel* (it contained a naturally

occurring alloy that was approximately two-thirds gold and one-third silver) became the recognized standard medium for exchange in international trade in 1500 B.C. In 1350 B.C. Babylonians started to test the purity of gold. In 1200 B.C. the use of gold is extended and the Egyptians mastered the art of beating gold into leaf. In China little squares of gold was used as a form of money in 1090 B.C. Greeks and Jews began to practice alchemy in 300 B.C. In 58 B.C. Julius Cesar repaid all of Rome's debts in gold, after a victorious campaign in Gaul. Romans began issuing a gold coin (Aureus) in 50 B.C. and from this point gold was a common form for legal tender. Of course, as gold is the easiest of metals to work (and because of its value) it has constantly remained a material from which to create jewellery. With technical development, gold is nowadays also used in a wide range of electronic devices.

However for science, gold is more interesting, not in bulk but in its colloid form, gold nanoparticles (AuNPs). The history of AuNPs also dates back to ancient times when it was used for both decorative and medical purposes¹. For decorative purposes, e.g. glass, workers added gold and silver to the molten glass which dispersed during the heat treatment and resulted in a special type of glass, known as dichroic. The only complete example of such a glass can be found in the British museum, called the Lycurgus cup (Figure 1), which was probably made in Rome in ~300 A.D., and became the most famous example for AuNPs, in scientific fields. The colour of the glass changes from opaque green to translucent red when light is shone through it (transmitted light).

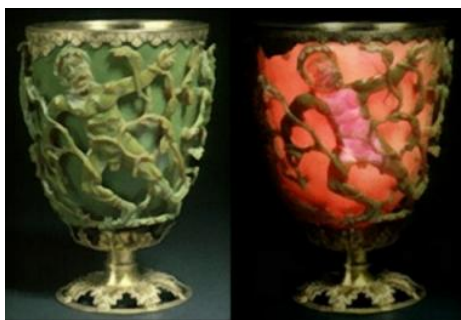


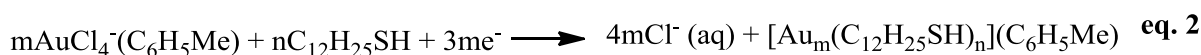
Figure 1 Lycurgus cup

Michael Faraday reported first, in 1857, the preparation of colloidal gold forming a deep red solution when gold chloride was reduced to gold using phosphorus. He suggested a relationship between size and colour². After Faraday, in 1951, J. Turkevich pioneered and reported the synthesis of AuNPs with sizes in a range of 10-20 nm, stabilized and suspended in water³. In 1994, Brust reported a two phase liquid-liquid method which provided stable 2 nm thiol-derivatised AuNPs soluble in organic solvents⁴.

II.1.1.2 Syntheses of AuNPs

Since Faraday's work, various methods of the synthesis of AuNPs were reported. A comprehensive review⁵ on the synthesis, physical properties and application of gold nanoparticles was written by Marie-Christine Daniel and Didier Astruc in 2004. The syntheses are usually based on the reduction of a soluble gold compound (e.g. $\text{HAuCl}_4 \cdot 3\text{H}_2\text{O}$) and adding capping agent for the stabilization. Various reducing agents, solvent media, capping agents and concentration were used in order to control the size, shape and size-distribution. Here we do not aim to present in detail the various methods but to highlight only the main methods.

The *Turkevich* method uses sodium citrate as both reducing and capping agent in boiling water which resulted 10-20 nm AuNPs^{3,6,7}. Changing the amount of citrate controlled the size (10-150 nm) but an increase in the size resulted in broad polydispersity⁸. The *Brust-Schiffrin* method was first carried out in two-phases (water – toluene) using dodecanethiol (DT) as a strong binding agent, sodium borohydride as the reducing agent and tetraoctylammonium bromide (TOAB) as the phase transfer reagent⁴, as illustrated in the equations below (eq. 1 and eq. 2) :



This method provides air stable AuNPs, with sizes ranging from 2 to 5 nm, functionalized with organic ligands (monolayer protected AuNPs), ready to be isolated and re-dissolved in apolar solvents without irreversible aggregation, due to the strong binding between gold and thiol. Many other works were published based on the Brust's method using different ligands to build up monolayer protected AuNPs e.g. phosphines⁹ or amines^{10,11}. These nanoparticles are sufficiently stable to carry out further reactions, e.g. ligand exchange¹² (see later), providing the opportunity to vary the ligands grafted to the core^{13,14}. These properties made this method especially interesting and most widely used, with small modifications, over the last two decades. One of the modification of this method, when it is carried out in a single phase, uses p-mercaptophenol as a capping agent¹⁵ or uses amine-borane complexes¹⁶, which results in very monodisperse particles with a size dispersity less than 5%. The size of the AuNPs can be controlled by changing the thiol/gold ratio, the speed and the temperature of the reduction step or the order of the addition of reactants^{17,18,19,20}.

Size modification can be carried out in many different ways: by applying careful adjustment of the reaction conditions in each step that provides nanoparticles with well

determined size and monodispersity, or by applying post-modification processes to narrow the dispersity of highly polydisperse nanoparticles e.g. *digestive ripening*^{21,22,23}. In the case of digestive ripening, polydisperse colloidal suspensions were refluxed in solvent in the presence of large excess of a surface-active ligand (e.g. thiol, amine, silane or phosphine) to reduce the size and dispersity. The careful control of the first case can be accomplished by *solid heat treatment*^{24,25,26} when the synthesis of nanoparticles with small size (~ 2 nm) is accomplished using a well-known process (Brust's) and evolved to larger sizes by heating in the presence of a phase transfer agent. In this case, the size of the nanoparticle is controlled thermodynamically due to the different thermal stability of AuNPs with different sizes (smaller nanoparticles have a lower melting point than larger ones). Monodisperse nanoparticles produced in this way form self-assembled 2D lattices (Figure 2). On the other hand, using a *seeded growth* synthesis^{27,28,29,30}, where the particle size is controlled by varying the ratio of seeds (the purpose of which is served by small nanoparticle as nucleation centres) to metal, also provides good monodispersity over a wide range of the sizes.

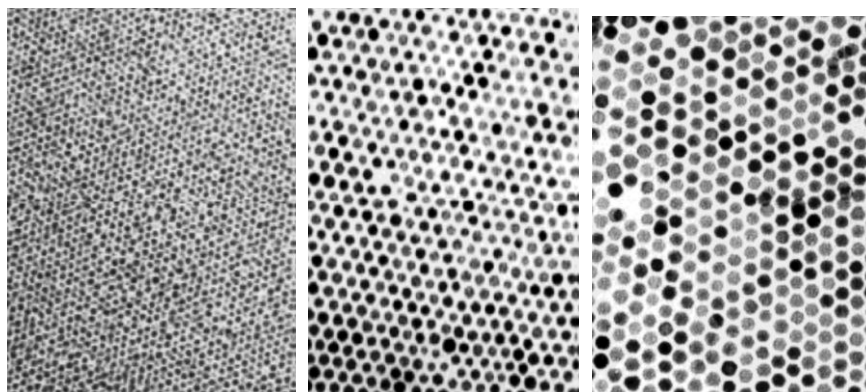


Figure 2 TEM images of DT-AuNPs heat treated at 150°C (3.4 nm), 190°C (5.4 nm) and 230°C (6.8 nm) (Teranishi²⁴)

II.1.1.3 Ligand-exchange and coupling on AuNPs

Monolayer protected AuNPs can be further reacted in *ligand-exchange reactions* providing the opportunity to vary the ligands and adjust the properties according to the experimental need. These reactions have a certain advantage compared to direct syntheses, where the ligands are often incompatible with the reaction conditions and the core size strongly depends on the applied ligand, limiting the structure and size of the nanoparticles. Also direct synthesis requires a significantly higher amount of ligand which can cause some difficulties from a synthetic point of view. However, direct synthesis of AuNPs with bifunctional capping agents is particularly interesting in that it enables control over the particle size and has the

capability for subsequent functionalization with functional groups providing 100% of coverage of the introduced ligand³¹. In ligand-exchange reactions, the size and structure of the nanoparticles remain the same or can be controlled independently of the ligand used. In the replacement step, either different ligands (e.g. phosphines^{32,33,34,35,36}) or thiols^{12,37,38,39,40,41} are exchanged for thiols. Complete replacement of the ligand, which build up on the original shell, is possible in case of triphenylphosphine (TTP) stabilized nanoparticles, which make them excellent precursors for other functionalized nanoparticle building blocks³³. Mechanistic studies also reveal a novel three-stage mechanism that can be used to control the extent of ligand exchange (Figure 3).

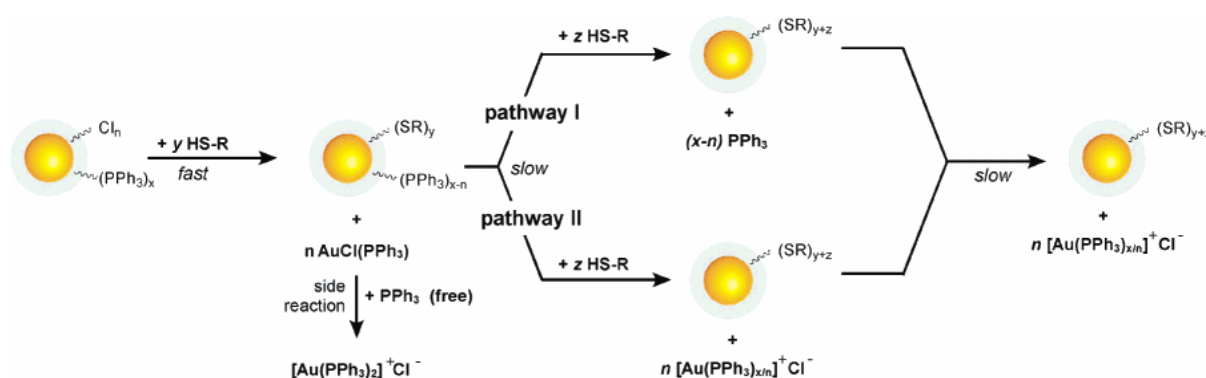


Figure 3 Proposed three-stage mechanism for the ligand exchange reaction between 1.5-nm Au_n -TTP and thiols. In the initial stage, part of the phosphine ligand shell is rapidly replaced in the form of $\text{AuCl}(\text{PPh}_3)$ until no more particle-bound chlorides are available. This initial phase is followed by removal of the remaining phosphine ligands either as free PPh_3 in solution (pathway I) or through direct transfer of PPh_3 to closely associated $\text{AuCl}(\text{PPh}_3)$ (pathway II). During the final stage, the completed thiol ligand shell is reorganized into a more crystalline state. Although treated as separate stages, it is most likely that the three stages overlap to a certain extent (Hutchison³³)

In the case of thiols, it was shown that complete replacement of the original thiol ligands is not possible but can be very close by increasing the ratio of the incoming ligands⁴⁰. The rate of place exchange decreases with the increase of the size of the original ligand in the protecting monolayer or the size of the entering ligand. The speed of the place exchange varies on the cluster surface: it takes place more quickly on the edges and vertices and more slowly at the near-edge and interior terrace sites¹². The alkanethiol of the original protecting shell can be exchanged to ligand bearing functional groups and in this way provides a functionalized mixed monolayer which can be subjected to further reactions (*coupling*) e.g. ω -bromo-functionalized AuNPs reacted with primary amines or alcohols in the presence of propionic anhydride¹⁴. The ω -bromo-functionalization of AuNPs proved to be especially useful as it can be easily converted to e.g. azide which can be further reacted in click-chemistry by introducing new ligands to the nanoparticle⁴² which functions as a secondary shell. Ester coupling reactions between AuNPs

bearing mixed shells of 11-mercaptoundecanoic acid / alkanethiol and 11-mercaptoundecanol / alkanethiol to form covalently networked AuNPs has also been demonstrated⁴³.

II.1.2 Liquid-crystalline Dendronized Gold Nanohybrids

The term hybrid materials is used in a very wide range of different materials, but by definition is the following⁴⁴: “a hybrid material is a material that includes two moieties blended on the molecular scale. Commonly one of these compounds is inorganic and the other one is organic in nature”. According to the possible interactions between the inorganic and organic species, two classes are distinguished: “*Class I* hybrid materials are those that show weak interactions between the two phases, such as van der Waals, hydrogen bonding or weak electrostatic interactions. *Class II* hybrid materials are those that show strong chemical interactions between the components”. Hybrid materials are of interest in many areas as the often dissimilar properties of the organic and inorganic parts are combined through their cooperative effects and their processing ability is increased. Hybrid materials can be built up from their building blocks using two approaches: on one hand, where the building blocks partially keep their molecular integrity which is still present in the final material, or the other one, when one or both structural units transform into a novel structure. Using building blocks with well-defined structures, which do not go through significant changes during the build-up of the hybrid systems, has the possibility for better structure-property prediction.

I.1.2.1 Dendronized gold nanohybrids

Our interest was focused on liquid-crystalline dendronized gold nanohybrids, but in this section, we will present some dendronized gold nanohybrids without liquid-crystalline behaviour. In the next section, we will describe those specific cases where these hybrid systems are liquid-crystalline and offer the possibility for self-assembly. Dendronized gold nanohybrids can be built up using dendrimers to encapsulate the AuNPs within their interior (dendrimer-encapsulated nanoparticles, DENs)^{45,46,47,48,49,50}, or the dendrimers can be grafted to the nanoparticles which can be positioned at the core: nanoparticle-cored dendrimers (NCDs), or at the periphery⁵¹.

Early examples show, that PAMAM dendrimers are effective for the preparation of **dendrimer encapsulated** AuNPs and depending on the concentration and the surface groups of the dendrimers, the size of the NPs can be adjusted⁴⁵. DENs also have potential as catalysts as the surfaces of the particles are accessible. They can be prepared by changing the composition of metal ions within the dendrimers and the following reduction of the composites results in

monodisperse, less than 3 nm, zero valent DENs, where the dendrimers act not only as a template but as a stabilizing agent and tuning the solubility⁴⁸. The size of the nanoparticles can be controlled through the initial metal ion / dendrimers ratio⁴⁷. Synthesis of hybrid AuNPs can be carried out by stabilizing (but not encapsulating), or encapsulating the AuNPs in new “clicked” dendrimers of generations zero to two (G0–G2) containing tri- and tetra-ethyleneglycol tethers^{49,50} (Figure 4). In first case, the AuNPs are bigger than the dendron, ~4.1 nm, and cannot be encapsulated. In the second case, the AuNPs are smaller ~1.9 nm, than the higher generation dendrimer, which are able to encapsulate them. DENs bring the combinations of the physical properties of the NPs and the dendrimers, which tune the solubility, stabilize the NPs and enhance catalytic selectivity and the surface reactivity.

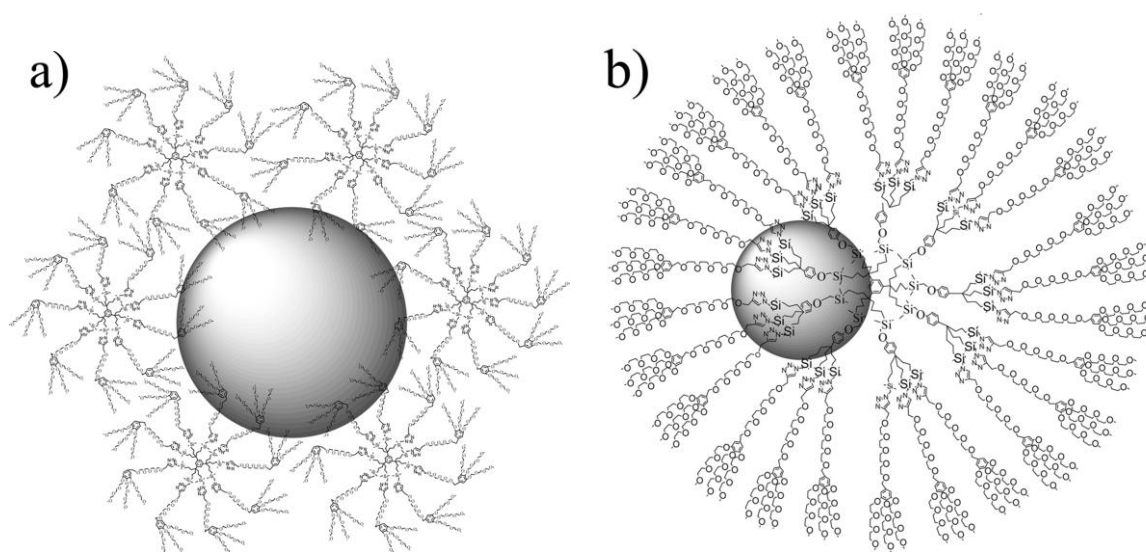


Figure 4 AuNPs stabilized by several G0 dendrimers; (b) G1 dendrimer-encapsulated AuNPs. (Astruc⁵⁰)

Nanoparticle-cored dendrimers have advanced the preparation, stability and control of hybrid materials. These hybrid materials can be built up using a direct synthesis method^{52,53,54,55,56,57}, ligand-exchange^{57,63,58,59} reactions or coupling reactions^{42,60,61,62}. In the case of *direct synthesis*, dendrons bearing a thiol or disulphide anchoring function are grafted onto the AuNPs, surrounding the NPs as a homogenous layer. The first set of dendron-stabilized AuNP, via direct synthesis, was prepared using a modified Schiffrin reaction with Fréchet-type dendrons bearing single thiol groups (Figure 5) and resulted in stable, monodisperse AuNPs with small cores⁵³. No significant change was observed in the core size by changing dendrimers/gold ratio. Another team also used Fréchet type dendrons but used disulphide wedges for the synthesis of NCDs and reported that increasing the generation number of the

dendritic wedges decreased the number of the connected units which results in low surface area coverage. This not passivated part of the Au cluster is available for catalytic activity⁵².

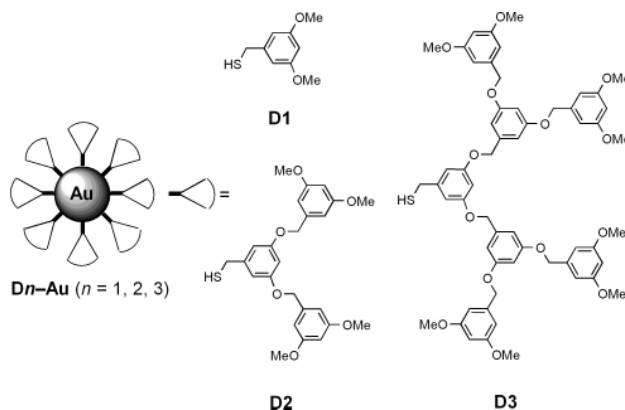


Figure 5 Schematic illustration of dendron-stabilized AuNPs⁵³

Chechik *et al.* who also used disulphides but with *L*-Lysine based (Newkome-type) dendrimers. They reported that the size of the AuNPs decreased with increasing the dendritic generation number⁵⁴. The chemical stability of the hybrid structures was also investigated and it was concluded that better overall nanoparticle surface coverage provides better stability which is decreased by increasing the branching or appearance of hydrogen bonding⁵⁵. The connection between the core size and the generation number cannot be stated unequivocally as different observations were made as well: when the core size was found to increase when raising the generation number of poly(oxymethylphenylene) dendrons⁵⁶. In case of large dendrons where steric hindrance can hamper the direct reaction, mixtures of small linear ligands (dodecanethiol) can be used to resolve the difficulties and build up mixed shells, as it was shown in case of silylferrocenyl dendrons⁶³ which are suitable for application as sensors with a large dendritic effect for oxo-anions. AuNPs dendronized with conjugated dendrons (e.g. thiophene dendrons) were also synthesised via direct reaction⁶⁴ and more moderate fluorescence quenching was observed if longer spacer length and larger dendrons were applied, which makes them suitable for optoelectronic devices and photonic materials. Dendrons with ester functional groups on the periphery and disulphide anchoring function were also used for grafting to the AuNPs via direct synthesis⁶⁵. The same decrease as mentioned previously, in the density of the connected branching units when the generation number was increased occurred, but the hybrids remained stable. The esters on the periphery were converted to the corresponding sodium salt via hydrolysis providing water solubility and the hybrids exhibited micellar properties. This solubility and the capability to act as host cavities for guest molecules due to the large void spaces near to the metal core and the unpassivated surface area enable them to be used as catalytic nanoreactors⁶⁵. Dendrimers bearing a carbazole at the periphery

and amine anchoring functions with different generation numbers were grafted onto the gold and a direct synthesis protocol was compared to ligand exchange, in which case the Au-NPs were protected by propane thiol or butyric acid, followed by subsequent ligand exchange with a carbazole-terminated thiol. The results indicated that the direct synthesis route generally yielded high surface functionality. However exchange was applied only on ligands so far but on higher generation dendrimers. There is also suggestion that ligand exchange was better in the case of butyric acid passivated AuNPs, but more experimental data is required for a clear statement. Electrochemical crosslinking of the carbazole was also carried out which resulted in a shift in the absorption and fluorescence.

Ligand-exchange in the case of dendritic moieties is carried out in similar ways to those described in the previous paragraph (II.1.1.3): first step, monolayer protected AuNPs are synthesised, followed by the partial exchange of the original ligands with dendrons bearing anchoring functions. Dendronized nanoparticles using Newkome-type dendrons with branched structure having carboxyl terminated functional groups were also prepared via a ligand exchange reaction, using 10 nm citrate capped AuNPs⁵⁹. Dendrons with different anchoring functions (disulphide, thiol and “di-anchored” disulphide groups) and generation numbers were taken into the reaction (Figure 6) and reactivity was investigated by determination of the relative surface coverage.

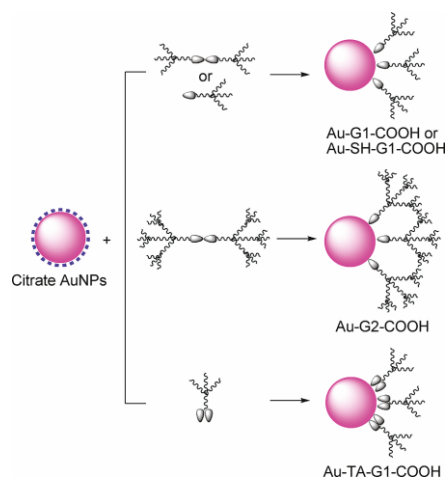


Figure 6 Schematic view of ligand-exchange reaction of citrate protected AuNPs with Newkome-type dendrons bearing different anchoring function with different generation numbers⁵⁹

The highest surface coverage resulted in the case of the “di-anchored” disulphide dendron but still lower than in the case of 11-mercaptoundecanoic acid. This result is explained by steric hindrance which, on one hand does not support the grafting of the disulphide and on the other hand does not allow tight packing due to the branched structure. Astruc applied not only direct reaction but also ligand-exchange to construct dendronized gold nanoparticles. In the first case,

not dendrons but only ligands, (amidoferrocenyl)alkanethiols⁵⁸, were used to exchange the dodecanethiol on the AuNPs with different lengths of spacer (11 and 6 C atoms) and it was observed that no higher than 38% ligand content of the organic mixed shell can be achieved, if the longer spacer was applied, which was in agreement with previous work of Murray¹². Introducing ferrocenyl (AFAT) dendrons via ligand exchange reaction further decreased the rate as low as only ~5%⁶³ (Figure 7). Increasing the generation number via ligand-exchange reaction did not work due to steric hindrance and direct synthesis with mixed ligands was applied (see above).

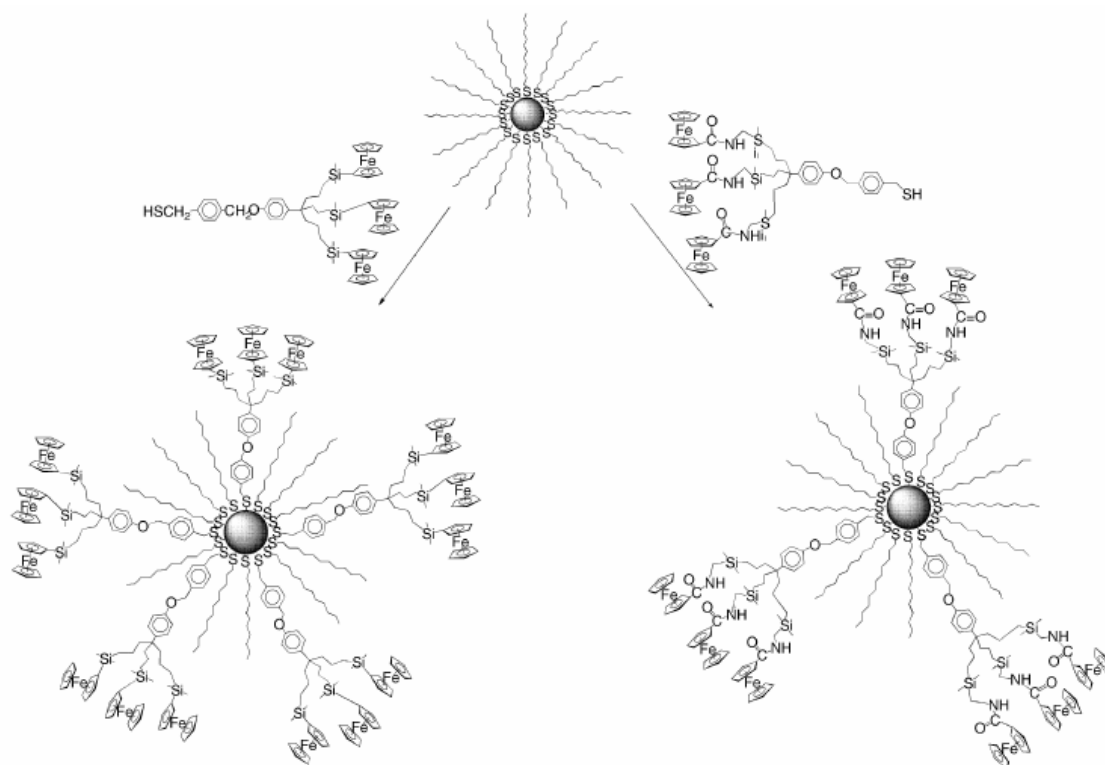


Figure 7 Synthetic scheme for AFAT-AuNPs via ligand substitution method⁶³

In the case of *coupling reactions*, the monolayer of the AuNPs can be functionalized (mixed or homogeneous shell) and is capable for further reactions. The nanoparticle through these functional groups can be reacted with dendrons in a coupling reaction in a single or multi-step. This approach can overcome the problem of the direct synthesis that requires a large excess of dendrons with anchoring functions, and with little control over the size of the AuNPs and can also provide a better coverage than the ligand-exchange reaction. However, 100% of binding is not achievable in many cases which leave mixed shell with active functional groups. Ester coupling reactions, one of the most popular reactions for coupling, was already shown in previous section, when AuNPs with hydroxyl and carboxyl terminated functional groups were reacted to form covalent networks⁴³. For the case where the functional groups were induced by

a ligand-exchange reaction, there was only a partial presence of the functions in the termini. Dendritic AuNPs were built up by ester coupling reaction between V-shaped amphiphilic dendritic ligands with a carboxyl function and mercaptophenol-functionalized AuNPs⁶⁰, which led to 65 grafted dendrons on AuNPs with 2 nm size and unreacted mercaptophenols. In other ester coupling reactions, the AuNPs were functionalized with carboxylic acid termini and reacted with hydroxyl-functionalized dendrons by a single coupling reaction, according to the convergent approach⁶¹. The dendrimer's wedge density could be controlled, in the case of "Féchet-type" dendrons, by reacting AuNPs having different loadings of carboxylic acid groups⁶². Using different generation numbers results in different numbers of interior layers - unreacted carboxyl acid groups inside the dendrons - and dendritic wedge densities. Beside esterification coupling methods, "click" chemistry is also used for functionalization. During functionalization of AuNPs using "click" chemistry, difficulties such as low yield are encountered that contrast with the "easy" click reactions. It was shown that very precise control of the conditions (solvent, catalyst and atmosphere) is necessary to overcome this problem and results in quantitative yields between azido group terminated AuNPs and linear or dendronic alkenes⁴².

1.1.2.2 Liquid-crystalline gold nanohybrids and self-assembly

Fabrication of ordered structures which are relatively stable are great challenges. As top-down approaches are limited, bottom-up approaches, which are used for nanostructuring of elements to self-organize into 2D and 3D structures, are especially interesting. Nanoparticles doped in liquid crystals were reviewed by Hegman's group most extensively^{66,67,68} but will not be detailed here. In the latest reviews there are also included a part on liquid crystalline nanoparticles which is our main interest as these materials that can solve the long term stability problems. Donnio and Nealon also reviewed the developments in the field of discrete thermotropic liquid-crystalline nanoparticle hybrids, with special emphasis on the relationship between the nanoparticle morphology and the nature of the organic ligand coating and their resulting phase behaviour⁶⁹. Design concepts for liquid-crystalline metal based nanoparticles were partly adapted from liquid-crystalline fullerenes⁷⁰. Functionalization of AuNPs with mesogenic or protomesogenic ligands showing LC phases is a quite new area (calamatic^{71,72,73,74,75,76}, discotic^{77,78,79}, bent-core^{74,80,81,82}). The ways mesogens, protomesogens or dendritic ligands can be introduced to the AuNPs to form LC AuNPs are the same as were shown previously for classical AuNPs functionalization (paragraph I.1.2.1): a direct, a ligand-exchange or coupling (post-functionalization) method. In order to investigate the liquid crystalline

properties of the hybrids it is particularly important to assure the purity of the sample, as free ligands can modify the liquid crystalline behaviour.

The first report on LC AuNPs used the calamitic 10-[(trans-(4-pentylcyclohexyl)phenoxy)] decane-1-thiol as the ligand, which exhibited LC properties, in a direct synthesis of Brust's two phase method which resulted in 3 nm core size with homogeneous shell⁷². The thermodynamic behaviour of the hybrid was quite different from the calamitic ligand. A similar procedure was applied using cyanobiphenyl with a C12 linker and thiol function⁷¹, in which case, beside the mesophase (unidentified) one dimensional arrangement was observed during annealing of the 2.7 nm cores size hybrids. Nematic gold hybrids were obtained^{83,84} in ligand exchange reactions where part of the hydrocarbon (~50%), from which the monolayer was built up from around the AuNPs, was replaced with a nematic mesogen (Figure 8).

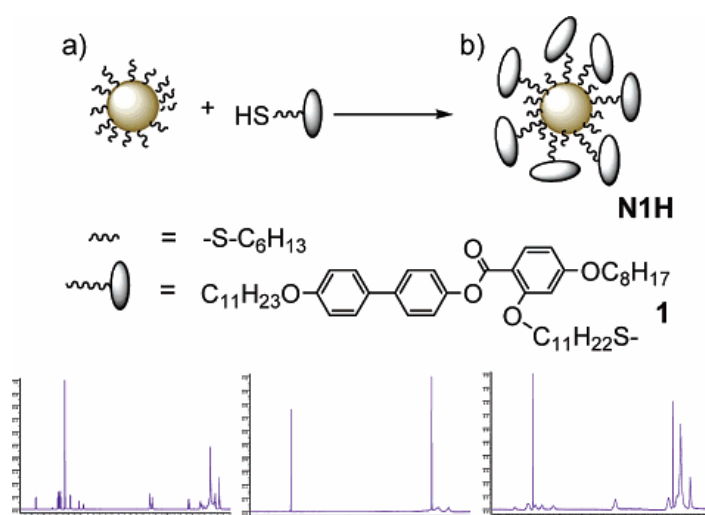


Figure 8 Top: Schematic representations; (a) (left) nanoparticles and (b) (right) exchange reaction yielding N1H. Middle: Chemical structure of the groups covering the particle surface (hexylthiol and mesogen). Bottom: NMR spectrum of mesogen 1 (left), NMR spectrum of hexylthiolfunctionalized nanoparticle; LC nanoparticle N1H (right). (Taken from Mehl⁸³)

The mesogens are rod-like where the spacer is attached on the side, which is also different from previous reports. The purity was confirmed by ¹H-NMR. The above described reaction was also carried out with a hydrocarbon chain length of C12 and comparing the two systems it was observed that the particle size and chain length modify the onset of the LC phase⁸⁴. Further investigation of these materials by Ungar and Mehl enlightened that these systems form highly ordered bulk arrays where the AuNPs form strings with rhomohedral or hexagonal columnar lattices⁸⁵. Similar systems were designed (L3) and investigated with mixed and homolithic shells⁸⁶ (Figure 9). While the two ligands with C6 long hydrocarbon co-ligand exhibit a similar

hexagonal columnar phase arrangement, using C12 long ligands, the AuL4 forms an anisotropic 3D structure of ordered NP strings in mutual register and with high birefringence. AuL3 has an optically isotropic face-centred cubic structure (Figure 9). The reason for the difference in the lower aspect ratio of the L3 mesogen and the dilution effect of the longer co-ligand was given. Without the co-ligand, AuL3 exhibits a (P_6/mmm) 3D hexagonal, non-birefringent structure.

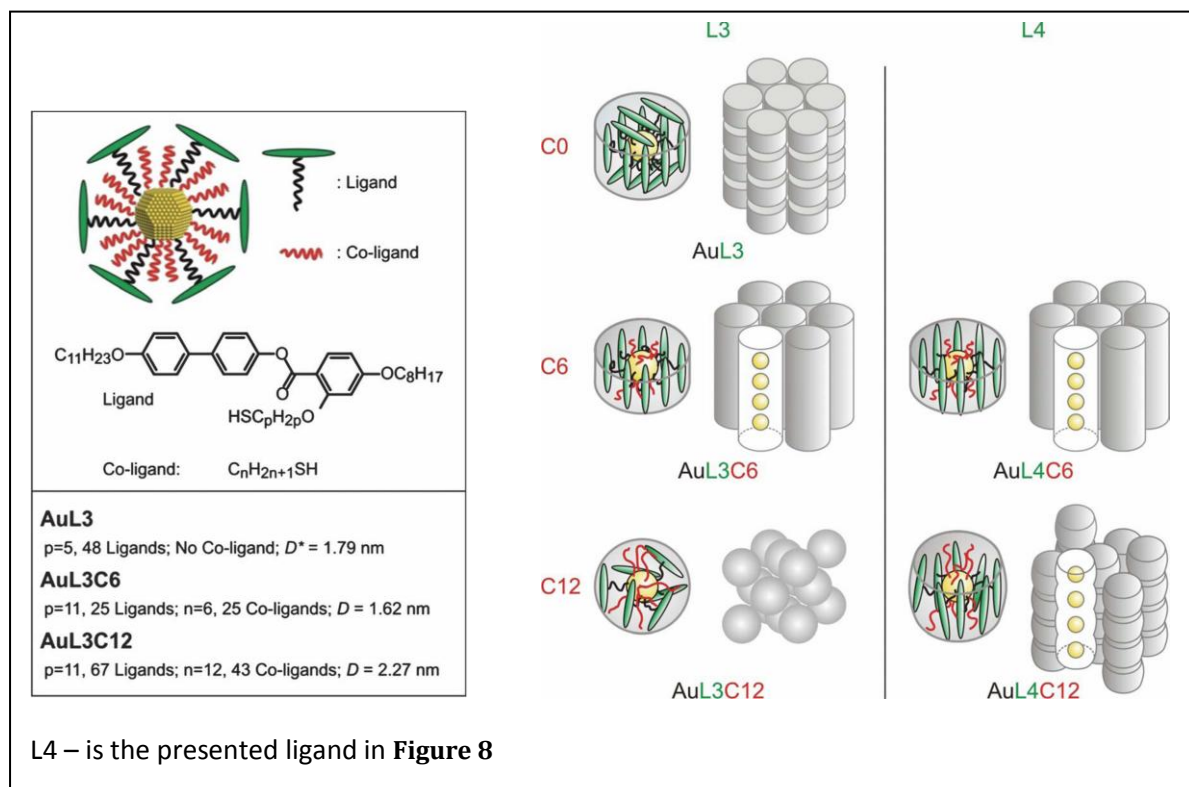


Figure 9 Schematic illustration of the different arrangements of ligands and co-ligands around a nanoparticle depending on the relative amount of co-ligand (red) and the length of the mesogenic ligand (green), and of the different resulting types of ordered self-assembly (taken from Mehl⁸⁶)

This work demonstrated that the self-assembly mode of NPs, and the distance between them in a defined direction can be controlled. Donnio et al. also applied a ligand exchange reaction to obtain dendronized AuNPs. In this case the dendritic ligand had a conical shape and itself did not exhibit liquid crystalline properties but the Au nanohybrids did. For first time, the dendrimer-coated AuNPs self-assembled on a surface and in the bulk, with 2D and 3D (body-centred cubic phase) positional order, respectively⁸⁷. Pocięcha et al. have presented Au nanohybrids, synthesised via ligand exchange reactions, which exhibit smectic or columnar phases after substitution of mesogenic rod-like or bent cores ligands⁷⁴. Goodby et al. carried out a detailed investigation on hybrid AuNPs where mesogenic cyanobiphenyl based thiols with different alkyl spacer were grafted to the AuNPs⁷³. Grafting the mesogenic ligands was carried

out using a ligand exchange reaction, but the original shell, which was triphenyl phosphine, was exchanged completely by the ligand resulting in a new homolitic shell with dense packing exhibiting a local rectangular arrangement.

Kanie and Ungar synthesised the first highly ordered simple-cubic thermotropic liquid crystal Au hybrids by coupling monodisperse AuNPs with amino substituted organic dendrons and obtained unconventional superlattices⁸⁸ (Figure 10). The effect of dendron generation and surface coverage on self-organization was investigated.

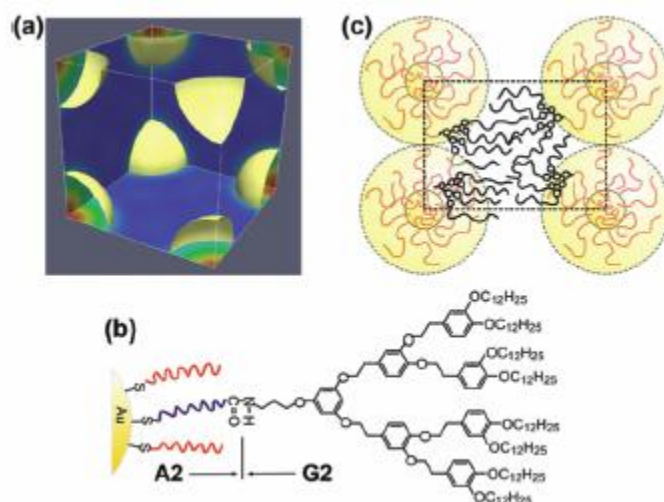


Figure 10 (a) 3D electron density map of a unit cell of the Pm3m SC phase reconstructed from the diffraction pattern in Figure 1g (blue, lowest density; red, highest density). The isoelectron surface delimits the spherical region of highest density (i.e., gold); organic matter fills the continuum. (b) Schematic of part of the double corona of a G2/ A2 NP. (c) (110) section through the unit cell. (taken from Kanie⁸⁸)

Deschenaux et al. also used coupling reactions to obtain dendronized AuNPs with liquid crystalline behaviour, but in this case “click chemistry” was applied⁸⁹. Liquid crystalline cyanobiphenyl based dendrons were attached to the AuNPs bearing azide functions resulting in an Au hybrid which exhibits SmA phase. Mehl et al. presented a novel approach for a coupling method³¹ where mesogenic groups were grafted to larger gold nanoparticles. AuNPs were protected by bifunctional capping agents, bearing an amine as the anchoring group. This was further functionalized with a mesogenic group which contained a long spacer and a siloxane group, resulting in a nematic Au hybrid.

Self-assembly of monolayer protected, monodisperse AuNP of different sizes were already presented by many different groups but grafting dendrons to AuNPs does not necessarily favour the self-organization. Self-assembly behaviour can be generated and controlled without formation of liquid crystalline phases in some case of dendronized gold

nanohybrids. Boudon made a comprehensive investigation of the effect of various liquid crystal dendrons attached to AuNPs via different synthesis protocols, such as direct synthesis, ligand exchange and coupling (using esterification method), on self-assembly⁹⁰. The direct synthesis led to full coverage and these dendronized AuNPs exhibited an unexpected organization where particles (1.2 nm core size) arranged themselves in evenly spaced rows⁹¹ (Figure 11) but this hybrid did not show mesomorphism. However, AuNPs bearing hydroxyl groups and dendronized via esterification using different mesogens, displayed a distinct mesophase under POM, but no phase transition was observed by DSC analysis and the mesophase was not confirmed⁹⁰.

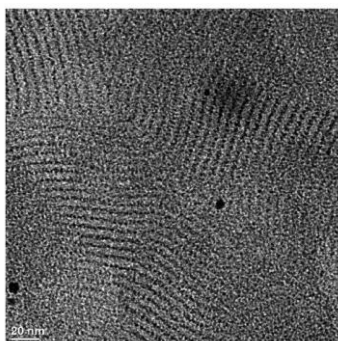


Figure 11 TEM Micrograph showing rows of 1.2-nm gold nanoparticles⁹¹

Torigoe et al. showed that grafting G1 and G2 Fréchet-type PPD dendrons, in direct synthesis, to AuNPs observed formation of spontaneous 1D arrays on carbon films⁵⁶. AuNPs capped by higher generation redox-active Fréchet type dendrons bearing a long alkyl chain thiol at the focal point also exhibit the spontaneous formation of 1D arrays⁹² (Figure 12).

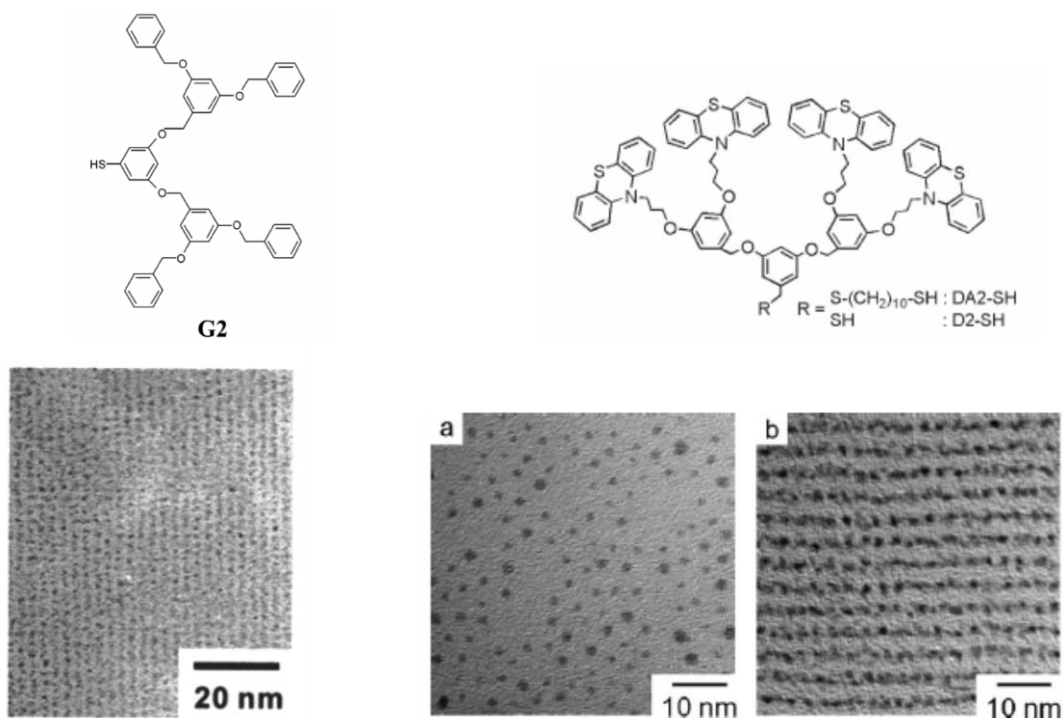


Figure 12 TEM micrographs of self-assembly of dendronized AuNPs; Left: taken from Torigoe⁵⁶, Right : taken from Fujihara⁹²

Using a direct synthesis, discotic, triphenylene based dendrons capped to AuNPs were synthesised and their self-assembly (hexagonal or 1D chain) was controlled by altering the ratio of methanol to toluene in the solvent⁹³ showing that the state of the surrounding organic ligands in solution influence the self-assembled structure of metal nanocores on the substrate.

II.1.3 Objective of the thesis, II.

As we presented in the previous chapter, liquid crystalline dendrimers are especially interesting because of their structural diversity and the ability to self-assemble into ordered supramolecular edifices. Because of this, protodendritic ligands emerge as prime candidates to build up metal-cored hybrid materials where liquid crystallinity can be induced which favour self-assembly into 2D or 3D networks. AuNPs based dendronized hybrid materials, as was introduced in the previous sections, are especially interesting because of their size-dependent and biocompatible properties and be used to develop nanomaterials, from which fabrication of ordered structures is possible.

The third part of this thesis, which is presented in Chapter II, involves the design and synthesis of gold nanohybrids where the core of the dendrimers, whose syntheses are described in the first chapter, is replaced by a gold nanoparticle. The objective is to obtain multifunctional compounds where specific properties of the two building blocks (inorganic – size dependent properties - and organic – flexibility, solubility, self-organizing ability) are combined within a single structure. We studied the relationship between the structure of the grafted protodendritic ligands and the self-assembly of these hybrid materials. Therefore, the goal was firstly to prepare monodisperse gold nanoparticles with good reproducibility and secondly to graft covalently the protodendritic ligands to them in order to induce self-assembly and investigate if liquid crystalline properties could be induced. With this study we also wanted to present the multi-faceted properties of dendrimers which is provided by the dendritic structure.

II.2 Results and discussion - Syntheses

II.2.1 *Synthesis of gold nanoparticles*

As was shown in the previous paragraph (II.1.1) many different techniques were developed to control the size and monodispersity of gold nanoparticles (AuNPs). In order to synthesise dendronized gold nanohybrids by a ligand-exchange reaction and later to be able to organize them into periodic arrays, AuNPs with well-defined and controlled size, low dispersity and, importantly, with good reproducibility have first to be prepared. Both types of ligands, 1-dodecanthiol (DT) and 1-octylamine, were used in the direct synthesis to protect the AuNPs from aggregation by forming a monolayer around the nanocrystal.

The reproducibility of the synthesis, that includes the control of both the monodispersity and size, is a crucial issue. Several different methods and modifications of the Brust's two phase methods were tested to obtain small ~ 2 nm particle sizes which can be used as a source for further reactions. We applied another modification of Brust's method, using DT as monolayer around the shell, which proved to be the most reproducible for the synthesis of ~ 2.1 nm AuNPs (experimental details are described in the experimental part). The synthesis followed the standard procedure where gold salt is dissolved in water and added to a vigorously stirred solution of tetraoctylammonium bromide (TOAB) in toluene which almost immediately transfers the gold to the organic phase as evidenced by the change of the colour from yellow to orange. This is followed by adding 1-dodecanethiol to the solution, resulting in the lightening of the colour. The next step, reduction, is carried out by adding NaBH_4 dissolved in water to the solution under continuous stirring resulting in the darkening of the organic phase, testimony to the formation of AuNPs (**G1**: 2.3 nm, **G2**: 2.1 nm) (Figure 13).

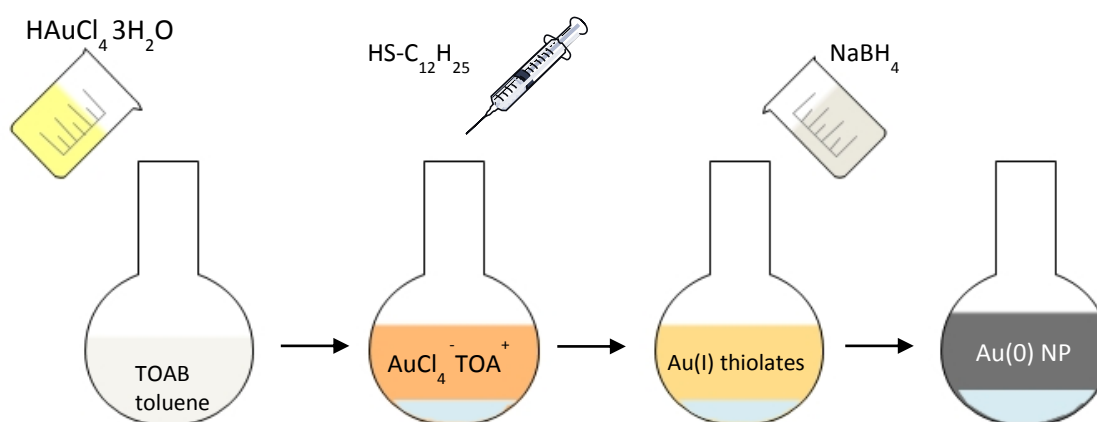


Figure 13 Modified Brust's two phase method applied for the synthesis of ~ 2 nm DT-AuNPs

To achieve optimal control of this method, several parameters were changed and their effect systematically investigated on the size, monodispersity and reproducibility of the AuNPs. Fine modification of the size was carried out by changing the DT: AuCl₄ ratio. In order to obtain smaller nanoparticles (**G3**, ~1.7 nm) the DT: AuCl₄ ratio was increased from 1:1 to 3:1 in more dilute conditions. The former was used to favour the formation of DT-AuNPs around 2.1 nm. We also aimed to simplify the reaction paths and for this reason we investigated other conditions e.g. the effect of the phases separation. The separation of the organic phase from the water phase before introduction of the DT did not improve the monodispersity or had little or no effect on the size (Figure 14), so to reduce the synthetic steps, this step was abandoned.

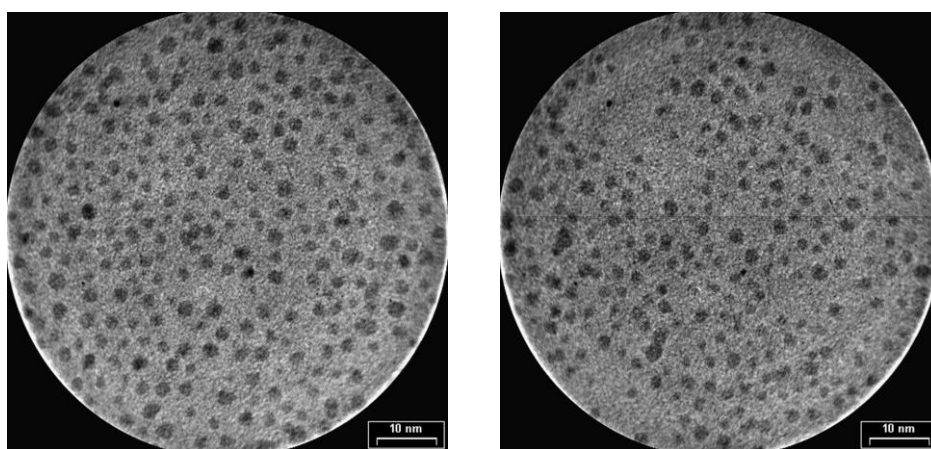


Figure 14 ~1.8 nm DT-AuNPs. Left: without phase separation, Right: with phase separation before introduction of DT in Brust's two phase method

To increase the size of the AuNPs, we applied two different methods according to the literature: "Seeding growth"²⁹ and "Solid heat treatment"^{24,26}. The scale up of the "Seed growth" method resulted in polydisperse DT-AuNP, in contrast to the "Solid heat treatment" for which monodispersed nanoparticles with size 2.8 and 5.6 nm were obtained by heating at 150°C and 170°C, respectively. Scale up of this method provided the same monodispersity but not the same size (7.7 instead of 5.6 nm heating at 170°C) (Figure 15).

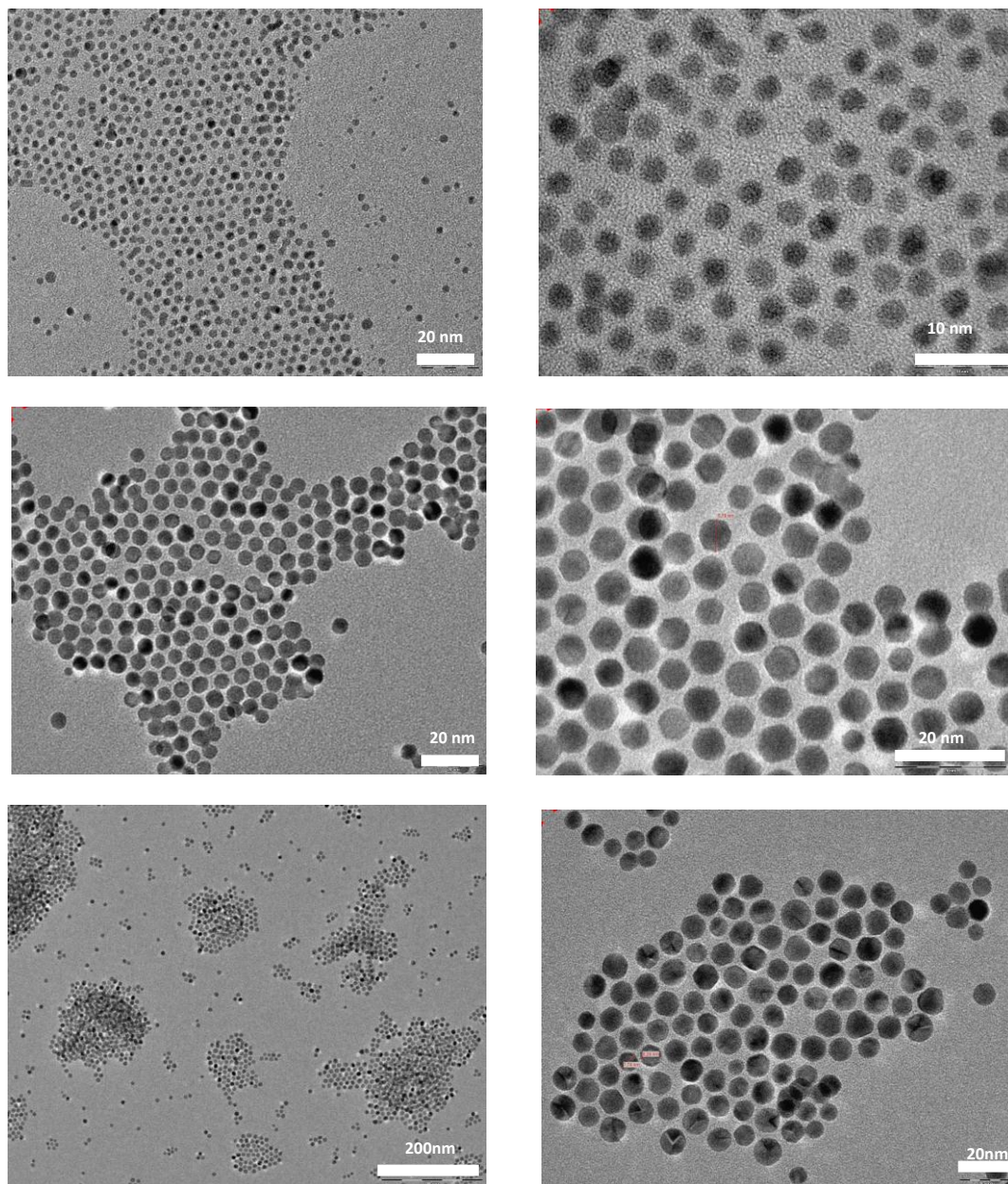


Figure 15 TEM images of DT-AuNPs treated according to “Solid heat treatment”:
 Top: 2.8 nm, $sd=0.48$, applied temperature 150°C, scale: 20 nm, 10 nm; middle: 5.6 nm, $sd=0.59$ nm,
 170°C, 20 nm, 20 nm; bottom: ~ 7.2 nm, 170°C at higher scale, 200nm and 20 nm

We also carried out direct synthesis using 1-octylamine (OA) as ligand for the monolayer in a more dilute system and using only two fold excess of the reducing agent. This resulted in monodisperse (5.4 nm, $\sigma=0.27$) and 3D self-assembly (over 400 nm, Figure 16) of the OA-AuNPs but the same result at larger scale under more concentrated condition, unfortunately, was not reproducible and for that reason will not be detailed.

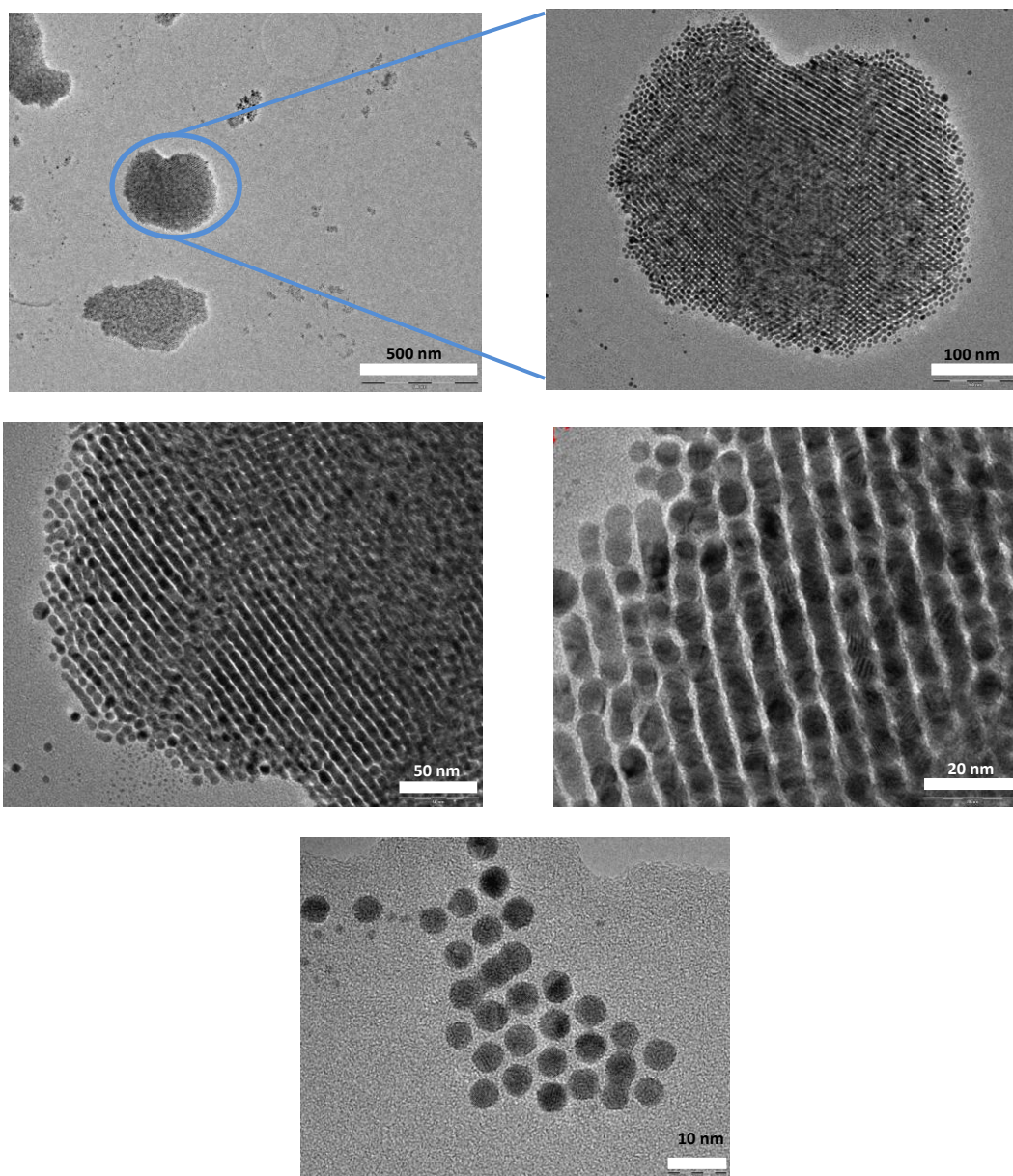
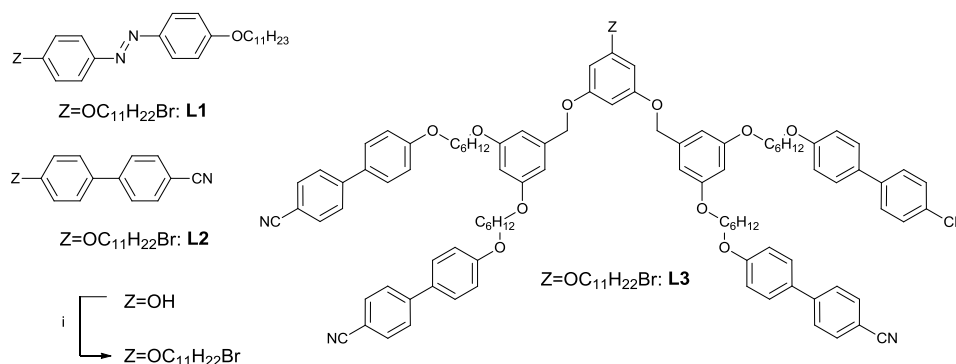


Figure 16 3D self-assembly of OA-AuNPs, ~5.4 nm

II.2.2 Synthesis of Ligands

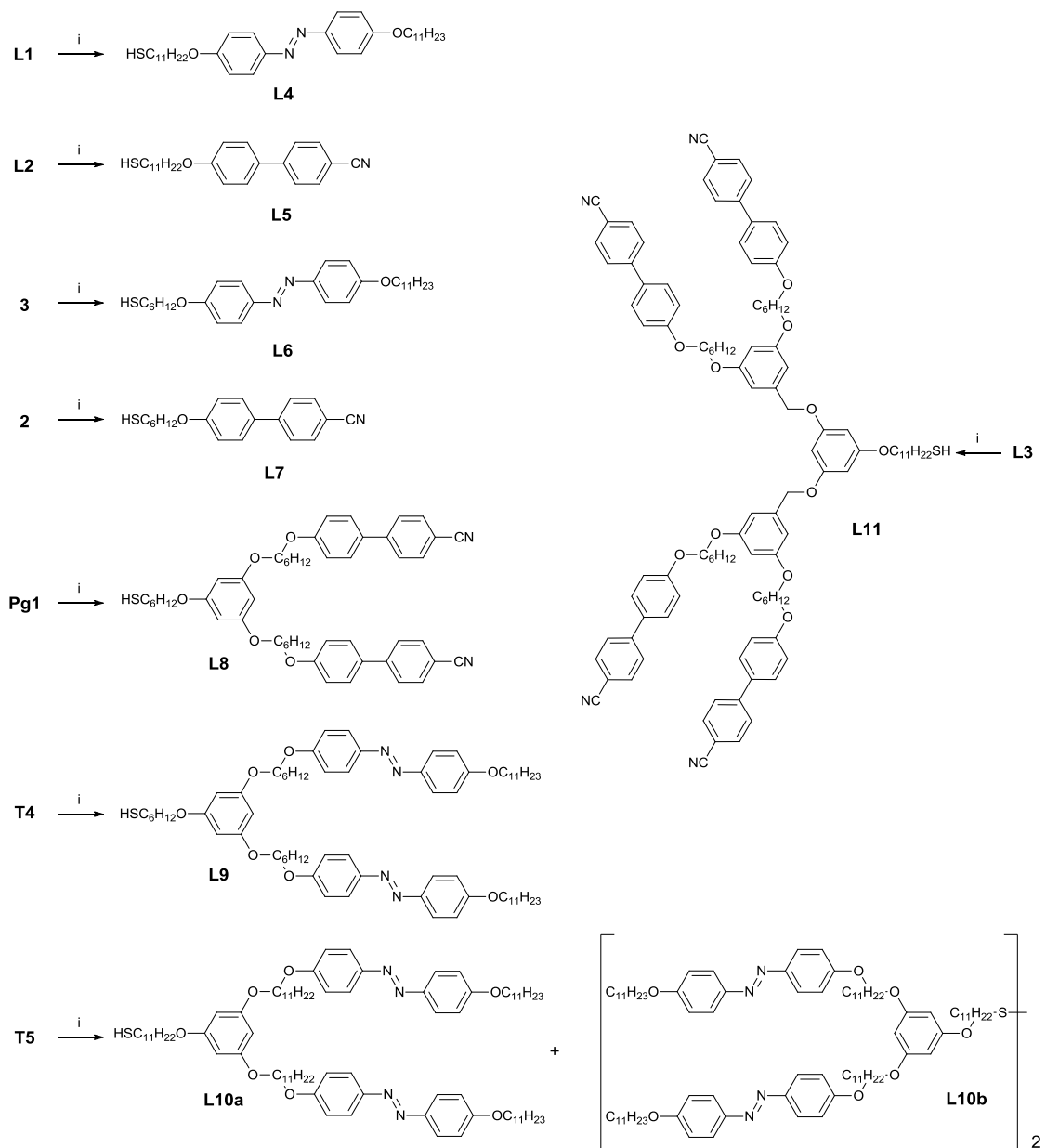
In order to build up dendronized gold nanohybrids, most commonly direct synthesis or solvent-mediated ligand exchange reactions can be used. In our case, all syntheses were performed using solvent-mediated ligand exchange reactions where the size and the monodispersity of the gold nanoparticles, used as a precursor, remain the same⁹⁴. In order to attach the protodendritic ligands to the gold, it has to have a strong binding function, e.g. thiol groups.

We used the DT-AuNPs, - their syntheses were presented in the previous section -, and thiol substituted protodendritic ligands as starting materials in the solvent-mediated ligand-exchange reaction. Various hydroxyl-based protodendritic ligands, which were used to build up the dendrimers (I.2), were derivatized with a bromoalkyl chain, which function as a spacer between the mesogenic part and the AuNPs (Scheme 2) in this case. Three ligands (**AZB**, **OCB** and **Ba8** (HO-PG(Ba₆OCB₂)₂)) were not previously appended with C11 long bromo-alkyl chains and for this reason they were bromoalkylated by 1,11-dibromoundecane via Williamson etherification (Scheme 1).



Scheme 1 Bromoalkylation of AZB, OCB, Ba8, *Reagents and conditions: (i) 1,11-dibromoundecane* K_2CO_3 , 18 crown-6, acetone/THF, reflux

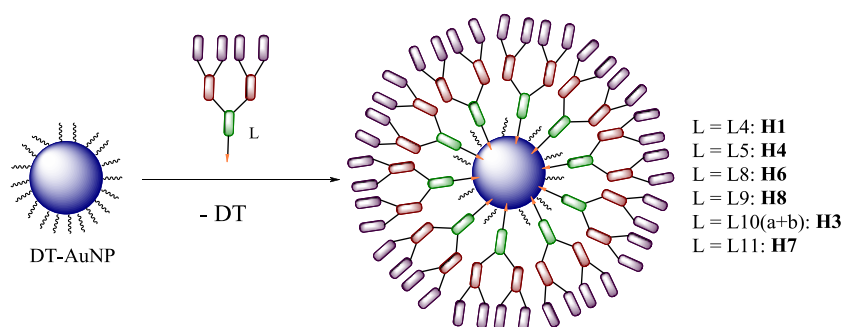
These bromide atoms could be easily converted to a thiol anchoring function, which made the ligands suitable for grafting to the AuNPs (Scheme 2). The bromide atoms on the ligands (L1, L2, L3, 2, 3, Pg1, T4, T5) were thiolated, in all case, using hexamethyldisilathiane (HMDS) agent and followed by addition of TBAF, 5 minutes later, to the solution. The following thiol substituted ligands were grafted to the gold (Scheme 2):



Scheme 2 Thiolation, Reagents and conditions: (i) HMDTS, TBAF, THF, 0°C

II.2.3 Synthesis of dendronized gold nanohybrids

Syntheses of gold nanohybrids were carried out in a solvent-mediated ligand-exchange reaction using dodecanethiol protected gold nanoparticles ~ 2 nm (DT-AuNP, the synthesis was described in the II.2.1 paragraph) and the thiolated protodendritic ligands (**L4**, **L5**, **L8**, **L9**, **L10(a+b)**, **L11**) as building blocks using CH_2Cl_2 as a solvent at room temperature (Scheme 3). In order to graft the prodendritic ligands to the DT-AuNPs, first the size of the AuNP and the number of dodecanthiol grafted to the surface had to be determined. The radius of nanoparticles was measured using TEM. According to the formulas (see below) the gold / DT number ratio was calculated for DT-AuNPs with different diameters (Table 1) and assuming that the ligand with thiol function will occupy the same surface area as the dodecanethiol, the required amount of ligand for the exchange reaction then was calculated.



Scheme 3 Solvent-mediated ligand exchange reaction; *Reagents and conditions: DT-AuNP, Li, CH_2Cl_2 , rt*

In the thiol-to-thiol exchange reaction increasing the incoming:outgoing thiol ratio results in a higher coverage of incoming thiol although above a ratio of 4 and over 24 hours, there is no significant improvement⁴⁰. For this reason in each case the ligands were used in ~ 3 -4 times excess compared to the grafted DT (see II.5.3).

The gold atoms occupy a volume of 0.017 nm^3 ($v_g = (4/3)\pi r^3 / 0.74$), where r is the atomic radius of gold atom, 0.74 nm is from the inter-atom distance in the bulk face-centered cubic (FCC) lattice in the polycrystalline core¹⁷, and assuming that the nanoparticles are spherical and the thiols each occupy⁹⁵ a surface area of 0.214 nm^2 , similar to the value observed on Au (111) surfaces, it is possible to calculate the number of gold atoms / particle and the thiol / gold ratio and to define a 'relative molecular mass'⁹⁶. However the calculated (theoretical value) weight percentage of the dodecanthiol (DT wt%), grafted to the nanoparticle, is low compared to the experimental values (weight percentage of the dodecanethiol or ligands, grafted to the surface of AuNPs measured by TGA). For two batches of dodecanethiol protected gold nanoparticles, which were used in the exchange reactions, the following values were

calculated from TEM and TGA measurements: D=2.13 nm, sd=0.43 nm, 24.62 wt% of DT and for 2.28 nm, sd=0.48 nm, 21.74 wt% of DT. This discrepancy is probably due to the assumption of a spherical model and the calculation of thiol on a flat Au(111) surface, but matches well with previous literature data where calculations were made on polyhedron shapes¹⁸.

$$N_{Au} = \frac{V_{Np}}{v_g} = \frac{4 * \pi * R^3}{3 * v_g}$$

$$N_{thiol} = \frac{S_{Np}}{a_{thiol}} = \frac{4 * \pi * R^2}{a_{thiol}}$$

$$M_{NP} = M_{Au} * N_{Au} + M_{thiol} * N_{thiol}$$

$$DT \text{ wt}\% = \frac{N_{DT}M_{DT}}{N_{DT}M_{DT} + N_{Au}M_{Au}}$$

N_{Au} – number of gold, V_{Np} - volume of the nanoparticle, $v_g = 0.017 \text{ nm}^3$ - volume of gold atom, R - radius of NP_{Au} , N_{thiol} – numer of thiol, $a_{thiol}=0.214 \text{ nm}^2$ – surface occupied by one thiol, S_{Np} – surface of the nanoparticle, $M_{Au} = 196.97 \text{ g/mol}$, M_{thiol} – molecular weight of thiol

D (nm)	R (nm)	V_{Np} (nm ³)	N_{Au}	S_{Np} (nm ²)	N_{thiol}	N_{Au} / N_{thiol}	S/V	DT wt%
1	0.5	0.523	30.78	3.14	14.67	2.10	6.00	32.77
1.6	0.8	2.144	126.09	8.04	37.56	3.36	3.75	23.35
1.8	0.9	3.052	179.53	10.17	47.54	3.78	3.33	21.31
2	1	4.187	246.27	12.56	58.69	4.20	3.00	19.59
2.1	1.05	4.847	285.09	13.85	64.71	4.41	2.86	18.84
2.2	1.1	5.572	327.79	15.20	71.02	4.62	2.73	18.14
2.3	1.15	6.367	374.55	16.61	77.62	4.83	2.61	17.48
2.4	1.2	7.235	425.56	18.09	84.52	5.04	2.50	16.88
2.5	1.25	8.177	481.00	19.63	91.71	5.25	2.40	16.31
3	1.5	14.130	831.18	28.26	132.06	6.29	2.00	13.97
4	2	33.493	1970.20	50.24	234.77	8.39	1.50	10.86
5	2.5	65.417	3848.04	78.50	366.82	10.49	1.20	8.88
6	3	113.040	6649.41	113.04	528.22	12.59	1.00	7.51
7	3.5	179.503	10559.02	153.86	718.97	14.69	0.86	6.51
8	4	267.947	15761.57	200.96	939.07	16.78	0.75	5.74
9	4.5	381.510	22441.76	254.34	1188.50	18.88	0.67	5.14
10	5	523.333	30784.31	314.00	1467.29	20.98	0.60	4.65

Table 1 Calculated Au / thiol ratios of AuNPs and molecular weight of DT

It is well known that metallic nanoparticles grow as polyhedra and that small NPs adopt the shape of various polyhedral clusters^{97,98}. The diameter measured by TEM is a mean diameter, which can be approximated to the diameter of the inscribed spheres and considering the most common polyhedra⁸⁷ (Table 2). It is possible to find relationships between such a diameter and polyhedral edges. Unlike to a sphere, which has a minimal surface, chains also can be grafted on the edges of the polyhedron^{18,87} which results in more grafted thiols and increases the weight percentage of the organic part. The surface and the volume of a great number of polyhedra were indexed and the number of gold atoms in their volume determined according to the in-sphere approximation⁸⁷ (Table 2). In the case of the dodecahedron, icosahedron, rhombicuboctahedron and rhombic dodecahedron the calculated surface (S) volume (V) ratio remains the same as at the spherical approximation (e.g. 2.86 at 2.1 nm diameter - Table 1), this results in the same weight percentage for the same ligand (e.g. 18.84 wt% of DT at D=2.1nm). However calculating with the mid-radius, (a tangent to every edge of the polyhedron) the calculated values are closer to the measured values (see Table 3, calculation for dodecahedron) but there is still a need to allow excess grafting on the edges.

All experiments were carried out with large excess of ligands compared to DT. The excess of the ligand were also larger than the difference between the spherical and polyhedron model and because of this the spherical approach were used for the calculation of the necessary molarity of the ligands.

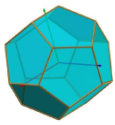

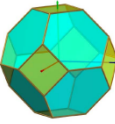

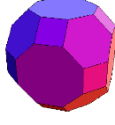
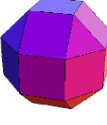
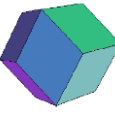
Polyhedron	Faces	$V/\text{\AA}^3$	$S/\text{\AA}^2$	$\frac{\phi}{\text{insphere}/\text{\AA}}$	$l/\text{\AA}$	V_{Np}	N_{Au}
Dodecahedron ¹ 	12◆	$7.66312l^3$	$20.64573l^2$	$2.227l$	9.43	6425.44	379.5
Icosahedron ¹ 	20▲	$2.18169l^3$	$8.66025l^2$	$1.5115l$	13.89	5850.95	345.6
Truncated Octahedron ² 	6■ +8◆	$11.31371l^3$	$26.78461l^2$	■ $2.82843l$ ◆ $2.4495l$	7.425 8.57	4630.49 7129.0	273.51 421.1
Cuboctahedron ² 	8▲ +6■	$2.35702l^3$	$9.4641l^2$	▲ $1.63299l$ ■ $1.4142ll$	12.86 14.85	5012.69 7717.5	296.1 455.9
Rhombitruncated Cuboctahedron ² 	12■ +8◆ +6●	$41.79899l^3$	$61.75517l^2$	■ $4.42l$ ◆ $4.18l$ ● $3.82l$	4.75 5.02 5.5	4482.9 5300.23 6944.38	264.8 313.1 410.2
Rhombicub-octahedron ² 	8▲ +18■	$8.71404l^3$	$21.46410l^2$	$2.4405l$	8.6	5551.9	327.95
Rhombic dodecahedron ³ 	12◆	$3.07920l^3$	$11.31371l^2$	$1.6323l$	12.865	6556.86	387.3

Table 2⁸⁷ Selection of common polyhedrons associated to metallic particles and their specific properties when the insphere diameter is $\Phi=21\text{\AA}$. l is the polyhedron edge;

D (nm)	In-sphere			DT wt%	Midsphere			DT wt%
	<i>l</i>	$S_{Np}(nm^2)$	$V_{Np}(nm^3)$		<i>l</i>	$S_{Np}(nm^2)$	$V_{Np}(nm^3)$	
1	0.45	4.16	0.69	32.77	0.38	3.01	0.43	36.42
1.6	0.72	10.66	2.84	23.35	0.61	7.71	1.75	26.37
1.8	0.81	13.49	4.05	21.31	0.69	9.76	2.49	24.14
2	0.90	16.65	5.55	19.59	0.76	12.05	3.42	22.27
2.1	0.94	18.36	6.43	18.84	0.80	13.28	3.95	21.43
2.2	0.99	20.15	7.39	18.14	0.84	14.58	4.55	20.66
2.3	1.03	22.02	8.44	17.48	0.88	15.93	5.20	19.94
2.4	1.08	23.98	9.59	16.88	0.92	17.35	5.90	19.27
2.5	1.12	26.02	10.84	16.31	0.95	18.83	6.67	18.64
3	1.35	37.46	18.73	13.97	1.15	27.11	11.53	16.04
4	1.80	66.60	44.40	10.86	1.53	48.19	27.33	12.53
5	2.25	104.07	86.72	8.88	1.91	75.30	53.38	10.28
6	2.69	149.86	149.86	7.51	2.29	108.44	92.24	8.72
7	3.14	203.97	237.97	6.51	2.67	147.60	146.48	7.57
8	3.59	266.41	355.22	5.74	3.06	192.78	218.65	6.68
9	4.04	337.18	505.77	5.14	3.44	243.99	311.32	5.98
10	4.49	416.27	693.79	4.65	3.82	301.22	427.05	5.42

Table 3 Specific properties (*V*, *S*, *l*) of dodechaderon calculated for insphere ($r_{mi} \approx l \cdot 1.113516364$) and midsphere ($r_m \approx l \cdot 1.309016994$) and weight percent of the grafted dodecanethiol

II.3 Results and discussion - Characterization

II.3.1 Characterization of gold nanoparticles

DT-AuNPs are reasonable stable in solid phase and can be easily re-dissolved in apolar solvents (e.g. toluene, CH₂Cl₂, ...), providing the possibility to characterize them in solvent (UV/Vis), in solid phase (TGA) or crystallize or precipitate them from solvent for characterisation (Transmission Electron Microscopy (TEM)). The size, monodispersity and self-assembly - if it existed - of DT-AuNPs were determined using (TEM) as the primary technique and TGA - this was used to determine the weight ratio of organic part of the hybrids (II.3.3)- and UV/Vis spectroscopy as complementary techniques (Figure 17). The resolution of TEM is significantly higher than light microscopy, allows observing objects of a few angstroms. The contrast depends on the electron density of the material, which allows us to observe the gold core, due to its high density. However to characterize nanoparticles with diameter smaller than 2 nm is fairly difficult, as below this range the metal core cannot be easily distinguished from the background, which is, in our case, carbon coated copper grids. After taking images of the samples the next task is to count them. To have a representative value of the size dispersion, it is ideal to count more than one thousand particles. We have used the program, ImageJ, to create a binary image (threshold) to count and determine the size of the particles. This provides a much more accurate method than counting "by eye and by hand" but still does not exclude errors completely⁹⁹. High magnification is required and it is ideal to measure ~ 2 nm particles at scale of 23-13 pixels/nm and for 5-8 nm at 15-8 pixels/nm but in this case the calculation has to be carried out on several pictures and counting more thousand particles. This also decreases the accuracy of the overall measurement as for all individual images the setting has to be adjusted separately. The preparation of the sample affects the self-assembly and can be carried out using different techniques. "Drop casting" is when a highly diluted dispersion of the nanoparticle in toluene dropped on the grid allowing the nanoparticles to move freely. As the solvent evaporates slowly (toluene is ideal as it is not volatile and in this way slow evaporation can be assured) capillary forces draw the nanoparticles together helping the self-assembly on the surface of the grid. The other technique is to drop a diluted dispersion of the nanoparticles in toluene on the surface of water. The solvent evaporation causes their 2D self-assembly on the water surface but due to more free movements, the expansion of the assembly size can be increased; the layer is removed by dipping the grid on the surface (Figure 20).

Characterization

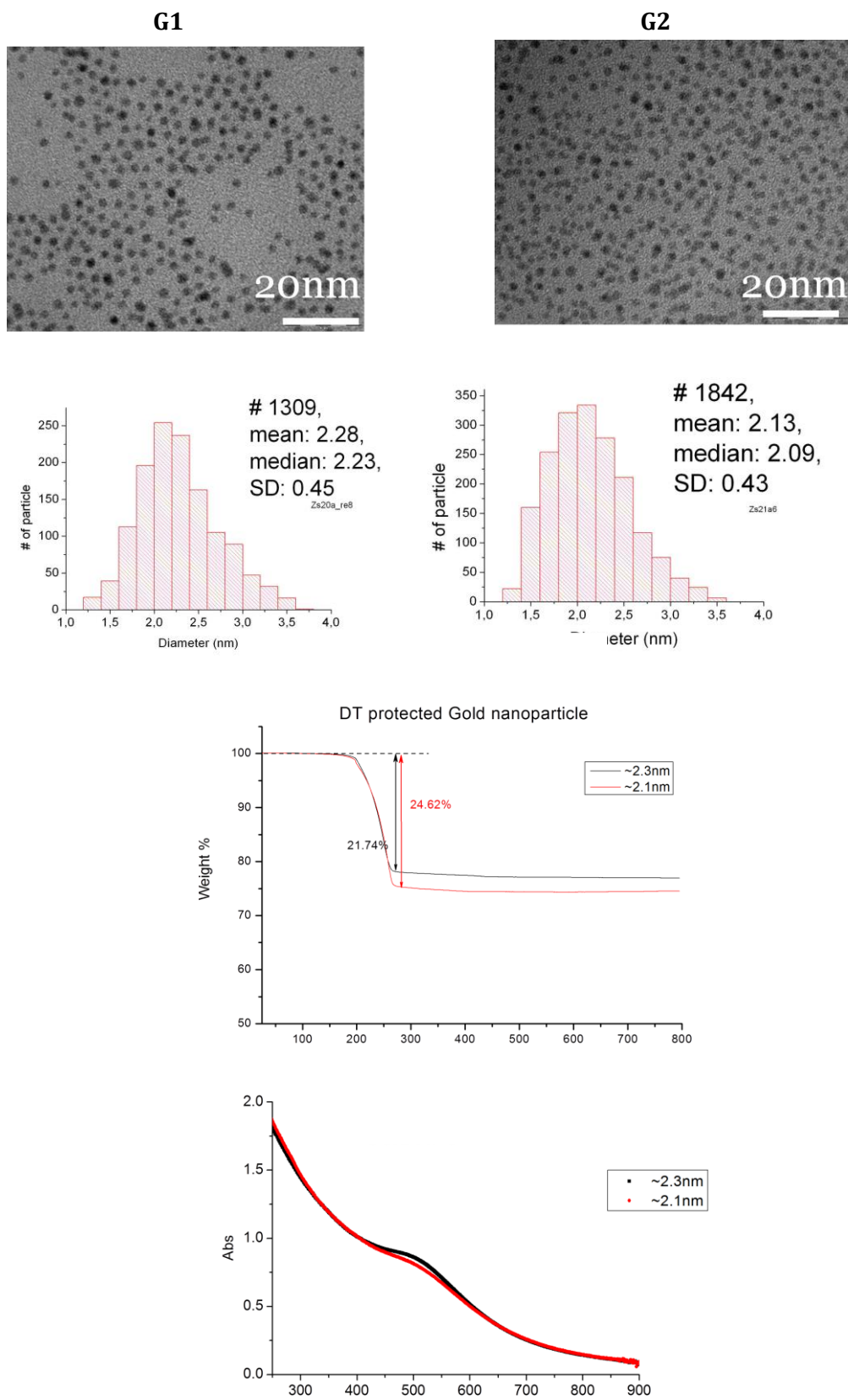


Figure 17 Characterization of DT-AuNPs (G1 and G2) by TEM image, NPs size was determined using ImageJ program (top), TGA (middle) and UV/Vis spectroscopy (bottom)

The TGA experiments indicate that 1-dodecanethiol is more readily decomposed when it is grafted to the gold. Decomposition temperature of the 1-dodecanthiol is at 350°C but when it is grafted to the gold the decomposition temperature decrease down to ~270°C. Smaller core size has higher surface ratio which result in higher weight % of organic part. Small (~0.2 nm) size differentiation is already attainable by TGA measurements (Figure 17).

Optical properties of the nanoparticles including the intensity and energy of its surface plasmon bands are strongly correlated to the NP size^{100,101}. Incident electromagnetic field induces coherent oscillation of the surface conduction electrons¹⁰², the so called surface plasmon resonance (SPR). When the spherical particle size is much smaller than the wavelength of the incident electromagnetic field the oscillating electric field induces coherent oscillation of the surface conduction electrons locally around the nanoparticle with a frequency known as the LSPR¹⁰³ (localized surface plasmon resonance) (Figure 18). The frequency of SPR and LSPR depends on the dielectric constant of the medium¹⁰⁴, ϵ_m , resulting in changes in the colour of colloidal gold with the dielectric constant of the solvent or surrounding medium^{105,101}. LSPR spectra can easily be tuned from the near-UV through the visible spectrum¹⁰⁶ and even into the mid-IR by changing the size or shape of the nanoparticles.

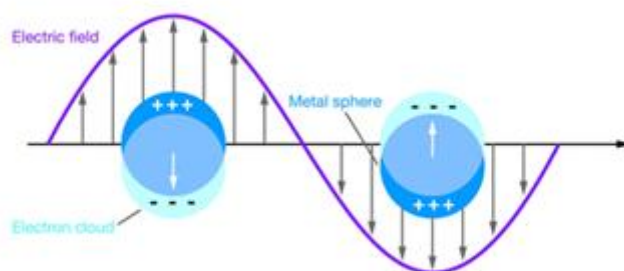


Figure 18 Schematic illustration of localized surface plasmon band (taken from Willets¹⁰⁷)

UV/Vis spectroscopy allows us to estimate the size of the nanoparticle¹⁰⁸ above 2 nm (below this size, resonances are not visible) as there is a clear relationship between extinction coefficient (ϵ^*) and mean particle size⁹⁶. Increasing the particle size results in redshift of the maxima of the absorption spectra and changes in the plasmon band shape. At sizes ~2 nm almost no plasmon resonance is observed, at size ~3 nm a weak plasmon band arises and the maxima can be distinguished and at 6 nm a strong absorption band is observed (Figure 19). The very small change in the plasmon band of G1 and G2 indicates the small difference in size (Figure 17), which is agreement with the TEM observations.

Characterization

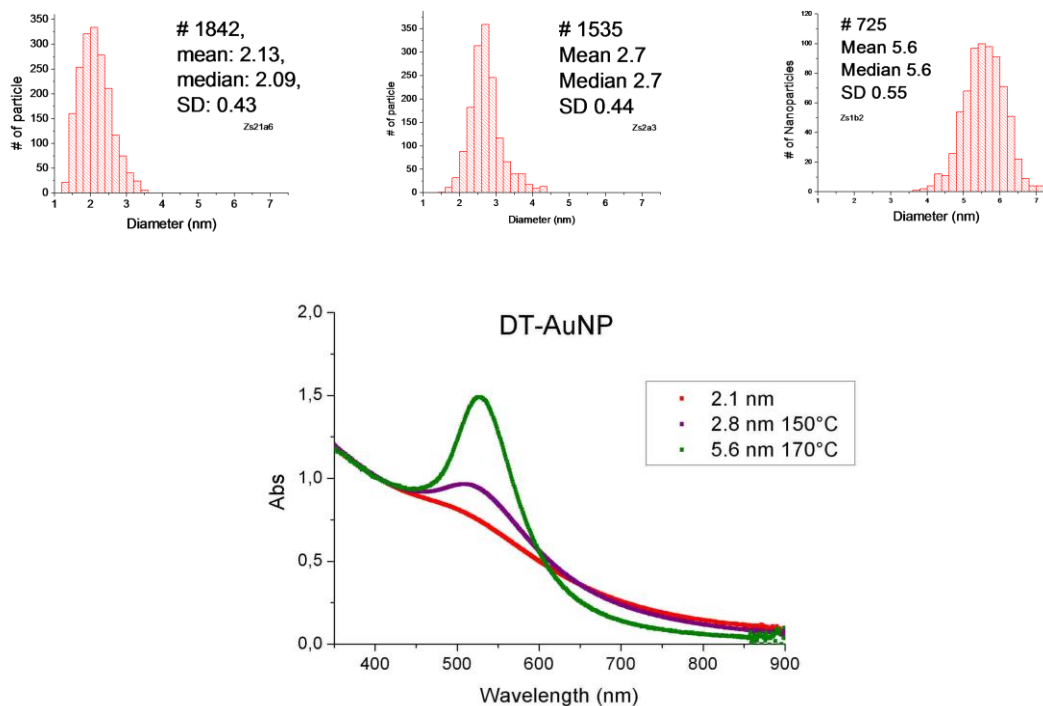


Figure 19 Size distribution and plasmon band of DT-AuNPs at different size

As in most cases we worked with size ~ 2 nm, UV/Vis spectra were used as a complementary technique to confirm the small size by the absence of intense absorption in addition to TEM which is the most accurate technique.

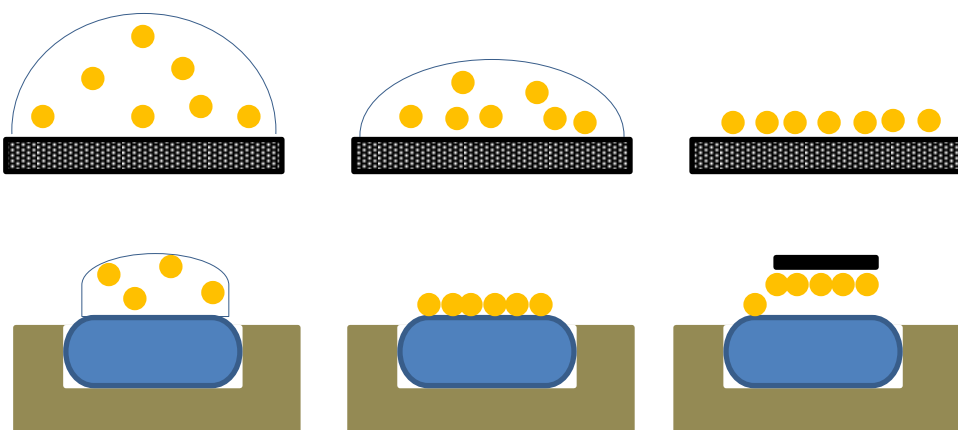


Figure 20 Sample preparation for TEM: (top) “drop casting” (bottom) self-assembly on “water/apolar solvent surface

II.3.2 Characterization of Thiols

The most convenient way to track if the reaction was successful is NMR spectroscopy. In case of thiolation of the bromide functional groups, the triplet of the methylene protons next to the bromide at 3.44ppm has disappeared and a doublet of triplet has appeared at 2.53ppm which correspond to the 2H of the methylene next to the thiol group. The triplet of the thiol proton has also appeared at 0.89ppm (representative $^1\text{H-NMR}$ spectrum is shown at Figure 21).

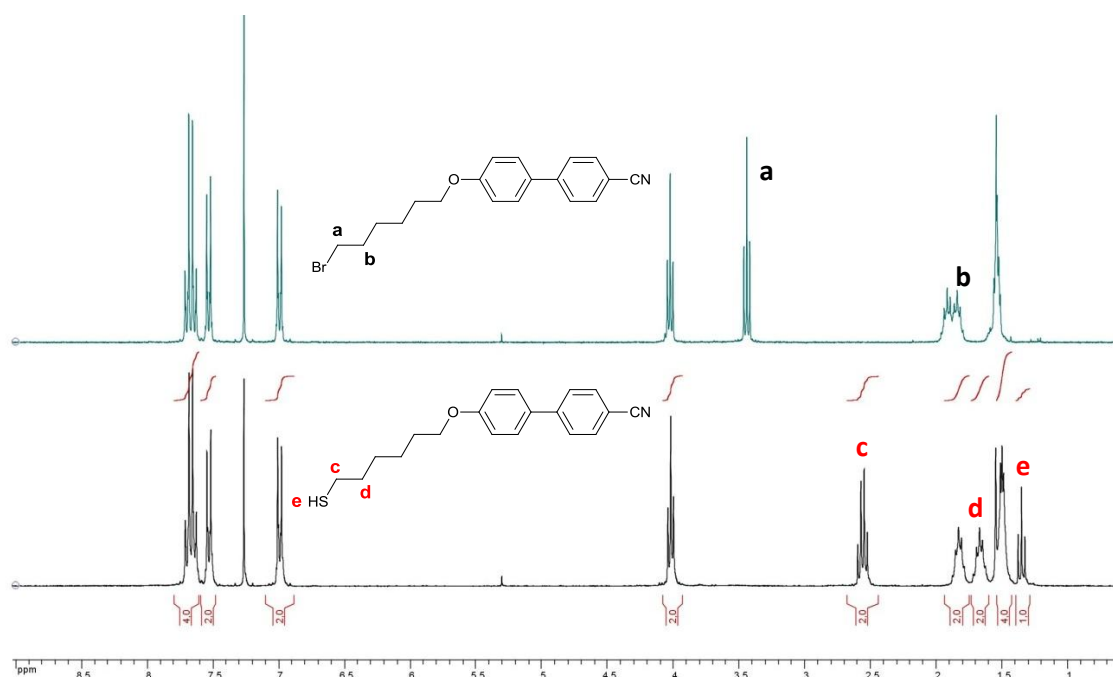


Figure 21 $^1\text{H-NMR}$ spectra of **2** and **L6**

In some cases, during thiolation not only the thiol but the disulphide by-product is formed. In this case a triplet of the methylene groups, next to the disulphide bond, is seen at 2.68ppm on the $^1\text{H-NMR}$ spectra (representative spectra: Figure 22) as well as the corresponding carbon of these methylene groups at 39.22ppm at the $^{13}\text{C-NMR}$ the (representative spectra: Figure 23).

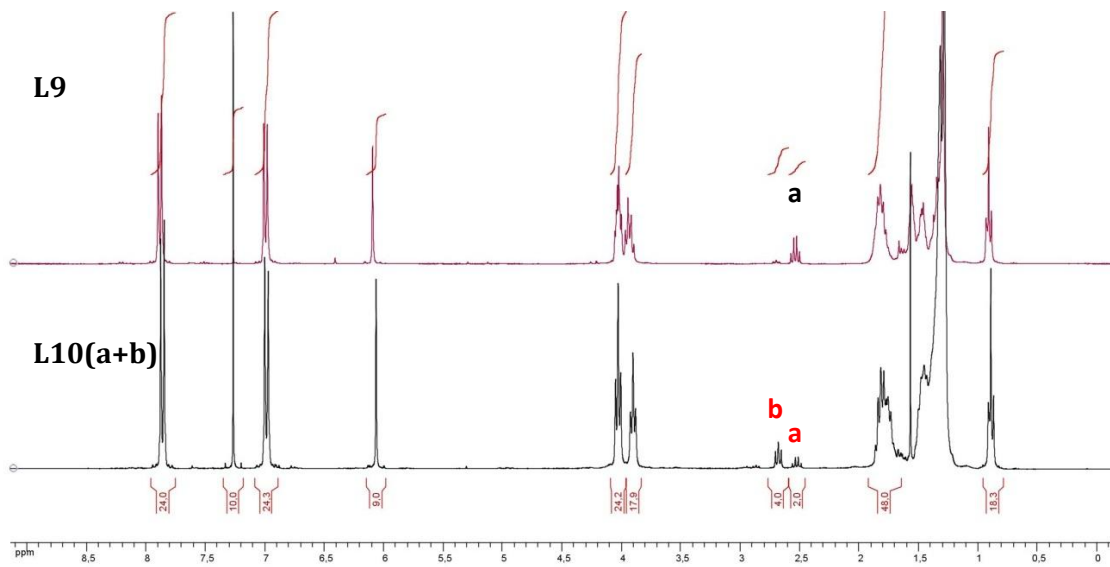


Figure 22 $^1\text{H-NMR}$ spectra of **L9** and **L10(a+b)**

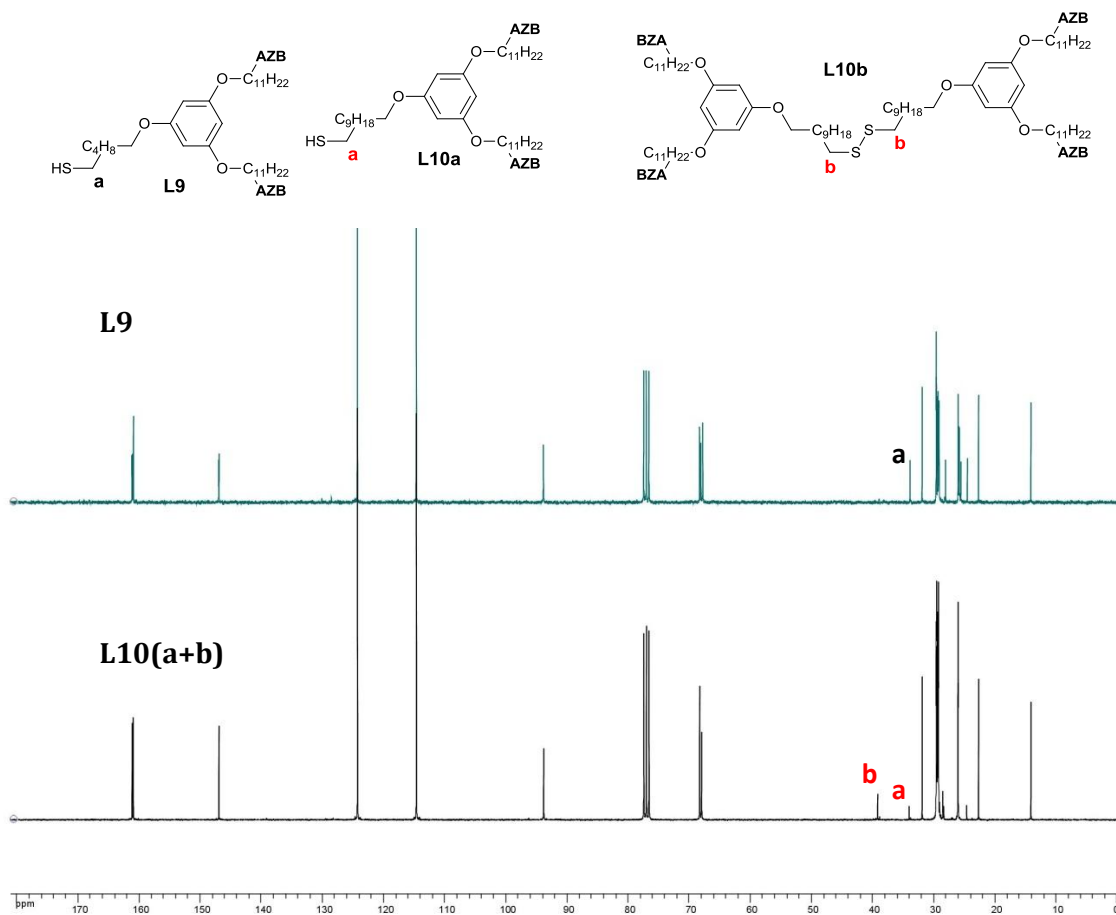


Figure 23 $^{13}\text{C-NMR}$ spectra of **L9** and **L10(a+b)**

Thermal behaviour

The thermal behaviour of the ligands was investigated by TGA, DSC, POM and SAXS measurements, but the complete characterization is still in progress. The onset of thermal decomposition (defined at the weight loss greater than 5%) of most of the ligands starts at $\sim 300^\circ\text{C}$ (**L5**, **L10**, **L11** at 300°C ; **L7**, **L9** at 270°C ; **L8** at 330°C) except **L4** which starts at a lower temperature of around 230°C (Figure 24).

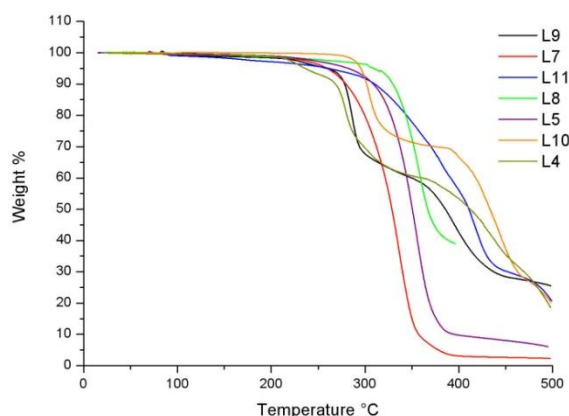


Figure 24 Thermal decomposition curves of ligands bearing thiol function. TGA was carried out under inert atmosphere at $10^\circ\text{C}/\text{min}$ rate

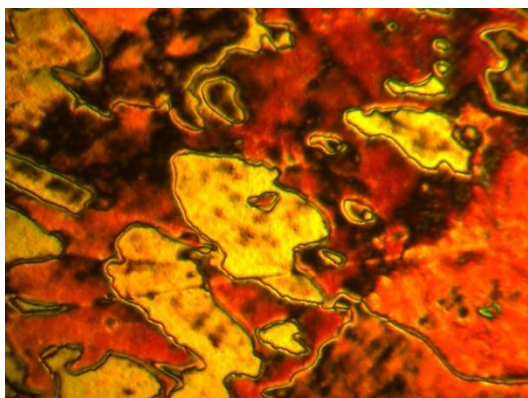
Most of the thiolated ligands exhibit mesomorphic behaviour (nematic or smectic), but **L9**, which has no mesophase; **L5** and **L8** have only monotropic phase but the nematic phase of the **L8** remains stable during the subsequent heating. Most of the OCB containing ligands has nematic phase and the AZB ligands have smectic, but to identify the exact type of the phases needs further analysis which is in progress. The thermal transition temperatures are collected in Table 5 and two representative POM texture are shown in Figure 25.

Table 4 Phase transition temperatures (°C) and corresponding enthalpy ΔH (J.g⁻¹) or specific heat variation ΔC_p (J.g⁻¹.°C⁻¹)^{a,b}

L7 (HS ₆ OCB)	
<i>h1</i> Cr	53.55 (74.3) N 65.05 (2.1) I
<i>c1</i> I	66.2 (-4.1) N 7.7 (-30.2) Cr
<i>h2</i> Cr	45.3 (80.4) N 66.5 (2.2) I
L5 (HS ₁₁ OCB - ligand of H4))	
<i>h1</i> Cr	69.1 (103.9) I
<i>c1</i> I	68.1 (-6.9) M 56.5 (-105.5) Cr
L4 (HS ₁₁ AZB (ligand of H1))	
<i>h1</i> Cr	77.5 (16.7) Cr' 98.1 (101.0) M 103.0 (22.9) I
<i>c1</i> I	103.3 (-27.0) M 91.5 (-101.2) Cr
L9 (HS ₆ PG ₆ AZB ₂ (ligand of H8))	
<i>h1</i> Cr	85.6 (83.4) I
<i>c1</i> I	83.2 (-10.1) Cr 57.9 (-15.2) Cr
L8 (HS ₆ PG ₆ OCB ₂ (ligand of H6))	
<i>h1</i> Cr	63.8 (61.7) I
<i>c1</i> I	28.6 (-0.4) N -3.5 (0.6) G
<i>h2</i> G	-4.5 (-0.5) N 25.7 (0.2) I
L10 (HS ₁₁ PG ₁₁ AZB ₂ + (S ₁₁ PG ₁₁ AZB ₂) ₂)	
<i>h1</i> Cr	71.2 (33.3) Cr' 78.7 (10.8) M1 89.3 (16.0) I
<i>c1</i> I	93.0 (16.5) M1 78.0 (-2.1) M2 61.5 (-35.8) ^c Cr''' 58.1 (-) Cr' 49.1 (-) Cr
<i>h2</i> Cr	73.2 (35.8) ^c Cr' M1 (-) Cr'' 89.5 (16.0) I
L11 (HS ₁₁ BA ₆ OCB ₄ (ligand of H7))	
<i>h1</i> G + Cr	48.0 (-) Cr 74.0 (46.5) M 99.7 (0.3) N 116.4 (0.1) I
<i>c1</i> I	60.8 (-1.6) N 19.7 (0.6) G
<i>h2</i> G	24.1 (0.5) N 59.3 (3.4) M' 72.0 (-24.9) Cr 89.4 (1.9) Cr' 98.0 (22.6) N 115.1 (0.2) I

^aOnset temperature (DSC), Cr: crystalline phase, M: mesophases, N: nematic phase, I: isotropic liquid;
^bFirst heating (*h1*), first cooling (*c1*), second heating (*h2*); ^cCumulated enthalpy

L7 (48°C)



L11 (57°C)

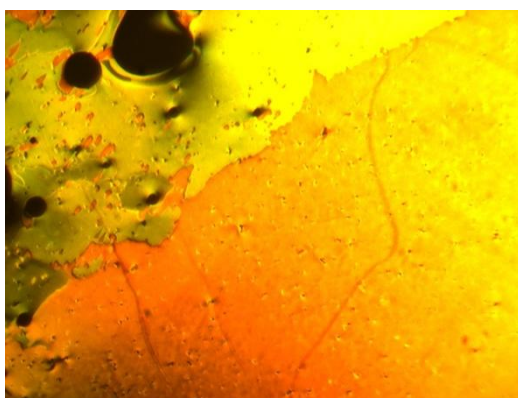


Figure 25 Representative POM texture of **L7** and **L11**

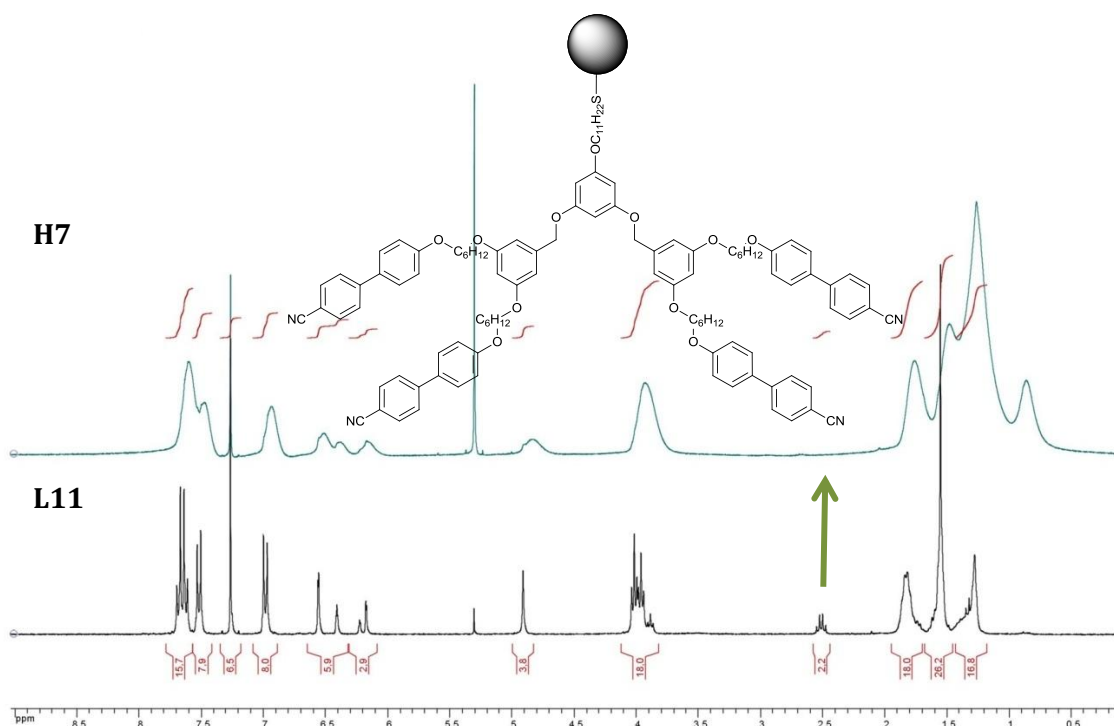


Figure 27 $^1\text{H-NMR}$ spectra of H7 and the ligand L11

The dendronized gold-hybrids were also characterized by UV-Vis spectroscopy. The spectra of the hybrids closely resemble of the sum of the absorption spectra of the building blocks (DT-AuNP and ligands) (Figure 28). The minimal change of the surface plasmon band also confirms, with TEM measurements, little or no change in the average particle size.

The proportion of the grafted ligands to the gold surface area was estimated by evaluation of TGA results (Figure 29 and Figure 30) and $^1\text{H-NMR}$ spectra. The calculated results by the two techniques corroborate each other. But this can be only an estimation as the broadened peak of the $^1\text{H-NMR}$ spectra cannot allow precise calculation, or the TGA as the degradation temperature of the dodecanethiol and the ligands overlap. The complete thermal decomposition temperature of the dodecanethiol occurs at $\sim 270^\circ\text{C}$ (see II.2.1) and its weight percentage was taken at this temperature. In most cases the complete decomposition of the organic part was complete at 550°C or 600°C . The TGA data indicates that the remaining weight of the sample correspond to the weight of the gold. The thermal decomposition of the organic part appears to occur in more than one stage: the first stage is the result of the more rapid degradation rate of the DT and the further stage is the decomposition of the ligands, which takes

place in several stages as well (see II.2.2). Figure 29 and Figure 30 displays TGA curves of the hybrids and the corresponding DT-AuNP.

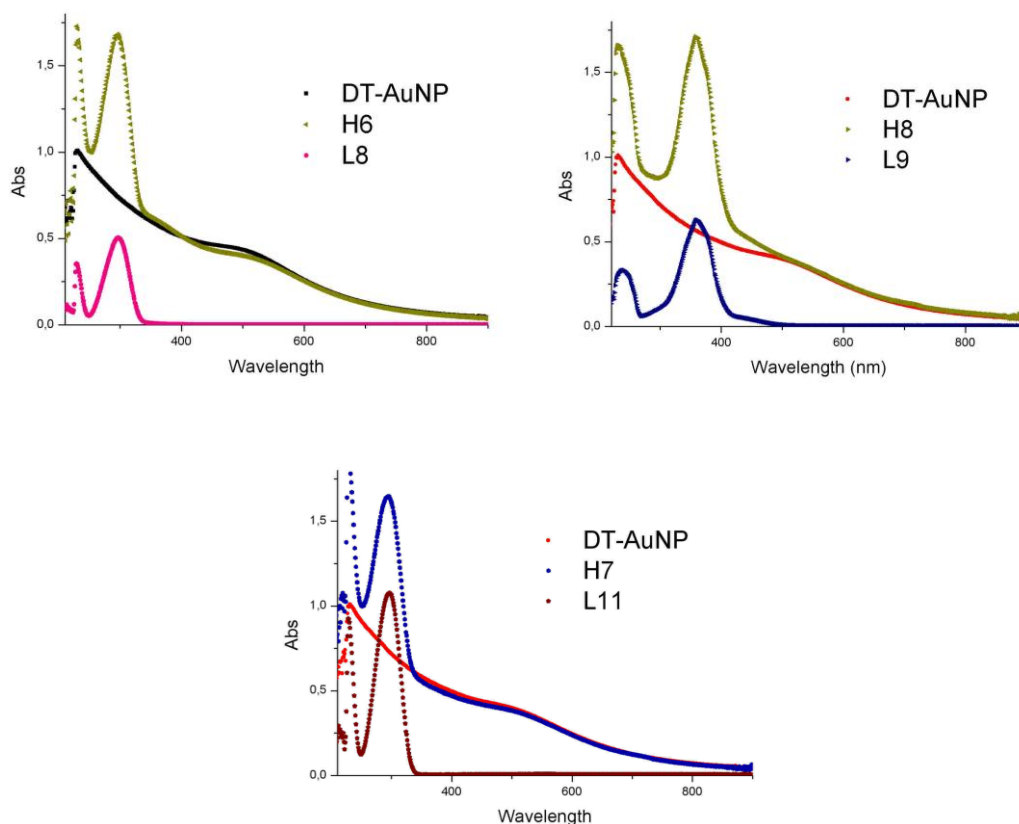
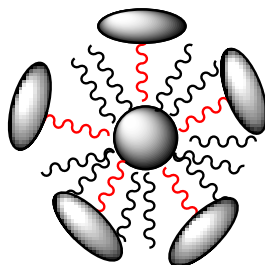
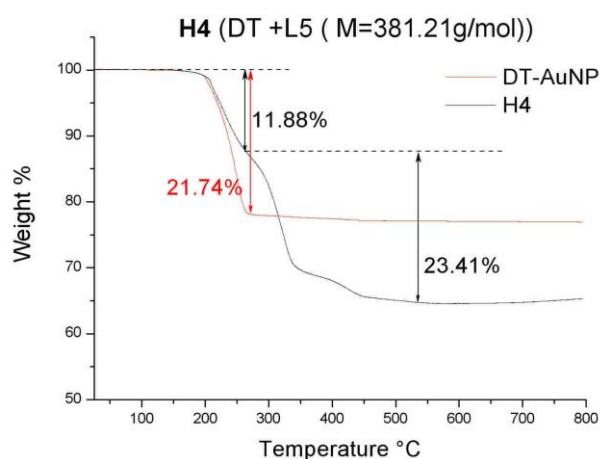


Figure 28 UV/Vis spectra of Hybrid (H6, H7 and H8) and their building blocks. The solvent is CH_2Cl_2 and the ligands concentration 10^{-8} mol/ml, the spectra of the hybrids were normalized at 264 or 252nm and the DT-AuNP at 405nm

Despite that, in all cases, when a large ($\sim 4x$) excess of replacement ligands were introduced, shows no more than 50% of replacement and increasing the size of the ligands this ratio further decreased. This is due to the enlarged size of the ligand, which has strong steric hindrance:

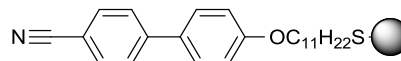


Characterization

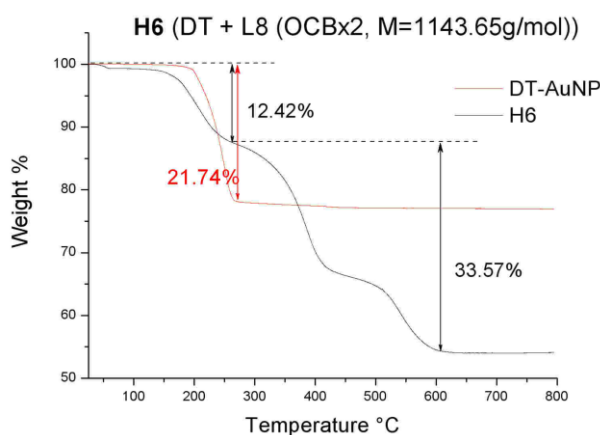


H4

$$\#DT/\#L5 = 0.96$$

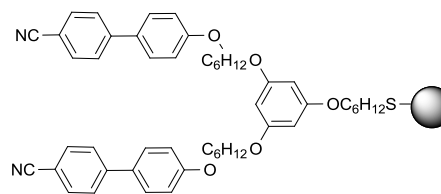


$$\phi = 2.3 \text{ nm}$$

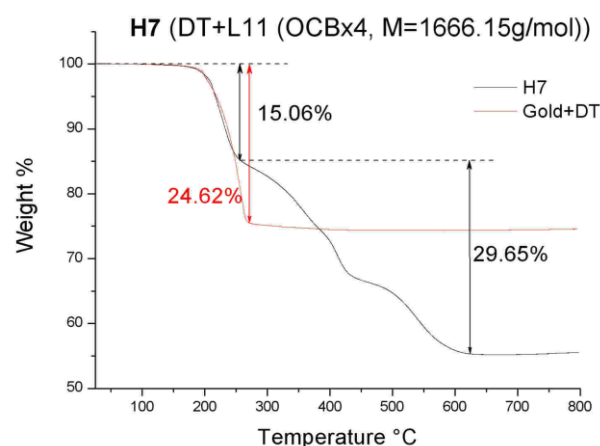


H6

$$\#DT/\#L8 = 1.46$$

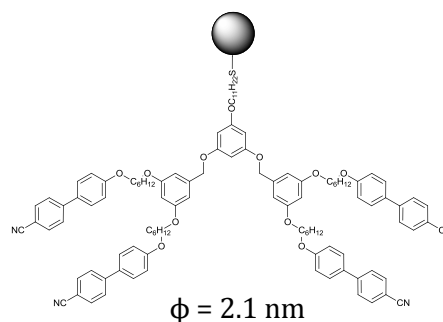


$$\phi = 2.3 \text{ nm}$$



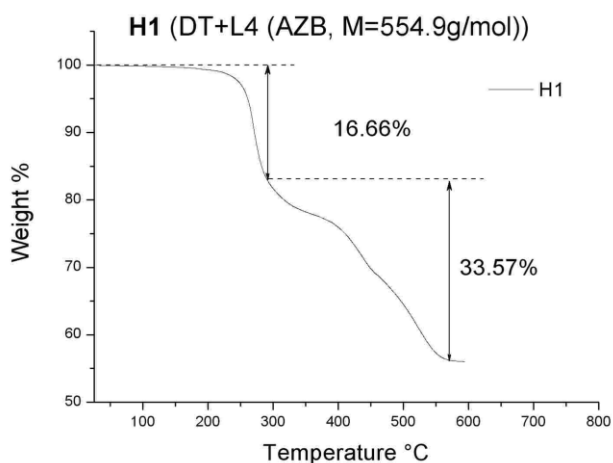
H7

$$\#DT/\#L11 = 4.2$$



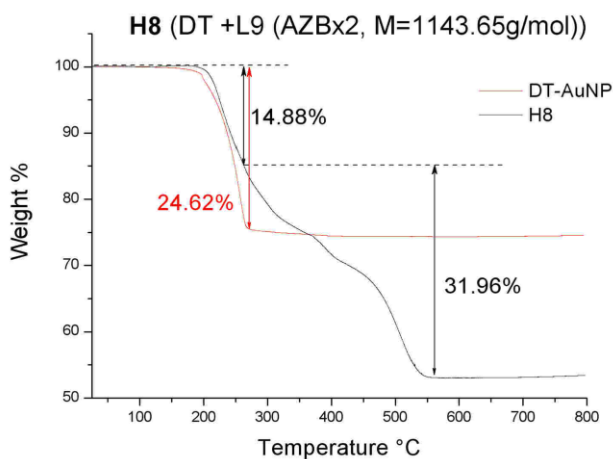
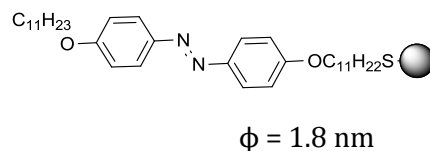
$$\phi = 2.1 \text{ nm}$$

Figure 29 TGA of Hybrids (grafted OCB derivatives) and the corresponding DT-AuNP; mol ratio of grafted Ligands compared to DT. TGA was carried out under inert atmosphere at 10°C/min rate



H1

$$\#DT/\#L4 = 1.37$$



H8

$$\#DT/\#L9 = 2.64$$

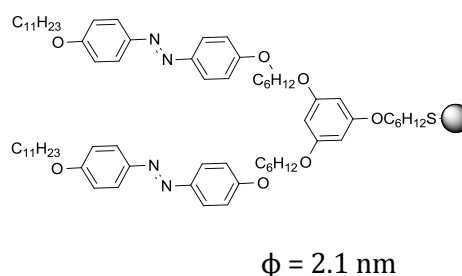


Figure 30 TGA of Hybrids (grafted AZB derivatives) and corresponding DT-AuNP; ratio of grafted Ligands compared to DT. TGA was carried out under inert atmosphere at 10°C/min rate

The number of gold atoms and thiols in the hybrids were calculated (Table 5) using the TGA data (for the calculation of the ratio of the building blocks), the TEM measurements (to determine the diameter of the particle) and the volume of the nanoparticle which was calculated by taking the average volume of the polyhedrons listed in Table 2 (but calculated using the midsphere dimensions). These calculations allow us to determine the number of the mesogenic ligands in the cross section area. The results of these calculations indicate a very compact arrangement of the thiols on the surface of the particle if we compare to the theoretical value (0.214 nm²). This difference comes from the fact that the theoretical value was calculated on flat surface and does not consider that the thiol can occupy the edges and vertexes of the polyhedron.

	H4 (L5)	H6 (L8)	H7 (L11)	H1 (L4)	H8 (L9)
N_{DT}	71.1	89.0	80.3	62.1	82.5
N_L	74.0	60.8	19.1	45.4	31.2
N_{Au}	395.8	395.8	301.3	189.7	301.3
$S \text{ (nm}^2\text{)}$	18.6	18.6	15.52	11.4	15.52
$V \text{ (nm}^3\text{)}$	6.73	6.73	5.12	3.23	5.12

Table 5 Number of building block construct the hybrids The values were calculated from the TGA data and taking the average volume of the polyhedra (Table 2) calculated at the midsphere;

Also we have to consider that the standard deviation of the size of the particles is about ~ 0.4 nm which gives a great error in the surface-volume ratio of small particles (Figure 31) in the range from 1 to 3 nm diameter the ratio of the surface and core is exponentially decrease in a few angstrom change.

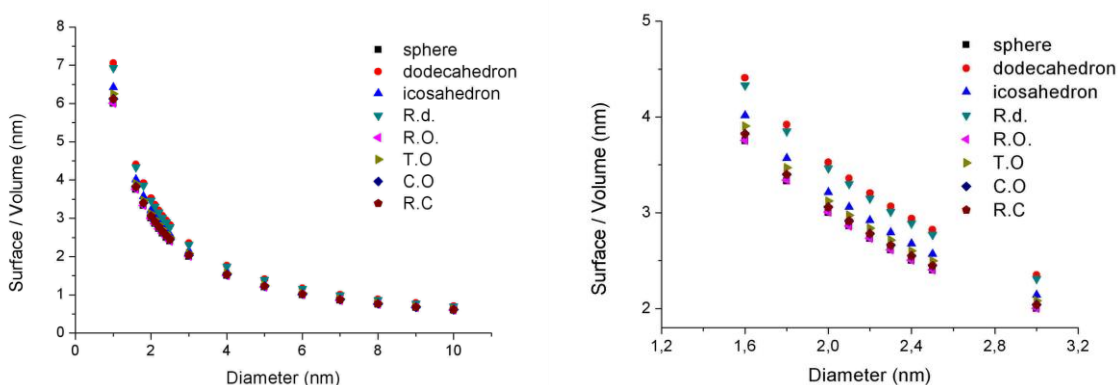


Figure 31 Ratio of the surface-volume in the function of particle size (diameter) of different polyhedrons

II.3.4 *Self-Assembly of dendronized gold nanohybrids*

In this section we will present the different characterizations that were carried out on the dendronized gold nanohybrids by different techniques such as TEM, POM, DSC. SAXS and small-angle neutron scattering (SANS) measurements have also been carried out but at this stage the analysis of the results are still in progress. Using these preliminary results and comparing them with the building blocks (DT-AuNPs and ligands), we will briefly attempt to indicate self-organization and give preliminary interpretation of the mesomorphic behaviour. Unequivocal determination of the mesomorphism of the dendronized gold nanohybrids is complicated and requires many different techniques. As it was already mentioned, it is crucial to purify the hybrids to ascertain that the measured properties are not coming from the free mesogenic ligands. The purity of the dendronized gold hybrids has been shown in the previous section and therefore it can be stated that all the mesomorphic behaviours, if existing, come solely from the hybrids'.

Firstly, TEM observations were made on the samples which were prepared by evaporating slowly a drop of diluted dispersion of the samples on a carbon coated copper grid (dispersions were made using THF or toluene, depending on the solubility), or on water and then dipping the grid on the surface (II.3.1). This was followed by POM and DSC investigations and finally by SAXS and SANS measurements. The three small DT-AuNPs (**G1** (2.3 nm), **G2** (2.1 nm), **G3** (1.8nm)) which were used as building blocks in the solvent mediated exchange reactions are monodisperse and the core size of the AuNP after the reaction remained the same (II.3.1, II.3.3).

In the case of the cyanobiphenyl containing ligands, when the zero and first generation thiolated dendrons (**L5** and **L8**) were attached to **G1** to build up the two hybrids, **H4** and **H6**, respectively, it improved the organization on the surface according to the TEM observations, showing larger domains and more continuous coverage, when compared to DT-AuNP (**G1**) (Figure 32). In parallel, using similar TEM areas for the different systems (**G1**, **H4**, **H6**) the density is quasi-doubled (~2 times more AuNPs are calculated after averaging several countings). Moreover, as the generations number of the dendrons is increased (H4 → H6) a slight improvement of the ordering may also be observed. The DSC traces indicate complicated thermal behaviours with several thermal events occurring at different temperatures than the phase transitions of the relevant free ligands (Figure 32) e.g. melting temperature of **L5** is not traceable in the DSC curve of the corresponding hybrids (**H4**). However when hybrids were observed under POM no obvious texture characteristic of LC has been seen. Further

investigations are necessary to prove the presence of the mesophase (see later), as these two techniques are clearly not determining.

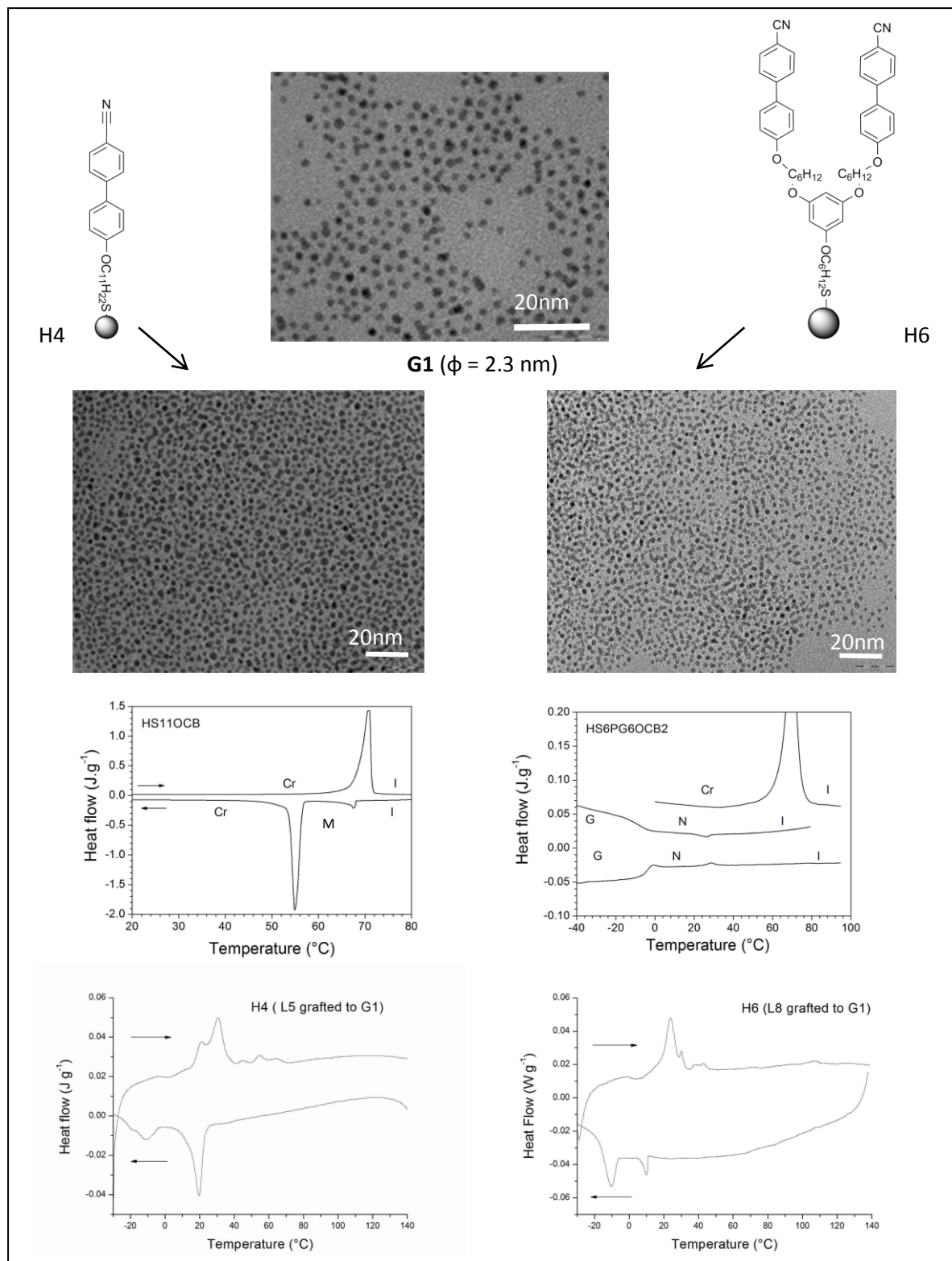


Figure 32 TEM image (sample is deposited on the grid by “drop casting”, dispersed in THF) of G1, H4 and H6 (top), DSC trace of the ligands - middle (L5 - left; L8 - right), DSC trace of the hybrids - bottom (H4 - left, H6 - right)

In the case of **H7** (where the second generation BA based thiolated ligand, **L11** was attached to **G2**), distinct 2D organization occurs and extends over much larger domains, when compared to the lower generations; over $2 \mu\text{m}^2$ is covered continuously by the dendronized gold particles similar to a “carpet” (monolayer of the hybrid overlap even on the holes of the grid) (Figure 33). The hybrid cores are positioned from each other at similar distances and surrounded by the thick organic layer where the ligands of the particular hybrids entangle and provide a strong enough holding force which enables them to cover the holes on the grid (Figure 33). All over the areas, short strings of the hybrids are formed and can be seen. In this case, no phase transitions were indicated on DSC traces which is very different from the corresponding ligand (Figure 33). POM observations did not indicate obvious mesophase in this case neither, however during heating under the microscope a viscosity change could be observed but without any typical texture.

Characterization

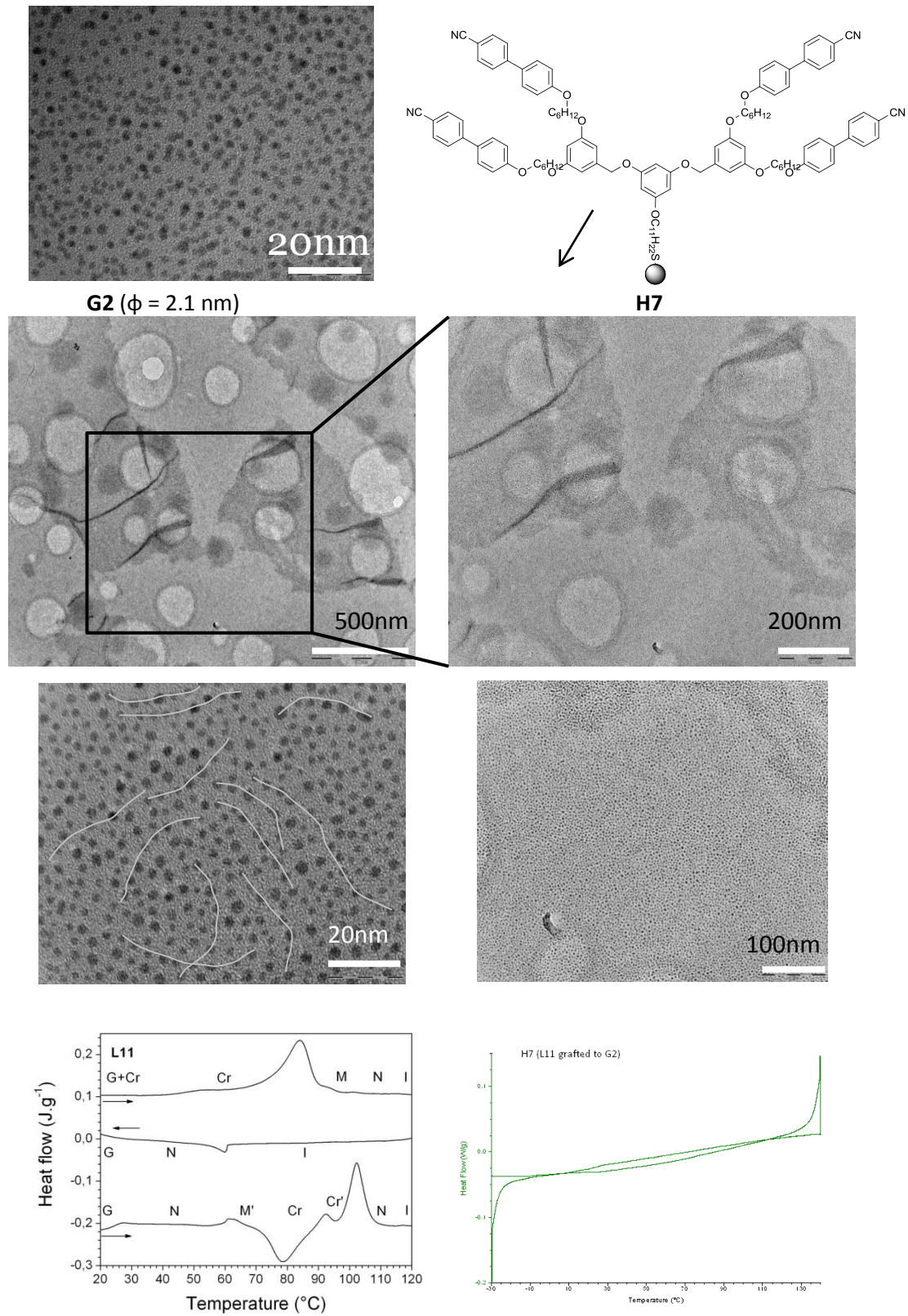


Figure 33 TEM image (sample is deposited on the grid by dipping the grid on the surface of the water) of G2, (top, left) and H7 (middle and bottom, at 500, 200, 100 and 20 nm scale); dark grey areas: multilayer of the hybrid, circles: edge of the holes on the grid; bottom: DSC trace of L11 (left) and H7 (right)

In the case of the AZB containing hybrids, when **H1** and **H8** (the zero and first generation thiolated dendrons, **L4** and **L9** were attached to **G3** and **G2**, respectively), compared to the relevant DT-AuNPs (**G3** and **G2**) no significant improvement in the self-organization was observed in the case of **H1**, but the increase of the generation number results with a more dense and homogenous coverage of the surface under TEM observation (Figure 34). Beside the improved self-organization, **H8** does exhibit texture under POM observation but of an unknown nature, and these observations were not clearly confirmed by DSC analysis as only uncharacteristic DSC traces were recorded, which is different from its ligand (**L9**) (Figure 35).

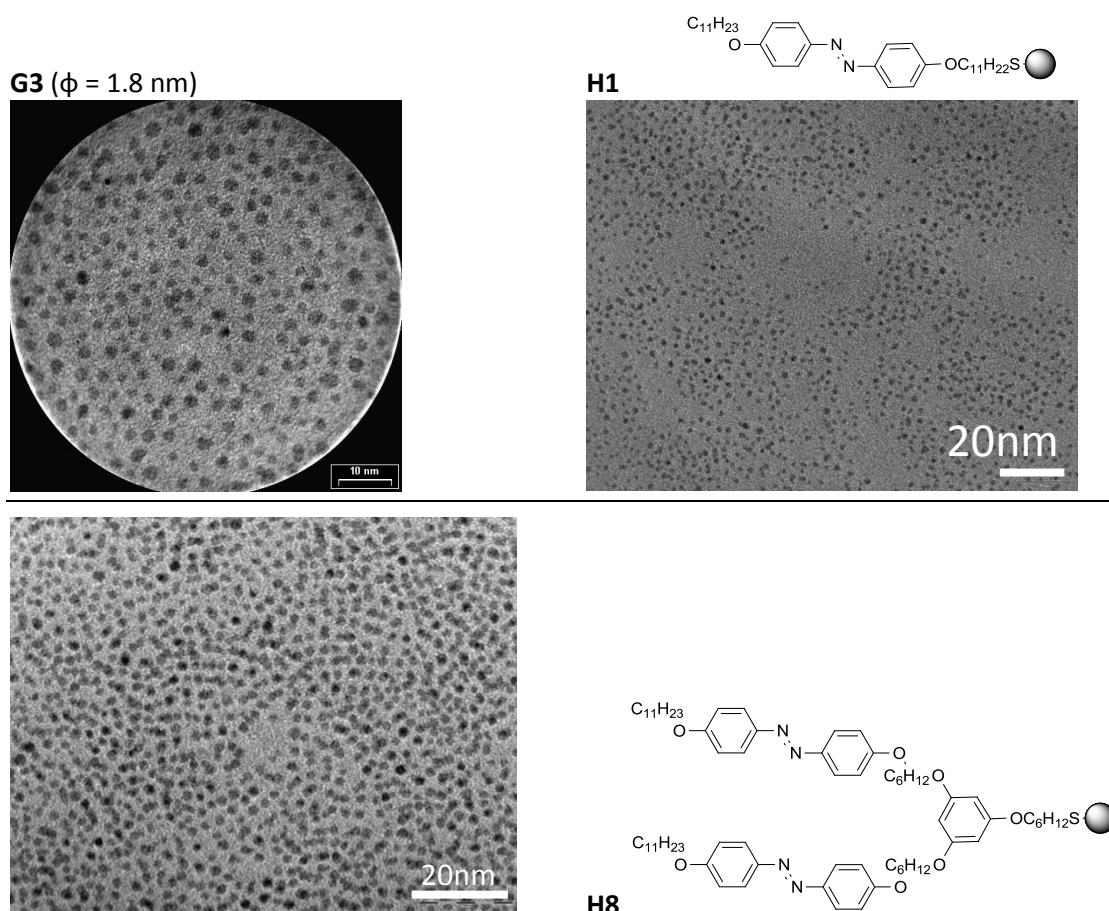


Figure 34 TEM image (sample is deposited on the grid by “drop casting”, dispersed in toluene) of G3 and H1 (top), H8 (bottom);

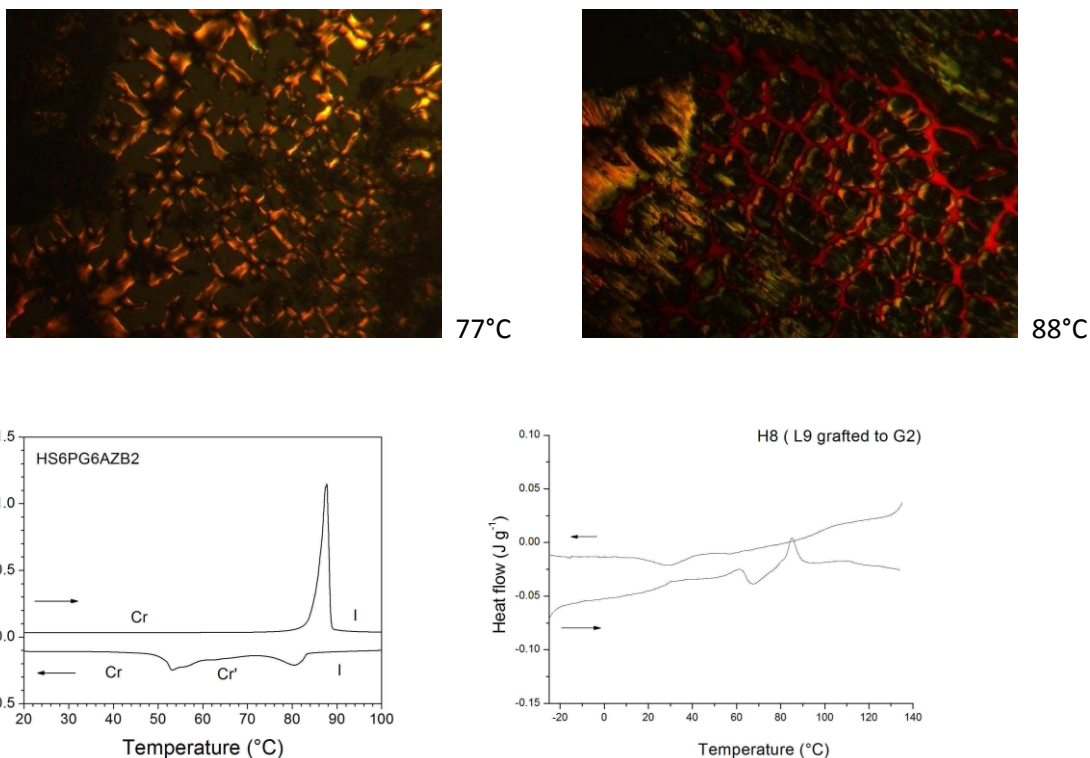


Figure 35 POM micrograph of H8 at 77 and 88°C, DSC trace of the ligands (L9) – bottom left, and of the hybrid (H8) – bottom right

The SAXS and SANS characterizations of the mesomorphic behaviour of the hybrids are under progress and therefore will not be discussed here in details. The SAXS pattern of the **H1** and the grafted ligand (**L4**) are presented on Figure 36. Both sets of patterns are different, suggesting changes of the supramolecular organization. In the pattern of the hybrid two diffuse scattering are observed around 5.4 and 2.7 nm, clearly distinct from the reflections coming from the lamellar periodicities of the crystal and the smectic phase of the ligand. This indicates that the observed phase is intrinsic to the hybrid. Due to their different shapes, we assume that the signal at 5.4 nm corresponds to some embryo of layering and that at 2.7 nm is likely the mean lateral distance between the hybrids. The diffracting signals are nevertheless broad, suggesting that the ordering is rather short-range and not extended to too large distances. Thus, two arrangements are possible and consisting of the alternation of layers of NPs, aliphatic spacers with tails, and mesogens; and the other of alternation of layers of NPs, aliphatic spacers, mesogens, which are strongly tilted, and aliphatic tails, as shown in the figure below (Figure 36). This organization is likely imposed by the cylindrical conformation adopted by the hybrid, with a segregation of the mesogens at the poles of the NPs and the DT chains around the equator. These possibilities, which cannot be discriminated, were suggested by considering the surface area of the hybrid, obtained by $S_H = V_H/d$ (where V_H is the theoretical volume of the hybrid). S_H

was calculated to be close to 1000\AA^2 in case of **H1**, which divided by half of the mesogen numbers giving the mesogenic cross section $\sim 57\text{\AA}$.

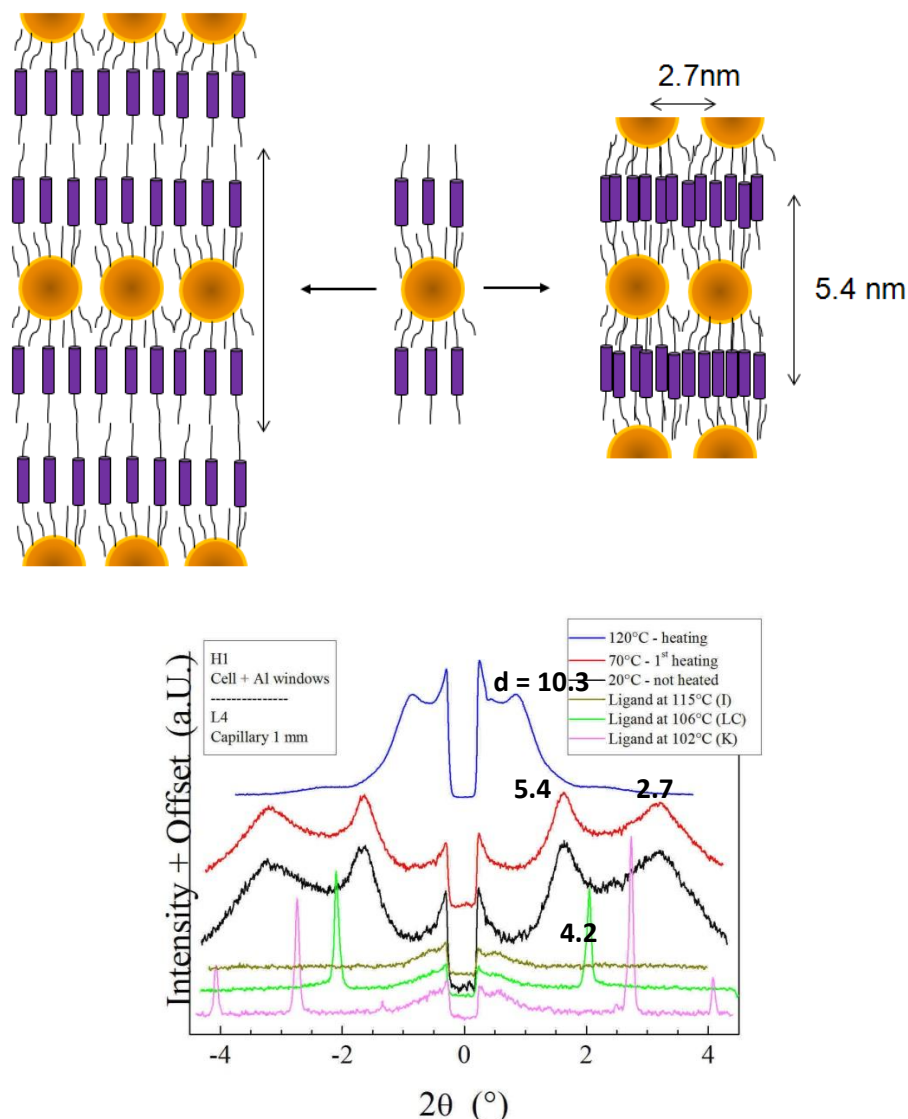


Figure 36 Two proposed models for the self-organization of **H1** (top); In one case (left) the repeating units include the aliphatic tails of the mesogens, which are strongly tilted, in the other case (right) the mesogens overlap and this is the sequence of the repeating units; SAXS pattern of **H1** and the corresponding ligand **L4** (bottom),

Increasing the generation number of the flexible protodendritic ligands results in more dense packing of the mesogens around the NP core and the number of mesogens is increased, *e.g.* the number of AZB mesogens is ~ 1.4 times more around the NP core in the case of **H8** when compared to the **H1**. Similar increase can be observed when the zero and first generation OCB mesogens grafted to the AuNPs: ~ 1.6 times more mesogen is surrounded in **H6** than in **H4**. The number of mesogens in none of these cases doubled as could result from the increased generation number, which indicates that steric hindrance, using aliphatic chains with C6 length,

occurs. However if the flexibility of the dendritic ligand decreases – using BA branching points - increasing the generation number does not increase further the number of the mesogens, when compared to the zero generation, due to strong steric hindrance (e.g. in **H7** the number of mesogens are roughly the same as in **H4**). These calculations are in agreement with the TEM observation where, in that case, when the zero (**H1**, **H4**) and first (**H8**, **H6**) generation dendrons grafted to the NPs the variation level of the distance between the NPs' core is higher, indicates a segregation of the mesogenic groups. When the second generation BA dendron grafted to the NPs the distances between the cores are almost equal and the NPs most likely surrounded equally with the mesogenic ligand and no segregation occurs. Thus, it seems evident that the nature of the ligand (generation and branching) strongly influences the ability of the hybrids to self-organize on surface (2D) and in the bulk (3D) as LC phase.

II.4. Conclusions and outlooks

In this part of the work, we aimed to synthesise dendronized gold nanohybrids to induce mesomorphic behaviour which could favour the self-assembly of 2D or 3D networks. The design and the structure of the hybrids is based on the dendrimers which were presented in the previous chapter (Figure 37).

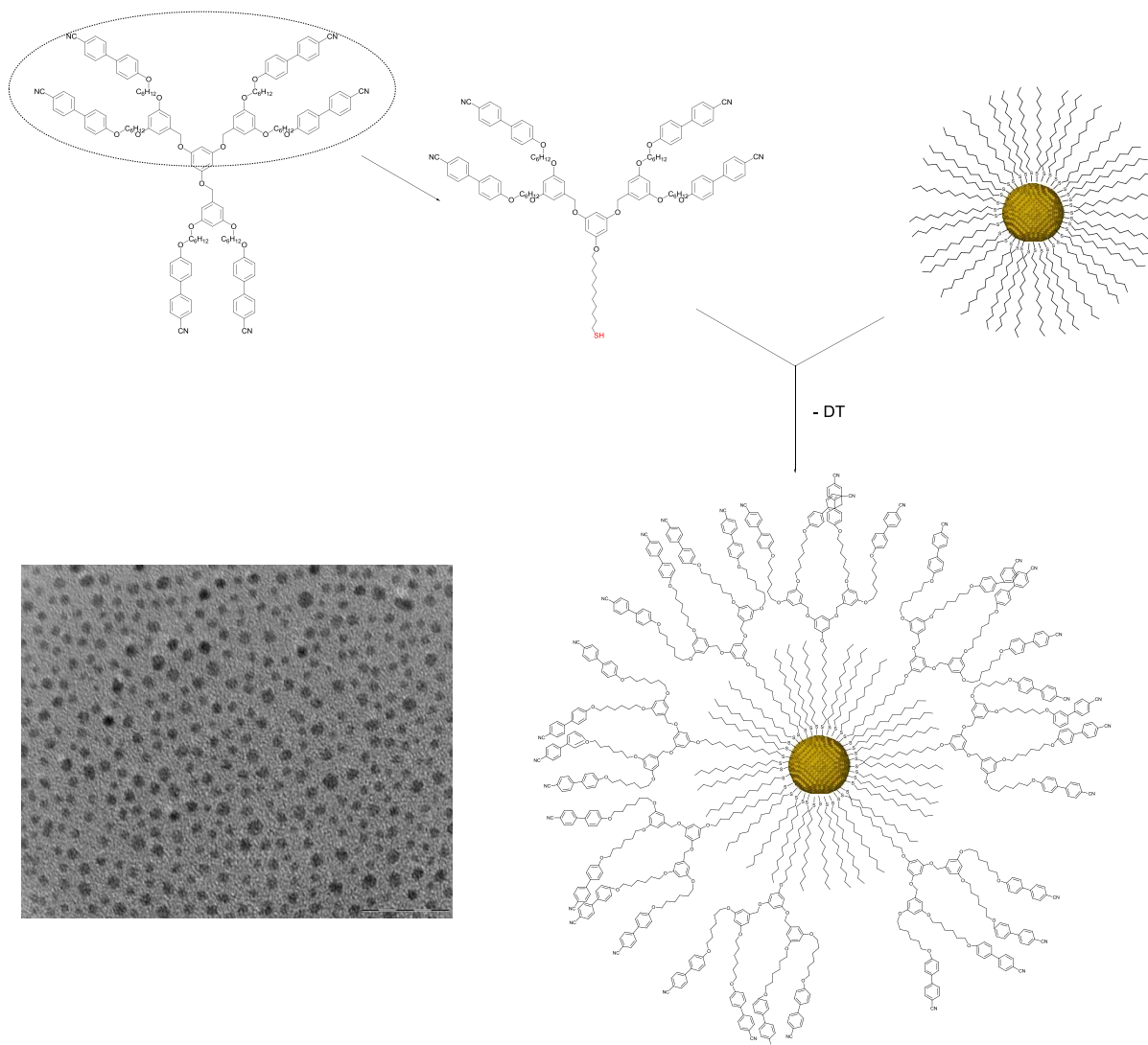


Figure 37 Representative example of synthesis of gold nanohybrids by ligand exchange reaction using protodendritic ligands of the dendrimers

For the synthesis of dendronized gold nanoparticles many different methods are available, such as ligand exchange, direct synthesis or coupling reactions. We could not undertake direct synthesis because of the huge excess of organic ligands which are required and reduced control over the size of the AuNPs that would be formed. Coupling reactions are promising possibilities but in our case the additional reactions steps could strongly reduce the

yield of the ligands which led us to the decision to use solvent-mediated ligand-exchange reactions, which allows a good control over the size of the AuNPs and only a reasonable excess of the ligand is required.

Monodisperse small (2nm) DT-AuNPs with good reproducibility were synthesised using a modification of the Brust's two phase method and these were used as a building block for the synthesis of the hybrids. The mesogenic and protodendritic ligands were used from the synthesis of the dendrimers, described in Chapter I. Long bromo-alkyl spacers (C6 or C11) were attached to the protomesogenic parts which could be easily converted into a thiol anchoring function which was used because of its strong binding energy with gold. The successful synthesis of the gold nanohybrids and their purity were confirmed by NMR spectroscopy. This was essential to allow the investigation of the mesomorphic behaviour of the hybrids.

On average, increasing the generations number of the protodendritic ligands promoted the self-assembly. A non-characteristic mesophase of the hybrid of the first generation azobenzene derivative could be observed by POM. However, the strongest induction of self-assembly - 2D self-assembly over a square micron area - was observed by TEM when the second generation cyanobiphenyl derivative was attached to the AuNPs. The number of mesogens around the NP core is increased with the generation number of the PG based flexible protodendritic ligands and according to the TEM observation some segregation tendency could be observed. However no increase in the mesogenic groups occurred around the core when the second generation BA dendrons grafted to the core, but provided a uniform coating around the NPs (*i.e.* no separation between DT and BA dendritic ligands). This indicates that the nature and the flexibility of the ligands has crucial role in the self-organization tendency and the achievable maximum mesogenic density. The purity of the hybrids was confirmed by NMR and the purification process itself was carried out using size-exclusion chromatography. This technique proved to be effective in this size range. However, a further increase of the size of the ligand can fail using this method, due to the decreased size difference between the hybrid and the ligand and because of the size limit of the Bio-gel.

SAXS and SANS measurements for the verification and determination of the mesophases of the hybrids have also been carried out. The analyses of these results are however complex and time consuming and not completed at the time of the writing and are still in progress.

Outlooks

The complete study of the self-assembly and the mesomorphic behaviour of the hybrids by SAXS and SANS measurements will allow the determination of the origin of the self-assembly - whether it is induced by the AuNPs or the grafted ligands - and help in a better understanding of the organization process. By changing the structures (*e.g.* type of the mesogens, the generation number or the length of the spacer) and the density of the grafted ligands on the hybrids would allow studying the correlation between these structural changes and the surface self-assembly and the LC properties. Multi-functionality can be induced by increasing the variety of the functional groups in the grafted ligands and different physical properties can be tuned.

It would also be interesting to carry out optical experiments with azobenzene containing gold hybrids because of their photoresponsive properties. For instance the AuNPs can be theoretically moved due to mass transport of the azobenzene moiety and promote the self-organization (*e.g.* building up strings with layer periodicity) by photo-induction.

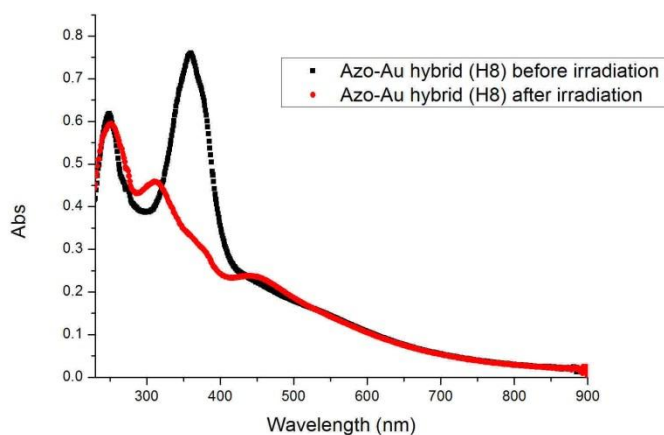


Figure 38 Absorption spectra of gold hybrid with azobenzene moiety (**H8**) in CH₂Cl₂; black: before exposure (mainly *trans* form), red: after light exposure (mainly *cis* form)

II.5 Experimental part

Size exclusion chromatography was used to purify the gold nanohybrids. Bio-Beads S-X beads are neutral, porous styrene divinylbenzene copolymer beads. The S-X1 bead has exclusion limits from 600 to 14,000 Daltons. This range makes it particularly suitable for the fractionation and separation of low molecular weight organic polymers and other hydrophobic substances. The amount of divinylbenzene crosslinkage determines the pore size, and hence the molecular weight exclusion limit of a particular gel in this series. Pore dimensions and exclusion limits are also influenced by the eluent employed; maximal expansion of the matrix is achieved with relatively nonpolar, aromatic solvents. The beads are typically used with benzene, xylene, carbon tetrachloride, THF and mixtures of solvents. Gel permeation is the mode of separation which occurs with Bio-Bead S-X beads. Large compounds, greater than the molecular exclusion limit, pass through the column unhindered, whereas small compounds, within the molecular weight operating range, will be retained in the column. The small compounds permeate the pores and thus they take longer to pass through the column. This mechanism requires an eluent which is mobile, and, therefore the beads must always be used in a column mode (Bio-Beads S-X Beads, Instruction manual).

Description of all other instruments and solvents see previous chapter.

II.5.1 Gold Nanoparticles

In this paragraph only the preparation of those DT-AuNPs will be detailed of which synthesis was reproducible and was used further in the synthesis of gold nanohybrids.

G1 (~2.3 nm) and G2 (~2.1 nm)

The procedure for the synthesis of ~2 nm DT-AuNP is the following: To a vigorously stirred solution of TOAB (2.036 g, 3.72 mmol) in toluene (90 ml) 5 ml aqueous solution of $\text{HAuCl}_4 \cdot 3\text{H}_2\text{O}$ (0.360 g, 0.91 mmol) was added. The toluene phase quickly turned orange from the transfer of the AuCl_4^- into the organic phase. After few minutes 1-dodecanethiol (DT, 0.235 ml, 0.96 mmol) was added to the solution, which caused lightening in the colour, and stirred further 20 minutes before the NaBH_4 (0.345 g, 8.94 mmol) dissolved in deionized water (5ml) was added dropwise. The organic phase became very dark and stirred for 24 hours at room temperature. The organic phase was separated from the water phase, concentrated under reduced pressure and suspended in 150 ml methanol. The mixture was kept in the fridge overnight and the solvent from the brown precipitate was decanted. This washing procedure was repeated several

times with ethanol and acetone. The DT-AuNPs were dried resulting in black viscous solid. The reaction was repeated with good reproducibility, resulting similar size and monodispersity.

G3 (~1.8 nm)

DT-AuNP with diameter size ~1.8 nm was synthesised in a similar way as it is described above with the following parameters: TOAB (0.819 g, 1.50 mmol) in toluene (50 ml), HAuCl₄·3H₂O (0.202 g, 0.51 mmol) in 17 ml deionized water, 1-dodecanethiol (DT, 0.36 ml, 1.50 mmol), NaBH₄ (0.345 g, 8.94 mmol) in 17 ml deionized water.

II.5.2 Thiolated ligands

General procedure for bromoalkylation:

A large excess (5-8 equiv.) of 1,11-dibromoundecane was added to a mixture of phenolic alcohol (1 equiv.) and anhydrous K₂CO₃ (2 - 3 equiv.) in THF or acetone and was refluxed under argon for 48 h. The cooled reaction mixture was filtered. The residue was dissolved in CH₂Cl₂ and washed sequentially with water and sat. aq. NaCl. The organic layer was dried over anh. Mg₂SO₄, filtrated and concentrated. The product was further purified using a silica gel column if necessary.

General procedure for the thiolation:

Hexamethyldisilathiane (HMDS) was added in excess (1.2 - 1.5 equiv.) to a solution of bromide derivative (1 equiv.) in dry THF at -10°C. After 5 minutes, tetra-*n*-butylammonium fluoride (TBAF, 1M solution in THF, 1.2 - 1.5 equiv.) was added. The reaction mixture was stirred for 30 minutes at the same temperature and a further 2 hour at room temperature. The reaction mixture was diluted with CH₂Cl₂ and the solution washed with a saturated solution of NH₄Cl. The organic layer was dried over anh. Mg₂SO₄, filtrated and concentrated. The crude product was purified by silica gel column chromatography.

(L1), 4-(11-Bromoundecyloxy)-4'-undecaneoxyazobenzene

The product was prepared according to the general procedure of *bromoalkylation* and isolated as a yellow solid, 0.626 g, 77% (Mol. Wt: 601.7 g/mol), from **AZB** (0.498 g, 1.35 mmol) and 1,11-dibromoundecane (2.0 mL, 6.71 mmol) using acetone (11 ml) as solvent. (Scheme 1)

Experimental

¹H NMR (CDCl₃): δ 7.87 (d, J=8.9Hz, 4H), 6.99 (d, J=8.9Hz, 4H), 4.04 (t, J=6.6 Hz, 4H), 3.42 (t, J=6.9 Hz, 2H), 1.94–1.74 (m, 6H), 1.54–1.22 (m, 30H), 0.89 (t, J=6.8 Hz, 3H);

(L2), 4'-(11-Bromoundecyloxy)biphenyl-4-carbonitrile

The product was prepared according to the general procedure of *bromoalkylation* and isolated as a white solid 3.538 g, 80% (Mol. Wt: 428.41 g/mol), from 1,11-dibromoundecane (11.5 ml, 48.88 mmol) and 4'-hydroxy-4-biphenylcarbonitrile (**OCB**) (2.013 g, 10.31 mmol) using acetone (60 ml) as solvent. The cooled reaction mixture was filtered. The filtrate was concentrated on rotary evaporator and suspended in ethanol and refrigerated. The crystalline part was separated by filtration and dried under vacuum. (Scheme 1)

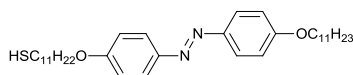
¹H-NMR (CDCl₃): δ 7.67 (q, J=8.1Hz, 4H), 7.53 (d, J=8.8Hz, 2H), 7.00 (d, J=8.8Hz, 2H), 4.02 (t, J=6.6Hz, 2H), 3.41 (t, J=6.9Hz, 2H), 1.96-1.72 (m, 4H), 1.60-1.16 (m, 14H);

(L3)

The product was prepared according to the general procedure of *bromoalkylation* and was isolated as a white viscous material 0.513 g, 91%, (Mol. Wt: 1712.98 g/mol), from 1,11-dibromoundecane (0.65 mL, 2.76 mmol) and **Ba8** (HO-PG(Ba₆OCB₂)₂, 0.489 g, 0.33 mmol) using THF (5 mL) as solvent and CH₂Cl₂ to CH₂Cl₂:EtOAc (10:1) as the eluent for silica gel column chromatography. (Scheme 1)

¹H-NMR (CDCl₃): δ 7.65 (#q, J=8.1Hz, 16H), 7.52 (#d, J=8.7Hz, 8H), 6.99 (#d, J=8.7Hz, 8H), 6.58 (d, J=2.2Hz, 4H), 6.43 (t, J=2.2Hz, 2H), 6.25 (t, J=2.2Hz, H), 6.19(d, J=2.2Hz, 2H), 4.93 (s, 4H), 4.02 (t, J=6.4Hz, 8H), 3.97 (t, J=6.4Hz, 8H), 3.90 (t, J=6.7Hz, 2H), 3.40 (t, J=6.9Hz, 2H), 1.95-1.72 (m, 18H), 1.65-1.48 (m, 18H), 1.40-1.24 (m, 14H); **¹³C NMR** (CDCl₃): δ 161.03, 160.63, 160.47, 159.74, 145.23, 139.07, 132.54, 131.35, 128.31, 127.06, 119.06, 115.10, 110.10, 105.88, 100.88, 94.58, 94.49, 70.14, 68.00, 67.89, 33.98, 32.82, 29.49, 29.44, 29.39, 29.34, 29.18, 29.15, 28.74, 28.15, 26.03, 25.87, 25.84

(L4), 4-undecyloxy-(11-mercapto)-4'-undecaneoxyazobenzene

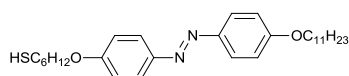


According to the general procedure of *thiolation*, the product was isolated as a yellow solid 0.418 g, 72% (Mol. Wt: 554.87 g/mol) from 4-(11-bromoundecyloxy)-4'-

undecaneoxyazobenzene (**L1**) (0.597g, 1.04 mmol), HMDTS (0.33ml, 1.56mmol), TBAF (1.35 ml, 1.35 mmol), using CHCl₃:cuclohexane (2:1) as the eluent for silica gel column chromatography. (Scheme 2)

¹H NMR (CDCl₃): δ 7.99 (d, J=8.9Hz, 4H), 7.01 (d, J=8.9Hz, 4H), 4.05 (t, J=6.5 Hz, 4H), 2.53 (dt, J=7.1Hz, 7.3Hz, 2H), 1.96–1.52 (m, 6H), 1.50–1.20 (m, 31H), 0.89 (t, J=6.8 Hz, 3H); ¹³C NMR (CDCl₃): δ 161.18, 161.16, 146.97, 124.28, 114.67, 68.35, 68.32, 34.04, 31.91, 29.61, 29.60, 29.57, 29.52, 29.49, 29.39, 29.36, 29.34, 29.23, 29.07, 28.38, 26.03 ,24.64, 22.68, 14.11

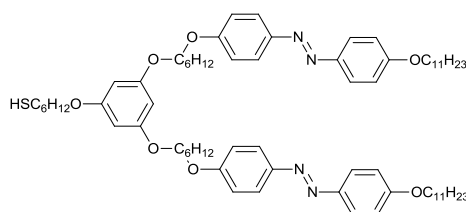
(L6), 4-undecyloxy-4'-(6-mercapto)-hexaneoxyazobenzene



According to the general procedure of *thiolation*, the product was isolated as a yellow solid 0.331 g, 84% (Mol. Wt: 484.74 g/mol) from **3** (0.434 g, 0.816 mmol), HMDTS (0.26 ml, 1.23 mmol) and TBAF (1.10 ml, 1.10 mmol), using CHCl₃ as the eluent for silica gel column chromatography. (Scheme 2)

¹H NMR (CDCl₃): δ 7.87 (d, J=8.9Hz, 4H), 6.99 (d, J=8.9Hz, 4H), 4.04 (t, J=6.4Hz, 4H), 2.56 (dt, J=7.3, 7.3 Hz, 2H), 1.96-1.60 (m, 6H), 1.55-1.20 (m, 21H), 0.91 (t, J=6.8 Hz, 3H); ¹³C NMR (CDCl₃): δ 161.20, 161.07, 147.03, 146.95, 124.30, 114.68, 114.66, 68.35, 68.12, 33.90, 31.92, 29.62, 29.60, 29.58, 29.40, 29.34, 29.23, 29.12, 28.09, 26.03, 25.56, 24.54, 22.69, 14.11

(L9)



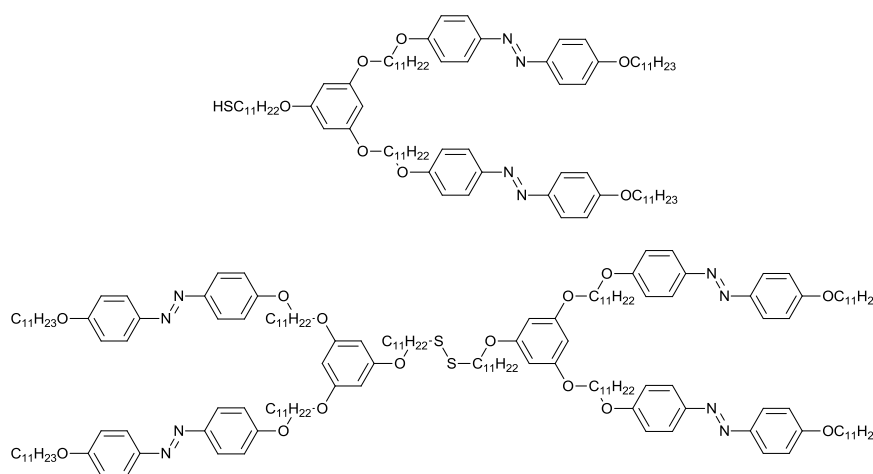
This was made according to the general procedure of *thiolation*, the product was isolated as a yellow solid 0.218 g, 60% (Mol. Wt: 1143.65 g/mol) from **T4** (0.380 g, 0.32 mmol), HMDTS (0.09 ml, 0.48 mmol) and TBAF (0.50 ml, 0.50 mmol), using CH₂Cl₂:Petroleum ether (20:1) as the eluent for silica gel column chromatography. The disulphide by-product was also isolated. (Scheme 2)

Experimental

¹H NMR (CDCl₃): δ 7.89 (d, J=9.0Hz, 8H), 7.00 (d, J=9.0Hz, 8H), 6.10 (s, 3H), 4.12-3.84 (m, 14H), 2.54 (dt, J=7.3, 7.3 Hz, 2H), 1.96-1.70 (m, 14H), 1.70-1.20 (m, 46H), 0.91 (t, J=6.8 Hz, 6H); **¹³C NMR** (CDCl₃): δ 161.22, 161.11, 160.97, 147.01, 146.97, 124.32, 114.68, 93.91, 68.35, 68.16, 67.84, 33.92, 31.94, 29.64, 29.60, 29.43, 29.37, 29.26, 29.20, 29.18, 28.11, 26.06, 25.91, 25.86, 25.60, 24.55, 22.72, 14.15

MALDI-ToF: m/z: Calcd for C₇₀H₁₀₂N₄O₇S: 1142.75; found: 1143.705 (M+1)

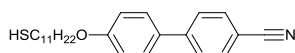
(L10a) and (L10b)



The product was prepared according to the general procedure of *thiolation*, from **T5** (0.707 g, 0.50 mmol), HMDTS (0.16 ml, 0.76 mmol) and TBAF (0.66 ml, 0.66 mmol), using THF (6 ml) as a solvent and CHCl₃ as the eluent for silica gel column chromatography. The reaction resulted 0.547g ~50-50mol% of the product and disulphide by-product (according to ¹H-NMR results, see in synthesis part), (disulphide: Mol. Wt: 2706.07 g/mol; Thiol: Mol. Wt: 1354.05 g/mol) which were not separated from each other. (Scheme 2)

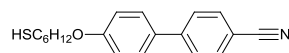
NMR data of the mixed compound:

¹H NMR (CDCl₃): δ 7.86 (d, J=8.8Hz, 24H), 6.99 (d, J=8.8Hz, 24H), 6.07 (s, 9H), 4.03 (t, J=6.6Hz, 24H), 3.90(t, J=6.5Hz, 18H) 2.68 (t, J=7.3Hz, 4H), 2.54 (dt, J=7.3, 7.3 Hz, 2H), 1.96-1.70 (m, 42H), 1.70-1.20 (m, 169H), 0.91 (t, J=6.8 Hz, 18H); **¹³C NMR** (CDCl₃): δ 161.18, 161.00, 146.98, 124.31, 114.67, 93.86, 68.34, 68.02, 39.22, 34.07, 31.94, 29.73, 29.63, 29.60, 29.57, 29.42, 29.41, 29.36, 29.29, 29.26, 29.08, 28.56, 28.40, 26.08, 26.06, 24.65, 22.71, 14.14

(L5) 11-mercapto-(4-cyanobiphenyl-4'-oxy)undecane

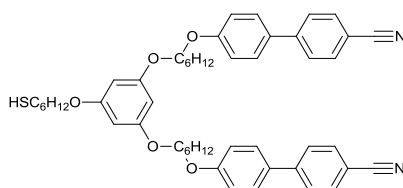
According to the general procedure of *thiolation*, the product was isolated as a white solid 0.686 g, 31% (Mol. Wt: 381.57 g/mol) from 11-bromo-(4-cyanobiphenyl-4'-oxy)undecane (**L2**) (2.477 g, 5.78 mmol), HMDTS (1.90 ml, 9.01 mmol), TBAF (8.00 ml, 8.00 mmol), using THF as solvent (40 ml) and CH₂Cl₂:Petroleum ether (20:1) as the eluent for silica gel column chromatography. The disulphide by-product was also isolated (0.840g, 1.10 mmol, Mol. Wt: 761.15 g/mol). (Scheme 2)

¹H-NMR (CDCl₃): δ 7.67 (#q, J=8.2Hz, 4H), 7.53 (#d, J=8.6Hz, 2H), 7.0 (#d, J=8.7Hz, 2H), 4.01 (t, J=6.6Hz, 2H), 2.53 (dt, J=7.3Hz, 7.3Hz 2H), 1.81 (quintet, J=7.0Hz, 2H), 1.62 (quintet, J=7.0Hz, 2H), 1.54–1.22 (m, 15H); ¹³C NMR (CDCl₃): δ 159.83, 145.30, 132.55, 131.28, 128.31, 127.07, 119.07, 115.11, 110.08, 68.20, 34.02, 29.52, 29.48, 29.35, 29.22, 29.05, 28.35, 26.03, 24.63

(L7) 6-mercapto-(4-cyanobiphenyl-4'-oxy)hexane

According to the general procedure of *thiolation*, the product was isolated as a white solid 0.418 g, 80% (Mol. Wt: 311.44 g/mol) from 6-bromo-(4-cyanobiphenyl-4'-oxy)hexane (**2**) (0.600 g, 1.67 mmol), HMDTS (0.45 ml, 2.40 mmol), TBAF (2.30 ml, 2.30 mmol), using CH₂Cl₂:Petroleum ether (20:1) as the eluent for silica gel column chromatography. The disulphide by-product was also isolated. (Scheme 2)

¹H-NMR (CDCl₃): δ 7.67 (#q, J=8.3Hz, 4H), 7.53 (#d, J=8.8Hz, 2H), 7.0 (#d, J=8.8Hz, 2H), 4.02 (t, J=6.4Hz, 2H), 2.56 (dt, J=7.3Hz, 7.3Hz, 2H), 1.83 (quintet, J=6.8Hz, 2H), 1.67 (quintet, J=6.9Hz, 2H), 1.54–1.44 (m, 4H), 1.35 (t, J=7.8Hz); ¹³C NMR (CDCl₃): δ 159.75, 145.27, 132.55, 131.37, 128.33, 127.09, 119.07, 115.10, 110.11, 67.98, 33.87, 29.10, 28.06, 25.55, 24.52

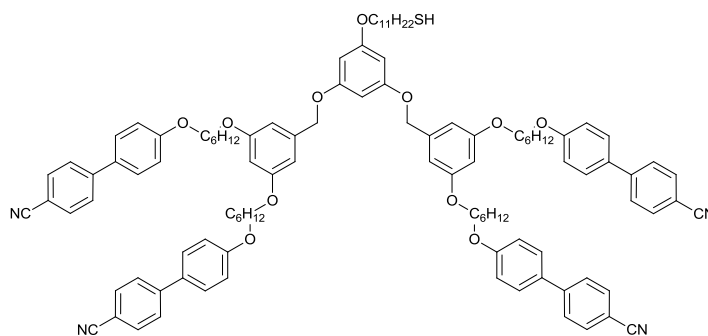
(L8)

Experimental

According to the general procedure of *thiolation*, the product was isolated as a yellowish viscous solid 0.215 g, 99% (Mol. Wt: 797.06 g/mol) from **Pg1** (0.231 g, 0.27 mmol), HMDTS (0.08 ml, 0.43 mmol), TBAF (0.40 ml, 0.40 mmol), using CH₂Cl₂:EtAc (30:1) as the eluent for silica gel column chromatography. (Scheme 2)

¹H-NMR (CDCl₃): δ 7.66 (#q, J=7.5Hz, 8H), 7.53 (#d, J=8.7Hz, 4H), 7.0 (#d, J=8.7Hz, 4H), 6.09 (s, 3H), 4.02 (t, J=6.4Hz, 4H), 3.98-3.86 (m, 6H), 2.54 (dt, J=7.3Hz, 7.3Hz 2H), 1.96-1.70 (m, 10H), 1.70-1.40 (m, 14H), 1.35 (t, J=7.8Hz, 1H); ¹³C NMR (CDCl₃): δ 160.95, 159.77, 145.26, 132.55, 131.34, 128.32, 127.07, 119.06, 115.13, 110.10, 93.94, 93.90, 77.46, 77.04, 76.61, 68.03, 67.84, 33.88, 29.19, 29.17, 29.12, 28.06, 25.89, 25.85, 25.58, 24.53

(L11)



According to the general procedure of *thiolation*, the product was isolated as a white paste, 0.316 g, 64% (Mol. Wt: 1666.15 g/mol) from **L3** (0.508 g, 0.30 mmol), HMDTS (0.08 ml, 0.43 mmol), TBAF (0.40 ml, 0.40 mmol), using CH₂Cl₂ as the eluent for silica gel column chromatography. The disulphide by-product was also isolated. (Scheme 2)

¹H-NMR (CDCl₃): δ 7.65 (#q, J=8.1Hz, 16H), 7.52 (#d, J=8.7Hz, 8H), 6.99 (#d, J=8.7Hz, 8H), 6.58 (d, J=2.2Hz, 4H), 6.43 (t, J=2.2Hz, 2H), 6.25 (t, J=2.2Hz, 1H), 6.19 (d, J=2.2Hz, 2H), 4.93 (s, 4H), 4.02 (t, J=6.4Hz, 8H), 3.97 (t, J=6.4Hz, 8H), 3.90 (t, J=6.7Hz, 2H), 2.52 (dt, J=7.3Hz, 7.3Hz 2H), 1.95-1.72 (m, 18H), 1.65-1.48 (m, 18H), 1.40-1.24 (m, 15H); ¹³C NMR (CDCl₃): δ 161.03, 160.63, 160.47, 159.74, 145.23, 139.07, 132.55, 131.35, 128.32, 127.06, 119.06, 115.10, 110.10, 105.88, 100.88, 94.58, 94.49, 70.14, 68.00, 67.88, 34.02, 29.51, 29.47, 29.36, 29.18, 29.15, 29.05, 28.35, 26.03, 25.87, 25.84, 24.63

MALDI-ToF m/z: Calcd for C₁₀₇H₁₁₆N₄O₁₁S: 1664.84; found: 1665.75 (M+1)

II.5.3 Dendronized Gold Nanohybrids

Gold nanoparticles (DT-AuNP; see synthesis 0) and the ligands with thiol function were dissolved in CH_2Cl_2 , according to Table 6, where the proportions were determined according to the description in II.2.3 - and stirred for 24 hours at room temperature. After the solvent was evaporated under reduced pressure, the crude product was purified twice using Bio Beads SX-1 beads, swollen in CH_2Cl_2 . The purity was confirmed by $^1\text{H-NMR}$ (see paragraph II.3.3).

Hybrid →	H1	H4	H6	H7	H8
DT-AuNP	G3	G1	G1	G2	G2
$\phi_{\text{DT-AuNP}}$ (nm)	1.8	2.3	2.3	2.1	2.1
$m_{\text{DT-AuNP}}$ (g)	0.104	0.060	0.063	0.061	0.060
Ligand →	L4	L5	L8	L11	L9
M (g/mol)	554.9	381.21	797.06	1666.15	1143.65
n_{DT} (mmol)	1.10×10^{-1}	5.21×10^{-2}	5.47×10^{-2}	5.71×10^{-2}	5.61×10^{-2}
Ligand excess ~	4x	4x	4x	3x	3x
m_{L} (g)	0.2442	0.079	0.173	0.281	0.190
Solvent (ml)	6.00	3.00	3.00	2.50	2.50

Table 6 Quantity of materials used in ligand exchange reaction

II.6 References

- ¹ F. Antonii, *Panacea Aurea-Auro Potabile*; Bibliopolio Frobeniano, Hamburg, **1618**
- ² M. Faraday, *Phil. Trans. R. Soc.* **1857**, *147*, 145-181
- ³ J. Turkevitch, P. C. Stevenson, J. Hillier, *Discuss. Faraday Soc.* **1951**, *11*, 55-75
- ⁴ M. Brust, M. Walker, D. Bethell, D. J. Schiffrin, R. Whyman, *J. Chem. Soc., Chem. Commun.* **1994**, 801-802.
- ⁵ M. C. Daniel, D. Astruc, *Chem. Rev.* **2004**, *104*, 293-346
- ⁶ J. Kimling, M. Maier, B. Okenve, V. Kotaidis, H. Ballot, A. Plech, *J. Phys. Chem. B* **2006**, *110*, 15700-15707
- ⁷ B. V. Enustun, J. Turckevich, *J. Am. Chem. Soc.* **1963**, *85*, 3317-3328
- ⁸ G. Frens, *Colloid & Polymer Science* **1972**, *250*, 736-741
- ⁹ W. W. Weare, S. M. Reed, M. G. Warner, J. E. Hutchison, *J. Am. Chem. Soc.* **2000**, *122*, 12890-12891.
- ¹⁰ Heath, J. R.; Brandt, L.; Leff, D. V. *Langmuir* **1996**, *12*, 4723-4730.
- ¹¹ Green, M.; O'Brien, P. *Chem. Commun.* **2000**, 183-184.
- ¹² Hostetler, M. J.; Templeton, A. C.; Murray, R. W. *Langmuir* **1999**, *15*, 3782-3789
- ¹³ Templeton, A. C.; Hostetler, M. J.; Kraft, C. T.; Murray, R. W., *J. Am. Chem. Soc.* **1998**, *120*, 1906-1911.
- ¹⁴ Templeton, A. C.; Wuelfing, W. P.; Murray, R. W., *Acc. Chem. Res.* **2000**, *33*, 27-36
- ¹⁵ M. Brust, J. Fink, D. Bethell, D. J. Schiffrin, C. Kiely, *J. Chem. Soc., Chem. Commun.* **1995**, 1655
- ¹⁶ N. Zheng, J. Fan, G. D. Stucky, *J. Am. Chem. Soc.*, **2006**, *128*, 6550-6551
- ¹⁷ D.V. Leff, P.C. O'Hara, J.R. Heath, W.M. Gelbart, *J. Phys. Chem.*, **1995**, *99*, 7036-7041
- ¹⁸ M. J. Hostetler, J. E. Wingate, C.-J. Zhong, J. E. Harris, R. W. Vachet, M. R. Clark, J. D. Londono, S. J. Green, J. Stokes, G. D. Wignall, G. L. Glish, M. D. Porter, N. D. Evans and R. W. Murray, *Langmuir*, **1998**, *14*, 17-30
- ¹⁹ R. L. Whetten, J. T. Khoury, M. M. Alvarez, S. Murthy, I. Vezmar, Z. L. Wang, P. W. Stephen, C. L. Cleveland, W. D. Luedtke, U. Landman, *Adv. Mater.* **1996**, *5*, 428-433
- ²⁰ Y. Li, O. Zaluzhna, B. Xu, Y. Gao, J. M. Modest, Y. Y. J. Tong, *J. Am. Chem. Soc.* **2011**, *133*, 2092-2095
- ²¹ Prasad, B. L. V.; Stoeva, S. I.; Sorensen, C. M.; Klabunde, K. J., *Langmuir* **2002**, *18*, 7515-7520
- ²² X. M. Lin, C. M. Sorensen, K. J. Klabunde, *J. Nanopart. Res.* **2000**, *2*, 154
- ²³ B. L. V. Prasad, Savka I. Stoeva, Christopher M. Sorensen, and Kenneth J. Klabunde *Chem. Mater.* **2003**, *15*, 935-942
- ²⁴ T. Teranishi, M. Miyake, S. Hasegawa, T. Shimizu, *Adv. Mater.* **2001**, *13*, 1699-1701
- ²⁵ T. Teranishi, *C.R.Chimie*, **2003**, *6*, 979-987
- ²⁶ T. Shimizu, T. Teranishi, S. Hasegawa, M. Miyake, *J. Phys. Chem. B* **2003**, *107*, 2719-2724
- ²⁷ N. R. Jana, L. Gearheart, Murphy, C. J. *Adv. Mater.* **2001**, *13*, 1389
- ²⁸ C. Ziegler, A. Eychmueller, *J. Phys. Chem. C*, **2011**, *115*, 4502-4506.
- ²⁹ N. Jana, L. Gearheart, C. J. Murphy, *Langmuir* **2001**, *17*, 6782-6786.
- ³⁰ J. Rodríguez-Fernandez, J. Pérez-Juste, F. J. García de Abajo, L. M. Liz-Marzan, *Langmuir* **2006**, *22*, 7007
- ³¹ C. H. Yu, C. P. Schubert, C. Welch, B. J. Tang, M. G. Tamba, G. H. Mehl, *J Am Chem Soc.* **2012** *134*, 5076-5079
- ³² L. O. Brown, J. E. Hutchison, *J. Am. Chem. Soc.* **1997**, *119*, 12384-12385

- 33 G. H. Woehrle, L. O. Brown, J. E. Hutchison, *J. Am. Chem. Soc.* **2005**, *127*, 2172 – 2183
- 34 J. Petroski, M. H. Chou, C. Creutz, *Inorg. Chem.* **2004**, *43* (5), 1597-1599
- 35 Y. Shichibu, Y. Negishi, T. Tsukuda, T. Teranishi *J. Am. Chem. Soc.* **2005**, *127*, 13464-13465
- 36 G. H. Woehrle, M. G. Warner, J. E. Hutchison, *J. Phys. Chem. B* **2002**, *106*, 9979-9981
- 37 R. L. Donkers, Y. Song, R. W. Murray, *Langmuir* **2004**, *20*, 4703-4707
- 38 M. Montalti, L. Prodi, N. Zaccheroni, R. Baxter, G. Teobaldi, F. Zerbetto, *Langmuir* **2003**, *19*, 5172-5174
- 39 S. Perumal, A. Hofmann, N. Scholz, E. Ruhl, C. Graf, *Langmuir* **2011**, *27*, 4456–4464
- 40 A. Kassam, G. Bremner, B. Clark, G. Ulibarri, R. B. Lennox, *J. Am. Chem. Soc.* **2006**, *128*, 3476-3477
- 41 R. Guo, Y. Song, G. Wang, R. W. Murray, *J. Am. Chem. Soc.* **2005**, *127*, 2752-2757.
- 42 E. Boisselier, L. Salmon, J. Ruiz and D. Astruc, *Chem. Commun.*, **2008**, 5788
- 43 D. J. Tognarelli, R. B. Miller, R. R. Pompano, A. F. Loftus, D. J. Sheibley, M. C. Leopold, *Langmuir* **2005**, *21* 11119-11127.
- 44 G; Kickelbick, *Hybrid Materials: Synthesis, Characterization, and Applications*, Wiley-VCH, Weinheim, **2007**
- 45 K. Esumi, A. Suzuki, A. Yamahira and K. Torigoe, *Langmuir*, **2000**, *16*, 2604
- 46 R. M. Crooks, M. Zhao, L. Sun, V. Chechik, L. K. Yeung, *Acc. Chem. Res.* **2001**, *34*, 181-190
- 47 Y. G. Kim, S. K. Oh, R. M. Crooks, *Chem. Mater.* **2004**, *16*, 167-172
- 48 R. W. J. Scott, O. M. Wilson, and R. M. Crooks, *J. Phys. Chem. B* **2005**, *109*, 692-704
- 49 E. Boisselier, A. K. Diallo, L. Salmon, J. Ruiz and D. Astruc, *Chem. Commun.*, **2008**, 4819–4821
- 50 E. Boisselier, A. K. Diallo, L. Salmon, C. Ornelas, J. Ruiz, D. Astruc, *J. Am. Chem. Soc.* **2010**, *132*, 2729–2742
- 51 C. Cordovilla, S. Coco, P. Espinet, B. Donnio, *J. Am. Chem. Soc.* **2010**, *132*, 1424–1431
- 52 K. R. Gopidas, J. K. Whitesell, M. A. Fox, *J. Am. Chem. Soc.* **2003**, *125*, 6491-6502
- 53 M.-K. Kim, Y.-M. Jeon, W. S. Jeon, H.-J. Kim, S. G. Hong, C. G. Park, K. Kim, *Chem. Commun.* **2001**, 667-668
- 54 C. S. Love, V. Chechik, D. K. Smith, C. Brennan, *J. Mater. Chem.* **2004**, *14*, 919-923
- 55 C. S. Love, I. Ashworth, C. Brennan, V. Chechik, D. K. Smith, *J. Colloid Interface Sci.* **2006**, *302*, 178-186
- 56 S. Nakao, K. Torigoe, K. Kon-No, T. Yonezawa, *J. Phys. Chem. B* **2002**, *106*, 12097-12100
- 57 C. Danda, R. Ponnampati, P. Dutta, P. Taraneekar, G. Patterson, R. C. Advincula, *Macromol. Chem. Phys.* **2011**, *212*, 1600–1615
- 58 A. Labande, J. Ruiz, D. Astruc, *J. Am. Chem. Soc.* **2002**, *124* (8), 1782-1789.
- 59 T. J. Cho, R. A. Zangmeister, R. I. Maccuspie, A. K. Patri, V. A. Hackley, *Chem. Mater.*, **2011**, *23*, 2665
- 60 E. R. Zubarev, J. Xu, A. Sayyad, J. D. Gibson, *J. Am. Chem. Soc.* **2006**, *128* (15), 4958-4959
- 61 E. C. Cutler, E. Lundin, B. D. Garabato, D. Choi, Y.-S. Shon, *Mater. Res. Bull.* **2007**, *42*, 1178-1185
- 62 Y.-S. Shon, D. Choi, J. Dare, T. Dinh, *Langmuir* **2008**, *24*, 6924-6931
- 63 D. Astruc, M. C. Daniel, J. Ruiz, *Chem. Commun.* **2004**, 2637-2649
- 64 S. Deng, T. M. Fulghum, G. Krueger, D. Patton, J.-Y. Park, R. C. Advincula *Chem. Eur. J.* **2011**, *17*, 8929 – 8940

- ⁶⁵ K.R. Gopidas, J.K. Whitesell, M.A. Fox, *J. Am. Chem. Soc.*, **2003**, *125*, 14168 – 14180
- ⁶⁶ U. Shivakumar, J. Mirzaei, X. Feng, A. Sharma, P. Moreira, T. Hegmann, *Liq. Cryst.* **2011**, *38*, 1495-1514
- ⁶⁷ T. Hegmann, H. Qi, V. M. Marx, *J. Inorg. Organomet. Polym. Mater.* **2007**, *17*, 483-508
- ⁶⁸ O. Stamatoiu, J. Mirzaei, X. Feng, T. Hegmann, *Top. Curr. Chem.* **2012**, *318*, 331-393
- ⁶⁹ G. L. Nealon, R. Greget, C. Dominguez, Zs. T. Nagy, D. Guillon, J.-L. Gallani, B. Donnio, *Beilstein, J. Org. Chem.* **2012**, *8*, 349-370.
- ⁷⁰ R. Deschenaux, B. Donnio, D. Guillon, *New J. Chem.* **2007**, *31*, 1064-1073
- ⁷¹ I. In, Y. W. Jun, Y. J. Kim, S. Y. Kim, *Chem. Commun.* **2005**, 800-801
- ⁷² N. Kanayama, O. Tsutsumi, A. Kanazawa, T. Ikeda, *Chem. Commun* **2001**, 2640-2641
- ⁷³ M. Draper, I. M. Saez, S. J. Cowling, P. Gai, B. Heinrich, B. Donnio, D. Guillon, J. W. Goodby, *Adv. Funct. Mater.* **2011**, *21*, 1260-1278
- ⁷⁴ M. Wojcik, W. Lewandowski, J. Matraszek, J. Mieczkowski, J. Borysiuk, D. Pocięcha, E. Gorecka, *Angew. Chem. Int. Ed.* **2009**, *48*, 5167-5169
- ⁷⁵ M. Wojcik, M. Kolpaczynska, D. Pocięcha, J. Mieczkowski, E. Gorecka, *Soft Matter* **2010**, *6*, 5397-5400
- ⁷⁶ J. Zhang, J. K. Whitesell, M. A. Fox, *Chem. Mater.* **2001**, *13*, 2323-2331.
- ⁷⁷ S. Kumar, S. K. Pal, P. S. Kumar, V. Lakshminarayanan, *Soft Matter*, **2007**, *3*, 896-900.
- ⁷⁸ S. Kumar, *Chem. Soc. Rev.* **2006**, *35*, 83-109
- ⁷⁹ B. R. Kaafarani, *Chem. Mater.* **2011**, *23*, 378-396
- ⁸⁰ R. A. Reddy, C. Tschierske, *J. Mater. Chem.* **2006**, *16*, 907-961
- ⁸¹ J. Etxebarria, M. B. Ros, *J. Mater. Chem.* **2008**, *18*, 2919-2926
- ⁸² Marx, V. M.; Girgis, H.; Heiney, P. A.; Hegmann, T., *J. Mater. Chem.*, **2008**, *18*, 2983-2994
- ⁸³ L. Cseh, G. H. Mehl, *J. Am. Chem. Soc.* **2006**, *128*, 13376-13377
- ⁸⁴ L. Cseh, G. H. Mehl, *J. Mater. Chem.* **2007**, *17*, 311-315
- ⁸⁵ X. Zeng, F. Liu, A. G. Fowler, G. Ungar, L. Cseh, G. H. Mehl, J. E. Macdonald, *Adv. Mater.* **2009**, *21*, 1746-1750
- ⁸⁶ X. Mang, X. Zeng, B. Tang, F. Liu, G. Ungar, R. Zhang, L. Cseh, G. H. Mehl, *J. Mater. Chem.*, **2012**, *22*, 11101-11106
- ⁸⁷ B. Donnio, P. García-Vázquez, J. L. Gallani, D. Guillon, E. Terazzi, *Adv. Mater.* **2007**, *19*, 3534-3539
- ⁸⁸ K. Kanie, M. Matsubara, X. Zeng, F. Liu, G. Ungar, H. Nakamura, A. Muramatsu, *J. Am. Chem. Soc.*, **2012**, *134*, 808-811
- ⁸⁹ S. Mischler, S. Guerra, R. Deschenaux, *Chem. Commun.*, **2012**, *48*, 2183-2185
- ⁹⁰ Julien Boudon, Dendrimer-Based Gold Nanoparticles: Syntheses, Characterization and Organization; *Thesis*, **2009**
- ⁹¹ S. Frein, J. Boudon, M. Vonlanthen, T. Scharf, J. Barberá, G. Süß-Fink, T. Bürgi, R. Deschenaux, *Helv. Chim. Acta* **2008**, *91*, 2321-2337
- ⁹² Y. Komine, I. Ueda, T. Goto, H. Fujihara, *Chem. Commun.* **2006**, 302-304
- ⁹³ M. Yamada, Z. Shen, M. Miyake, *Chem. Commun.* **2006**, 2569-2571.
- ⁹⁴ M. G. Warner, S. M. Reed, J. E. Hutchison, *Chem. Mater.* **2000**, *12*, 3316.

- ⁹⁵ H. Sellers, A. Ulman, Y. Schnidman, J.E. Eilers, *J. Am. Chem. Soc.*, **1993**, *115*, 9389
- ⁹⁶ G. A. Rance, D. H. Marsh, A. N. Khlobystov, *Chem. Phys. Lett.* **2008**, *460*, 230-236
- ⁹⁷ B. Donnio, D. Guillon, *Adv. Polym. Sci.* **2006**, *201*, 45;
- ⁹⁸ S. Barnard, L. A. Curtiss, *Chem. Phys. Chem.* **2006**, *7*, 1544;
- ⁹⁹ G. H. Woehrle, J. E. Hutchison, S. Ozkar, R. G. Finke, *Turk.J.Chem.* **2006**, *30*,
- ¹⁰⁰ G. Mie, *Ann. Physik* **1908**, *25*, 377-445
- ¹⁰¹ P. Mulvaney, *Langmuir* **1996**, *12*, 788-800
- ¹⁰² K. L. Kelly, E. Coronado, L. L. Zhao, G. C. Schatz, *J. Phys. Chem. B* **2003**, *107*, 668-677
- ¹⁰³ AJ Haes, CL Haynes, AD McFarland, S Zou, GC Schatz, RP Van Duyne. *MRS Bull.*, **2005.30**, 368-375
- ¹⁰⁴ MM Miller, AA Lazarides, *J. Phys. Chem. B* **2005***109*,21556-65
- ¹⁰⁵ S. Underwood, P. Mulvaney, *Langmuir* **1994**, *10*, 3427-3430
- ¹⁰⁶ T.R. Jensen, M. Duval Malinsky, C.L. Haynes, and R.P. Van Duyne, *J. Phys. Chem*, **2000**, *104*, 10549.
- ¹⁰⁷ K.A. Willets, R.P. Van Duyne, *Annu. Rev. Phys. Chem.* **2007**, *58*, 267-297
- ¹⁰⁸ A. V. Gaikwad, P. Verschuren, E. Eiser, G. Rothenberg, *J. Phys. Chem. B* **2006**, *110*, 17437-17443

Résumé de la Thèse

Synthèse de dendrimères et nanohybrides dendronisés, auto-organisés, et étude de leurs propriétés physiques

Contexte et objectifs de thèse

La chimie supramoléculaire est un concept extrêmement puissant pour l'élaboration programmée d'assemblées de petites molécules en réseaux ordonnés, fonctionnels, complexes et variés, car basée sur de simples critères d'interactions associatives non-covalentes et de reconnaissance moléculaire; il suffit de constater que tous les organismes vivants sont constitués d'éléments auto-assemblés. Cette approche présente de nombreux intérêts scientifiques fondamentaux et appliqués et est de plus en plus considérée dans les sciences de la vie ou des matériaux. Parmi ces systèmes moléculaires d'une très grande diversité structurale capables de s'organiser spontanément en superstructures ordonnées, il y a les cristaux liquides, qui émergent régulièrement comme des candidats idéaux dans de nombreuses technologies modernes. Cette classe de matériaux dynamiques et stimulables, qui combine à la fois ordre et fluidité au sein même de structures périodiques de basse dimensionnalité, devient aussi souvent incontournable dans le développement de nouvelles technologies et biotechnologies dont les applications dépendent de l'ordre moléculaire (l'optoélectronique, le photovoltaïsme, la détection, l'amplification du signal, la théranosutique, etc...). Du fait de ces agencements moléculaires réguliers et homogènes, il est attendu une amplification des propriétés de la molécule unique par des effets coopératifs, de même que de nouvelles propriétés peuvent émerger par effets synergétiques. L'élaboration et le choix des blocs moléculaires élémentaires (forme, force d'interaction, spécificité et directionnalité) permettent de prédire partiellement la nature de ces assemblées supramoléculaires et leurs fonctions.

La majorité des mésogènes thermotropes de bas poids moléculaires possède une structure simple, dont la partie rigide et anisotrope (bâtonnets, disques) est équipée de chaînes aliphatiques flexibles: des mésophases nématiques et/ou smectiques sont observées pour les structures bâtonnets, alors que des structures colonnaires sont observées pour les matériaux en forme de disque. Ces dernières années, d'énormes avancées ont été réalisées dans l'élaboration des cristaux liquides, avec par exemple les mésogènes boomerangs (ou banane) qui génèrent toute une variété de nouvelles mésophases polaires, ou des molécules de grande taille (mais parfaitement monodisperses) à architectures plus complexes (supermolécules) comme les oligomères, intermédiaires structuraux des petites molécules et des polymères. Il s'agit de molécules multifonctionnelles (insertion et hiérarchisation de fonctions supplémentaires au

sein de l'édifice oligomérique) qui sont en général formées d'unités pro-mésogènes standard, connectées entre elles par des espaceurs flexibles, pouvant générer des systèmes linéaires ou à architectures ramifiées, tels des polyèdres ou des dendrimères. Également, ces supermolécules dendritiques sont aussi très prometteuses pour l'élaboration de nanostructures hybrides incluant des nanoparticules métalliques. En particulier, selon la taille et la forme de ces dernières, et la structure et la densité de greffage des parties dendritiques sur la nanoparticule, de nouveaux matériaux intéressants pour des applications en plein essor comme l'optoélectronique ou la spintronique (nano-transistors, méta-matériaux, quantum dots, etc...) peuvent voir le jour grâce à une organisation bi- ou tridimensionnelle déduite d'un auto-assemblage en phases mésomorphes.

Pour ce travail de thèse, nous nous sommes intéressés dans une première partie à la conception et la synthèse de nouveaux matériaux multifonctionnels (systèmes moléculaires dendritiques de zéro et première génération) capables d'être élaborés en films minces anisotropes et doués de propriétés photo-induites. Ce travail a été réalisé dans le cadre d'un réseau européen de type Marie Curie (ITN, Initial Training Network) intitulé "Functional Liquid Crystalline Dendrimers: Synthesis of New Materials, resource for New Applications" (acronyme "Dendreamers"). C'est la raison pour laquelle un des principaux objectifs de la thèse a été réalisé en collaboration avec un partenaire du réseau, localisé à Postdam (Allemagne) au Fraunhofer Institute for Applied Polymer Research, et spécialisé dans l'étude des propriétés optiques. Nous avons également réalisé l'étude complète des propriétés mésomorphes de ces nouveaux matériaux et de dérivés structuraux par la diffraction des rayons X aux petits angles. Dans une seconde partie, nous avons voulu profiter de l'expertise déjà acquise au sein de notre département (DMO) dans le domaine des architectures dendritiques pour fonctionnaliser des nanoparticules d'or avec des ligands dendritiques mésogènes afin d'organiser ces particules dans des structures mésomorphes; le but, bien entendu, est de profiter de cette organisation supramoléculaire pour pouvoir adresser plus facilement ces nanoparticules in fine. Les objectifs principaux de cette partie sont tout d'abord la synthèse d'une "bibliothèque" de nanoparticules mésomorphes dendronisées, et ensuite la caractérisation de réseaux simples formée par l'auto-assemblage des particules précédentes.

Synthèse et caractérisation de dendrimères multifonctionnels pour des applications en optique

Les films optiques anisotropes sont aujourd'hui d'un très grand intérêt pour créer des éléments essentiels de différents dispositifs comme le stockage optique d'informations ou pour d'autres composants optiques comme des polariseurs anisotropes. Dans cette perspective, le

photo-alignement de cristaux liquides photosensibles présente des avantages certains par rapport à d'autres techniques conventionnelles d'orientation comme la technique de Langmuir-Blodgett ou le brossage; on peut ainsi obtenir un bon contrôle de la direction d'orientation à température ordinaire. De plus, l'orientation photo-induite par une lumière polarisée peut être significativement améliorée par un recuit dans le domaine de température de la mésophase. C'est ainsi que des dérivés de l'azobenzène ou de cinnamate peuvent être envisagés pour de telles applications.

Actuellement, de nombreux polymères cristaux liquides photosensibles, contenant des mésogènes et des fluorophores distribués de façon aléatoire le long de la chaîne polymère, sont utilisés pour élaborer des films optiques anisotropes, mais ne conduisent pas en général à la bonne proportion ou à la bonne séquence de groupes fonctionnels. A l'inverse, les oligomères, qu'ils possèdent une structure linéaire (dimères, trimères, etc..) ou branchée (polypèdes, dendrons et dendrimères) ont démontré leur potentialité de par leur régularité structurale (topologie contrôlée, poids moléculaire bien défini) alliés à une bonne solubilité et une faible viscosité. De plus, une fois qu'ils ont été fonctionnalisés à dessein, ils peuvent présenter des mésophases ordonnées de basse dimensionnalité, très homogènes. Ainsi, utiliser des dendrimères cristaux liquides plutôt que des polymères semble une approche intéressante pour l'élaboration de films minces anisotropes. Afin d'élaborer les meilleurs matériaux pour être préparés en films minces anisotropes présentant les propriétés optiques souhaitées, nous avons tout d'abord conçu et synthétisé plusieurs trimères (dendrimères de génération zéro, Figure 1) susceptibles de satisfaire aux conditions requises, à savoir:

- une transition vitreuse supérieure à 25°C;
- une propension à former des films facilement;
- une faible tendance à l'agrégation pour des concentrations élevées de chromophores;
- une présence d'un état amorphe ou mésomorphe;
- un état photosensible.

Les chromophores mésogènes (par exemple du type alkoxyazobenzène) ont été incorporés dans la structure moléculaire en proportions variables. Plusieurs séries de mésogènes trimères à base de phloroglucinol (PG) et portant des groupes terminaux de type azobenzène (AZB), alkoxy-biphénylène (BPH) ou alkoxy-cyanobiphényl (OCB) en proportions variées, ont été synthétisées. Les systèmes finaux sont homolithiques (une seule brique) et hétérolithiques (briques différentes) selon le cas; par la suite, ils seront abrégés sous la forme $PG_zAZB_xBPH_{3-x}$ ou $PG_zAZB_xOCB_{3-x}$ où $z = 6$ ou 11 est la longueur de l'espaceur entre PG et les unités mésogènes périphériques (Figure 1). Par la suite, de nouvelles supermolécules

dendritiques ont été synthétisées et étudiées du point de vue de leurs propriétés mésomorphes uniquement. Il s'agit de la première génération des dendrimères à base de PG avec un espaceur contenant six groupes méthylène ($PG_6AZB_{2x}BPH_{6-2x}$ ou $PG_6AZB_{2x}OCB_{6-2x}$), et des dendrimères à base d'alcool benzylique (BA) et d'un espaceur à six méthylènes ($BA_6AZB_{2x}BPH_{6-2x}$ ou $BA_6AZB_{2x}OCB_{6-2x}$).

La préparation de tous les dendrimères a été réalisée par méthode divergente (Schéma 1) ou convergente (Schéma 2) selon la réactivité des groupes fonctionnels ou des dendrons. Différents types de couplage ont été utilisés entre le cœur phénol hydroxyl ou les points de branchement et le dérivé hydroxyl (réaction de Mitsunobu) ou bromé (éthérisation de Williamson).

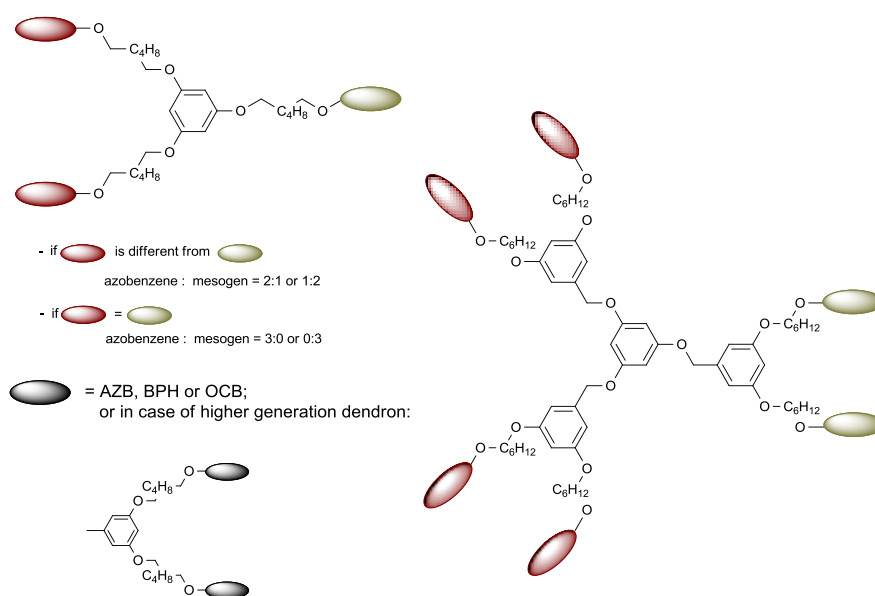


Figure 1: Structure schématique des dendrimères synthétisés comportant différentes proportions de groupes fonctionnels photochromes/mésogènes

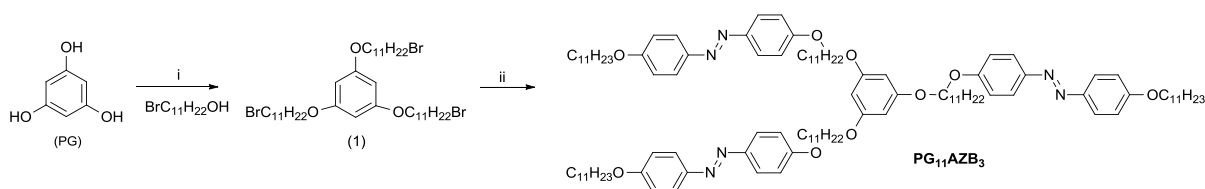


Schéma 1: Procédure de synthèse divergente des trimères homolithiques (illustration de la synthèse de $PG_{11}AZB_3$); réactifs et conditions: (i): DIAD, PPh_3 , THF; (ii): 4-(6-bromohexyloxy)-4'-(hexyloxy)azobenzène, K_2CO_3 , DMF

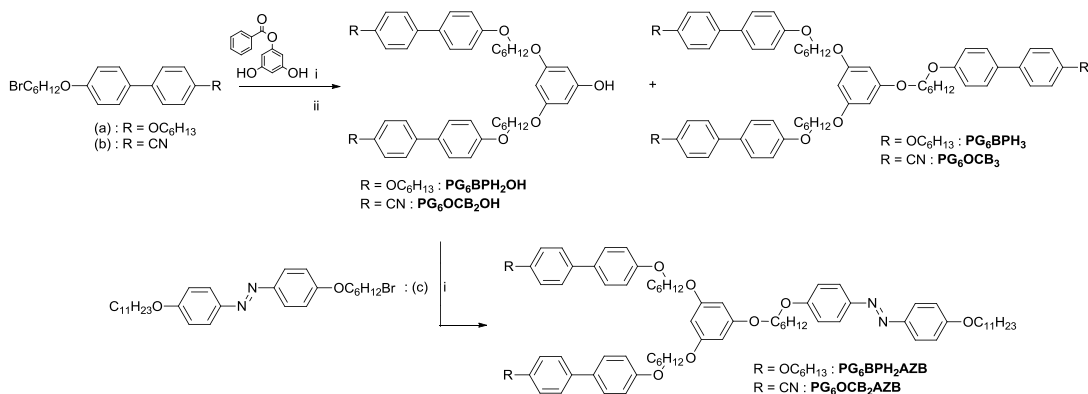


Schéma 2 Synthèse des trimères hétérolithiques (illustration de la synthèse de PG₆OCB₂AZB et de PG₆BPH₂AZB); *réactifs et conditions*: (i) K₂CO₃, KI, 18 crown-6, DMF or acetone; (ii) KOH, THF/H₂O, reflux

La photogénération d'une anisotropie optique à la suite de l'irradiation polarisée des trimères a conduit à des résultats prometteurs (Figure 2). Par exemple, le composé PG₆OCB₂AZB présente un dichroïsme de 0.77 (irradiation à 356 nm), valeur relativement grande si on la compare à celles habituellement obtenues avec des systèmes polymériques mésomorphes.

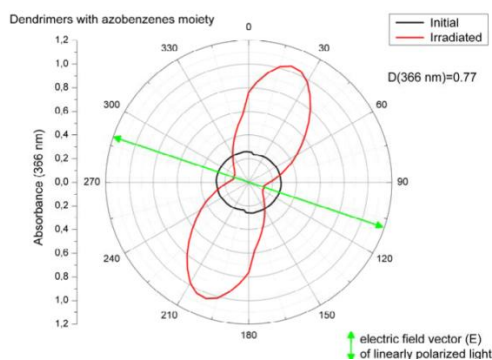


Figure 2 Absorbance de PG₆OCB₂AZB dans l'état initial et après irradiation

La Figure 2 montre une décroissance de l'absorption dans la direction parallèle au vecteur champ électrique de la lumière polarisée, et un fort accroissement de l'absorption dans la direction perpendiculaire. La différence d'absorption globale entre le film dans son état initial et le film une fois irradié indique une orientation différente des groupes azobenzène par rapport au film initial (alignement préférentiel des chromophores dans le plan du film).

Nous avons déterminé les propriétés mésomorphes des trimères en utilisant les techniques d'analyse thermique différentielle, de microscopie optique en lumière polarisée et de diffraction des rayons X aux petits angles (Figure 3). La nature de la mésophase dépend fortement du mésogène et de la topologie, quant à la stabilité thermique elle dépend essentiellement de la proportion relative entre les différents mésogènes. Les deux dérivés azobenzène homolithiques (PG₆AZB₃ and PG₁₁AZB₃) sont mésomorphes et présentent une phase smectique C, la stabilité de cette phase diminuant significativement quand la longueur de

l'espaceur est réduite. L'échange du groupe azobenzène par un groupe biphenylène dans la série $PG_6AZB_3 \rightarrow PG_6AZB_2BPH \rightarrow PG_6BPH_2AZB \rightarrow PG_6BPH_3$ n'améliore pas les propriétés liquide-cristallines qui sont d'ailleurs totalement perdues dans le composé homolithique contenant le groupe biphenylène; par contre, une phase smectique C est maintenue dans les deux composés hétérolithiques. Quand les groupes azobenzène sont échangés séquentiellement par des groupes fortement mésogènes, comme les groupes cyanobiphényl, selon la série $PG_6AZB_3 \rightarrow PG_6AZB_2OCB \rightarrow PG_6OCB_2AZB \rightarrow PG_6OCB_3$, le mésomorphisme est considérablement amélioré avec l'apparition de mésophases énantiotropes et sur de larges domaines de température. Les deux composés hétérolithiques présentent une phase smectique A et PG_6AZB_2OCB présente une phase smectique B. Dans le cas du composé OCB homolithique, la mésophase est très fluide et a été caractérisée comme une phase nématique. Les mesophases smectiques des trimères possèdent une structure en double couche, avec une ségrégation parfaite des différentes unités constituantes des mésogènes dans la mésophase. Des modèles ont été expliqués et décrits de façon efficace grâce aux volumes moléculaires partiels et calculs des sections moléculaires transverses aux différentes interfaces, générés par la structure multibloc des molécules.

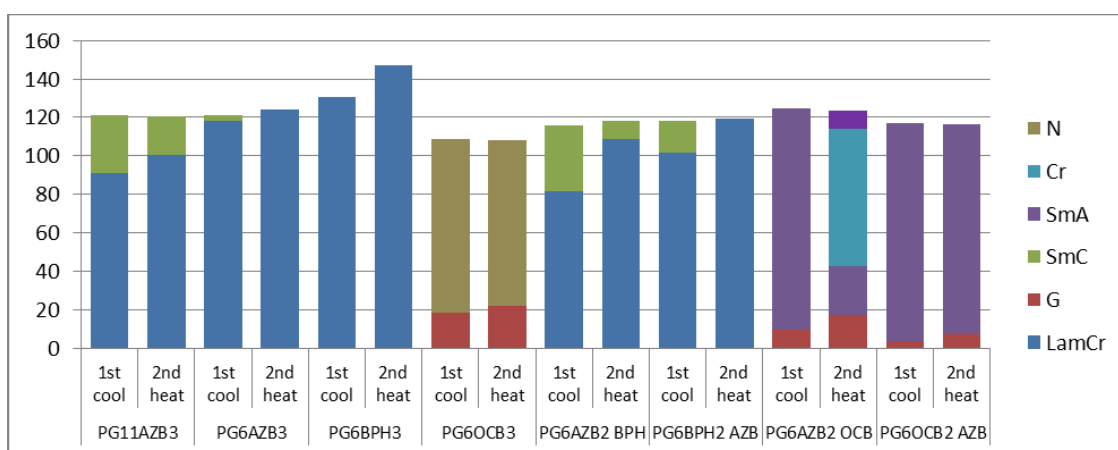


Figure 3: Mésomorphisme des trimères

Afin d'évaluer l'effet de variations structurales sur le mésomorphisme de ces systèmes, comme la génération, la longueur de l'espaceur entre points d'embranchements, et la nature du cœur central, d'autres systèmes ont été synthétisés. L'étude des propriétés mésomorphes des dendrimères de premier génération à base de PG et de ceux à base de BA a montré une amélioration notable du mésomorphisme, avec l'observation de mésophases de type smectique (M1 et M2) énantiotropes sur de larges domaines de températures (Figure 4) et, dans certains cas avec des T_g au-dessus de température ambiante. Les études par diffraction des rayons X montrent que la ségrégation à l'échelle moléculaire est partiellement conservée, due à la taille et la flexibilité du cœur dendritique de premier génération.

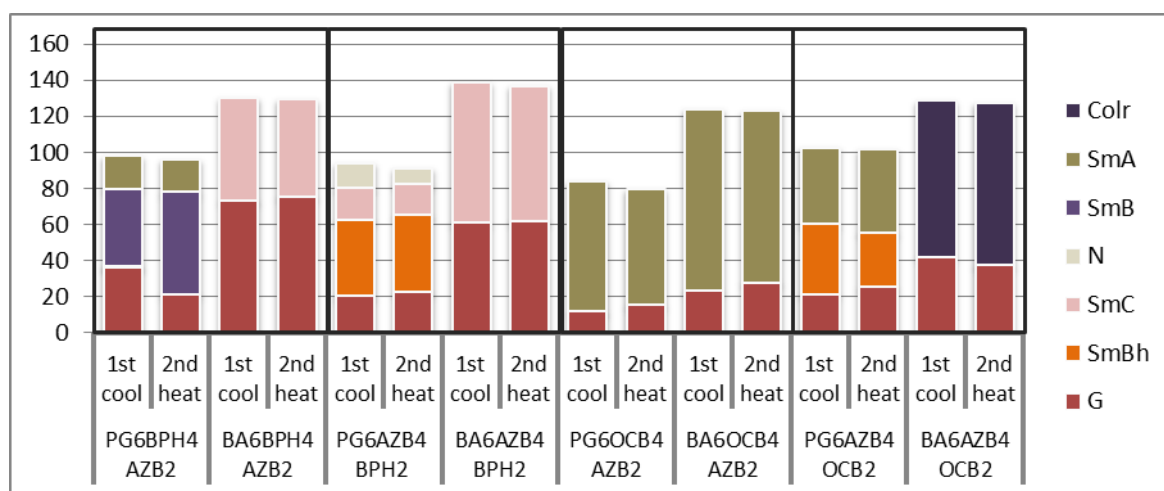
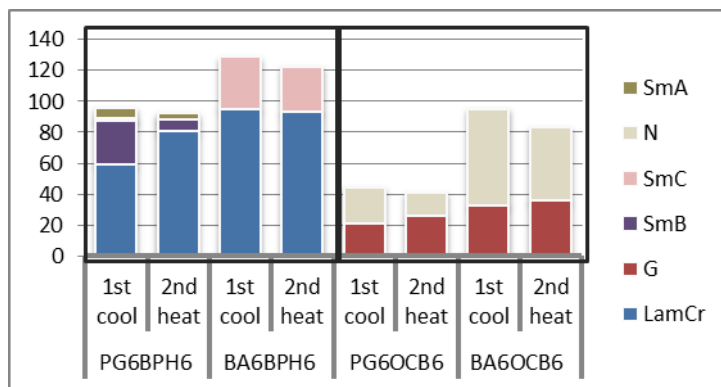


Figure 4: Diagrammes comparatifs des transitions de phase des dendrimères de premier génération homolithiques (en haut) et hétérolithiques (en bas) à base de PG et BA.

Hybrides dendronisés

Le développement de nanomatériaux par assemblage d'espèces organiques et inorganiques, actuellement privilégié au laboratoire, vise à promouvoir des petits objets doués de propriétés magnétiques/optiques capables de s'auto-organiser et manipulables/adressables par les techniques de microscopie en champ proche. L'auto-organisation dans le volume puis sur des réseaux 2D et 3D est essentielle pour réaliser de nouveaux dispositifs pour lesquels l'ordonnancement spatial est indispensable au fonctionnement (mémoires magnétiques, calculateurs supramoléculaires, capteurs, etc...) et à l'émergence de nouvelles propriétés.

A cet égard, les cristaux liquides sont tout à fait remarquables car ils sont capables de s'auto-organiser en diverses structures de basse dimensionnalité, ils sont fluides, et donc sans défaut à l'échelle de plusieurs centaines de microns (auto-organisables et autoréparables), et sont sensibles à leur environnement. Préalablement aux applications et utilisations envisagées, un travail exploratoire et fondamental dans ce domaine est donc primordial.

Les dendrimères sont uniques de par leur structure arborescente et régulière, où chaque génération peut remplir une ou plusieurs fonctions spécifiques (hiérarchisation des fonctions), et se prêtent également à la synthèse modulaire, c'est-à-dire que les synthons sont facilement permutable, permettant une modulation des propriétés physico-chimiques. Par exemple, des molécules stimuli-sensibles connectées sur des dendrimères susceptibles d'assurer une fonction physique ou chimique, permettraient aux propriétés de l'ensemble d'être contrôlées par des stimuli externes. Dans de tels systèmes, les dendrimères doivent également être élaborés pour promouvoir l'auto-organisation de ces hybrides, tout en contrôlant la distance entre nano-objets. Il apparaît alors prometteur et pertinent de développer la fonctionnalisation de nanocristaux (particules métalliques, oxydes ou alliages) par des dendrimères comme lien ou interface moléculaire, pour en faciliter la manipulation. La fabrication de nanostructures hybrides hiérarchisées de type cœur-couronne, constituées d'un cœur inorganique et multivalent sur lequel sont greffés des dendrons polyfonctionnels permet de réaliser des structures moléculaires inédites, tout en offrant des perspectives d'applications remarquables, par exemple pour l'électronique moléculaire ou l'électronique de spin pour lesquelles on peut tirer parti de la synergie des propriétés de chaque composant. L'objectif est d'obtenir des composés multifonctionnels en associant certaines propriétés de la partie inorganique à celles de la partie moléculaire (flexibilité, solubilité, fonctionnalité, stabilité, auto-organisabilité) au sein d'une structure unique. Cette combinaison chimique peut se traduire par des effets coopératifs additifs autant que synergiques. Il existe de très nombreuses publications concernant des nanoparticules non mésomorphes, fonctionnalisées par des ligands sans propriété particulière. Par contre, il existe beaucoup moins d'exemples de nanoparticules fonctionnalisées par des ligands mésomorphes et/ou optiquement actifs dans la littérature. L'auto-organisation peut en outre faire émerger des propriétés supplémentaires que les constituants initiaux seuls n'ont pas (métamatériaux).

Pour la synthèse des matériaux nanohybrides, nous nous sommes attachés à élaborer une méthode reproductible de préparation de nanoparticules d'or ayant une taille bien définie, en particulier en faisant varier plusieurs paramètres de la méthode de Brust. Nous avons ainsi pu mettre au point une méthode pour préparer des nanoparticules relativement monodisperses entre 2 à 6 nm de diamètre recouvertes d'une monocouche organique inerte (dodécane-thiol) (Figure 5) de façon reproductible.

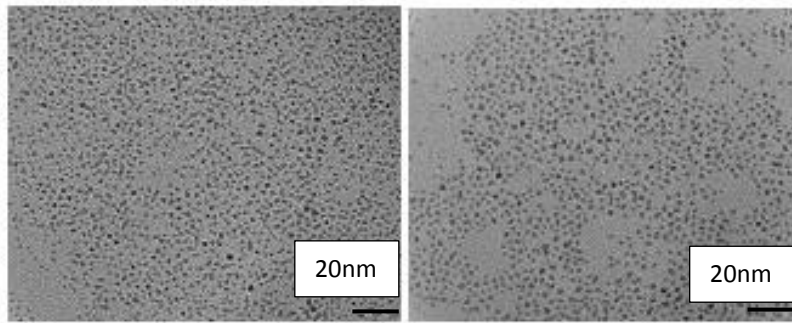


Figure 5: Nanoparticules d'or de 2,3 nm de diamètre

Pour accroître la taille des nanoparticules, un traitement thermique a été réalisé en présence de l'agent de transfert de phase, avec pour résultat l'obtention de nanoparticules d'or de 3 et 6 nm de diamètre pour des températures appliquées de 150 et 170°C respectivement (Figure 6).

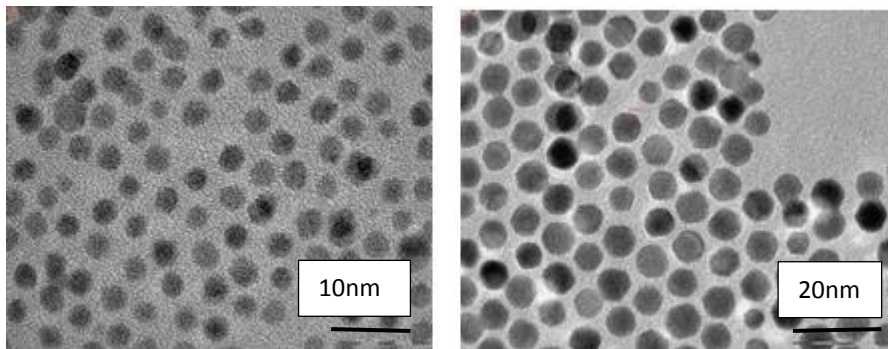


Figure 6: Nanoparticules d'or de 3 et 6 nm de diamètre obtenues après traitement thermique

Les matériaux nano-hybrides ont été ensuite obtenus à partir de ces nanoparticules d'or et de différents ligands dendritiques mésogènes par réaction d'échange par le biais de la fonction d'ancrage thiol (Figure 7). Les dendrons ont été obtenus à partir des précurseurs dendritiques obtenus dans la première partie de cette thèse. A la fonction hydroxyle libre des dendrons, a été connectée une longue chaîne alkyle (undécylène) terminée par une fonction bromure.

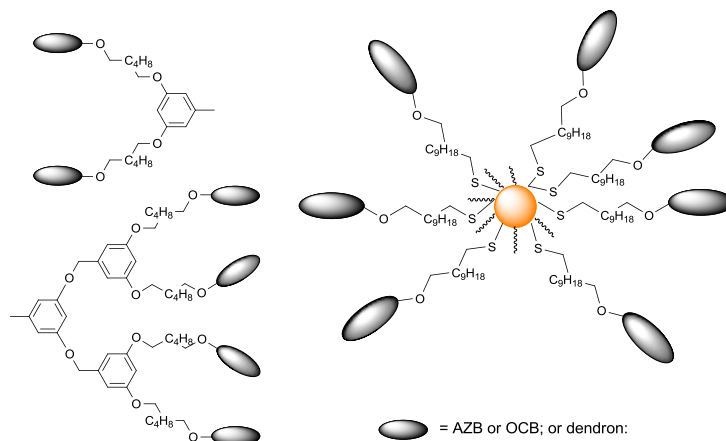


Figure 7: Nanoparticules d'or fonctionnalisées par des groupes mésogènes

Pour greffer les ligands prodendritiques, le bromure du point focal a été transformé en une fonction thiol (**L**), (Schéma 3) et celle-ci a été utilisée pour fonctionnaliser les nanoparticules d'or par réaction d'échange dans un solvant. La purification par une technique bio-gel a permis de séparer les nanohybrides des ligands organiques. Cette méthode a été efficace dans le cas des petits ligands, mais beaucoup moins dans le cas des ligands de poids moléculaire plus important, du fait de l'encombrement stérique.

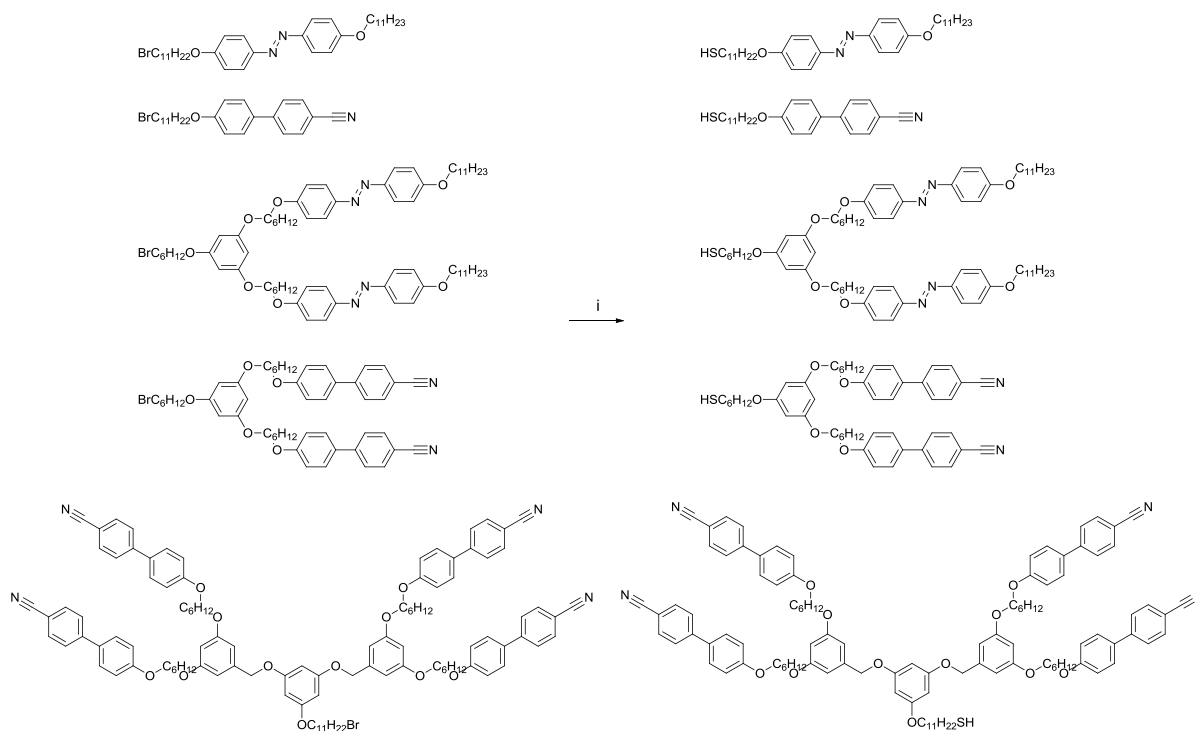


Schéma 3 Synthèse des ligands prodendritiques (**L**) portant la fonction thiol. Réactifs et conditions : (i) HMDTS, TBAF, THF, 0 °C

Les hybrides ont été caractérisés par microscopie électronique en transmission (MET), ce qui a permis de vérifier que la réaction d'échange n'a pas dégradé la nanoparticule et que le greffage de mésogènes promeut une distribution homogène des nanoparticules sur la surface de la grille (drop-casting). Le taux de substitution et le ratio ligand/dodécane-thiol ont été évalués par thermogravimétrie et RMN du proton. Les propriétés thermiques et d'auto-organisation des hybrides dendronisés ont été évaluées, ou sont en cours d'évaluation. Les ligands dendritiques sont eux-mêmes mésomorphes, alors que leur greffage sur la surface des NPs d'or de 2 nm environ induit un comportement thermique complexe et assez difficile à évaluer. En effet, ce type de matériaux induit des organisations supramoléculaires inédites, constituées de réseaux binaires, un premier sous-réseau formé par les parties organiques, et un second généré par les nanoparticules. Des premières mesures de diffraction des rayons X et neutrons permettent d'affirmer dans certains cas la formation de mésophases lamellaires. Ces deux sous-réseaux

bien que joints peuvent présenter des morphologies différentes: dans certains cas, les parties organiques s'organisent en mésophases de type smectiques, et selon la génération le sous-réseau de nanoparticules est soit isotrope (distribution aléatoire), soit dans le plan ou 3D. Les ligands de petite taille ne permettent pas d'améliorer le comportement mésomorphe de façon notable.

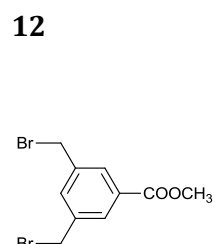
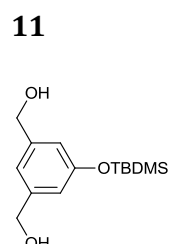
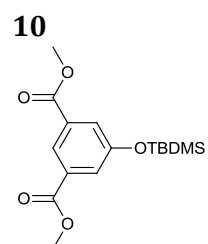
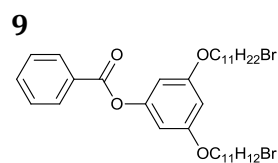
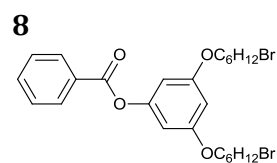
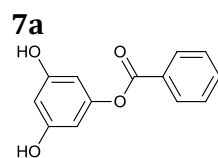
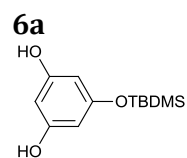
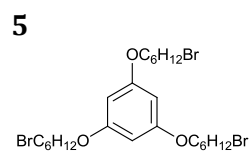
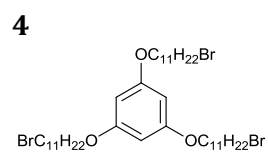
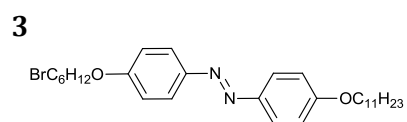
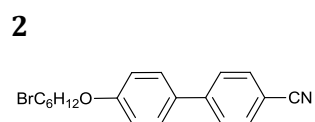
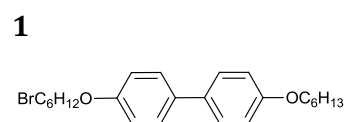
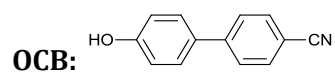
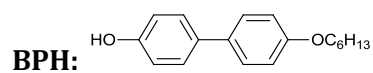
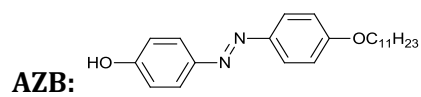
Conclusion

Nous avons synthétisé avec succès de nouveaux trimères présentant une forte anisotropie optique (dichroïsme de 0,77 (356 nm)), et des dendrimères de supérieure génération qui satisfont à certaines conditions, comme de présenter une valeur de transition vitreuse supérieure à la température ambiante et aussi un domaine mésomorphe sur une plage de température relativement grande. Nous avons également synthétisé différents types de dendrimères où des chromophores ont été introduits avec différents groupes fonctionnels mésogènes; une étude systématique en fonction de la proportion de groupes mésogènes a permis de bien cerner leur influence sur les propriétés mésomorphes des matériaux finaux.

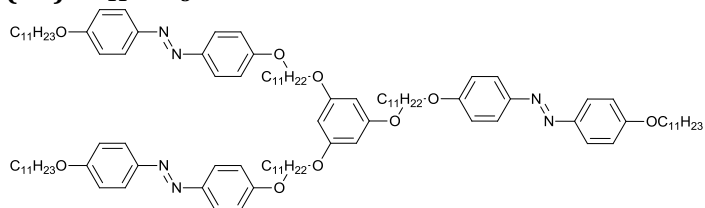
Enfin, des nanoparticules d'or recouvertes d'une monocouche organique ont été synthétisées, puis fonctionnalisées avec divers ligands dendritiques. Les mesures de diffraction des rayons X ne permettent pas cependant à elles seules de caractériser de façon univoque la nature des mésophases de l'ensemble des hybrides. D'autres expériences, notamment de diffusion des rayons X et de neutrons ont été menées; mais le traitement complexe des données obtenues n'en est qu'au stade préliminaire à l'heure actuelle et des conclusions hâtives seraient inappropriées.

Annex

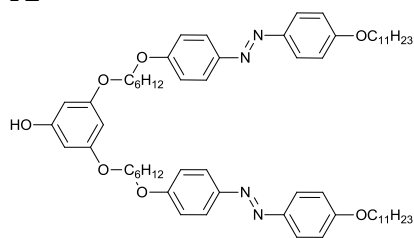
List of compounds



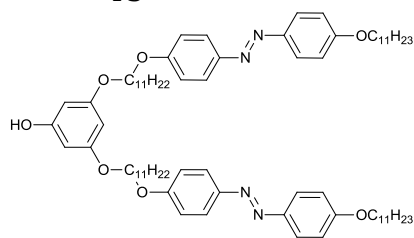
(T1) PG₁₁AZB₃



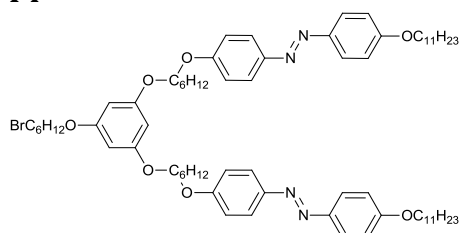
T2



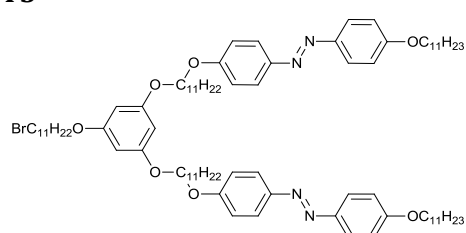
T3



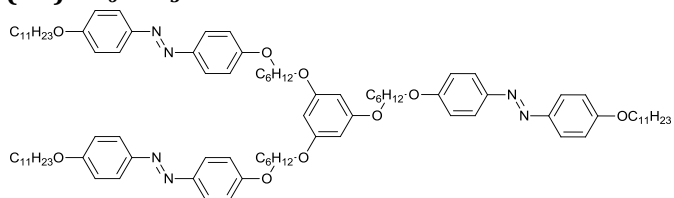
T4



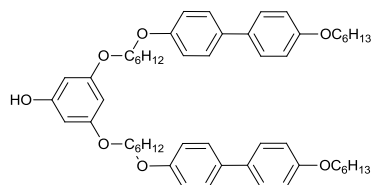
T5



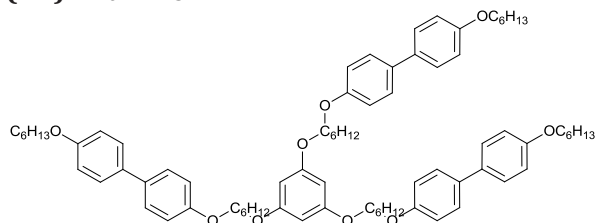
(T6) PG₆AZB₃



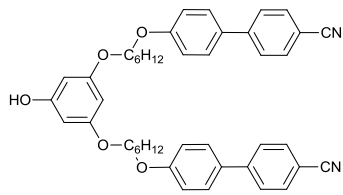
T7



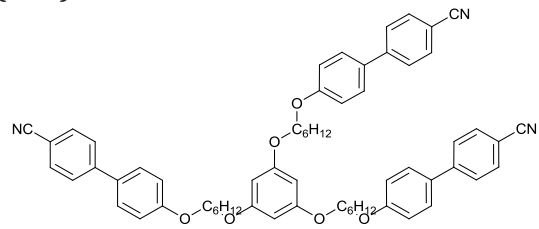
(T8) PG₆BPH₃



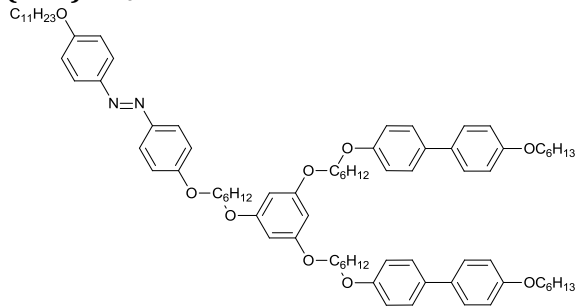
T9



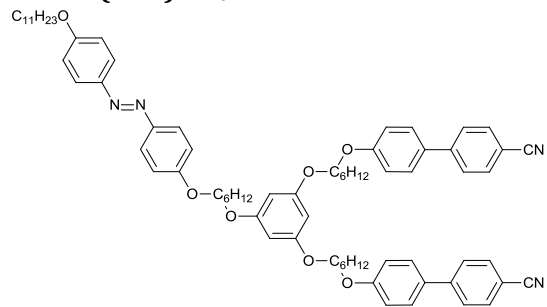
(T10) PG₆OCB₃



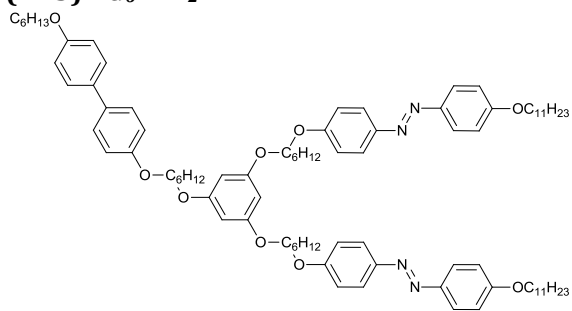
(T11) PG₆BPH₂AZB



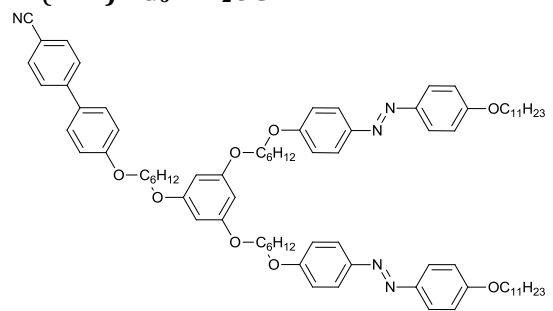
(T12) PG₆OCB₂AZB



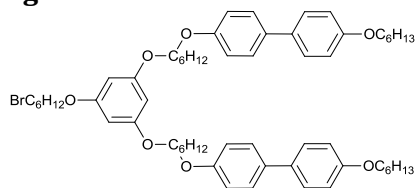
(T13) PG₆AZB₂BPH:



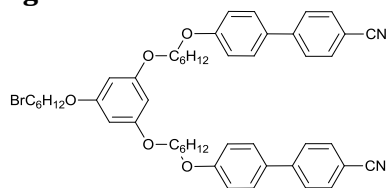
(T14) PG₆AZB₂OCB:



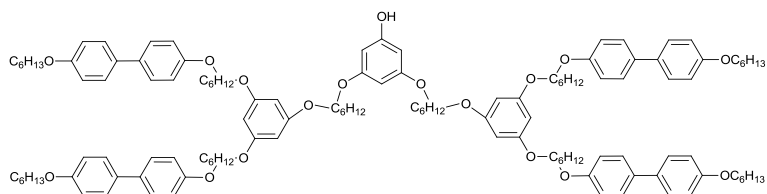
Pg1



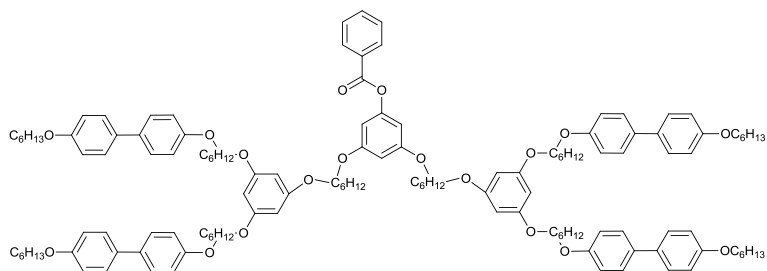
Pg2



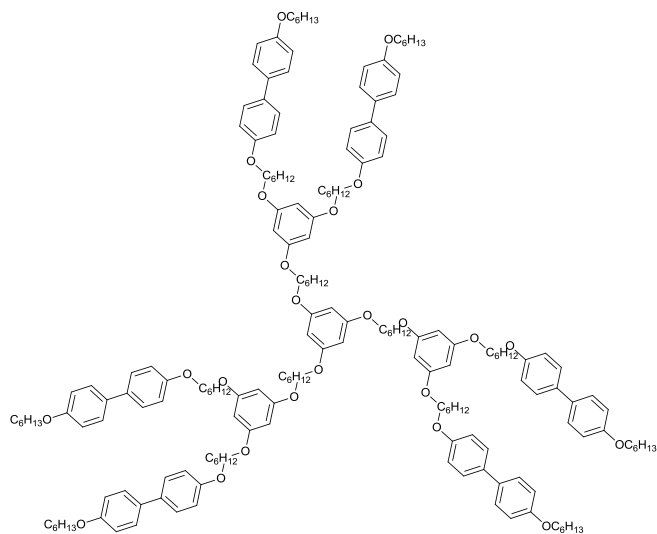
Pg3



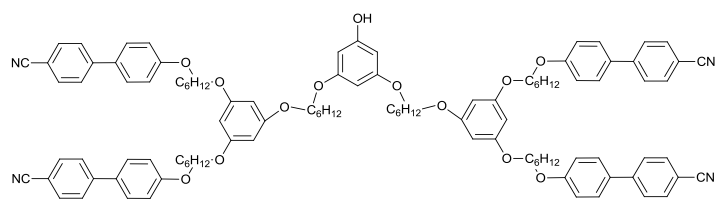
Pg4



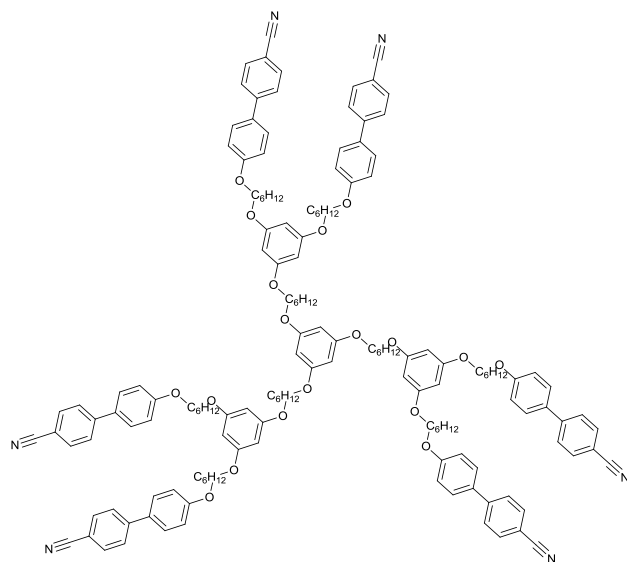
(Pg5) PG₆BPH₆



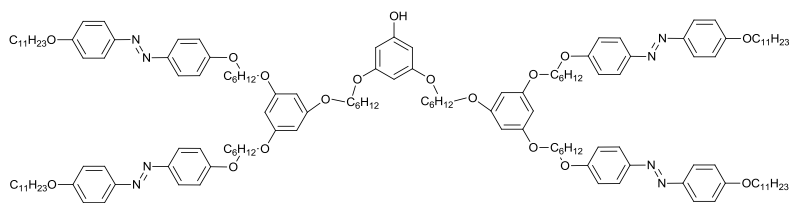
Pg6



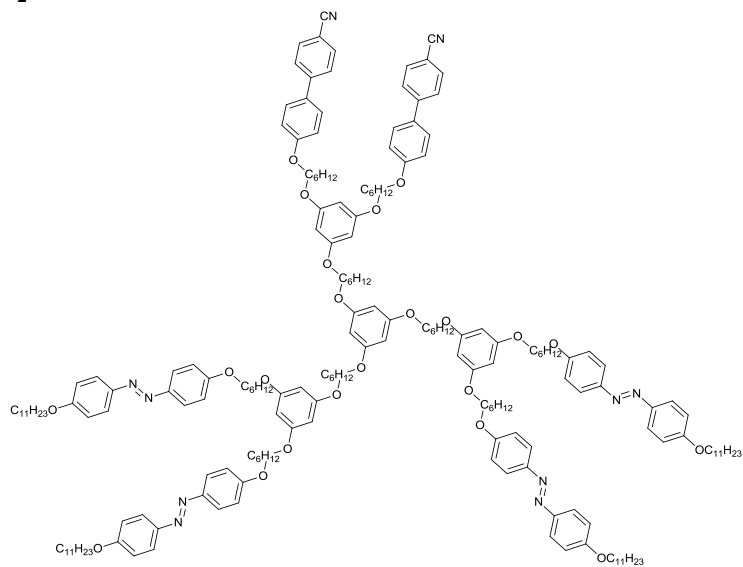
(Pg7) PG₆OCB₆



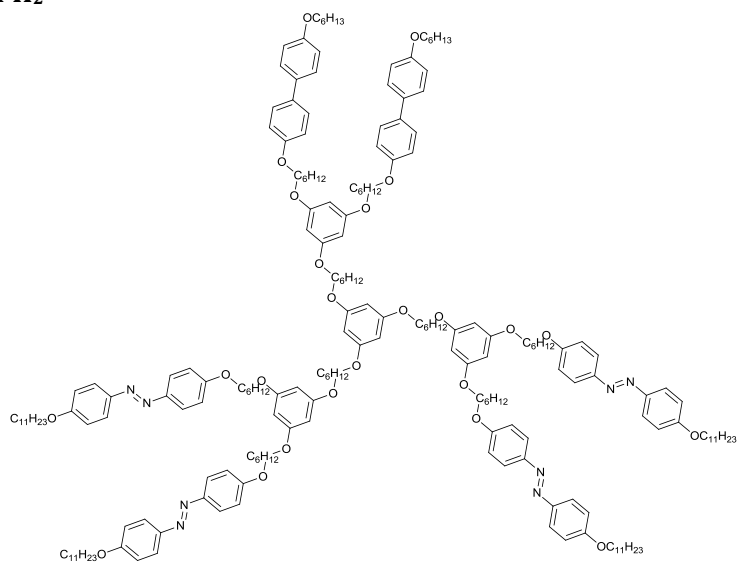
Pg8



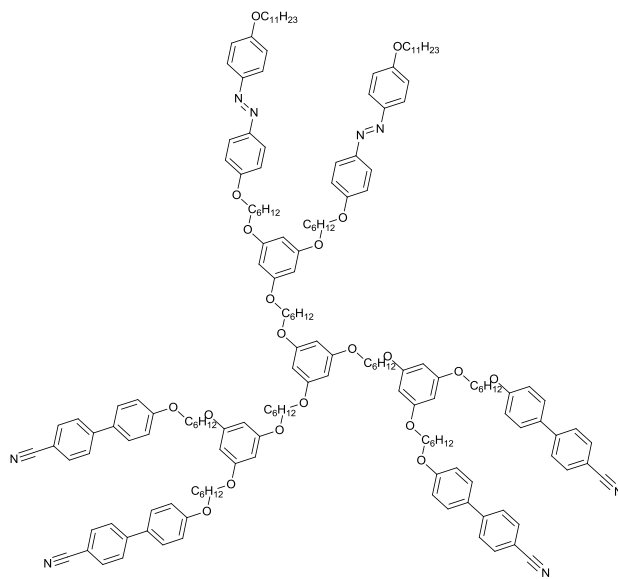
(Pg9) PG₆AZB₄OCB₂



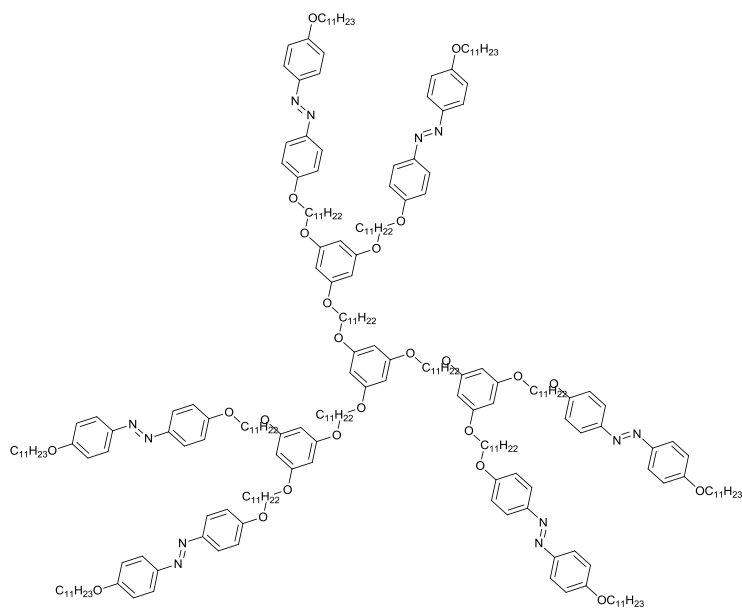
(Pg10) PG₆AZB₄BPH₂

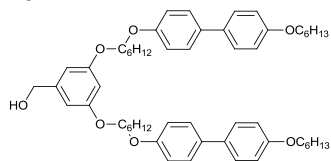
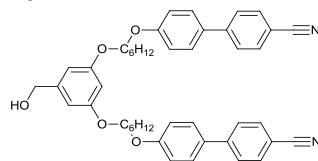
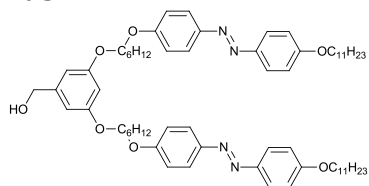
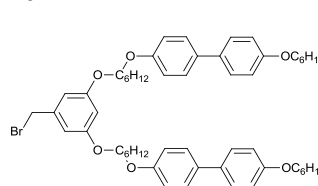
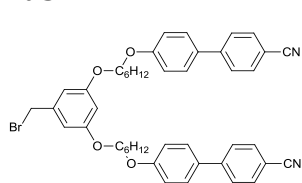
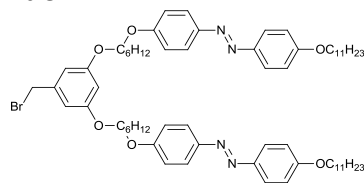
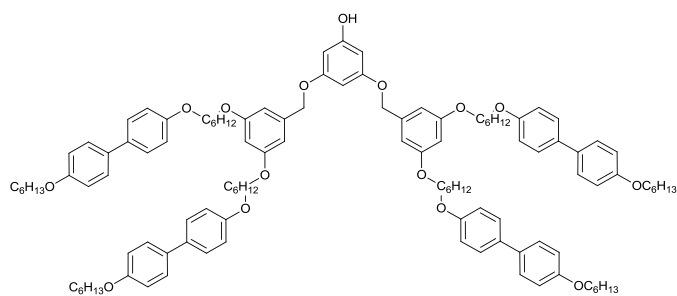
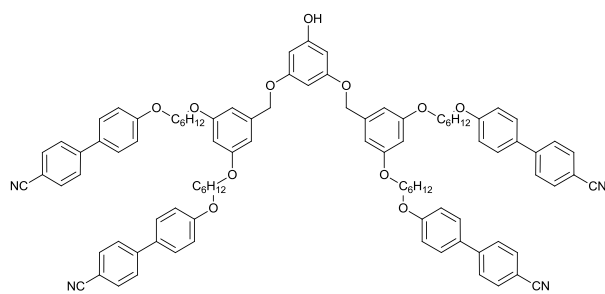


(Pg11) PG₆OCB₄AZB₂

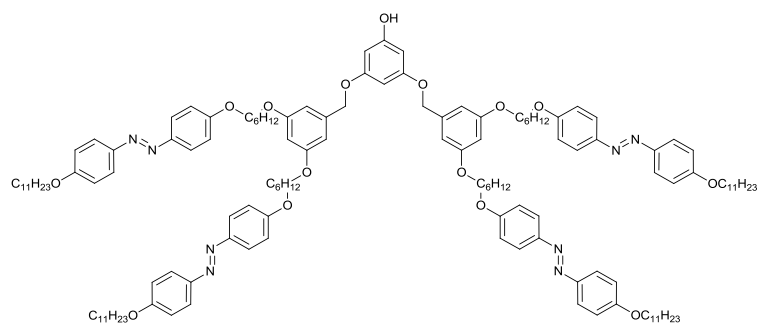


(Pg14) *PG₁₁AZB₆*

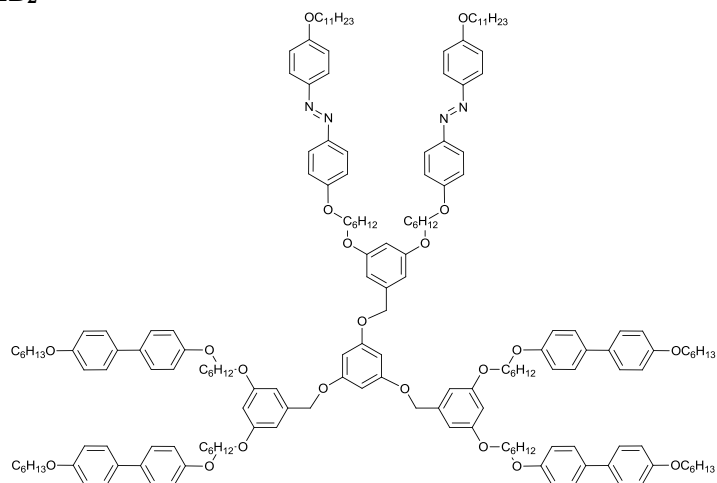


Ba1**Ba2****Ba3****Ba4****Ba5****Ba6****Ba7****Ba8**

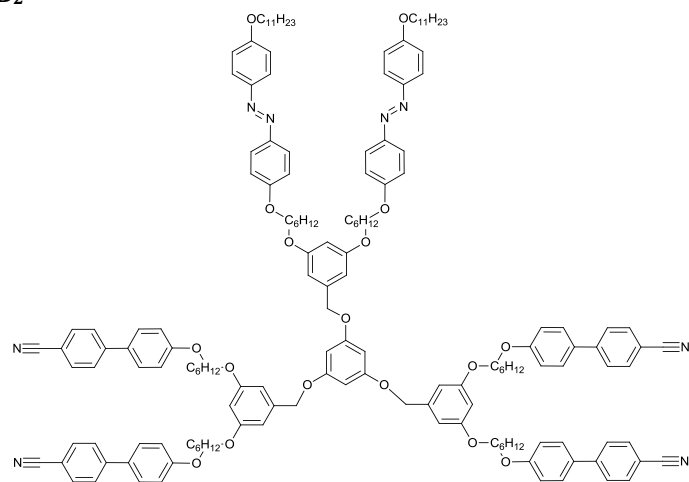
Ba9



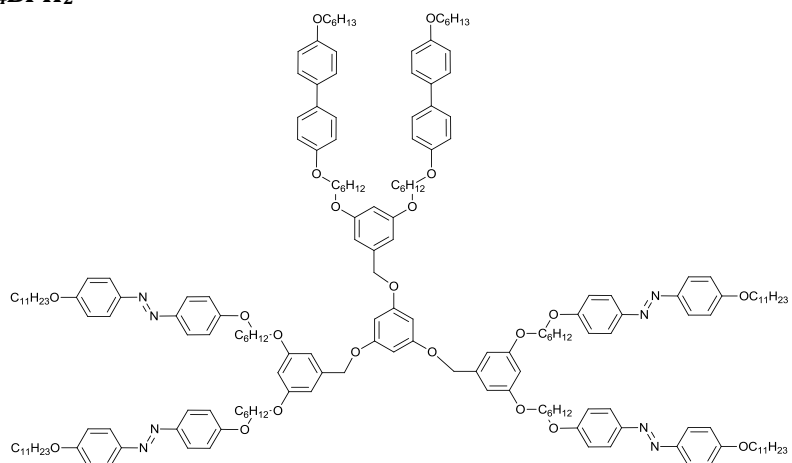
(Ba10) BA₆BPH₄AZB₂



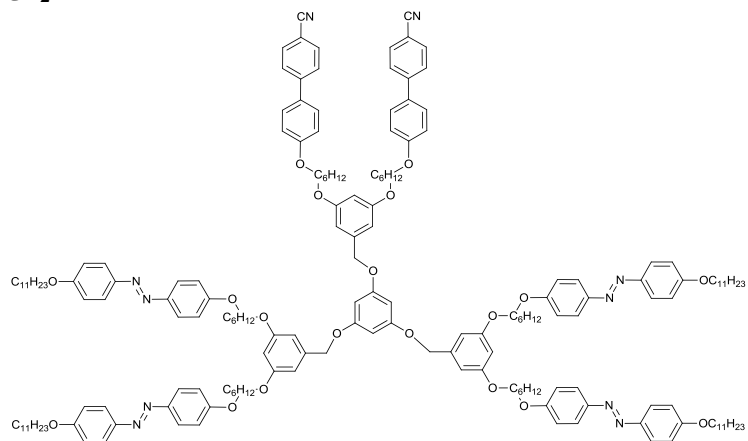
(Ba11) BA₆OCB₄AZB₂



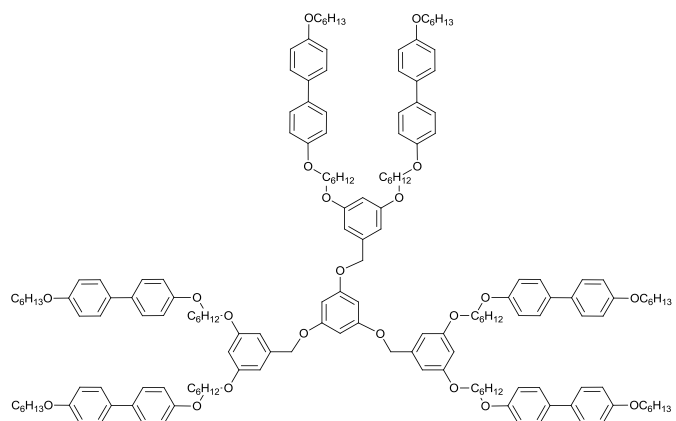
(Ba12) BA₆AZB₄BPH₂



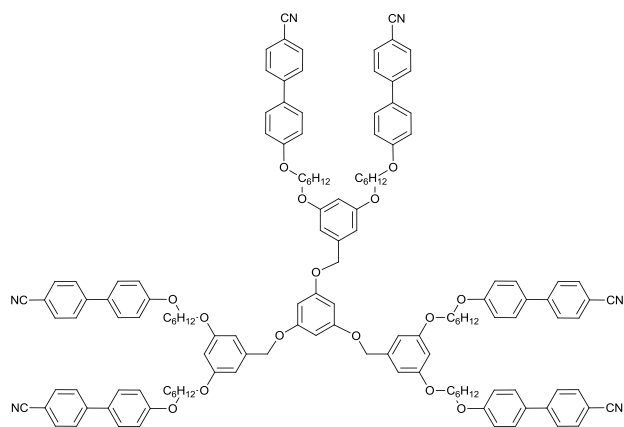
(Ba13) BA₆AZB₄OCB₂



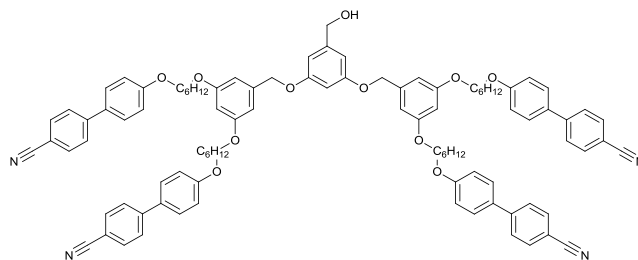
(Ba14) BA₆BPH₆



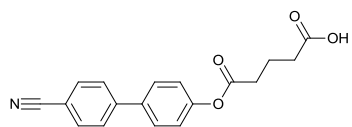
(Ba15) BA₆OCB₆



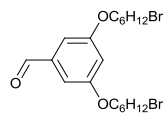
Ba16



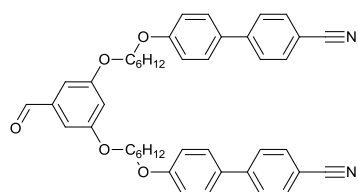
C1



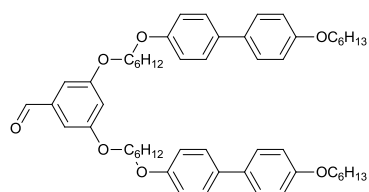
C3



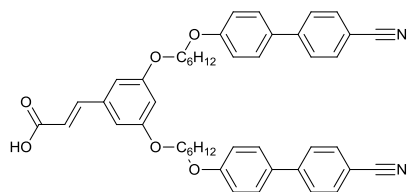
C4



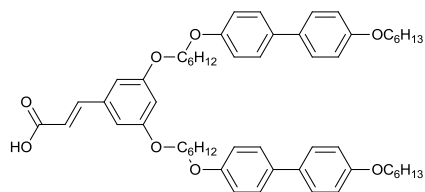
C5

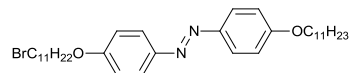
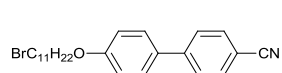
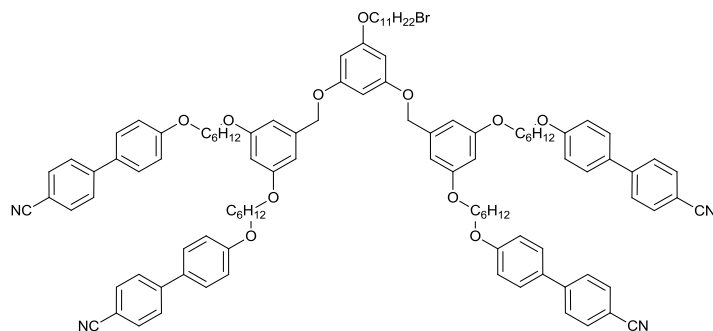
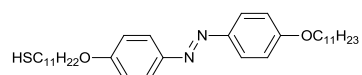
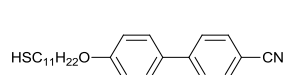
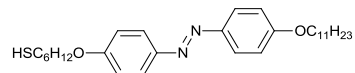
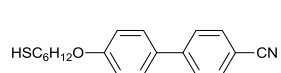
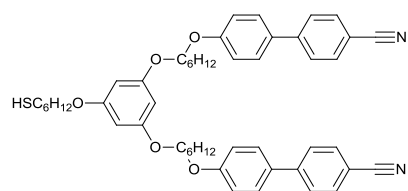
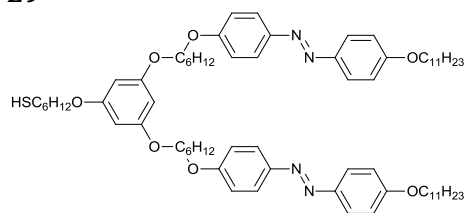
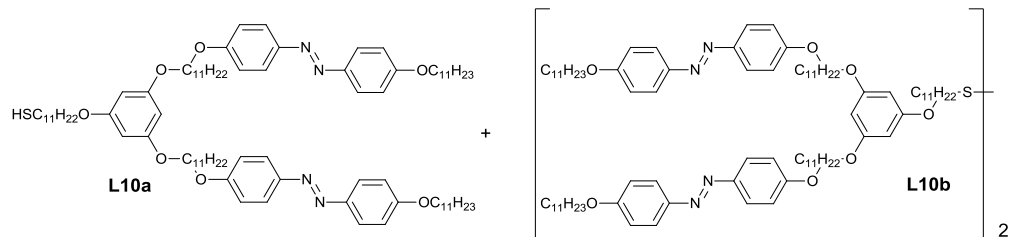


C6

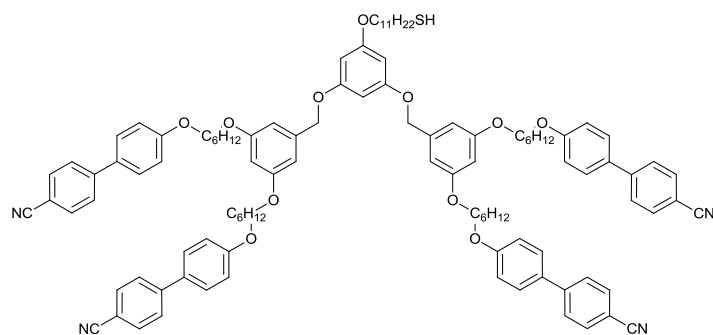


C7

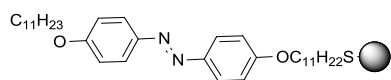


L1**L2****L3****L4****L5****L6****L7****L8****L9****L10**

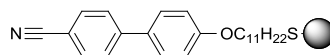
L11



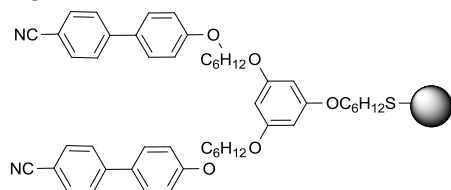
H1



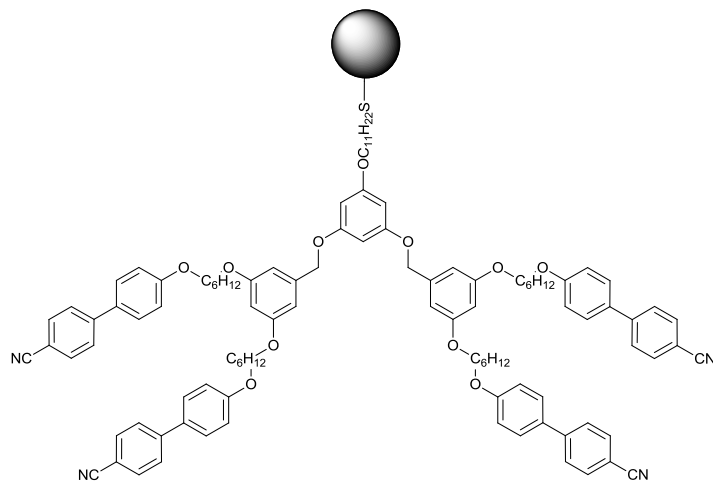
H4



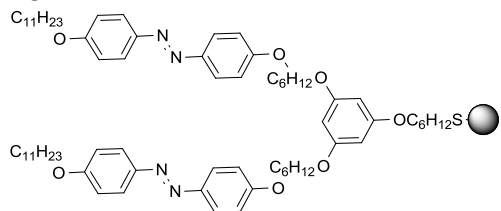
H6



H7



H8



Synthèse de dendrimères et de nanohybrids dendronisés, auto-organisés et étude de leurs propriétés physiques

Pour ce travail de thèse, nous nous sommes intéressés dans une première partie à la conception et à la synthèse de nouveaux matériaux multifonctionnels (LC, photosensible, systèmes moléculaires dendritiques) capables d'être élaborés en films minces anisotropes et doués de propriétés photo-induites. Nous avons réalisé l'étude complète des propriétés mésomorphes de ces nouveaux matériaux et de dérivés structuraux (en fonction de la connectivité dendritique intrinsèque) par la diffraction des rayons X aux petits angles; l'étude de leurs propriétés optiques a également été effectuée. Dans une seconde partie, nous avons fonctionnalisé des nanoparticules d'or avec des ligands dendritiques mésogènes afin d'organiser ces particules dans des structures mésomorphes. Les objectifs principaux de cette partie sont tout d'abord la synthèse d'une "bibliothèque" de nanoparticules mésomorphes dendronisées, et ensuite la caractérisation de réseaux simples formée par l'auto-assemblage des particules précédentes.

Mots-clés: azobenzène, cristaux liquides, dendrimères mésomorphes, nanoparticules, anisotropie optique, photosensibilité, auto-assemblage, systèmes supramoléculaires

On the one hand, we focused on the design and synthesis of multifunctional materials (liquid crystalline, photoresponsive) which are suitable for making thin films where photoinduced optical anisotropy and surface relief gratings can be generated. The mesomorphic behaviour of these dendrimers was investigated and also their optical properties. On the other hand, we grafted structurally related protodendritic mesogenic ligands to monodisperse gold nanoparticles to elaborate liquid crystalline hybrids in order to self-organize NPs in periodic arrays. A set of dendronized gold nanohybrids was synthesized to carry out this study.

Key-words: azobenzene, liquid crystals, mesomorphic dendrimers, nanoparticles, optical anisotropy, photoresponsive, self-assembly, supramolecular systems